Seismic Vulnerability Reduction of Historical Masonry Towers by External Prestressing Devices

Dissertation

submitted to and approved by the

Department of Architecture, Civil Engineering and Environmental Sciences
University of Braunschweig – Institute of Technology

and the

Faculty of Engineering
University of Florence

in candidacy for the degree of a
Doktor-Ingenieur (Dr.-Ing.) /
Dottore di Ricerca in "Riduzione del Rischio da Catastrofi Naturali su Strutture ed Infrastrutture" *)

by

Adolfo Preciado Quiroz
Born 16 October 1977
from Colima, Mexico

Submitted on	12 September 2011
Oral examination on	04 November 2011
Professorial advisors	Prof. H. Budelmann
	Prof. G. Bartoli

2011

*) Either the German or the Italian form of the title may be used.

Tutors:

Prof. Harald Budelmann – Technische Universität Braunschweig

Prof. Gianni Bartoli – Università degli Studi di Firenze

Doctoral course coordinators:

Prof. Udo Peil – Technische Universität Braunschweig

Prof. Claudio Borri – Università degli Studi di Firenze

Examining committee:

Prof. Udo Peil – Technische Universität Braunschweig

Prof. Harald Budelmann – Technische Universität Braunschweig

Prof. Joachim Stahlmann – Technische Universität Braunschweig

Prof. Hocine Oumeraci – Technische Universität Braunschweig

Prof. Gianni Bartoli – Università degli Studi di Firenze

Prof. Andrea Vignoli – Università degli Studi di Firenze

Prof. Luca Facchini – Università degli Studi di Firenze

Prof. Anna Saetta – Università IUAV di Venezia

To my wife Karlita and

my parents Rosa Margarita and Adolfo,

with all my love

Abstract

Existing historical masonry towers are distributed all over the world and constitute a relevant part of the architectural and cultural heritage of humanity. Their protection against earthquakes is a topic of great concern among the scientific community. This concern mainly arises from the strong damage or complete loss suffered by this group of structures due to these catastrophic events and the need and interest to preserve them. Although the great progress in technology, seismology and earthquake engineering, the preservation of these brittle and massive structures still represents a major challenge. This thesis describes a methodology aimed at managing the seismic risk of historical masonry towers, including the assessment of risk and the remedial measures to attain its reduction. The seismic risk of a certain historical structure located in a seismic zone is determined by the conjunct of the seismic hazard and its structural vulnerability. In the introductory chapters an intensive literature review is presented objected at describing the main aspects that determine the earthquake hazard of a site, the structural vulnerability of historical masonry towers and the recommended in literature to manage the seismic risk. Since the seismic hazard is unavoidable and is not in our hands to reduce it or modify it, therefore this research work aims at reducing the structural vulnerability of historical towers by the implementation of prestressing devices, in order to attain the seismic risk reduction. The devices are vertically and externally located inside the towers in order to give to the retrofitting the characteristic of reversibility, respecting in all senses the architectonic and historical value of the structure. This thesis addresses two main key stages on the seismic risk management of historical towers. The first stage corresponds to the assessment of the seismic risk with the combination of intensive numerical simulations and a suitable constitutive model able to satisfactorily represent the nonlinear behavior of masonry. In order to obtain numerical models more reliable and representative of real structures they are validated with key-behavioural characteristics reported in literature, observed damages after real earthquakes and calibrated with real physical data (mechanical and dynamic) obtained by experimental in-situ campaigns. The post-tensioned devices intend to improve the seismic performance of the towers and to reduce the expected damage with the application of a uniform overall distribution of compressive stresses to the masonry to increase strength, ductility, energy dissipation and confinement, achieving with these improvements the seismic risk reduction. The risk assessment of historical masonry towers and the possible achievement of the risk reduction are the main characteristics of the proposed methodology. The second key stage corresponds to the validation of the proposal by the demonstration of its effectiveness in two real historical masonry towers located in seismic zones. The first case study corresponds to the Cathedral of Colima, Mexico and the second one to the medieval tower "Torre Grossa" of San Gimignano, Italy. Finally, the advantages and limitations of this proposal in the seismic risk management of historical towers are described.

Keywords: Historical masonry towers, earthquake hazard, structural vulnerability, seismic risk management, retrofitting, external prestressing, prestressing force, smart materials

Acknowledgements

Starting from the very beginning, I thank to the Director of the Faculty of Civil Engineering Prof. Francisco J. Guzmán Nava and the Dean Prof. Miguel A. Aguayo López from the Universidad de Colima (Mexico) for the economic support to start my doctoral studies.

The reported research in this thesis was possible thanks to the scholarship made available by the German Research Foundation (Deutsche Forschungsgemeinschaft, DFG), which is gratefully acknowledged.

The research was developed at the Institute of Building Materials, Concrete Structures and Fire Protection (iBMB) of the Technische Universität Braunschweig (Germany) and at the Department of Civil and Environmental Engineering (DICEA) of the Università degli Studi di Firenze (Italy) in the framework of the International Research Training Group "Risk Management of Natural and Civilization Hazards on Buildings and Infrastructure".

I would like to record my gratitude to Prof. Harald Budelmann from the Technische Universität Braunschweig for the opportunity to join the doctoral course as well as for both his wise advice and polite treatment in everything. In the same manner I would like to thank to Prof. Gianni Bartoli from the Università degli Studi di Firenze for sharing with me his great professional experience, advices and kindness.

Special thanks to Dr. Silvio T. Sperbeck from GRS Berlin for the fruitful discussions and kind support in the first years of this research, as well as for his care and friendship since the first time we met.

Thanks to Prof. Agustín Orduña Bustamante and Prof. Guillermo Roeder Carbo, Universidad de Colima and Dr. Juan Carlos Araiza Garaygordóbil, WJE, for their support and encouragement since the time I was working for my Master´s Degree until present. To Dr. Gregory Penelis, PCE, Dr. Paolo Clemente, ENEA, Dr. Maria G. Castellano, FIP Industriale and Dr. Michele Betti, DICEA, for the fruitful discussions about related topics to this work.

My gratitude to Prof. Sergio Lagomarsino and Dr. Chiara Calderini from the Università degli Studi di Genova for their authorization and support in implementing their material model in my research.

I thank to Prof. Udo Peil and Prof. Claudio Borri for conceiving and leading this international doctoral course, as well as to all the colleagues of iBMB and DICEA for both academic and social interactions.

I would like to express my deepest gratitude to my wife Karla, to my parents Rosa Margarita and Adolfo, to my sisters Claudia, Rocío and Margarita, and to my little brother Alvaro for their love and invaluable support in everything. This thesis is dedicated to them.

Florence, Italy, December 2011 Adolfo Preciado Quiroz

Contents

Chapter 1

Introduction

1.1 Introduction

Existing historical masonry towers with different characteristics and functions are distributed all over the world and constitute a relevant part of the architectural and cultural heritage of humanity. These important vertical structures were built either isolated or commonly included in different manners in the urban context, such as built as part of churches, castles, municipal buildings and city walls. Bell and clock towers, also named civic towers, were built quite tall with the important purpose of informing people visually and with sounds by ringing bells and striking clocks about time and extraordinary events such as civil defence or fire alarm, and moreover to call the community to social meetings. Another reason that led to the construction of tall civic towers, especially in the medieval cities of Italy, was that they were seen as a symbol, representing by the height and architecture sophistication the richness and power of the great families.

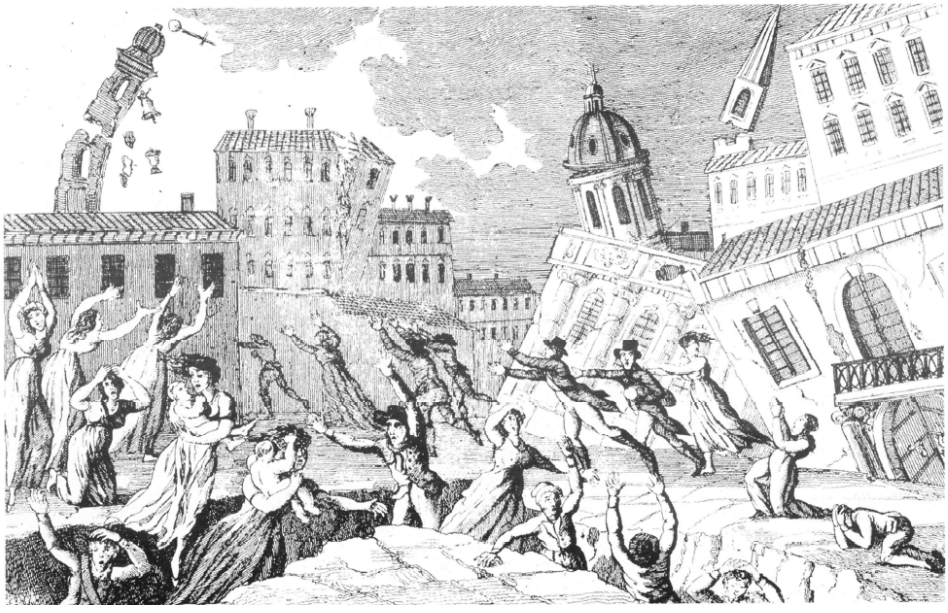

Figure 1.1: Earthquake of Naples, Italy, on July 26th, 1805 [Kozak and Thompson, 1991]

Strong damage or complete loss suffered by the cultural patrimony when subjected to considerable earthquake ground motion has been occurring throughout the history of humanity as illustrated in Figure 1.1, which shows the effects of the historical earthquake occurred in Naples, Italy in 1805. The occurrence of these unexpected and unavoidable events has demonstrated that historical masonry towers are one of the most vulnerable structural types to suffer strong damage or collapse as depicted in Figure 1.2. Their protection is a topic of great concern among the scientific community. This concern mainly arises from the observed damages after every considerable earthquake and the need and interest to preserve them. Although the recent progress in technology, seismology and earthquake engineering, the preservation of these brittle and massive monuments still represents a major challenge. These vertical structures are slender by nature. The slenderness (H/L) of towers is the single most decisive factor affecting their seismic performance, characterized by a ductile behavior similar to that of cantilever beams, failing in a predominant flexural mode. Moreover, the seismic vulnerability of historical masonry towers is increased by certain important aspects. These correspond to the presence of adjacent buildings, large openings at belfries, nonlinear behavior of masonry since low lateral loads due to its poor tensile strength, lack of good connection between structural elements, high vertical loading and progressive damage (see section 2.4.6).

Figure 1.2: San Bernardino church undamaged and observed damage after the 6.3 magnitude earthquake of L'Aquila, Italy on April 6th, 2009 [Bazrafshan, 2009]

In the context of the *seismic risk management of the built environment* there are two main stages that are recommended in literature to be carried out as a measure to attain the protection of the cultural heritage. These stages correspond to the *seismic risk assessment* and *seismic risk reduction.* The achievement of these two main stages represents a huge task. The seismic risk of a certain historical structure located in a seismic zone is determined by the conjunct of the *seismic hazard* and its *structural vulnerability*. The seismic risk is also named in the relevant literature and known within

the research community as *seismic vulnerability*. Nowadays, there is a great variety of methodologies aimed to assess the seismic vulnerability of structures (see section 2.3.2).

Seismic vulnerability assessment of ancient masonry buildings is an issue of most importance at present time. The main difficulty is the nonlinear behavior of masonry generated by the presence and development of cracks since very low horizontal load levels due to its poor tensile strength. This behavior, combined with the dynamic characteristics of the seismic action represents a major challenge [Orduña et al., 2008]. As aforementioned, the seismic risk of a structure depends on the conjunct of the hazard and the vulnerability of the structure. Since the seismic hazard is unavoidable and is not in our hands to reduce it or modify it, the seismic risk reduction of historical towers may be attained by reducing their structural vulnerability with the implementation of prestressing devices, which is the main objective of this thesis. The prestressing devices are vertically and externally located inside the towers in order to give to the retrofitting the characteristic of reversibility (see section 3.3.1), which is definitely the most important aspect when modern techniques are implemented, respecting in all senses the architectonic and historical value of the structure.

This thesis addresses two main *key issues* on the seismic risk management of historical masonry towers. The *first issue*, *the hypothesis*, corresponds to the possibility of assessing their seismic risk by combining intensive numerical simulations with a suitable constitutive model able to satisfactorily represent the nonlinear behavior of masonry in static and dynamic conditions. In order to obtain numerical models representative of real structures and more reliable results, they are validated with key-bahavioral characteristics reported in literature, observed damages after real earthquakes and calibrated with real physical data (mechanical and dynamic) obtained by experimental campaigns. The post-tensioned devices intend to improve the seismic performance of the towers and to reduce the expected damage with the application of a uniform overall distribution of compressive stresses to the masonry to increase *ductility*, *strength to lateral loads and energy dissipation*, achieving with these improvements the seismic risk reduction. The seismic risk assessment of historical masonry towers and the possible achievement of the seismic risk reduction are the main characteristics of the *proposed methodology*. The *second issue*, *the validation of the hypothesis*, corresponds to the demonstration of the effectiveness of the proposal in two real historical masonry towers located in seismic zones of Mexico and Italy.

1.2 Objectives

1.2.1 General objective

The general objective of this thesis consists on the investigation of the effectiveness of different external prestressing devices (such as steel, fiber reinforced plastics, shape memory alloys and combinations) as a retrofitting measure for the seismic risk reduction of historical masonry towers.

1.2.2 Particular objectives

The following partial objectives aim to achieve the above mentioned general objective:

- To describe the main aspects that determine the earthquake hazard of a site and the structural vulnerability of historical masonry towers reported in literature;
- To review the previous contributions in the seismic risk management (assessment and its reduction by prestressing) of cultural heritage;
- To validate the static and dynamic nonlinear response of the applied constitutive model for masonry with experimental results available in literature, key-behavioral characteristics and failure modes common of historical masonry structures;
- To validate the super-elastic and damping response of the applied constitutive model for shape memory alloys with experimental results available in literature;
- To propose a methodology for the seismic risk management of historical masonry towers by means of external prestressing devices;
- To propose a prestressing device and an optimal prestressing level able to effectively reduce the seismic risk of historical towers and to discuss the results;
- To select two historical masonry towers located in seismic zones of Mexico and Italy and to obtain all the relevant information and seismic hazard characteristics;
- To develop experimental campaigns in-situ to characterize the main mechanical and dynamic parameters of the case studies by means of testing equipment;
- To implement the proposed methodology in the case studies in order to validate its suitability.

1.3 Organization of the document

Chapter 1 presents the introduction of the thesis and situates the specific contributions to the scientific knowledge in a more general context. The general objective is described and the particular objectives to achieve it.

Chapter 2 is an intensive literature review objected at describing the earthquake hazard and its characterization, existing approaches for the seismic vulnerability evaluation of buildings in general and the seismic behavior and failure mechanisms of historical masonry structures. Moreover, the most important aspects which determine the seismic vulnerability of historical masonry towers are described.

Chapter 3 corresponds to a second intensive literature review regarding the two main stages of the seismic risk management specifically applied in cultural heritage (masonry structures), the assessment of risk, and its reduction by means of prestressing.

Chapter 4 describes the first stage of the proposed methodology to manage the seismic risk of historical masonry towers. It is developed through the seismic risk

assessment of four virtual historical masonry towers commonly found in Europe. As a first approximation, the 3D FE models are evaluated by linear elastic procedures. The models and the numerical results are validated with theoretical back ground and reported experimental data on similar real towers. The capability of the applied material model to simulate the nonlinear behavior of masonry is validated with reported experimental examples. The seismic hazard is qualitatively determined by the damage grades of the EMS-98 and the limit states of the performance-based design philosophy EC-8, and quantitatively by the seismic coefficient. As a final approximation, intensive numerical simulations developed through a series of nonlinear static and dynamic analyses are carried out for the earthquake evaluation of the towers. The results in terms of seismic response and failure mechanisms are validated with key-behavioral characteristics reported in literature and observed damages after real earthquakes.

Chapter 5 presents the second stage of the proposal corresponding to the seismic risk reduction of historical masonry towers. Firstly, the capability of the applied material model to simulate the superelastic response of SMA is validated with reported experimental results. An extensive parametric study on a selected tower is carried out based on more than 100 nonlinear static simulations aimed at investigating the impact in the seismic performance of different parameters such as tendon material (steel, FRP and combinations with SMA), prestressing level, changes in tendon forces and SMA superelasticity. Afterwards, from the parametric study is proposed a device and three prestressing levels based on the desirable seismic performance enhancement and the earthquake hazard. The suitability of the proposal is validated through the three different failure modes identified in the virtual towers of chapter 4 by assessing the level of seismic risk reduction between original conditions and retrofitted. The risk reduction is assessed by combining the capacity curves with the seismic hazard qualitatively by the EC-8 and EMS-98 and quantitatively by the seismic coefficient.

Chapter 6 includes applications of the proposed methodology for the seismic risk management (assessment and reduction) in two real historical masonry towers located in seismic zones, in order to validate the approach and to prove its effectiveness. The case studies correspond to the north bell tower of the Cathedral of Colima, Mexico and the medieval tower “Torre Grossa” of San Gimignano, Italy. The 3D FE models of the towers are calibrated with experimental data in the dynamic field and validated as in the case of the virtual towers. The seismic risk assessment and reduction are developed through two approaches with different level of refinement. Firstly, by the pushover method, assessing the seismic performance of the towers in original state and retrofitted with the proposed device and prestressing force levels. The seismic hazard is included in qualitative terms at the capacity curves for different damage grades and limit states, and quantitatively by the seismic coefficient. Secondly, by the capacity spectrum method, relating the converted capacity curves and the seismic demand of the site.

Finally, chapter 7 summarizes and presents the most important conclusions derived from this research work. Moreover, some unsolved issues and recommendations for further research are mentioned.

Chapter 2

Earthquake Hazard and Structural Vulnerability

2.1 Introduction

The present chapter is objected at describing an intensive literature review regarding the earthquake hazard and its characterization, existing approaches for the seismic vulnerability evaluation of buildings in general and the seismic behavior and failure mechanisms of historical masonry structures. Moreover, all the most important aspects which determine the seismic vulnerability of historical masonry towers are described. A deep understanding of all these aspects is the basis towards the achievement of their risk reduction, by means of decreasing their seismic vulnerability with prestressing devices, which is the main objective of this thesis. As a complement, chapter 3 presents a second intensive literature review on the relevant theoretical background about the two main stages of the seismic risk management specifically applied to cultural heritage (masonry structures), the assessment of risk and its reduction by means of prestressing.

2.2 Global seismicity

Earthquakes caused more than 1.5 million deaths worldwide during the 20th Century. In the beginning of the 21st Century the number of deaths was about half a million. This is an unacceptable finding, because earthquakes can no longer be regarded as natural disasters, since the main cause of this huge number of casualties is the inadequate seismic resistance of structures, which could be avoided. Earthquakes do no kill people, but the building collapse can do it [Gioncu and Mazzolani, 2011]. By means of modern techniques for spatial supervision such as the Global Positioning System (GPS), advanced computational tools and seismological information, the seismologists have recognized the main faults generating earthquakes around the world and are able to measure the movements of the different tectonic plates (Fig. 2.1) and to investigate the rupture process of earthquakes. The main plate boundaries (seismic zones) of the world are integrated by the *Circum-Pacific Ring* (also named Ring of Fire due to the presence of very active volcanoes), the *Alpine-Himalayan Belt* and the *Mid-Atlantic Ridge* (Fig. 2.1).

USGS [2011] describes that approximately 90% of the world earthquake energy and 80% of the largest earthquakes occur along the Ring of Fire. The next most seismic zone is the Alpine-Himalayan Belt (5 to 6% of the earthquake energy and 17% of the largest earthquakes) which extends from Java to Sumatra through the Himalayas, the Mediterranean and the Atlantic. The Mid-Atlantic Ridge is the third most prominent earthquake belt. It is an underwater mountain range of the Atlantic Ocean which extends from Iceland to Antarctica (see Figs. 2.1 and 2.2).

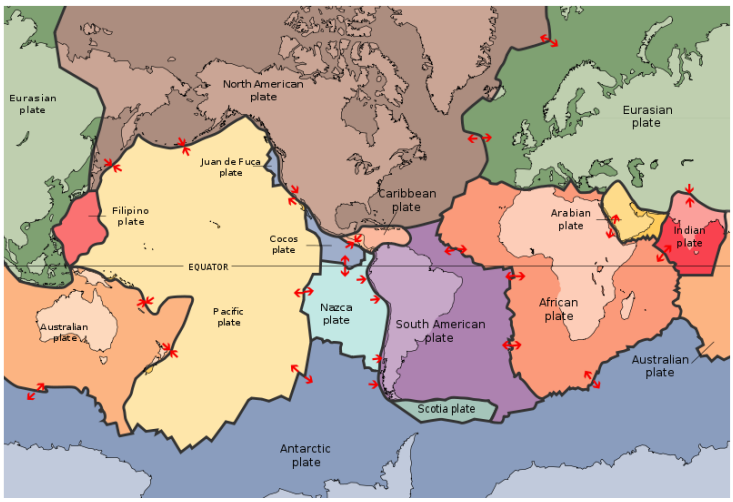

Figure 2.1: Tectonic plates of the world [USGS, 2011]

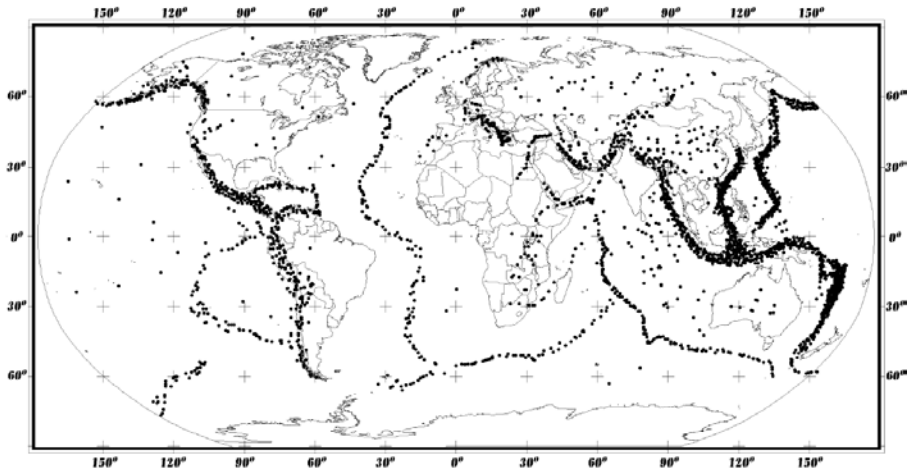

Figure 2.2: Global seismicity map of earthquakes M > 6 occurred since 1966 [Bolt, 1999]

The location of epicenters of earthquakes with magnitude higher than six clearly delineates the three main seismic zones of the world, the Ring of Fire in the left and right part of the map, the Alpine-Himalayan Belt from the right to the central upper part and the Mid-Atlantic Ridge in the central part (Fig. 2.2). The continuous movements of the tectonic plates (interplate) and micro plates (intraplate) generate every year

thousands of earthquakes around the world with different magnitudes as presented in table 2.1. It could be observed that statistically about 800 earthquakes of moderate magnitude take place annually; per month ten strong and about two major earthquakes occur; one great earthquake per year and one very great at 20 years. Anyway, these earthquake observations (table 2.1) and global seismicity map (Fig. 2.2) do not give enough information about earthquakes in terms of source and inherent characteristics, which are fundamental for the seismic hazard characterization of a zone.

Description	Magnitude	Average annually
Very great	> 9.0	1 at 20 years
Great	8.0 – 8.9	1
Major	7.0 – 7.9	18
Strong	6.0 – 6.9	120
Moderate	5.0 – 5.9	800
Slight	4.0 – 4.9	6200
Minor	3.0 – 3.9	49000
Very minor	2.0 – 2.9 1.0 – 1.9	about 1000 per day about 8000 per day

Table 2.1: Frequency of occurrence of earthquakes based on statistics since 1900 [Mazzolani, 2002] and [USGS, 2010]

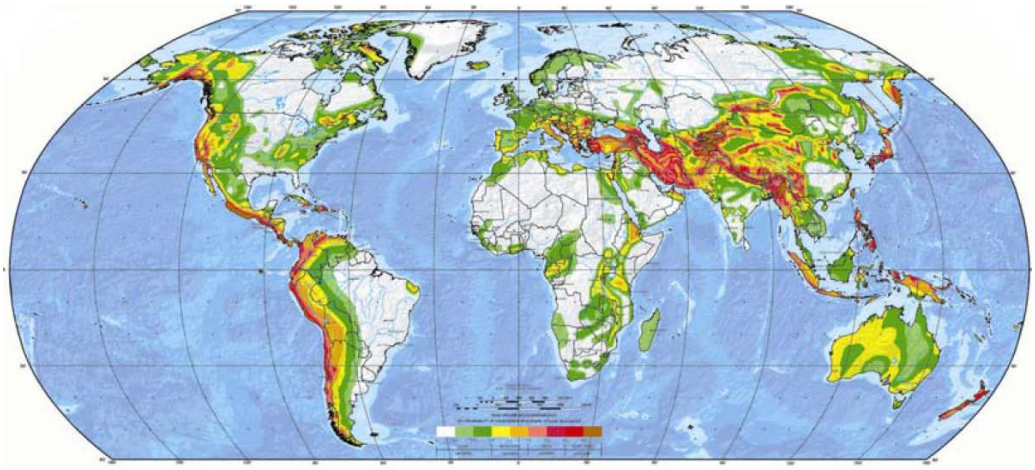

Figure 2.3: Global seismic hazard map [GSHAP, 2010]

By combining the results of different projects based on probabilistic approaches of the world seismic activity, GSHAP [2010] proposes a global seismic hazard map in an attempt to homogenize the Peak Ground Acceleration (PGA) expected at 10% probability of exceedance in 50 years and a return period of 475 years for rock sites, without taking into account models of seismic source zones (Fig. 2.3). The colors white, light green and dark green represent a low seismic hazard zone (0 – 0.08g), yellow and orange a moderate hazard (0.08 – 0.24g), pink and light red a high hazard (0.24 – 0.4g)

and dark red and brown a very high seismic hazard zone with PGA higher than 0.4g. In accordance to Figure 2.3, it is expected for the case studies of this thesis a *very high seismic hazard* for Colima, Mexico and a *moderate hazard* for San Gimignano, Italy. Table 2.2 presents the most destructive historical earthquakes occurred in Mexico and Italy. Some of them are reviewed in detail afterwards (see chapter 6). For more details about earthquakes and effects over structures the reader is referred to the works of Kramer [1996], Chopra [2001], Bazan and Meli [2003] and Gioncu and Mazzolani [2011].

Year	Date	Location	Magnitude	Deaths
1908	28.12	Messina, Italy	7.5	83000
1985	19.09	Mexico City	8.1	20000
1995	09.10	Colima, Mexico	8.0	48
1997	26.09	Umbria, Italy	5.9	11
2003	21.01	Colima, Mexico	7.5	17
2009	06.04	L´Aquila, Italy	6.3	281

Table 2.2: Great historical earthquakes occurred in Mexico and Italy of 20th Century and beginning of 21st Century [SMIS and EERI, 2006] and [Gioncu and Mazzolani, 2011]

2.3 General aspects on seismic risk assessment

Nowadays there is an enormous variety of methodologies to assess the seismic risk of buildings, the first main stage of the seismic risk management, and exists a big confusion within the scientific community regarding which is the best procedure to follow for assessing this risk and the measures to take for its reduction.

The application of risk management towards several disciplines has led to the development of a great diversity of definitions and methods. As a result, a unified methodology to define and to evaluate the risk is indispensable for a rational quantification, comparison and treating [Sperbeck, 2009]. Mena [2002] affirms that the seismic risk of buildings directly depends on the conjunct of the seismic hazard of the site and the self vulnerability of the structure. It means that the seismic risk assessment of a certain building or group of buildings located in a zone with seismic hazard allows indicating the level of structural damage that could result by the action of an earthquake, depending on the vulnerability level of the structure itself. Analyzing the above mentioned, in general, it is worth noting that the seismic risk of buildings may be satisfactorily assessed by taking into account the seismic hazard of the site and the vulnerability of the structure. Next paragraphs present the definition of these terms commonly found in the literature of seismic protection of structures.

Seismic risk corresponds to the conjunct of the potential social, economic and cultural consequences in the built environment and persons due to earthquakes.

Seismic hazard is the probability of occurrence of a potential damaging earthquake, characterized for being an inevitable event out of human control.

Seismic vulnerability represents the amount of damage that could be present in a building as a consequence of the occurrence of an earthquake of certain intensity.

The amount of damage identified in the seismic vulnerability assessment of buildings depends on many factors such as intensity of the seismic action, soil conditions, constructive materials, state of previous damages and structural elements. Another important aspect to consider is whether the structure was designed to resist earthquakes (nowadays buildings) or only to withstand their own self weight, like in the case of most of the historical constructions. Another interesting definition of seismic vulnerability is presented by Sandi [1986], where the author defines it as an intrinsic property of the structure, a characteristic of its own behavior due to the action of an earthquake described trough a law of *cause-effect,* where the cause is the seismic action and the effect is the damage.

2.3.1 Seismic hazard characterization

In general terms the seismic hazard level of a certain zone depends on its proximity to a seismic source with events of enough magnitude to generate significant seismic intensities at the zone under study. The earthquake source is mainly due to the released energy generated by the abrupt movements of the tectonic plates of the earth´s crust, presented in the contact zone between plates (*interplate*), in geological faults inside of a plate (*intraplate*) or in the subducting slab beneath the contact between plates (*intraslab:* shallow 30 – 70 km, intermediate 70 – 300 km and deep > 300 km).

When the strain accumulated in the rock exceeds its capacity limit in the asperity, the *fault ruptures*, rock masses are abruptly displaced and seismic waves begin to radiate from the fault. As the rupture propagates, it successively releases the *strain energy* stored along the activated part of the fault. Therefore, each point of the rupture surface contributes, with a certain time of delay, to the total picture of *seismic waves*, which interfere with each other at a certain distance from the causative fault and give rise to a quite complicated wave train [Kulhanek, 1990]. The seismic waves lose energy as they propagate through the earth along the travel path. The rate at which the earthquake ground motion decreases with the distance is a function of the *source*, *seismic wave types*, *regional geology*, *topography* and *inherent earthquake characteristics*. These major factors affect the severity of the ground shaking at the site. The attenuation varies depending on the source type [Gioncu and Mazzolani, 2011]. Based on observations developed in different recorded accelerograms types, Filiatrault [1996] classifies the effects of the seismic wave types in function of the distance from the epicenter: *Near-source sites*, where all the wave types (body and surface) are present (P, S, L and R); for *intermediate-source sites*, the P-wave disappears due to the very important attenuation, being only present the S, L and R waves; and for *far-source sites*, only the surface waves remain (L and R). Gioncu and Mazzolani [2002] describe that there are four site classifications in function of the distance from the epicenter: *epicentral-site*, including the area around the epicenter (with a radius equal to the *source depth*); *near-source site* (near-field site), for an area within a distance of

about 25-30 km from the epicenter; *intermediate-source site* (intermediate-field site), for an area within a distance of 150 km from the epicenter; *far-source site* (far-field site), an area located more than 150 km. Mena [2002] affirms that the ground shaking intensity and collateral effects mainly depend on the geology and topography of the site, but definitely on the inherent earthquake characteristics (e.g. hypocenter, mechanism, magnitude, intensity, duration and content of frequencies).

Somerville [2000] describes that the first step in the evaluation of the seismic hazard of a zone is to characterize the seismic source to understand the characteristics of earthquakes. Generally are used simplified methods and models based in *statistical laws* to define the *probability of occurrence* in intervals of time for different intensities and expected maximum accelerations. However, these models involve many uncertainties that lead to the adaptation of other studies, resulting with this, in a rough representation of the real seismic hazard characteristics of the site under study. Woo [1992] and Mucciarelli and Magri [1992] describe that these uncertainties are even higher in areas with sporadic seismicity where previous studies are scarce. A good starting point towards the assessment of the seismic hazard of a site with these characteristics could be the study of *historical earthquakes and damages*. Due to the fact that this historical data is qualitative, the evaluation could be complemented with *probabilistic studies* and the opinion of experts.

Statistical seismology is a relatively new field, which applies statistical methodologies to earthquake data in an attempt to raise new questions about earthquake mechanisms and to make some progress towards earthquake characteristic prediction [Vere-Jones et al., 2005 and Vere-Jones, 2006]. But the main question to be agreed is: can the physics of earthquakes be a statistical problem [Turcotte, 1999].

Giovinazzi [2005] indicates that two universally recognized approaches exist for seismic hazard assessment: the *deterministic* and the *probabilistic*. The deterministic considers each seismic source separately and determines the occurrence of an earthquake of specified size at a specified location. The probabilistic combines the contributions of all relevant sources and allows characterizing the rate at which earthquakes and particular levels of ground motions occur.

Gioncu and Mazzolani [2011] describe that a seismic hazard analysis must be carried out on the basis of the earthquake type. For intraplate earthquakes, the major faults and sources are not well known (the epicenter positions are undetermined) and the hazard assessment is more difficult than for the interplate earthquakes (move along a well defined fault). For this type is possible to use statistical methodologies, which in contrast, are useless for intraplate earthquakes due to the absence of sufficient data on the same site. Analyzing all the aforementioned in this section, in general terms, the seismic hazard characterization of a certain zone under study is recommended to be estimated by considering a combination of seismological, geophysical, geological and geotechnical studies with the history of earthquakes, damages and the experts' opinion.

2.3.2 Methodologies of seismic vulnerability assessment

Seismic vulnerability assessment of buildings is an issue of most importance at present time and is a concept widely used in works related to the protection of buildings. Nevertheless, there is not a rigorous and widely accepted definition of it. In general terms, vulnerability measures the amount of damage caused by an earthquake of given intensity over a structure. However, "amount of damage" and "seismic intensity" are concepts without a clear and rigorous numerical definition [Orduña et al., 2008].

The selection of a suitable methodology for the development of the seismic vulnerability evaluation of buildings mainly depends on the nature and objective of the study, as well as the reliability of the expected results. It means that is possible to assess the seismic vulnerability of a large group of buildings in a quite general manner (roughly) following simple methodologies (qualitative), or to only evaluate one building in a detailed way by means of refined methodologies (quantitative). Qualitative methodologies allow obtaining a qualification of the buildings or group of buildings in terms of seismic vulnerability that could range from low to high, whereas the quantitative ones in numerical terms (e.g. ultimate force and displacement capacity). Caicedo et al. [1994] describe that there is an extensive variety of methodologies proposed by different authors for the seismic vulnerability assessment of buildings. The selection of a certain methodology of evaluation depends on the next aspects: nature and objective of the study, available information, characteristics of the building or group of buildings under study, suitable methodology of assessment (qualitative or quantitative) and the organism which will receive the results of the study (e.g. government, scientific organizations, companies and so on). Dolce [1994] classifies the methodologies of seismic vulnerability evaluation in four main groups depending on the available information: empirical, analytical, experimental and hybrid.

2.3.2.1 Empirical methodologies

These approaches are considered as qualitative and are widely used for the seismic vulnerability assessment of the built environment. Safina [2002] affirms that an especial characteristic of the empirical methods is that they are so subjective because are based on the acquired experience by observed damage on different types of buildings due to earthquakes. These methods are used when the available information is limited and to perform a preliminary evaluation of a building or a large group of buildings at territorial scale in a fast way. These qualitative evaluations are commonly developed in-situ by means of a questionnaire of evaluation and visual inspections. The results give a grade of seismic vulnerability to every building ranging from low to high. The most used empirical methods are included by the *vulnerability class* and the *vulnerability index*.

Vulnerability class

These methods classify the buildings in vulnerability classes based on the seismic performance that similar typologies of buildings have shown after relevant earthquakes.

The results are considered quite subjective and therefore the use of the vulnerability class methods is limited to preliminary assessments. One of the most famous methods commonly found in the relevant literature is the developed by the European Macroseismic Scale EMS-98 [Grünthal, 1998]. This proposal classifies the seismic vulnerability of a building in six vulnerability classes ranging from A to F (A: high vulnerability and F: low vulnerability). It evaluates the materials of the structure (masonry, concrete, steel, or wood) and the level of seismic design (table 2.3).

Type of Structure		Vulnerability Class					
		A	**B**	**C**	**D**	**E**	**F**
MASONRY	Rubble stone, fieldstone.	X					
	Adobe (earth brick)	X	1				
	Simple stone	0	X				
	Massive stone		1	X	0		
	Manufactured units	0	X	0			
	With slabs of reinforced concrete		1	X	0		
	Reinforced or confined			0	X	1	

X: most probable class; 1: probable range; 0: range of less probability, exceptional cases

Table 2.3: Summary of the EMS-98 only considering masonry

If two groups of buildings are subjected to exactly the same earthquake shaking, and one group performs better than the other, then it can be said that the buildings that were less damaged had lower seismic vulnerability (more earthquake resistance) than the ones that were more damaged [Grünthal, 1998]. Table 2.3 presents a resume of the classification of masonry structures in vulnerability classes of the EMS-98. During the visual inspections of the actual state of the structure the user can select the most probable class of vulnerability, or the probable ranges mainly considering the engineering experience [Preciado and Orduña, 2008]. Safina [2002] used the empirical methodology of the EMS-98 for the seismic vulnerability assessment of 64 hospitals located in Barcelona, Spain. With the results, the author elaborated a preliminary diagnostic, classifying the buildings in groups of less and more vulnerability. As a first stage the author collected all the specific information available of every one of the 64 hospitals, and in a subsequent stage applied the EMS-98 method to assign to each building a vulnerability class (low, medium or high).

Preciado [2007] and Preciado et al. [2007] satisfactorily assessed the seismic vulnerability of 15 historical buildings (mainly churches) of the XIX century located in Colima, Mexico. This study was developed as a result of the serious observed damage in most of the cultural patrimony after the M7.6 earthquake [SMIS and EERI, 2006] occurred on January, 21st, 2003. The EMS-98 was applied in the 15 buildings in order to obtain their vulnerability class. Additional information was considered for the

evaluations, such as plans, characteristics of constructive materials, historical analysis, structural configuration and observed damage state. The results showed that eight of the buildings obtained a high vulnerability class, five an intermediate and the rest a low class. The most vulnerable historical constructions corresponded to the churches as it was expected. Specifically, the parameters that contributed with their high vulnerability were the deficient conservation level, damage state, heavy and slender bell towers, vaulted roofs and heavy cupolas.

Vulnerability index

These methods are commonly used to identify and to characterize the potential seismic deficiencies of a building or group of buildings by means of a qualification by points to every significant component of the structure. This allows to the user the determination of a seismic vulnerability index. One of the most famous methods usually found in the relevant literature corresponds to the developed by Benedetti and Petrini [1984] and the GNDT [1990]. This method has been widely used in Italy during the last years and has been upgraded as a result of the continuous experimentation and observed damage of certain types of structures (mainly unreinforced masonry buildings) after earthquakes of different intensities, resulting in an extensive database of damage and vulnerability. The method is integrated by 11 parameters (see table 2.4) that were compiled in a questionnaire for the assessment of the buildings by means of visual inspections. As a result of its continuous use by many researchers around the world, the original questionnaire developed by the GNDT has suffered several changes, mainly based in past experiences or adaptations to structures of certain characteristics located in another place different to Italy. An example is the questionnaire of Aguiar et al. [1994] to assess the seismic vulnerability of unreinforced masonry buildings in Spain.

i	**Parameter**	***Ki A***	***Ki B***	***Ki C***	***Ki D***	***Wi***
1	Organization of the resistant system	0	5	20	45	1.0
2	Quality of the resistant system	0	5	25	45	0.25
3	Conventional resistance	0	5	25	45	1.5
4	Position and foundation	0	5	25	45	0.75
5	Horizontal diaphragms	0	5	15	45	1.0
6	Floor configuration	0	5	25	45	0.5
7	Configuration of elevation	0	5	25	45	1.0
8	Maximum separation between walls	0	5	25	45	0.25
9	Typology of the roof	0	15	25	45	1.0
10	Non structural elements	0	0	25	45	0.25
11	Conservation level of the building	0	5	25	45	1.0

Table 2.4: Numerical scale of the vulnerability index (I_v) for unreinforced masonry buildings [Benedetti and Petrini, 1984]

The use of table 2.4 is not a complicated task, during the visual inspections is selected for every one of the 11 parameters a vulnerability class A, B, C, or D, (A: low vulnerability, D: high vulnerability). Depending on the parameter and the selected class, the method assigns a numerical value (*Ki)* ranging from 0 to 45 that is affected for a coefficient of importance (*Wi)* between 0.25 and 1.5. This coefficient was assigned by the GNDT taking into account the opinion of experts and passed experiences. It reflects the importance of each parameter in the evaluation of the seismic vulnerability of the structure. As a final stage the seismic vulnerability index (I_v) of the building could be obtained with the use of Eq. 2.1.

$$Iv = \sum_{i=1}^{11} Ki\, Wi \qquad [2.1]$$

Analyzing Eq. 2.1 and table 2.4, it could be observed that the vulnerability index defines a scale of values ranging from 0 to the maximum reachable 382.5 (100%), allowing to obtain a range in the order of $0 < I_v < 100$. This range of vulnerability index could be used afterwards as a conclusion to determine a seismic vulnerability class (e.g. low $I_v < 15$, medium $15 \leq I_v < 35$ or high $I_v \geq 35$) comparable to the empirical method of the EMS-98. Palencia et al. [2005] evaluated the seismic vulnerability of an educational building located in a high seismic zone by means of the GNDT method and the questionnaire developed by Aguiar et al. [1994]. The authors found that the building presented an important vulnerability index (highly vulnerable) and concluded that as a consequence of a considerable earthquake the building could present important damages or collapse. Preciado [2007] and Preciado et al. [2007] analyzed the seismic vulnerability of the 15 historical buildings located in Colima, Mexico as a second stage by the GNDT method. In this study the base questionnaire developed by Aguiar et al. [1994] was modified in order to assess historical masonry constructions located in high seismic zones of Mexico. The modified questionnaire was applied in 15 buildings by visual inspections in order to identify and characterize the potential structural deficiencies corresponding to the eleven parameters shown in table 2.4. The vulnerability index was obtained and interpreted in terms of vulnerability class as aforementioned. The results showed that 14 buildings (most of them churches) obtained a high vulnerability class and only one a medium vulnerability. The identified most vulnerable buildings by the empirical approaches (vulnerability class and vulnerability index) were selected to analyze them with more refined and reliable methodologies such as the analytical ones.

2.3.2.2 Analytical methodologies

This group of approaches for the seismic vulnerability assessment of buildings are mainly computerized numerical methods based on the classical theories of elasticity and plasticity, and in more recent years in the theories of cracking and damage. The approaches that have gained more acceptance within the structural engineering

community are integrated by the finite element method (FEM) and the limit analysis (see section 3.2.3). These quantitative methods have the common characteristic that both are more refined and require many parameters for modeling the real physical characteristics of the actual structure, representing with this more time consuming. Compared with the rough empirical methodologies that permit to evaluate a building or a large group of buildings at territorial scale in a fast way (preliminary evaluations); the quantitative methods are most commonly used to evaluate the seismic vulnerability of *essential buildings* that require especial attention. It could be the case of the *seismic protection of historical buildings*, hospitals, museums, schools and so on.

The analytical methodologies consist of developing as a first step a geometrical representation of the structure under study mainly by the generation of a 3D model with computational tools. The process of the model´s generation depends on the selected method of analysis, FEM or limit analysis. Afterwards, the mechanical properties of the materials that constitute the structure are assigned to the initial model, as well as boundary conditions. Together with a suitable constitutive material model able to satisfactory represent the behavior of the structure (see section 3.2.2), the model is statically or dynamically assessed. These evaluations are linear or nonlinear depending on the aim of the study and the action under analysis (e.g. self weight, seismic loading, wind, and so on) in order to define the levels of damage in the structure (vulnerability).

2.3.2.3 Experimental methodologies

These methods consist in the implementation of tests with the purpose of determining the mechanical and dynamic characteristics of a certain existing structure. Generally, the mechanical properties of a structure are assessed in laboratory and in-situ, whereas the dynamic investigations are mainly developed in-situ. The mechanical tests aim to determine the characteristics of the constructive materials of the building (strengths, density, Young´s modulus, Poisson´s ratio, and so on). By the other hand, the main objective of the dynamic investigations is to obtain the natural frequencies and vibration modes of the structure by means of especial equipment (e.g. accelerometers). For the selection of the equipment is recommended to consider factors such as economy, simplicity and effectiveness. With this especial equipment is possible to evaluate the contributions of the horizontal constraints generated by neighbor buildings (boundary conditions) in the dynamic behavior of the building under study.

The dynamic characterization of buildings allows to the user to obtain relevant information of the actual damage state of a structure under study before or after the occurrence of an earthquake (damage scenario) [Safina, 2002]. In the work of Abruzzese and Vari [2004] the authors affirm that the experimental methodologies represent a fundamental stage towards the seismic vulnerability assessment of constructions. For detailed information about the experimental methodologies the reader is referred to section 3.2.1 of this thesis.

2.3.2.4 Hybrid methodologies

This last classification corresponds to a combination of methods for the seismic vulnerability evaluation of buildings (empirical, analytical and experimental). In the generation of an initial analytical model of a structure there are many assumptions and uncertainties regarding the determination of geometry, material properties, support and boundary conditions. All these issues and moreover considering the skills in numerical modeling and engineering experience of the user generate distrust about the reliability of the results. Due to this, the initial analytical model has to be compared with the real physical characteristics (mechanical and dynamic) of the structure obtained with the experimental methods. It could be done for example by comparing the frequencies and vibration modes of the initial analytical model with those obtained in the dynamic experimental campaigns. If the difference is satisfactory, the analytical model and the solution are assumed to be in agreement, otherwise the assumptions and uncertainties in the determination of the model have to be calibrated or updated, obtaining with this an analytical model more reliable and representative of the structure under study (analytical-experimental). Another possible use of the hybrid methods corresponds to the combination of the empirical, analytical and experimental approaches. It means that after assessing the seismic vulnerability of a group of buildings by the empirical methods, an organized list by level of vulnerability (low, medium and high) could be generated, selecting from it the most vulnerable and important to analyze them by more refined methods such as the analytical-experimental. In this way more reliable results towards the seismic vulnerability of the buildings are obtained.

2.4 Seismic behavior and failure mechanisms of historical masonry structures

This complementary section aims to present all the relevant information needed for the seismic vulnerability assessment of historical masonry towers. As a first stage, the most important characteristics of ancient masonry structures are described by considering aspects such as history and uses, most common typologies, physical and main mechanical properties as well as behavior-failure. Subsequently, an identification of the seismic behavior and failure mechanisms of unreinforced masonry walls under in-plane and out-of-plane horizontal loading is presented. Moreover, all the most important aspects that determine the seismic vulnerability of historical masonry towers are described.

2.4.1 Historical masonry

Masonry is known as the combination of stones or bricks with a mixture named mortar that aims to bind the construction units together and to fill the gaps between them. Unreinforced masonry is one of the main materials commonly found worldwide in ancient buildings, due to the fact that the use of this especial material as structure goes back to the first civilizations that populated the earth.

(a) (b) (c)

Figure 2.4: Masonry of dry joints used in historical structures; (a) segment of one of the pyramids of Cairo, Egypt; (b) Inca wall in Peru and (c) Aztec ruins in Mexico

In Mesopotamia the ancient cultures used to implement masonry of adobe as main constructive material in their structures. Adobe is integrated by sun-dried clay bricks placed together with mortar of the same material. By the other hand, in Egypt, carved stone with no mortar between units (named as well masonry of dry joints) was used for the edification of their pyramids. This typology of masonry was widely used in America by the Aztec culture in Mexico and the Inca in Peru (Fig. 2.4). Whereas the Maya culture used for the edification of their pyramids and temples carved stone in combination with mortar made of burnt fragments of lime stone (Fig. 2.6).

(a) (b)

Figure 2.5: Roman ancient masonry structures made of stone and fired clay bricks; (a) the Coliseum (Flavian Amphitheatre) and (b) the forum of Nerva

The Romans in Italy used stones and fired clay bricks combined with enhanced mortars and innovative techniques for the construction of walls, arcs, vaults and domes in large structures mainly reinforced by buttresses (see Fig. 2.5). Mortars in ancient structures were mainly integrated of clay or lime in combination with water. In some cases other materials or compounds used to be added to the mortar for increasing its capacity of adherence, resistance, durability and for being more malleable during the construction. This is the case of the mortars used by the Romans named pozzolana, which is a normal mortar of lime enhanced with the addition of volcanic ashes. It allowed them to develop the first concrete which had important uses for the construction of their aqueducts, bridges and other important structures.

By the other hand in America, especially in the constructions of adobe in Mexico, fibers of vegetation, blood of animals and extract of nopal plants were used to enhance the units and mortar of clay. This aimed to reduce the contraction of the material generated by drying, and to enhance its resistance to the climate effects. It was until the end of the XIX century when the Portland cement was introduced, permitting to produce mortars of superior resistances than the lime ones, with faster hardening and higher elasticity modulus that increases the stiffness of the masonry. The presence of this mortar in historical constructions is commonly due to recent rehabilitation measures. SMIE and FICA [1999] affirm that the main important properties of mortars in general are their resistances, adherence with the unit, workability, durability, and impermeability.

(a) (b)

Figure 2.6: Masonry used by the ancient culture of the Mayas; (a) the pyramid of Chichen-Itza in Yucatan, Mexico and (b) ruins of a Maya temple

However, from the ancient time until now, masonry has been widely appreciated around the world by different important factors such as availability, durability, bioclimatic characteristics, and the main factor, which corresponds to its low cost in comparison with other materials such as steel and reinforced concrete.

2.4.2 Typologies of masonry used in historical structures

As it was above mentioned, in the construction of historical structures multiple typologies of masonry were used depending on many factors such as availability of materials, structural element to be built, constructive techniques and appearance. When referred to typologies of masonry in the construction of ancient buildings, it means that moreover of considering the different available materials (stones, sun-dried or fired clay bricks and mortars) and the structural element to be built (walls, cupolas, domes, arcs, vaults, buttresses and so on), the constructors had to take into account the arrangement of masonry (see Fig. 2.7). This order or assemblage is the way that units and mortar were placed together to conform the structural element, involving on it different constructive techniques. Meli [1998] describes that there is a huge variety of constructive modalities commonly found in the masonry of historical buildings and classifies them in two main groups. These correspond to the *organized or regular* masonry of bricks or carved stone with head and bed joints of mortar (Fig. 2.7a), and the *disorganized or irregular*, where the stones are placed without a complete carving (or natural) and irregularly distributed in a matrix of mortar (Fig. 2.7b). Another combination that could be found in historical constructions is the three-layers masonry (sack or three-leaf masonry), where the external layers have a regular arrangement (brick or stone) that works as a falsework for the infill commonly composed of rubble of other constructions mixed with mortar (Figs. 2.7c and d).

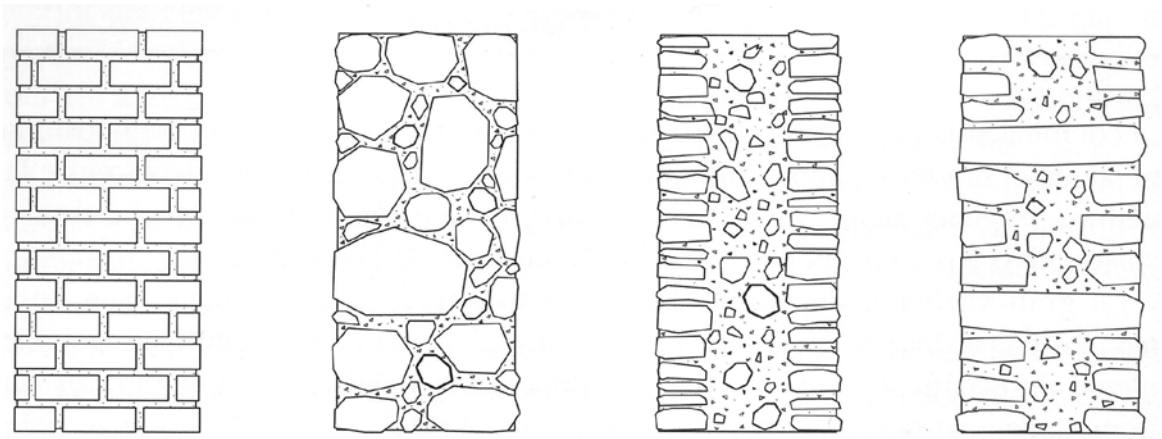

(a) (b) (c) (d)

Figure 2.7: Four arrangements of ancient masonry; (a) organized; (b) disorganized; (c) three-layers and (d) three-layers with anchorage stones [Meli, 1998]

Croci [1998] mentions in his work that six types of masonry have been the most commonly used in the construction of historical buildings. These mainly correspond to bricks of fired clay or carved stones with regular mortar joints; natural stones of different types and shapes; sack masonry (three-layer or three-leaf masonry); combined masonry, made of stone and bricks; masonry of dry joints (no mortar between units),

composed by rectangular pieces of carved stone; and bricks of sun-dried clay (adobe) with mortar of the same material.

2.4.3 Mechanical properties and behavior-failure of historical masonry

As aforementioned, there is a huge variety of masonry typologies commonly found in historical constructions. The behavior and failure modes of historical masonry as a composite are different than those of the units and mortar when considered by separate (see Fig. 2.8). It mainly depends on the physical characteristics of the composite (e.g. the arrangement shown in Fig. 2.7), mechanical properties of the material components, as well as the state of stresses (see table 2.5). The behavior and failure mechanisms of historical masonry structures could be influenced as well for important factors such as state of damage (cracking and deterioration) and the mechanical properties of the materials used in recent rehabilitations. It refers to the compatibility of materials, when is used in the rehabilitation works a material with different mechanical properties such as a higher elasticity modulus, it could lead to local stiffening on the structure and with this to concentration of stresses. The knowledge on the different mechanical properties and behavior of historical masonry as a composite can lead to a better understanding of the different failure modes of this anisotropic and complex material. Next paragraphs describe the main mechanical properties of historical masonry as well as behavior-failure modes when subjected to different state of stresses.

2.4.3.1 Compression

Compared to its poor tensile strength, masonry commonly presents an optimal performance when subjected to compressive loading. Its response and failure mechanisms rely on the interaction between units and mortar joints. The compressive behavior of masonry varies from one typology to another. It mainly depends on the material of the units and mortar, and in a global way by the arrangement (assemblage) of the masonry used in the structural element (see table 2.5).

Masonry	Density (kg/m^3)	E modulus (kg/cm^2)	Compressive strength (kg/cm^2)	Shear strength (kg/cm^2)
Adobe and clay mortar	1800	3000	2 - 5	0.5
Brick and clay mortar	1600	5000	5 - 10	1.0
Brick and lime mortar	1600	10000	15 - 20	2.0
Natural stone and lime mortar	2000	5000	10 - 15	0.5
Carved stone and lime mortar	2000	20000	30	2.0

Table 2.5: Average mechanical properties of five types of historical masonry [Meli, 1998]

The mechanical properties shown in table 2.5 could be obtained by in-situ and laboratory tests as previously mentioned in the experimental methodologies for

assessing the seismic vulnerability of buildings. This mechanical characterization of historical masonry structures is explained in detail in section 3.2.1.2 of this thesis.

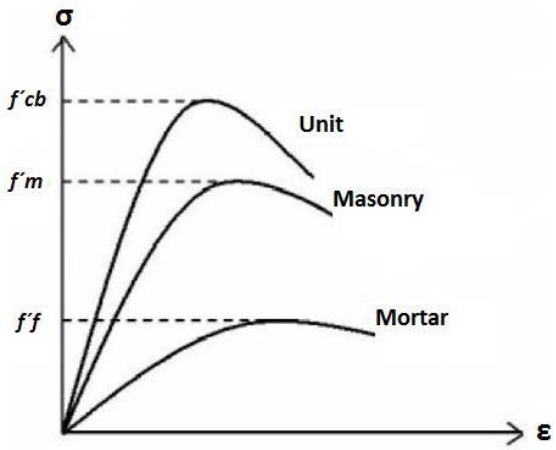

Figure 2.8: Stress-strain curve of masonry and its components under compression [Paulay and Priestley, 1992]

When masonry is under uniaxial compressive loading an interaction is presented between the component materials. This behavior is due to the fact that the units (Fig. 2.8) are the part which allow less deformation (units are stiffer than mortar) and constraint the strains of the mortar, generating with this a state of stresses represented by tension in the unit and by the other hand, compression in the mortar (see Fig. 2.9).

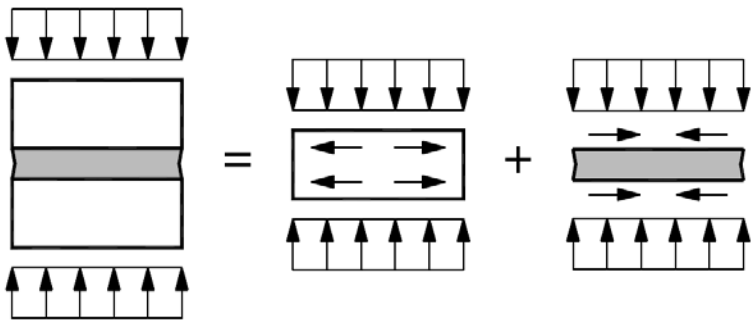

Figure 2.9: Uniaxial compressive behavior of masonry: schematic plane representation of stresses in the masonry components [Lourenço and Pina-Henriques, 2006]

If the compressive stresses are elevated they could generate the material yielding (exceeding of its resistance) and to lead as a consequence to an increasing of the probability of collapse of the structural element (see Fig. 2.10). In the work developed by Garcia [2007], the author comments that when historical masonry is subjected to high compressive loads the resistance of the conjunct directly depends on the typology of the

arrangement (regular or irregular) and the quality (mechanical properties) of units and mortar used in the construction.

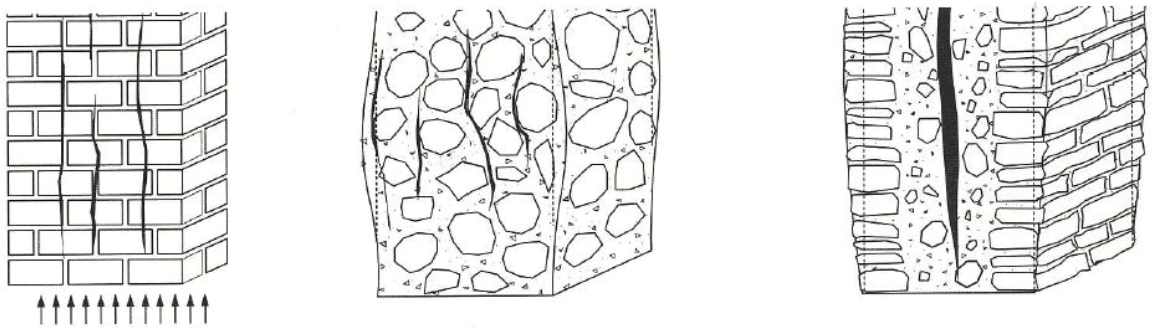

(a) (b) (c)

Figure 2.10: Failure modes due to high vertical loading; (a) transversal tension; (b) crushing and (c) separation due to weak plane [Meli, 1998]

Meli [1998] affirms that there are three typical failure mechanisms of historical masonry structures when subjected to high vertical loading. They mainly depend on the used masonry arrangement in the construction of the structural element (Fig. 2.7). In the organized masonry the failure mode is represented by a vertical propagation of cracks in units and mortar (see Fig. 2.10a) generated by transversal tension as above explained (Fig. 2.9). The second failure mechanism corresponds to a crushing of the mortar matrix and detachment of the stones in the disorganized masonry as shown in Figure 2.10b. The third failure mode is presented in the three layer masonry by a separation in vertical elements due to a cracking propagation in the weak plane integrated by the infill (Fig. 2.10c). These three failure mechanisms could definitely generate the collapse of the building. The failure mechanism presented in the sack masonry as shown in Figure 2.10c, with a separation of two vertical layers due to the weak material in the infill, generates a brittle behavior of the masonry element that could fail by buckling, generating with this the progressive or unexpected collapse of the building (e.g. the sudden collapse of the historical civic tower of Pavia, Italy in 1989).

Croci [1998] describes that the presence of a severe cracking parallel to the direction of loading (transversal tension) is the most commonly observed failure in masonry under high compression like in the case of the historical constructions. This local failure mechanism could represent catastrophic consequences to the structural conjunct if the rest of the elements are not capable to compensate the damage (unstable conditions), resulting in the global failure of the structure.

2.4.3.2 Tension

As aforementioned, masonry presents a quite good behavior under compressive loading compared with its poor tensile strength, which is quite low or almost zero. This issue is

due to the fact that the global strength of a masonry structural element is determined by the adherence or bond generated between mortar and units, and their own resistances.

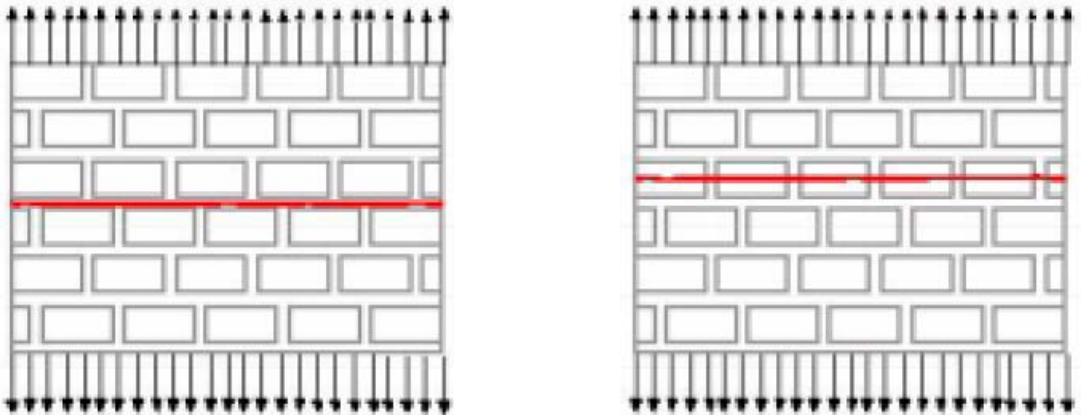

(a) (b)

Figure 2.11: Failure mechanisms of masonry under tensile loading; (a) failure of the bond between units and mortar and (b) failure of the units [Bonett, 2003]

Masonry structural elements subjected to uniaxial tensile loading perpendicular to the bed joints commonly present two main failure mechanisms as shown in Figure 2.11. The first failure mode corresponds to a horizontal cracking observed between units and mortar bed joints generated by a loss of bond (or adhesion). The second failure mechanism presents as well a horizontal cracking trough the units due to an exceeding of the tensile strength. Huster [2000] describes that a third possibility of failure may be taken into account when masonry is under uniaxial tensile loading. It refers to a cracking of the mortar joints due to an exceeding of the tensile strength, or named as well cohesion failure. When a masonry structure is under tensile loading the above mentioned three failures mechanisms could be present by separate, or in the worst case a combination of them. Even when masonry has a poor or almost zero tensile strength, the relevant literature recommends taking into account in the numerical simulations roughly values ranging from five to ten percent of its compressive strength.

2.4.3.3 Shear

The shear behavior of unreinforced masonry structures subjected to lateral forces generated by wind or earthquake ground shaking plays the most important role in the stability of the structure. Shear is usually presented in combination with compressive stresses caused by the effect of gravitational forces (self weight and upper levels). The adhesion, friction and tensile strength (cohesion) of the mortar joints in combination with the brittle tensile resistance of the units play an important role in the complex behavior and failure mechanisms of the structure under shear.

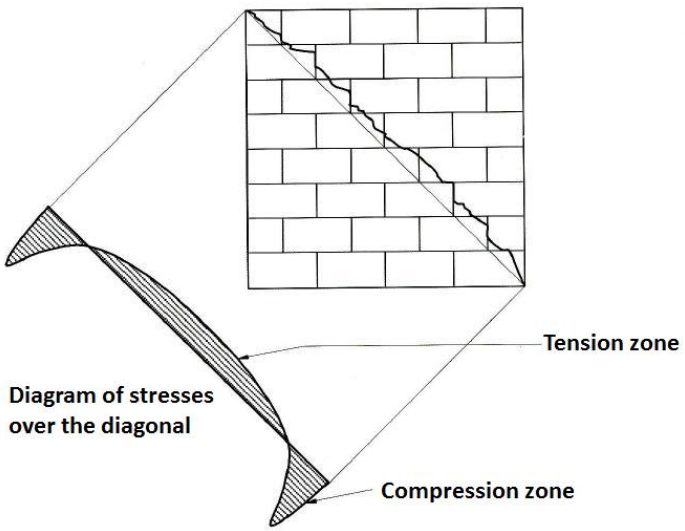

Figure 2.12: Failure in masonry under diagonal tension (shear) [Meli, 1998]

When a masonry structure is subjected to lateral loading (shear) in its plane, a state of tensile stresses is induced in the normal direction along the diagonal like the shown in Figure 2.12. Due to the low tensile strength of masonry, the failure mechanism is presented by a cracking distributed diagonally at 45^{o} that tends to separate the structural element in two parts. The position of the diagonal depends on the direction of the seismic loading or inertia forces, acting in this case at the left of the wall. Due to the alternation of the seismic loading in masonry walls subjected to earthquake motion, the cracking by two diagonals forming an X is commonly observed. Table 2.5 shows the average shear strength of five typologies of masonry usually found in historical structures. It could be appreciated that brick and carved stone masonry, both with lime mortar, present the same and highest shear strength of the five typologies.

2.4.4 In-plane behavior-failure of unreinforced masonry walls

The most important failure mode observed in unreinforced masonry walls subjected to alternated horizontal in-plane inertia loading corresponds to a diagonal double cracking as shown in Figure 2.13. When the size of these cracks is excessive, it generates a state of rapid stiffness degradation that could lead to a brittle collapse of the structure. Shear failure is presented in unreinforced masonry buildings when there is not enough density of walls in one of the plan directions X or Y, or by the presence of excessive openings (failure points) that substantially reduce the resistant area and generate the concentration of stresses. Therefore is commonly observed after a considerable earthquake the presence of large diagonal cracking at the corners of openings or at the complete wall as depicted in Figure 2.13. Sperbeck [2009] affirms that there are many influencing parameters on the failure mechanisms of in-plane loaded masonry walls. The most important ones correspond to the vertical load level, slenderness, support conditions in terms of top rotation (constrained or free) and material parameters.

Figure 2.13: Typical shear failure mode observed in unreinforced masonry walls after the 7.5 magnitude earthquake of Colima, Mexico in January 2003 [SMIS and EERI, 2006]

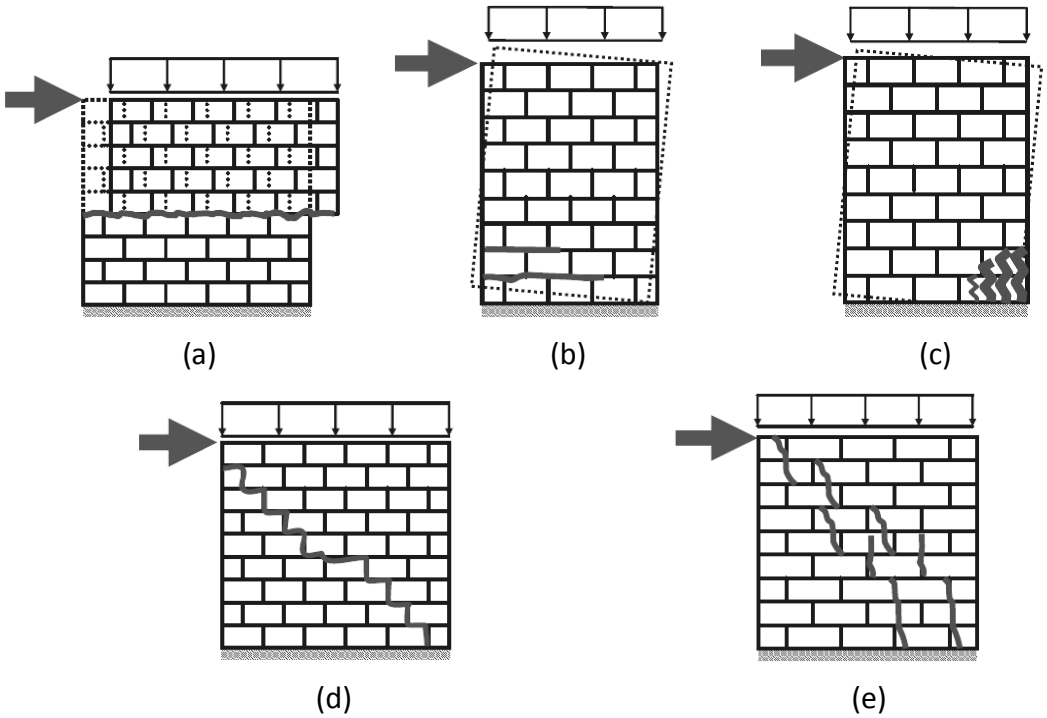

Figure 2.14: Static-monotonic tests on masonry walls; (a) bed joint sliding; (b) rocking; (c) toe crushing; (d) stepped cracking and (e) diagonal cracking [Mistler, 2006]

Several authors as Lourenço [1996] and Rots [1997], or more recently as Ötes and Löring [2006] and Mistler [2006] have observed by experimental tests on masonry walls subjected to in-plane static horizontal loading monotonically increased that the main failure mechanisms strongly depend on the vertical loading level and the quality of the mortar and units in terms of mechanical and physical properties. For low

vertical loading levels it could be mainly observed a failure by bed joint sliding as illustrated in Figure 2.14a. This is due to disequilibrium between the applied horizontal loading and the friction force which is calculated as the product of the normal force by the corresponding friction coefficient of the joints. This could lead to a horizontal cracking of the bed joints forming a sliding block. Poor quality mortars with low friction coefficient increase the probability of failure by sliding. For medium to high vertical loading is expected a failure mode mainly by diagonal tension that could be subdivided in stepped and diagonal cracking as shown in Figures 2.14d and e. The stepped cracking involves the failure by bonding (adhesion) or cohesion (failure by tensile strength) of the bed and head joints due to the presence of weak mortar (low friction coefficient), whereas the diagonal cracking could go through both, unit and joint by an exceeding of their tensile strength. Ötes and Löring [2006] and Mistler [2006] observed in compact and slender masonry walls subjected to static horizontal loading that other failure mechanisms could occur. This is due to a rocking of the structure by an uplifting of the wall base due to horizontal cracking and top rotation by low vertical loading, poor mortar or slenderness (Fig. 2.14b). As a consequence of this rocking, the failure of the wall is generated by toe crushing of the compressed area as shown in Figure 2.14c.

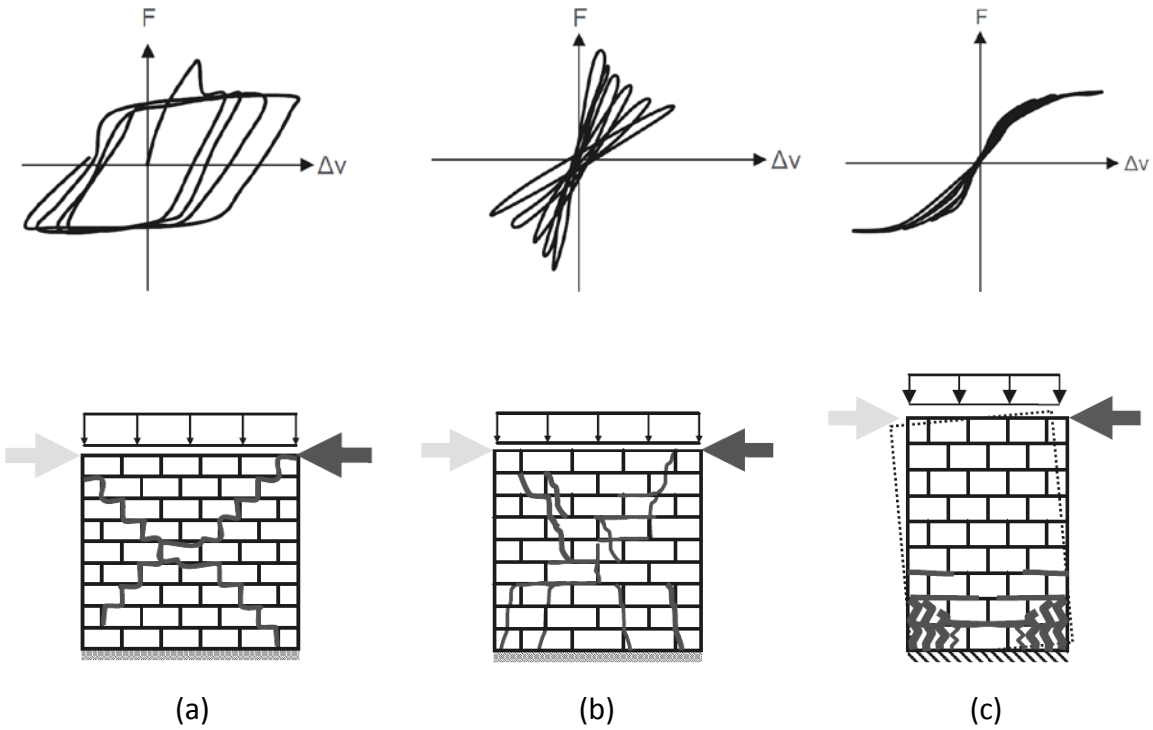

Figure 2.15: Static-cyclic tests on masonry walls; (a) stepped cracking; (b) diagonal cracking and (c) horizontal cracking and crushing [Mistler, 2006]

The assessment of the in-plane static-cyclic loading performance of different unreinforced masonry walls by experimental tests has been carried out by several authors such as Mistler [2006] and ElGawady et al. [2007]; and dynamically with shake-

table by Toranzo-Dianderas et al. [2004], and subjected to a series of seismic motions on an earthquake simulator by Badoux et al. [2002]. In all the cases the main objective was to investigate the walls shown in Figure 2.14 in terms of failure mechanisms, force-displacement and energy dissipation by means of the analysis of the qualitative and quantitative characteristics of the hysteretic behavior observed in the experimental tests (see Fig. 2.15). The force-displacement hysteretic response allows the evaluation of ductility and strength degradation as well as energy dissipation, which is represented by the area enclosed by the hysteresis loop. High ductility and high energy dissipation are desirable properties for structures subjected to considerable seismic actions.

The failure mode by steeped cracking of the wall depicted in Figure 2.15a presents a very ductile response but a relative low load capacity. This is due to the softening with very limited damage due to the cracking of head and bed joints. The alternation of loads in the test generates a mechanism of closing and opening of cracks that leads to high energy dissipation as it could be observed in the enclosed area by the large hysteresis loops. By the other hand, the failure by diagonal cracking presents an opposite behavior compared to the stepped cracking. It shows high horizontal load capacity and a low ductility that lead to less energy dissipation as depicted in the close hysteresis loops with small enclosed area of Figure 2.15b. This is due to the stiffness degradation of the wall presenting brittle behavior when the tensile strength of mortar and units is exceeded. The failure by rocking is observed by horizontal cracking due to bending, leading to a base (or foundation) disconnection. The rocking wall may sustain large lateral displacements with the absence of damage as a result of the rigid body rotation. The horizontal loading capacity is relative low. This behavior considerably increases the normal force, resulting in an explosive failure due to the crushing of the compressed zone. It presents a limited amount of energy dissipation as shown in the narrow hysteresis loops forming an “S” (Fig. 2.15c). Its main mechanism of energy dissipation is generated by means of radiation of energy to the ground by impact.

2.4.5 Out-of-plane behavior-failure of unreinforced masonry walls

The in-plane behavior and failure modes of unreinforced masonry walls under earthquake loading mainly depend of the slenderness, vertical loading level and the quality of the masonry components (mortar and units) in terms of mechanical and physical properties. When the seismic loading is presented perpendicular to the plane of the wall (out-of-plane), the structure shows different behavior and failure modes than those loaded in plane, mainly due to instability conditions and connectivity. Historical masonry buildings located in seismic regions were constructed considering empirical rules to mainly withstand their self weight satisfactorily; being with this, extremely vulnerable to horizontal inertia forces generated by the seismic action. Another important issue that plays an important role in the seismic vulnerability of historical buildings is the lack of good connection between elements at the corners or with the roof system due to the low tensile strength of masonry.

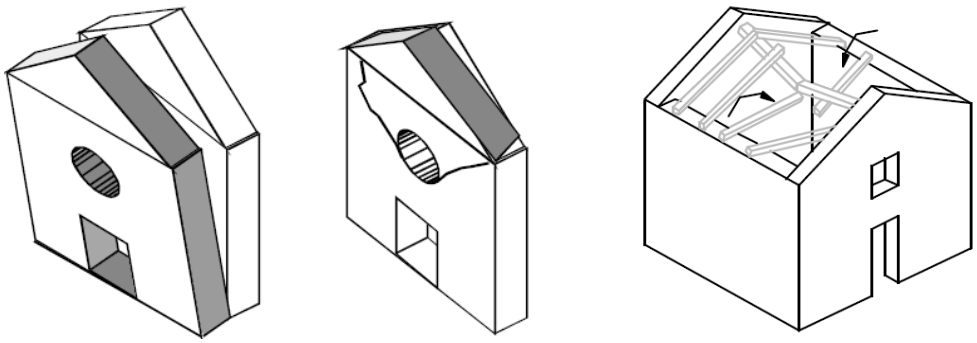

(a) (b) (c)

Figure 2.16: Typical out-of-plane failure modes of historical buildings; (a) façade overturning; (b) partial façade overturning and (c) collapse of the roof [D'Ayala, 2000]

As a result of the ground shaking, the walls could vibrate out-of their plane or to be pushed by other perpendicular walls, being separated of the rest of the structure and generating a state of instability (overturning moment > resistant moment) that could lead to their partial or total collapse (Figs. 2.16a and b). The elevated mass of cupolas and vaulted roofs of historical masonry buildings generate during an earthquake important inertia forces that could be transmitted out-of-plane to the support walls and façade because the cover does not behave as a rigid diaphragm as nowadays structures. This transmission of forces out-of plane could lead to the collapse of walls or façade by overturning or the failure of the roof system by instability (Fig. 2.16c).

2.4.6 Seismic vulnerability aspects of historical masonry towers

As stated in the introductory chapter, the seismic risk of a certain historical structure located in a seismic zone is determined by the conjunct of the seismic hazard and its structural vulnerability. Since the seismic hazard of the research zone is unavoidable, *the seismic risk reduction of towers* could be achieved by decreasing their structural vulnerability with the implementation of *prestressing devices*. Deep understanding of all the most important aspects determining the vulnerability of historical masonry towers in terms of behavior and failure modes is fundamental for the achievement of their seismic risk reduction, which is the main objective of this thesis.

2.4.6.1 Slenderness

Probably the single most decisive factor affecting the seismic behavior of a wall is its slenderness, commonly expressed in terms of aspect ratio (H/L). High slenderness walls ($H/L \geq 2$) are characterized by a ductile behavior, failing in a predominant flexural mode similar to that of cantilever beams. In low slenderness or compact walls ($H/L \leq 1$) the determining factor of the seismic performance is shear [Penelis and Kappos, 1997]. NTCDF [2004] and Bazan and Meli [2003] affirm that the seismic behavior of walls differs importantly depending of their slenderness. Compact walls ($H/L \leq 2$) are mainly

dominated by shear effects. By the other hand, slender walls (H/L ≥ 2) mainly behave as cantilever beams with generally low vertical loading, dominating the effect of flexion. If H/L > 4, the structure could be considered as excessively slender, being this the case of most of the historical masonry towers as depicted in Figure 2.19. This could cause the failure by flexion, shear, overturning by instability and transmission of elevated vertical loads to the foundation and soil (Fig. 2.17).

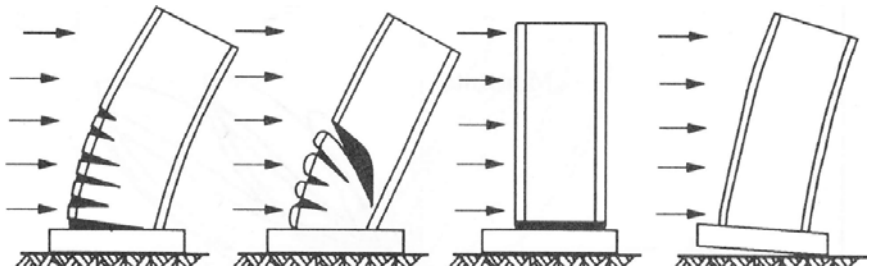

Figure 2.17: Failure modes of slender masonry structures; (a) flexion; (b) shear; (c) rocking: by base uplifting and (d) by foundation uplifting [Bazan and Meli, 2003]

2.4.6.2 Boundary conditions

The position of a historical masonry tower in the urban context is a very important aspect that influences the vulnerability of the structure [Sepe et al., 2008]. These boundary conditions (see Fig. 2.18) could strongly modify its seismic behavior and have big impact in the generation of different failure modes. Non-isolated towers were commonly built as part of churches or next to another building. The presence of adjacent walls or façades with different height than the tower and the lack of connection between elements due to the poor tensile strength of masonry could generate during an earthquake a detachment of the different bodies, vibrating in an independent way and hitting between them, leading to serious damages.

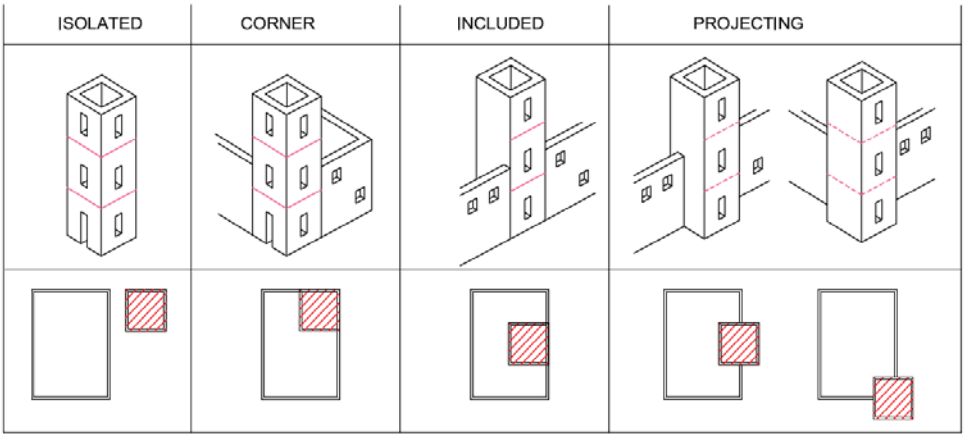

Figure 2.18: Position of the tower in the urban context [Sepe et al., 2008]

Curti et al. [2008] observed in 31 Italian bell towers (16 isolated and 15 with one or two shared sides with the church) damaged by the 1976 Friuli earthquakes (May M6.4 and September M6.1), that the presence of walls and façades adjacent to any tower at different heights are horizontal constraints that increase the seismic vulnerability of the tower by limiting its slenderness and by creating localized stiffening zones that could cause the concentration of important stresses.

2.4.6.3 Long-term heavy loads

Historical masonry towers were built as most of the historical buildings to withstand mainly the vertical loading generated by their self weight. The walls thicknesses used to be determined following empirical rules transmitted from generation to generation by trial and error mainly based on the height (in some cases taller than 60 m) and observed damages after earthquakes. This led to the construction of walls with enormous thicknesses, in some cases higher than 2 m. The roof system of historical masonry towers was usually made of the same material of the walls, even when reduced thicknesses were considered, the elevated mass of masonry generated problems of instability that could lead to its collapse even during the construction works. Due to this, is quite frequent to especially find in Italy masonry towers with a plane roof system integrated by wooden beams and fired-clay bricks. In Germany the masonry towers usually have a triangular timber roof externally covered by thin plates made of metal (copper). By the other hand, fired-clay bricks were frequently used in Mexico and in some cases volcanic stones of low density or artisanal clay vessels to make lighter the roof system.

Figure 2.19: Replica of the collapsed bell tower of "Piazza San Marco" in Venice, Italy

Historical masonry towers are slender structures under high vertical loading. This is due to the height, wall thickness, the presence of a roof system, the high density of masonry (see table 2.5) and heavy bells, leading to a concentration of high compressive

stresses at their base. All these issues and moreover taking into account the deterioration of masonry through the centuries (progressive damage) make historical masonry towers extremely vulnerable to suffer a sudden collapse by an exceeding of their compressive strength (see section 2.4.3.1), or in some cases the failure of the foundation or soil. These sudden collapses have been occurring since centuries ago in this type of structures. The most famous cases are reported e. g. in Binda et al. [1992], Macchi [1993], GES [1993] and Binda [2008]. They correspond to the sudden collapses of the bell tower of "Piazza San Marco", Venice in 1902 (a replica was built, see Fig. 2.19), the civic tower of Pavia in 1989 and the bell tower of the church of "St. Maria Magdalena" in Goch, Germany in 1992.

2.4.6.4 Local site effects and soil-structure interaction

Seismic hazard characteristics and soil conditions of the site are important aspects that determine the vulnerability of historical masonry towers. Seismic hazard of a certain site is the probability of occurrence of an earthquake. This depends on its proximity to a seismic source with events of enough magnitude to generate significant seismic intensities at the site under study. The source of the earthquake is mainly due to the released energy generated by the abrupt movements of the tectonic plates of the earth´s crust, presented in the zone of contact between plates or in geological faults inside of a plate. Ground motion strongly depends on the geology and topography conditions of the site as well as the inherent characteristics of the earthquake.

Figure 2.20: General view of the leaning tower of Pisa, Italy

The city of Tenochtitlan (now the historical center of Mexico City) was built by the Aztecs upon raised islets in Lake Texcoco. Due to this, the soil presents bad conditions, is very soft, and this modifies the basic characteristics of the seismic source by amplification of the ground motion, represented by low frequencies and high periods. This was the case of the earthquake occurred in 1985 (magnitude 8.1) in the Pacific coast of Michoacan, Mexico, causing thousands of deaths and strong damage to the built environment, mainly in Mexico City which is located more than 350 km away from

the epicenter. These low frequencies mainly affect slender structures like masonry towers because their fundamental vibration frequency is in the range of the predominant frequency of the ground motion (resonance phenomena). The high mass of the tower and flexibility due to its slenderness generate that the structure presents during an earthquake important top displacements. By the other hand, high frequencies and low periods mainly affect compact structures like most of the historical buildings. *Liquefaction* due to ground motion and instability conditions by *soil settlements* are geotechnical issues that depend on the site. The latter issue has been observed at the Metropolitan Cathedral of Mexico City since decades due to soft soil conditions. The most famous case presented in historical masonry towers is the leaning tower of Pisa, Italy. Since its construction in the XII century it started to incline, due to irregularities in the soil conditions, being with this quite vulnerable to overturning (see Fig. 2.20).

2.4.6.5 Seismic behavior and failure mechanisms

The excessive slenderness of historical masonry towers (H/L > 4) is characterized by a ductile behavior, failing in a predominant flexural mode similar to that of cantilever beams. Due to all these factors and its heavy mass, the lateral vibration at the top of the tower is considerably more amplified than the one of the base, generating with this important horizontal top displacements and inertia forces transmitted in-plane and out-of-plane by ground motion. This behavior could cause as aforementioned different failure modes generated by flexion, shear, base and foundation uplifting due to transmission of elevated vertical loads or poor soil conditions (Fig. 2.17). Moreover, the last could generate an amplification of the ground shaking very close to the natural frequency of the tower, leading to its failure by the resonance phenomena.

(a) (b)

Figure 2.21: Typical failure mechanisms of bell towers; (a) [Meli, 1998]; (b) Effects of the Colima earthquake (2003): damaged belfries and the *collapsed one at adjacent building*

Meli [1998] describes that during an earthquake historical masonry towers present important horizontal top displacements. The flexion generates horizontal cracks but rarely the overturning of the structure. This is due to the alternation of the direction of the movement that causes an opening and closing effect of these cracks, dissipating with the impact an important part of the energy induced by the earthquake. By the other hand, in bell towers, the presence of large openings at belfry could increase the vulnerability of the structure, being more frequent the failure by shear. Due to the strong damage, the belfry could collapse by instability, endangering the adjacent buildings and mainly people who could be inside or in the surroundings (see Fig. 2.21). Curti et al. [2008] observed in 31 Italian bell towers damaged by the 1976 Friuli earthquakes that the belfry is the most vulnerable part of the tower due to the presence of large openings, leading to the pillars to be slender and by the top masses. This amplifies the seismic motion causing critical effects in the higher part of the tower.

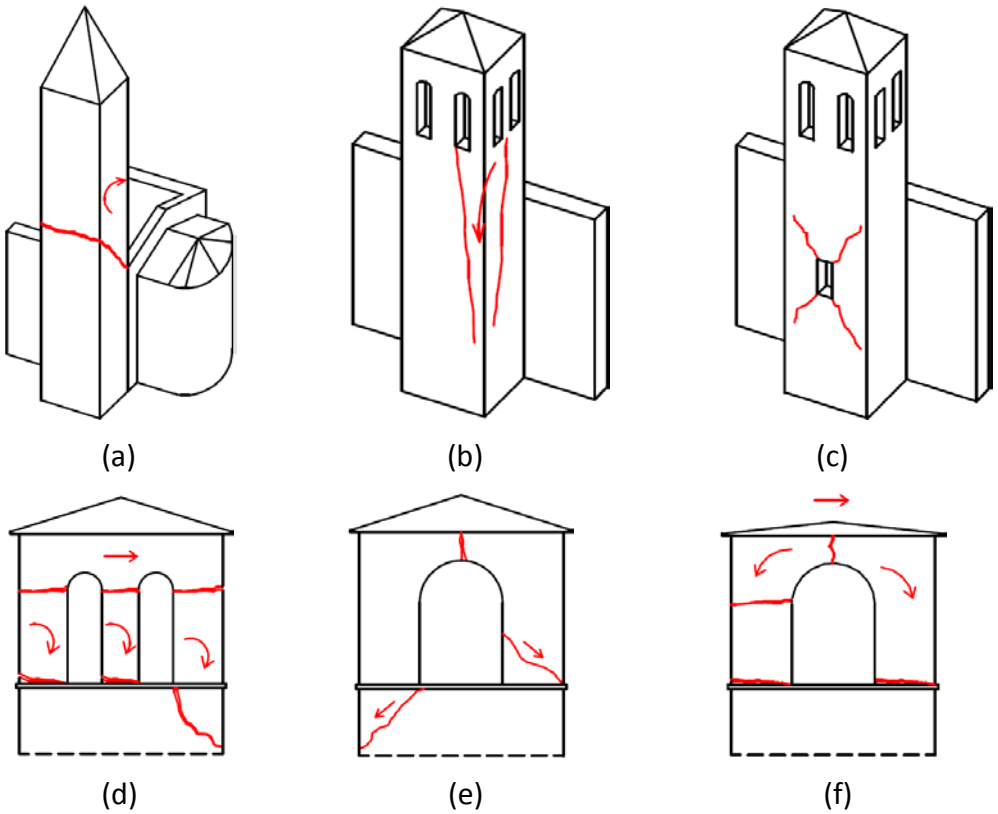

Figure 2.22: Damage mechanisms in masonry bell towers; (a-c) at the body of the tower and (d-f) at the level of belfry [Lagomarsino et al., 2002]

Based on observed damage after considerable earthquakes occurred in Italy, Lagomarsino et al. [2002] propose the damage modes commonly presented by historical masonry towers of Figure 2.22. The damage at the body (Fig. 2.22a) corresponds to horizontal cracking out-of-plane due to bending behavior and diagonal cracking by shear stresses in-plane by the contact with the façade of the church, leading to the

overturning of the tower over the nave (Fig. 2.22a). The type of damage of Figure 2.22b consists of vertical cracking in both planes due to horizontal tension, leading to the detachment of walls and their collapse by instability. By the other hand, the damage mode of Figure 2.22c is represented by alternated diagonal cracking in-plane due to shear. In this case the tower would not present collapse. The damages at belfries are mainly characterized by horizontal cracking by bending behavior and diagonal cracking by shear stresses when there is the presence of large openings, leading to collapse by overturning (see Figs. 2.22d-f).

2.4.6.6 Dynamic actions by bells swinging

In masonry bell towers is quite common the presence of large and heavy bells hanging from their respective supports and anchored in different places at belfry. The swinging of the heavy bells induces dynamic actions that could cause damage to the tower. This motion generates at the bell´s support elevated vertical and horizontal inertia forces that are transmitted to the structure. Considering that most of the towers were mainly built to withstand their vertical loading, results more critical the action of the induced horizontal forces that could generate cracking or the separation of structural elements due to the low tensile strength of masonry (Fig. 2.23). By the other hand, the excitation induced by the swinging of bells could be very close to one of the natural frequencies of the tower, leading to a high dynamic amplification of the structural response by resonance. For more detailed information about the dynamic actions by bells swinging the reader is referred to the works of Beconcini et al. [2001], Bennati et al. [2002] and Ivorra and Pallares [2006].

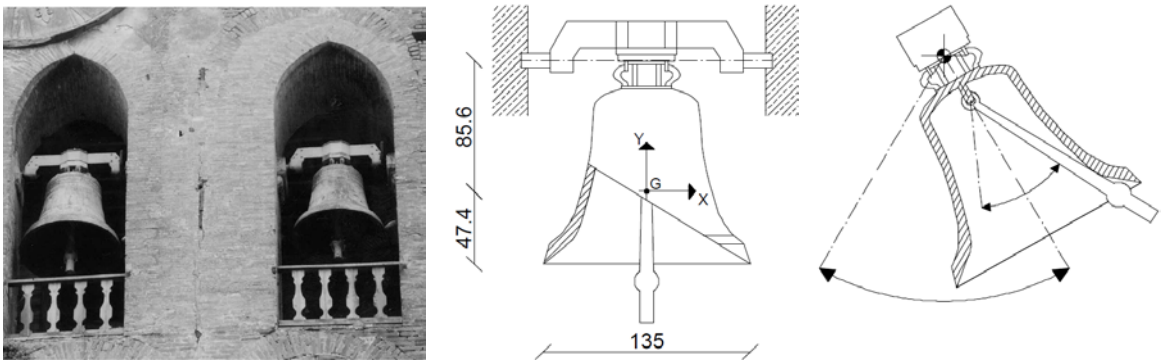

(a) (b) (c)

Figure 2.23: The bell tower of "Matilde" in Pisa, Italy; (a) location of bells at belfry and crack pattern; (b) bell dimensions (in cm); (b) bell swinging [Beconcini et al., 2001]

2.5 Summary

Seismic risk management of the built environment is integrated by two main stages, the assessment and the remedial measures to attain its reduction, and represents a huge task its achievement. The seismic risk of a certain structure located in a seismic zone is

determined by the conjunct of the seismic hazard and its structural vulnerability. The hazard level of a site mainly depends on its proximity to a seismic source, which is due to a fault rupture when the strain accumulated in the rock exceeds its capacity limit in the contact zone between tectonic plates (*interplate*), in geological faults inside of a plate (*intraplate*) or in the subducting slab (*intraslab*). The ground shaking mainly depends on the seismic source, geology and topography of the site, but definitely on the inherent earthquake characteristics. The source of intraplate earthquakes is diffuse, being a quite complicated task its characterization. In the case of interplate earthquakes is possible to use statistical methods, which in contrast, are useless for intraplate faults due to the absence of sufficient data on the same site. For fortune, low to moderate earthquakes occur in general in these faults. The seismic hazard characterization of a site is suggested to be estimated by considering a combination of studies (e.g. seismological, geophysical, and geological) with the history of earthquakes.

The most important methods of seismic vulnerability evaluation of buildings were mentioned. The selection of the method depends on different factors such as number of buildings, importance, available data, and aim of the study. The empirical methods satisfactorily allow the vulnerability evaluation of a single building or a large group of buildings at territorial scale in a fast and qualitative way. These methods are used to determine seismic scenarios before or after the occurrence of an earthquake. For assessing the vulnerability of an essential building the procedure is different and more in detail than in the qualitative and rough evaluations by empirical methods. The literature recommends applying a hybrid approach, which is a combination of the empirical, analytical and experimental methods, to obtain more reliable and quantitative results.

The main physical and mechanical properties of historical masonry were described. Subsequently, an identification of the seismic behavior and failure mechanisms of unreinforced masonry walls under in-plane loading was presented. This identification is quite difficult to predict and strongly depends on many factors such as physical (e.g. arrangement, slenderness and large openings) and mechanical properties of masonry, level of vertical loading and the magnitude of the transmitted inertia forces. All these factors play an important role in the determination of the behavior and failure patterns. By the other hand, the seismic performance and failure modes of unreinforced masonry walls loaded out-of-plane mainly depend on the bad connections between structural elements by the poor tensile strength of masonry and the presence of non-rigid diaphragms. This could lead to the collapse of the walls by overturning or the failure of the roof system by instability. Moreover, all the most relevant aspects that determine the seismic vulnerability of historical masonry towers in terms of behavior and failure modes were described. A deep understanding of all these aspects is very helpful towards the achievement of the seismic risk reduction, by means of decreasing the structural vulnerability with prestressing devices, which is the main objective of this thesis.

Chapter 3

Seismic Risk Management of Cultural Heritage

3.1 Introduction

This chapter presents a state-of-the-art about the two main stages of the seismic risk management specifically applied in cultural heritage (masonry structures), the risk assessment and its reduction by means of prestressing. The literature review is integrated by topics such as monitoring and diagnosis, constitutive material models, seismic analysis methods and retrofitting techniques with especial attention in prestressing. As aforementioned in chapter 1, a deep understanding of the actual scientific knowledge is the basis to propose a methodology for the seismic risk management of ancient masonry towers.

3.2 Seismic risk assessment

An intensive literature review on the existing methodologies for the seismic risk assessment of historical masonry structures is described in this section. First of all, the aiming and description of the monitoring and diagnosis campaigns is introduced. It includes experimental surveys developed in-situ and in laboratory, in order to identify the geometry, mechanical and dynamic characteristics, state of damages and modifications of the structure under study. Moreover, the need of the development of a constitutive material model for masonry is explained, as well as the main modeling strategies reported in the relevant literature, their advantages, disadvantages, uses and features. Finally, the fundamental basis and general characteristics of the applied masonry model in the intensive numerical simulations of this thesis are described.

3.2.1 Monitoring and diagnosis of historical masonry structures

The lack of information for a complete and detailed knowledge of the actual situation of an ancient building represents a huge task and by the other hand corresponds to a quite interesting issue in the context of the structural safety of the cultural heritage. The

implementation of monitoring and diagnosis surveys allows determining the structural characteristics of the construction under study, experimental data such as geometry of the structural elements, mechanical properties of the materials, state of damage, dynamic behavior, identification of past interventions and so on. The obtained experimental information of the actual state of the building represents the basis and reliability of the *seismic risk assessment* of the structure. Moreover, in a subsequent stage, the seismic risk could be treated by means of *retrofitting* measures aimed at *reducing the risk*. The structural characterization of an historical building could be developed by means of *in-situ and laboratory surveys,* supported nowadays by modern instruments and techniques, combined mainly with the knowledge and experience acquired throughout the years about this especial group of structures.

3.2.1.1 Structural identification and geometrical survey

The main objective of these preliminary studies is mainly to obtain the geometrical properties of the structural elements and their interaction with the rest of the structure, as well as support and boundary conditions and constructive irregularities. As a first stage, the development of an exhaustive historical analysis of the building is strongly recommended. This initial analysis allows obtaining information such as approximated date of construction, building materials, history of damages (e.g. fires, earthquakes, lightnings and so on) and the materials used in the intervention works. This information may be complemented with visual inspections to determine in a qualitative way the actual conservation state of the building and by means of photographs, video (e.g. endoscope device for examinations inside elements and gaps) and topographic instruments to develop the graphical representation (architectonic plans) of the entire structure. This is helpful to appreciate the architectonic distribution of spaces, geometry of constructive elements, elevations, details and so on. The structural identification and geometrical surveys permit as well a visual identification of the state of damages, such as crack pattern of structural elements and the conservation state of the building.

3.2.1.2 Mechanical characterization and state of damages

Once the structural and geometrical characteristics of the ancient building are known, is important to characterize as a second stage its dynamic and mechanical properties, as well as the identification of damages that the building has suffered throughout its existence. The mechanical characteristics and identification of damages could be obtained by means of two different approaches in dependency on the importance of the building and objective of the study. The first approach corresponds to a rough or rapid identification in a qualitative way, taking into account visual inspections and the opinion of experts. The second approach needs especial equipment for its development and represents more time consuming. It consists in quantitative identifications by means of experimental in-situ campaigns and laboratory tests. Nowadays, there is a huge variety of methods (minor-destructive and non-destructive tests) and equipment available for developing these identifications. A minor-destructive test corresponds to the in-situ core

extraction of the different structural elements (Fig. 3.1) with the use of modern drilling equipment. Afterwards, from this internal sampling several test-tubes are extracted in laboratory to obtain by compression loading the stress-strain curve, and from this, to determine the mechanical parameters of masonry. Meli [1998] affirms that these laboratory tests may be inaccurate and less representative when the type of masonry of the structural element is either irregular or three layers masonry, and in this case, these tests are only helpful for material identification of units and mortars. More representative results could be obtained by the in-situ application of the double flat-jack test as depicted in Figure 3.2.

Figure 3.1: Extracted cores of the façade of an historical masonry building [BGS, 2009*]*

In the case of historical masonry walls, especially in bell towers, the application of the double flat-jack test permits to determine the actual state of compressive stresses in different parts of the structure, especially at the base. These tests are helpful as well to assess the deterioration that the structure has suffered through the centuries (progressive damage) by means of evaluating the compressive stress-strain curve in order to obtain the mechanical parameters of masonry. Since historical masonry towers were built as most of the historical buildings to mainly withstand their self weight, an exceeding of their compressive strength make them extremely vulnerable to suffer strong damage or collapse by earthquake action or to suffer a sudden collapse in static conditions as mentioned in section 2.4.6.3. This experimental data is quite helpful to calibrate and to validate the analytical models of the structure (see section 2.3.2.4).

Historical masonry is a very heterogeneous material and the assessment of its mechanical characteristics is always a complicated task. This is due to the structure was built following empirical rules and available materials, and mainly to the continuous modifications throughout its existence. Nowadays, with the continuous technological advances there is an enormous variety of equipment available for the development of non-destructive tests in the cultural heritage.

(a) (b)

Figure 3.2: In-situ testing by double flat-jack in a historical masonry dome (Cathedral of Siena, Italy); (a) base distance measurement and (b) overall view [Bartoli et al., 2008]

One example of these modern equipments corresponds to the use of infrared thermal imaging and video for inspections. The obtained infrared thermal images of Figure 3.3 are helpful to identify constructive defects and damages (crack pattern and moisture by water infiltration), modifications such as sealed openings (windows or doors), hidden reinforcement elements inside the structure as iron bars (or more recently steel and concrete) and timber.

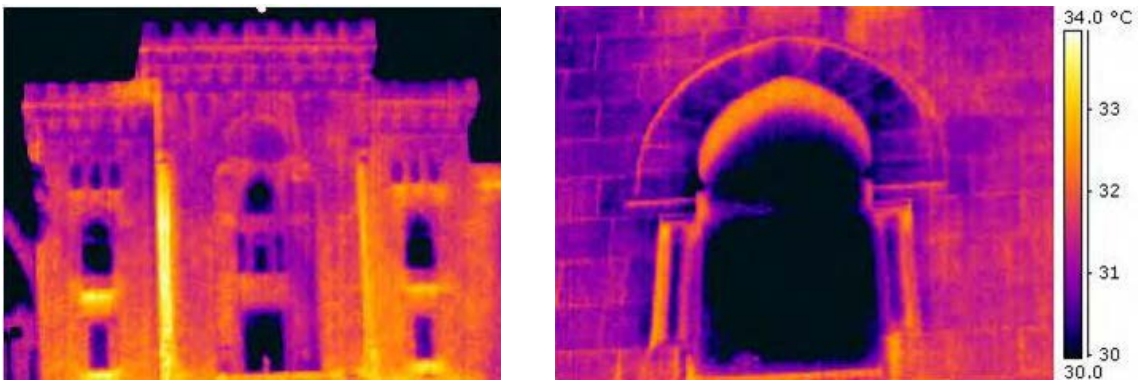

Figure 3.3: Infrared thermal images of an ancient masonry building [Rao, 2007]

3.2.1.3 Dynamic characterization

The dynamic characterization of structures represents a complementary and important stage of the monitoring and diagnosis surveys on old masonry structures. Different from the mechanical investigations, the dynamic experimental campaigns are mainly developed in-situ with the use of sensitive equipment such as accelerometers located at specific points of the structure. These dynamic investigations are carried out in buildings that require an especial attention as in the case of historical constructions in order to

obtain quantitative information of the natural frequencies and vibration modes. Araiza [2003] recommends that the selection of the equipment has to be based on factors such as economy, simplicity and effectiveness. These devices (Fig. 3.4) measure in a certain period of time the vibration of the structure when excited by ambient vibration such as wind or traffic, and in seismic zones by micro-seismicity. Rarely real earthquakes are recorded during these short experimental campaigns, at least that a permanent network of accelerometers has been installed and monitored in the building.

(a) (b)

Figure 3.4: Two types of classic accelerometers for the dynamic characterizations

The recorded signals by the ambient vibration tests are extracted from the devices and analyzed by numerical methods in combination with especial software to determine the parameters that govern the dynamic behavior of the structure, such as natural frequencies and corresponding vibration modes. Another method to assess the dynamic properties of a structure instead of recording ambient vibration consists on applying controlled forced excitation with a determinate frequency by means of equipment placed in-situ in the building or by dropping a mass in the ground nearby the foundation. The application of excitation by dropping masses is not well recommended in historical buildings to avoid structural damages or an excess of excitation. With the dynamic experimental campaigns is possible to determine as well the stiffness contribution induced by adjacent buildings or façades (see section 2.4.6.2) and to characterize the actual damage state of the structure before or after the occurrence of an earthquake by considering the influence of existing cracking on the dynamic response of the structure (stiffness degradation). Afterwards, this experimental data of the dynamic properties of the building could be independently used or in addition of the mechanical information to calibrate and to validate the analytical models, in order to obtain with this, a better approximation throughout the real behavior and damage state of the building (see section 2.3.2.4).

3.2.2 Material models for the analysis of historical masonry structures

In order to assess the seismic performance of a certain historical construction the engineer requires the development of *constitutive material models* able to satisfactorily represent the mechanical behavior of the materials under analysis, as well as the generation of the *structural model* mainly based on the monitoring and diagnosis

campaigns. The main objective of this section is to explain as a starting point the need of the development of a constitutive material model for masonry. Afterwards, an overview of the main modeling strategies for masonry is given, as well as their general description, advantages and disadvantages. Finally, the fundamental basis and general characteristics of the applied constitutive material model for masonry are described.

3.2.2.1 Modeling strategies for masonry structures

Compared to other structural materials, masonry presents nonlinear behavior since very low horizontal load levels due to its poor tensile strength. Moreover, the anisotropy of masonry in terms of behavior and failure mechanisms is mainly determined by the physical and mechanical characteristics of its components (mortar joints and units). The anisotropic and nonlinear behavior of masonry prevents the use of seismic analyses based in linear elastic principles because they are not representative of the real behavior of this material. The growing concern and interest for the seismic protection of historical constructions in recent decades has been a topic of very active research. This has led to the development of a considerable number of constitutive material models ranging from simplified to very accurate, able to simulate the nonlinear behavior of masonry when subjected to monotonic and cyclic loading. The selection of a suitable material model depends on the seismic analysis method, importance of the building, available data and reliability of the expected results.

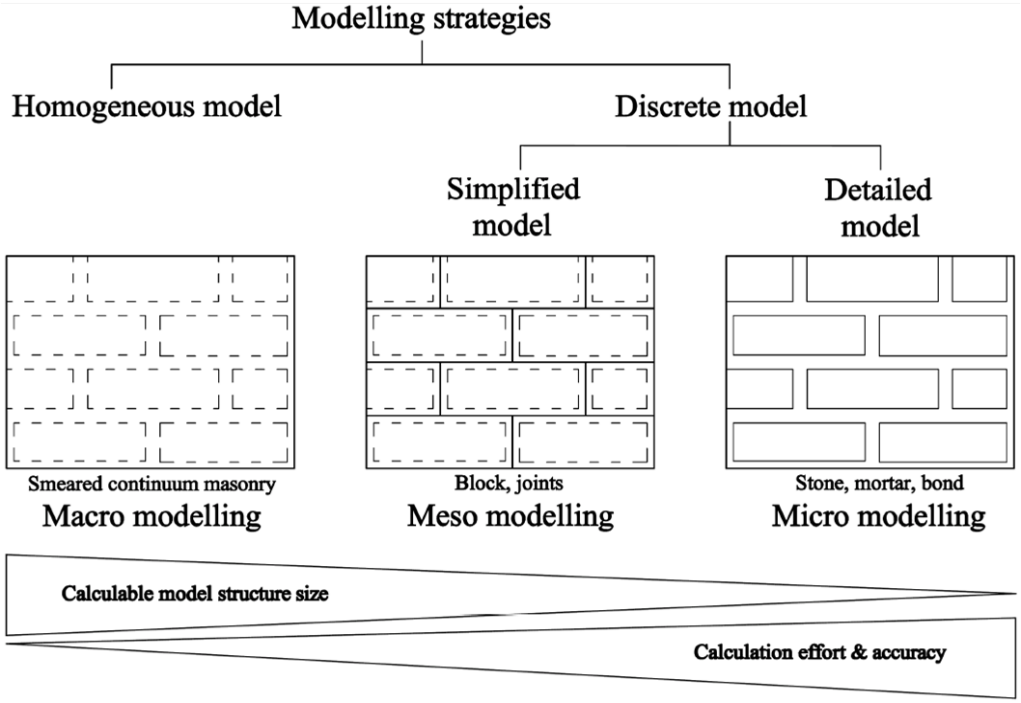

Figure 3.5: Overview of modeling strategies for masonry structures [Sperbeck, 2009]

In the framework of the FEM, three main modeling strategies for masonry are identified to be the most mentioned in the relevant literature as depicted in Figure 3.5. The micro-modeling of single elements (stone, mortar and their interface), also named discrete model is suitable and accurate for the seismic analysis of small structures, e.g. Lofti and Shing [1994] and Lourenço and Rots [1997]. Due to the large amount of needed time for the generation of the detailed structural model and the high calculation effort prevent the use of this approach in the seismic analysis of sophisticated and large-scale structures as in the case of historical constructions. By the other hand, the macro-modeling, also named smeared, continuum or homogenised model, considers masonry as an anisotropic composite material, e.g. Gambarotta and Lagomarsino [1997], Lourenço et al. [1998] and Schlegel [2004]. This simplifies the generation of the structural model, and due to the significantly reduction of the degrees of freedom, less calculation effort is needed, being considered with this, as a suitable constitutive material model for the seismic analysis of historical constructions. Compared to the discrete approach, the continuum model is relatively less accurate as depicted in Figure 3.5. This is due to the assumptions in the material model and also in the generation of the structural model. Another modeling strategy for masonry structures between the micro and macro approaches is the meso-modeling or also named simplified discrete model. In this approach the units are modeled as well as the interaction between mortar and unit as an average interface involving the properties of the mortar and the bond, e.g. Casolo and Milani [2010]. Even when this approach allows obtaining a balance between accuracy and needed time for the generation of the structural model and calculation effort, as in the case of the micro-modeling, the meso-modeling results unattractive for the seismic analysis of historical constructions.

3.2.2.2 Applied constitutive material model for masonry

This research work is not objected at developing a constitutive material model for masonry or to extend and existing one. In this section, the fundamental basis, advantages and disadvantages, uses and features of the applied material model developed by Gambarotta and Lagomarsino [1997] are described. The model is integrated in the commercial finite element program ANSYS® by means of subroutines. As above mentioned, the model is based on the macro-modeling approach which is considered as appropriate for the seismic assessment of historical constructions. The suitability of the material model in masonry structures has been proved through intensive numerical simulations against experimental results in the University of Genoa, e.g. Calderini and Lagomarsino [2006], and recently in the framework of the IGC 802 (risk management on the built environment) between the University of Braunschweig and the University of Florence, e.g. Urban [2007] and Sperbeck [2009]. The continuum damage model is based on a micromechanical approach where masonry is assumed as a composite medium made up of an assembly of units connected by bed mortar joints. The contribution of head joints is not considered. The constitutive equations are obtained by homogenizing the composite medium and on the hypothesis of plane stress

condition. Figure 3.6 shows the homogenised composite medium with its coordinate system and the representative volume element.

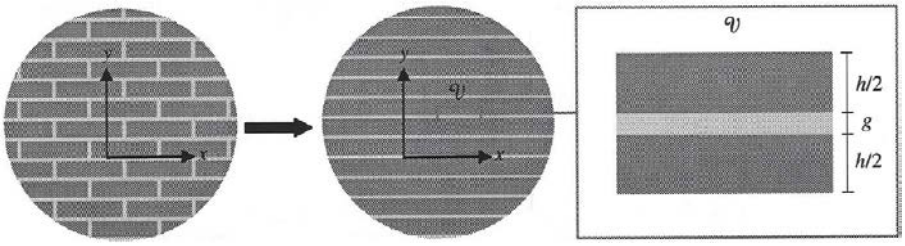

Figure 3.6: Masonry pattern and the representative volume element [Calderini, 2004]

The model is able to describe stiffness and strength degradation (Fig. 3.7) for structures monotonically loaded in-plane and out-of-plane as well as the hysteretic response by cyclic loading. Energy dissipation is possible through activated frictional mechanisms. Another important feature of this accurate material model is that is able to consider the evolution of damage in the units and mortar bed joints by especial damage parameters that are helpful to predict the structural failure mechanisms.

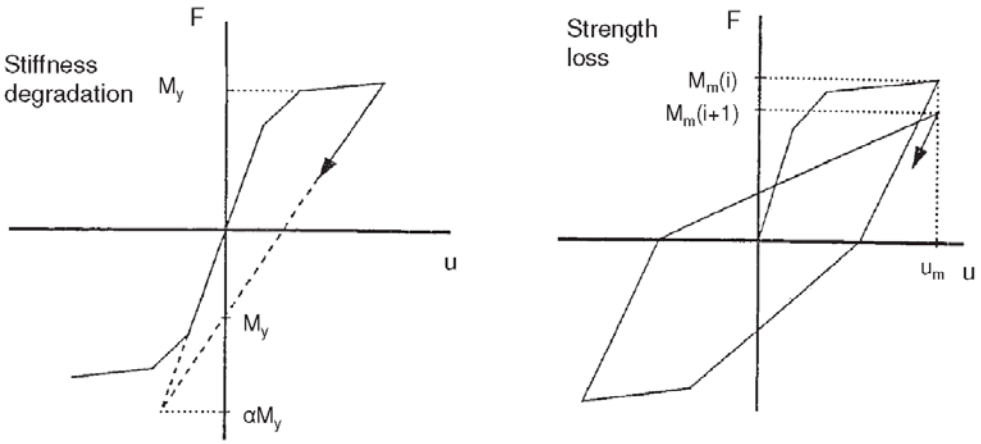

Figure 3.7: Stiffness degradation and strength loss [Urban, 2007]

In the next paragraphs the constitutive equations and the main assumptions that correspond to the basis of the model are briefly described. Eq. 3.1 describes the mean strain of masonry ε which is generated by an elastic contribution associated with an elastic equivalent continuum and an inelastic contribution determined by the damage process localised in the mortar bed joints ε_m^{pl} and units ε_b^{pl}. Here K_m represents the mean elastic tensor and σ the mean stress tensor.

$$\varepsilon = K_M \sigma + \varepsilon_m^{pl} + \varepsilon_b^{pl} \qquad [3.1]$$

$$\varepsilon = \{\varepsilon_x, \varepsilon_y, \gamma\}^t \quad [3.2]$$

$$\sigma = \{\sigma_x, \sigma_y, \gamma\}^t \quad [3.3]$$

The mean strain and stress tensors of Eqs. 3.2 and 3.3 may be expressed considering the defined axis for masonry of Figure 3.6 and the hypothesis of plane stresses. The inelastic strains of mortar and units presented in Eq. 3.1 may be further divided in extensions ε and sliding γ and are given by Eqs. 3.4 and 3.5. They are further determined for the mortar damage as presented in Eqs. 3.6 and 3.7, as well as for the unit damage in Eqs. 3.8 and 3.9.

$$\varepsilon_m^{pl} = \{0, \varepsilon_m, \gamma_m\}^t \quad [3.4]$$

$$\varepsilon_b^{pl} = \{0, \varepsilon_b, \gamma_b\}^t \quad [3.5]$$

Where in Eq. 3.6 H is the Heaviside function that takes into account the unilateral response of the interface, c_{mn} and c_{mt} are the inelastic compliance parameters for extensional and tangential mechanisms in the mortar bed joint. The friction at the interfaces is represented by f_i, it disapears if tensile stresses are present and limits the sliding in case of compressive stresses. α_m represents the mortar damage variable and α_b the unit damage variable. By the other hand, the Heaviside function H of Eq. 3.8 takes into account only the vertical compressive strain in the units. The sliding effect of the units is negligible compared to the mortar bed contribution. Due to this, if ε_m γ_m and ε_b are known, the strains in the representative masonry element may be determined.

$$\varepsilon_m = c_{mn}\alpha_m H(\sigma_y)\sigma_y \quad [3.6]$$

$$\gamma_m = c_{mt}\alpha_m(\tau - f_i) \quad [3.7]$$

$$\varepsilon_b = c_{bn}\alpha_b H(-\sigma_y)\sigma_y \quad [3.8]$$

$$\gamma_b = c_{bt}\alpha_b \tau \quad [3.9]$$

The inelastic contributions are governed by the evolution of the two damage variables α_m and α_b iteratively fitted in each load step during the numerical simulations. The evolution of damage is based on the theory of fracture mechanics by assuming that the damage energy release rate Y_m is ≤ than the toughness R, and that the toughness function $R(\alpha)$ depends on α as presented in Figure 3.8 for the evolution of damage in the mortar joints. This variable describes the loss of toughness at each node of the

representative masonry element. This loss could be defined as the reduction of the needed energy to generate further cracking, expressed as the percentage of the needed energy in the undamaged state.

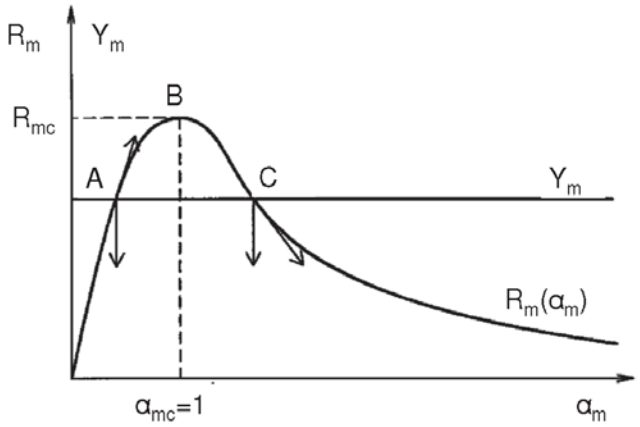

Figure 3.8: Damage function for the mortar joints, stable (A) and unstable evolution (B) [Gambarotta and Lagomarsino, 1997]

The failure limit states for mortar and unit damage are depicted in Figure 3.9. The homogenised material model is characterized by three yield surfaces determined by the tensile failure and sliding of the mortar joints considering the Coulomb friction law and the compressive failure of the units. The inelastic tangential compliance parameter for the units c_{bt} cannot be entered by a selected value, instead of it, it is automatically calculated in order to reduce the number of input parameters by the relationship of shear strength τ_{br} and the compressive strength σ_{br} by means of Eq. 3.10. In summary, if tensile stresses act in the mortar bed joints $\sigma_y \geq 0$, three damage mechanisms may become active: failure of the units, sliding and failure of the mortar bed joints. By the other hand, if the mortar joints are under compressive stresses $\sigma_y < 0$, then both damage mechanisms of units and mortar are activated.

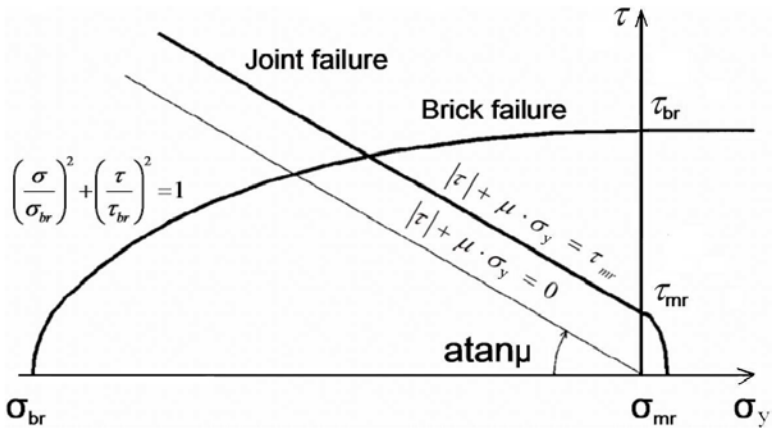

Figure 3.9: Mortar joint and brick failure domains [Gambarotta and Lagomarsino, 1997]

$$\frac{c_{bn}}{c_{bt}} = \frac{\tau_{br}^2}{\sigma_{br}^2} \qquad [3.10]$$

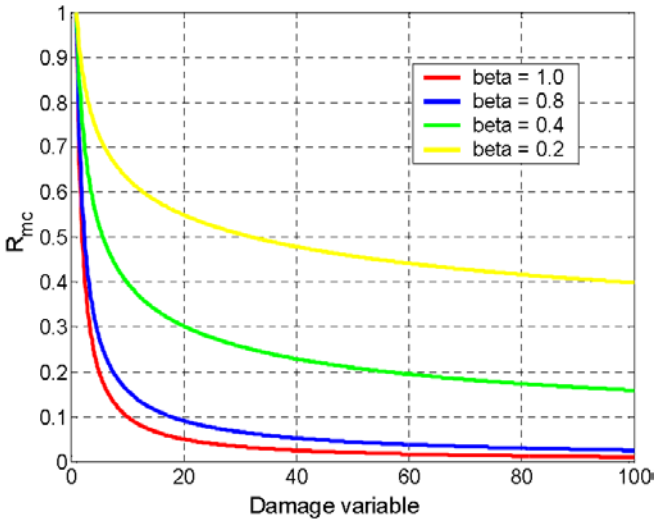

Figure 3.10: Loss of toughness with increasing damage [Urban, 2007]

$$R(\alpha) = \begin{cases} R_c \cdot \alpha & 0 < \alpha < 1 \\ R_c \cdot \alpha^{-\beta} & \alpha > 1 \end{cases} \qquad [3.11]$$

When a certain masonry structure presents cracking, it could behave brittle or ductile depending on many factors as explained in section 2.4.4. In the material model the softening parameter β characterizes whether the material behaves as brittle (β=1) or ideal plastic (β=0). To account for the post-peak behavior the resistance towards cracking could be described by Eq. 3.11. Where α is the damage parameter used in the material model (see Fig. 3.8), and by assigning different values of β in the range between 0 and 1, the loss of toughness with increasing damage may be represented as depicted in Figure 3.10. Besides the elastic parameters of masonry such as Young´s modulus, Poisson's ratio and density, the material model requires nine nonlinear parameters as presented in table 3.1. Calderini and Lagomarsino [2006] describe that the complete set of nonlinear parameters could be obtained by means of standard experimental tests and are described as follows:

- Force-control	- tensile strength of mortar joints (σ_m)
	- shear strength of units (τ_b)
- Displacement-control	- stress/strain shear behavior of mortar joints (τ_m, c_m, β_m, μ)
	- stress/strain compressive behavior of masonry (σ_M, c_M, β_M)

Based on extensive parametric investigations developed through numerical models of historical masonry structures, Urban [2007] proposes the material parameters presented in table 3.2.

Mortar joints:	**Strength:**	σ_m: tensile strength
		τ_m: shear strength
	Stress/strain:	c_m: shear inelastic compliance
		β_m: softening coefficient
	Friction:	μ : friction coefficient
Units and masonry:	**Strength:**	σ_M : compressive strength of masonry
		τ_b : shear strength of units
	Stress/strain:	c_M : normal inelastic compliance of masonry in compression
		β_M : softening coefficient of masonry

Table 3.1: Material parameters and related abbreviations of the constitutive model of Gambarotta and Lagomarsino [1997]

In order to assess the seismic response of an historical building is recommended to obtain these material parameters through detailed experimental campaigns like those mentioned in section 3.2.1.2. This is always a complex task, mainly due to the heterogeneity of masonry, the lack of representative samples and the need of non-destructive tests. In case that it is not possible to obtain all the material parameters, the ones proposed by Urban [2007] and the average mechanical properties of table 2.5 are recommended as a complement. However, these material parameters may be carefully selected because the response of the numerical model is very sensitive to them.

Parameter	**Value**	**Unit**
σ_m: tensile strength for mortar	0.25	Mpa
τ_m: shear strength for mortar	0.35	MPa
c_m: shear inelastic compliance for mortar	1	-
β_m: softening coefficient for mortar	0.7	-
μ : friction coefficient for mortar	0.6	-
σ_M : compressive strength of masonry	3.5	MPa
τ_b : shear strength of units	1.5	MPa
c_M : inelastic compliance of masonry in compression	1	-
β_M : softening coefficient of masonry	0.4	-

Table 3.2: Summary of material parameters and proposed values by Urban [2007]

3.2.3 Seismic analysis methods of historical masonry structures

After the monitoring and diagnosis campaigns developed on a certain historical construction, as a second stage, the engineer needs to elaborate the structural model, and together with a suitable constitutive material model able to satisfactorily represent the nonlinear behavior of masonry, to analyze the seismic performance of the structure. For this purpose, the application of analysis methods such as *FEM* and *limit analysis* is needed. These numerical approaches allow defining levels of damage generated in a structure by the occurrence of an earthquake. With the great scientific achievements in last decades in the generation of computational tools based on these methods, nowadays is possible to satisfactorily assess the seismic vulnerability of historical masonry structures with different variations in size and sophistication. This section aims to present general characteristics of the analysis methods under study, their fundamental basis, main advantages and disadvantages, as well as their uses in combination with several constitutive material models for masonry ranging from simplified to very accurate and different features.

3.2.3.1 Analysis by finite element method

The FEM is a numerical technique that was originated by the necessity of solving complex elasticity problems of stress analysis in the design of aircrafts, starting as an extension of the matrix method of structural analysis. The principles of this famous approach could be found in the works developed by Hrennikoff (1941) and Courant (1943) [Wikipedia, 2009]. With the continuous progress in the development of computational tools since the past decade until now, the use of FEM has proved to be useful in the analysis of historical masonry structures and has gained good acceptance within the structural engineering community. For the seismic assessment of complex historical masonry structures, the engineer needs to follow three main stages, the *pre-processing*, *solution* and *post-processing*. The *pre-processing* stage consists on the elaboration of the 3D structural model, mainly based on the monitoring and diagnosis campaigns. Once the geometry of the model is created, the appropriate finite element types with their respective real constants and material parameters are defined (linear or nonlinear depending on the analysis). Afterwards, by the mesh generation, the model is divided in finite pieces (elements and nodes) that adequately describe the model geometry and the defined input data. In the *solution* stage, boundary conditions and loads are defined, as well as the analysis type depending on the loading conditions and the needed response to assess. The analysis and proper understanding of the response results constitute the *post-processing* stage.

Analyses based on linear elastic principles are not representative of the real behavior of masonry structures. As previously mentioned, masonry presents nonlinear behavior since very low load levels due to its poor tensile strength. The most famous elastic assessments recently used for the assessment of historical buildings correspond to the static analysis of the dead load and the dynamic modal analysis. These allow assessing in a fast way and without the convergence problems of nonlinear analysis, the

vertical distribution of stresses, in order to identify zones of critical concentration and the main dynamic properties of the structure (natural frequencies and vibration modes). These preliminary linear elastic analyses are helpful as well to calibrate the initial models with the real structural information obtained in the experimental campaigns and to validate them, in order to obtain more representative models (see section 2.3.2.4).

The seismic response of a certain structure could be assessed by assuming that the earthquake action is constant throughout time (static), modeled as concentrated lateral inertia forces proportional to the mass. The most famous approach of this type corresponds to the traditional *pushover method*, which has been widely used since its development in the late 90's (see ATC-40 [1996] and FEMA-273 [1997]). In that time, very simplified material models were used, consisting on subsequent linear elastic analyses. The nonlinear behavior was induced to the model by localised changes in the elements presenting tensile stresses, by assigning a Young´s modulus reduction in order to represent the development of cracks and global stiffness degradation. The process is repeated until the structure becomes unstable or until a predetermined limit is reached, aimed at constructing in an approximated way the capacity curve of the building. Even when these subsequent analyses were considered as a practical and rapid tool without convergence problems, the exhaustive process of subsequently changing the model, the reanalysis, the reliability and interpretation of the results made it unattractive for engineering purposes. Recent developments and improvements of these approximated analyses and their use in masonry structures could be found in the works of Rots and Invernizzi [2004], Oliver et al. [2006] and Meza [2007].

With a suitable material model able to represent the nonlinear behavior of masonry combined with the structural model, is possible to automatically obtain by the pushover method the capacity curve of a structure. This curve represents the lateral displacement as function of forces monotonically increased to the structure. This curve is intended to represent a mass distribution by assuming a load pattern correlating the fundamental period of the structure, based on the assumption that is the predominant response. Analyzing this force-displacement diagram (base shear vs. top displacement) is possible to observe the resistance of the overall structure (ultimate lateral load capacity) and its ductility. The application of this approach is limited to structures with a fundamental period up to about one second ($T \leq 1$ s), for more flexible structures with a fundamental period greater than one second, it has to be considered in the analysis the effects of higher modes such as torsion (*adaptive pushover method*). Compared to a nonlinear dynamic analysis (time-history), the static pushover method does not give information about the hysteretic behavior of the structure, which is helpful to assess the strength degradation and the energy dissipation. This is due to the static analyses do not take into account motion and damping, and also not the main characteristics of the earthquake: maximum acceleration of the terrain expressed as a fraction of the gravity (PGA), duration of the intensive phase and vibration frequencies. Finally, changes in the modal properties due to the nonlinear behavior of masonry are not considered.

A disadvantage of using these sophisticated FEM models (combined with an accurate material model) in the practical assessment of structures is the large amount of needed time for the structural model elaboration, for performing the nonlinear analyses and for reaching proper results understanding. These should be used for structural analysis only in especial cases, as complex, important and large structures like monuments [Orduña, 2003].

3.2.3.2 Analysis by limit analysis method

Compared to the FEM that is based on both linear elastic and nonlinear plastic principles depending on the analysis type and objective of the study, in contrast the limit analysis approach is mainly based on the plasticity theory. Nielsen [1999] affirms that in the simplest way, this theory deals with materials that could present plastic deformations under constant loading until reaching values sufficiently high. These materials are named perfectly plastic and the approach that attempts to determine the bearing capacity and failure mechanisms of structures made of these materials is the limit analysis. The principles of this approach are related to Hooke and Coulomb in the XVII and XVIII centuries, followed by Kooharian [1952] and Heyman [1966, 1967 and 1969] who proposed the theoretical basis for its application in masonry structures. More recently, Orduña [2003] and Orduña and Lourenço [2005a, b] proposed a limit analysis procedure as a simplified tool to evaluate the seismic vulnerability of historical masonry structures. This approach considers that the nonlinear behavior of a masonry structure could be represented by rigid blocks interacting between them by means of frictional interfaces with no tensile strength. The constitutive model is based on a rigid-perfectly plastic material that does not need parameters of stiffness and softening, only strength parameters, being this the best advantage and attractive of the model. By the other hand, is not possible to evaluate the displacements and deformations of the structure.

For the pre-processing stage, the 3D structural model is developed based on the monitoring and diagnosis campaigns. The rigid blocks are modeled depending on the direction of the earthquake under analysis (+X, -X, +Y or –Y), observed damage after real earthquakes in similar structures and failure mechanisms reported in literature. The interaction between the 3D rigid blocks and foundation is modeled trough frictionant interfaces with no tensile strength. In the solution process the strength parameters are assigned to the structural model. By solving a mathematical programming problem that includes Eq. 3.12, yield conditions, flow rule, compatibility and complementary equations, it is possible to obtain relatively fast as a result the ultimate lateral load capacity of the model (load factor), failure mechanisms and stresses at the critical sections. Eq. 3.12 represents the equilibrium between the forces at the interfaces (Q) and the external loads applied to the blocks. Where Fc are the permanent loads, Fv the variable loads, α the load factor and B the equilibrium matrix.

$$F_c + \alpha F_v = BQ \qquad [3.12]$$

Giordano et al. [2007], Preciado [2007] and Orduña et al. [2007, 2008] have demonstrated that limit analysis by 3D rigid blocks represents a valuable and practical tool to approximately assess the in-plane and out-of-plane nonlinear behavior of ancient masonry buildings in seismic vulnerability studies. Compared to the refined FEM nonlinear models of an important historical building, the limit analysis model and the few needed material parameters, may be used as an advantage for preliminary assessments of historical constructions of small to medium size, as well as when the information of the building is limited or is needed to assess a group of buildings in a relative fast way. In the limit analysis, motion and damping are not considered as in the case of the FEM, nor the main characteristics of the earthquake and changes in the modal properties due to the nonlinear behavior of masonry.

3.3 Seismic risk reduction

This section describes an intensive literature review on seismic retrofitting measures of historical masonry structures, especially the practical application of uniaxial prestressed tendons. An overview based on the evolution of prestressing for the seismic protection of masonry structures (past and present) is presented. Old interventions in terms of used materials, aiming and existing applications are described. The overview is followed by a general description of modern prestressing for engineering purposes, based on the principles of prestressed concrete structures and its adaptation for the seismic retrofitting of historical masonry buildings, which is nowadays a topic of very active research all over the world. Moreover, the general characteristics and behavior of several prestressing devices of different materials are briefly described. These are included by traditional prestressing steel and smart materials such as fiber reinforced plastics and NiTi shape memory alloys of different fabricants. Finally, the presence of old and modern applications of prestressing in historical masonry towers is described.

3.3.1 Seismic retrofitting of historical masonry structures

Nowadays, there is a huge variety of techniques and materials available for the protection of historical masonry constructions. Among them, two main techniques are distinguished, the rehabilitation or restoration works and the retrofitting. The rehabilitation or restoration works aim to use materials of similar characteristics to the originals and to mainly apply the same constructive techniques, in order to locally correct the damage of certain structural elements, e.g. sealed up of cracks and reposition of mortar and units. In general terms, the objective of these works is to preserve the building in good conditions and in its original state, mainly to withstand the vertical loading generated by self weight. By the other hand, the structural retrofitting intends to use modern techniques and addition of advanced materials in order to mainly improve the seismic performance of the building, by increasing its ultimate lateral load capacity (strength), ductility and energy dissipation. Compatibility, durability and reversibility are the fundamental aspects recommended in literature to be taken into account when retrofitting is applied for the seismic protection of cultural heritage. A

good compatibility of deformations between materials is important in order to avoid a stress concentration that could generate damage to the rest of the structure. The durability of some retrofitting materials is not so easy to determine. This is due to the lack of capability verification to keep their mechanical properties and durability for centuries. Reversibility is definitely the most important aspect when modern techniques and materials are implemented in the seismic retrofitting of ancient buildings. If the applied technique is analyzed again and if is determined that it was not the best solution (e.g. compatibility and durability show deficiencies that increase the vulnerability) or when there is a new material or technique that allows a better seismic performance of the building, this old intervention could be substituted by the new one.

3.3.2 Prestressed masonry structures: Past and present

As above mentioned, nowadays there is a great variety of modern techniques and advanced materials for the seismic retrofitting of historical masonry buildings. The selection of the appropriate technique and materials depend on every case study and the purpose of the intervention. In the following pages an overview based on the evolution of prestressing as seismic retrofitting of historical masonry structures is described. This was done taking into account the main objective of this research work, which consists on the investigation of the effectiveness of different external prestressing devices (such as steel, fiber reinforced plastics, shape memory alloys and combinations) as a retrofitting measure for the seismic risk reduction of historical masonry towers.

(a) (b)

Figure 3.11: Presence of old prestressing in Italian historical monuments; (a) the Roman Coliseum and (b) vaulted structure in Pisa

Prestressing of masonry structures is not a recent retrofitting technique as it could be observed quite often in existing ancient masonry buildings in Italy (Fig. 3.11). Croci and D'Ayala [1993] and Croci [1995] affirm that past interventions were developed in the Roman Coliseum at the beginning of the XIX century to connect the internal walls

perpendicularly located to the external ring of the monument, in order to protect them against out-of-plane loading that could cause their overturning (see Fig. 3.11a). The addition of different types of metal bars (also named chains, belts and ties) was a common practice in past interventions of old constructions. Figure 3.12 shows several types of metal bars with their anchorages and tighteners of the same material. In order to generate the effect of prestressing the metal tie was usually heated to expand the material and when it returned to its normal temperature by means of the contraction, a shortening was generated, producing with this the active prestressing force. Throughout the history, the most frequent uses of old prestressing in ancient structures have been to tight and to connect walls to prevent overturning and to stabilize arches, vaults and cupolas that were damaged or identified as instable for an excess of opening or movement of their supports due to seismic forces (Fig. 3.11). The main disadvantages of these old metal bars were their heavy weight and the susceptibility of the material to suffer environmental attack represented by corrosion, reducing its resistance and damaging masonry by the volumetric change of the corroded bars leading to cracking and staining. Moreover, the difficulties to generate a good connection between bars and the excessive concentration of stresses induced by the anchorage to the masonry could lead to crushing. Another disadvantage was that there was no control or monitoring of the prestressing force, changing throughout the years by temperature, corrosion and by relaxation due to the deformation of masonry (creep).

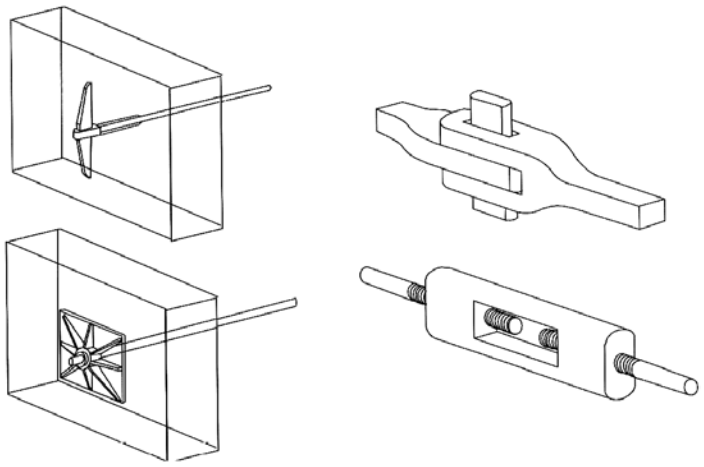

Figure 3.12: Metal bars with their anchorages and tighteners [Meli, 1998]

Modern prestressing had its principles at the beginning of the XX century with the development of prestressed concrete structures. The adaptation of this technique to the seismic protection of historical constructions has gained in recent decades especial interest for many researchers around the world and has been a topic of very active research. Prestressing consists of the application of a compressive force to masonry elements and may be achieved by post-tensioning high resistance steel tendons. The compressive force generates a uniform overall distribution of compressive stresses

aimed to enhance the tensile strength of masonry and structural stability at key locations identified in the seismic vulnerability evaluation (see Figs. 3.13 and 3.14).

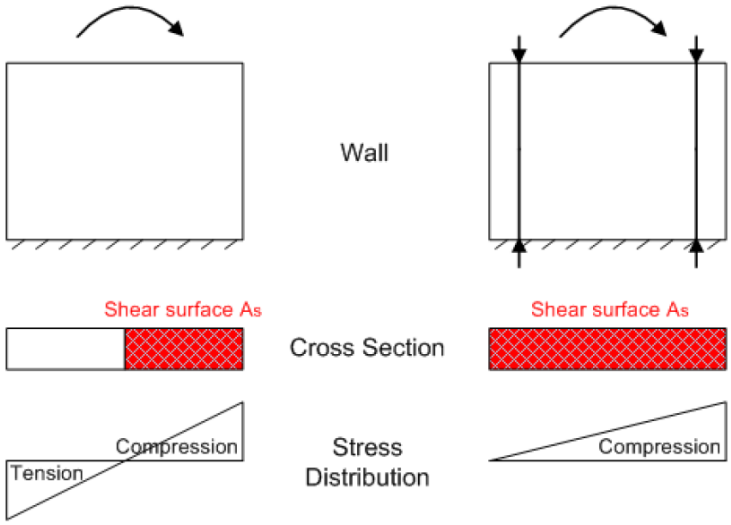

(a) (b)

Figure 3.13: Principle of shear surface reduction (A_s) in the nonlinear range; (a) wall in original conditions and (b) prestressed wall [Sperbeck, 2009]

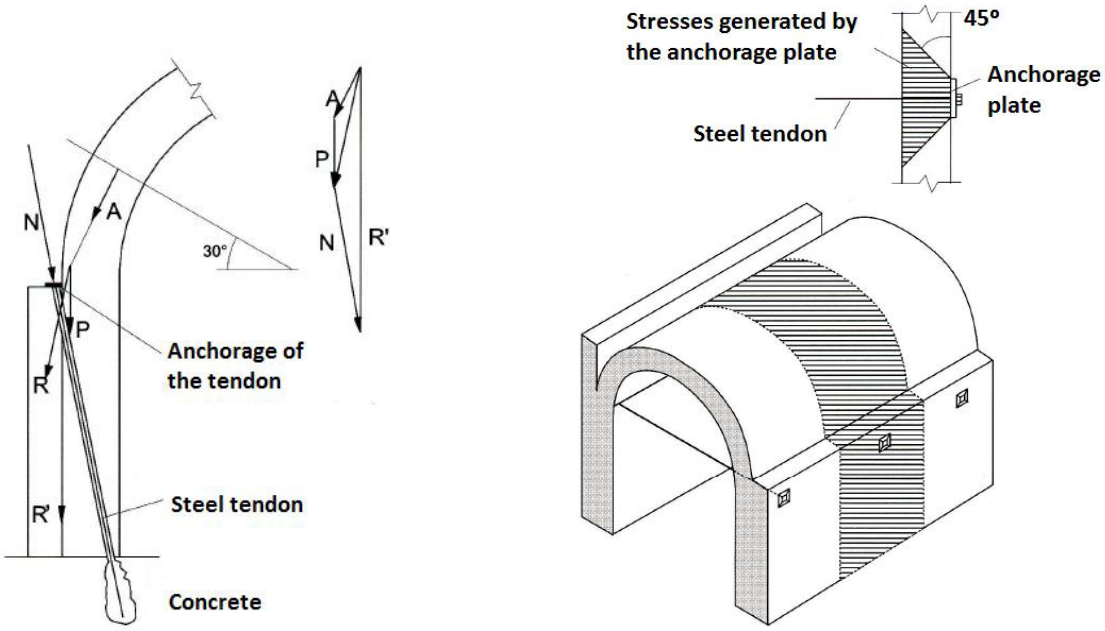

(a) (b)

Figure 3.14: Post-tensioned steel tendons in vaulted structures; (a) internal application (vertically) and (b) external application (horizontally) [Meli, 1998]

With the recent technological advances in drilling equipment and high resistance tendons of small diameters and low weight, is possible to apply prestressing in old constructions though holes of reduced diameter and great length that allows the internal insertion of tendons (Fig. 3.14a). This internal prestressing also protects the steel tendons against corrosion and is not so invasive for the architecture of the monument. From the structural point of view, the most important advantage of modern prestressing is that it could improve the seismic performance of masonry structures in terms of stability, strength and ductility. Another great advantage is the reversibility that permits the substitution for a better retrofitting measure. As in the case of the metal bars of the old prestressing and even with the enhancements on the high resistance steel tendons used in modern prestressing, they are still vulnerable to corrosion and the excessive concentration of stresses induced by the anchorage to the masonry.

3.3.3 Prestressing devices

This section is aimed at describing the general characteristics and behavior of several prestressing devices of different materials, including traditional prestressing steel and smart materials such as fiber reinforced plastics and NiTi shape memory alloys of different fabricants. In the context of this thesis a prestressing device is a structural member axially stressed in tension and is integrated in general terms by two main parts, the top and bottom anchorages and the tendon (Fig. 3.15). Normally, the used anchorage material for prestressed concrete and masonry structures has been of high resistance steel and more recently of innovative materials such as fiber reinforced plastics of different fibers (aramid, carbon and glass). By the other hand, the tendons could be commonly fabricated of both mentioned materials and shape memory alloys.

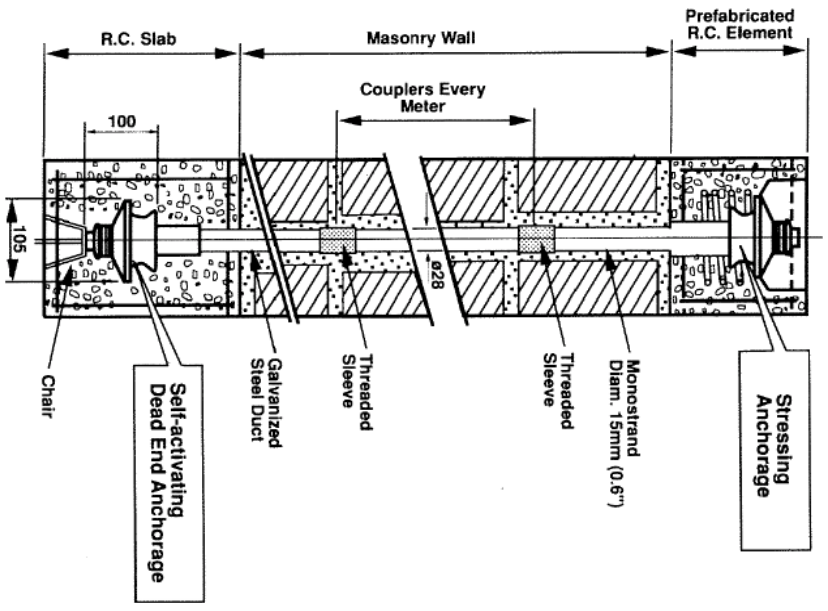

Figure 3.15: Typical prestressing device for masonry [Ganz, 1990]

3.3.3.1 Prestressing steel

Compared to conventional steel for reinforced concrete, prestressing steel was developed due to the need of a material of higher performance for its use in prestressed concrete structures. Nowadays, there is a great variety of prestressing steel, such as wires, strands, tendons (a group of strands or wires), bars and cables for bridges (a group of tendons) as depicted in Figure 3.16. The main properties of prestressing steel are the high tensile strength, ductility, bond, flexibility, low corrosion and low stress relaxation. As mentioned, relaxation has a great impact in the changes of prestressing forces with time. The main factors influencing this are creep (increase in deformation) and shrinkage (contraction by loss of water) of concrete.

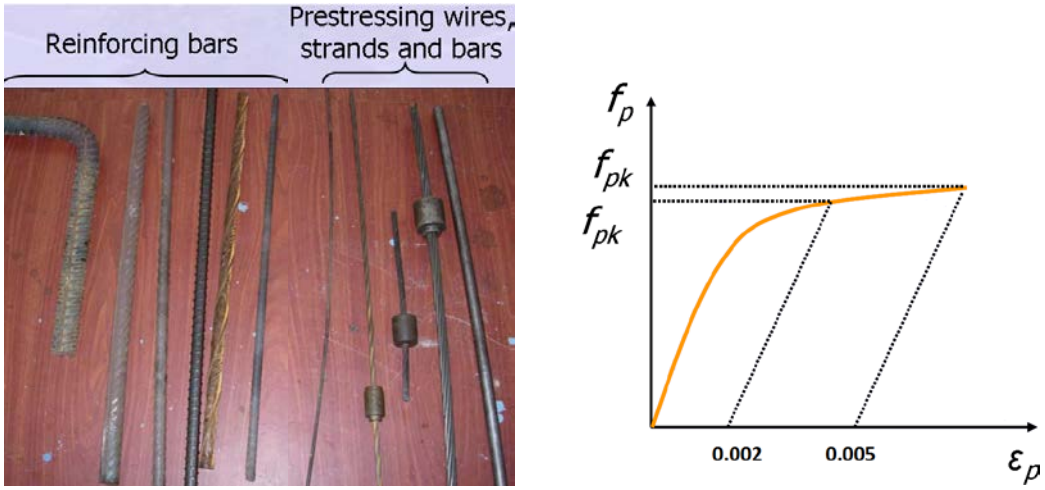

(a) (b)

Figure 3.16: Prestressing steel; (a) comparison with reinforced concrete steel and (b) characteristic stress-strain curve [Sengupta and Menon, 2009]

Type of prestressing steel	Tensile strength (MPa)	E modulus (MPa)
Cold drawn wire (5 - 7 mm)	1670 - 1860	210000
Cold drawn 7-wire strand (13 - 16 mm)	1770 - 1860	195000
Hot rolled bar (15 - 40 mm)	1030 - 1230	200000

Table 3.3: Main forms of prestressing steel and their mechanical properties

The stress-strain behavior of prestressing steel when subjected to uniaxial tension becomes nonlinear and inelastic at a strain of 0.2% (yield point) for a stress beyond of approximately 70% or 80% of the ultimate strength (Fig. 3.16b). Ganz [2001], DTES [2005] and Sengupta and Menon [2009] describe that there are three main forms of prestressing steel commonly used in prestressed structures as shown in table 3.3.

3.3.3.2 Fiber reinforced plastics

With the continuous technological progress in the chemical industry in past decades, several products of fiber reinforced plastics (FRP) composites have been introduced to the market for their use in prestressed concrete and more recently for the seismic retrofitting of historical masonry structures. Fibers of aramid (AFRP), carbon (CFRP) and glass (GFRP) have been used to manufacture bars, tendons (a group of bars), grids and plates with different shapes, sizes, colors and resistances.

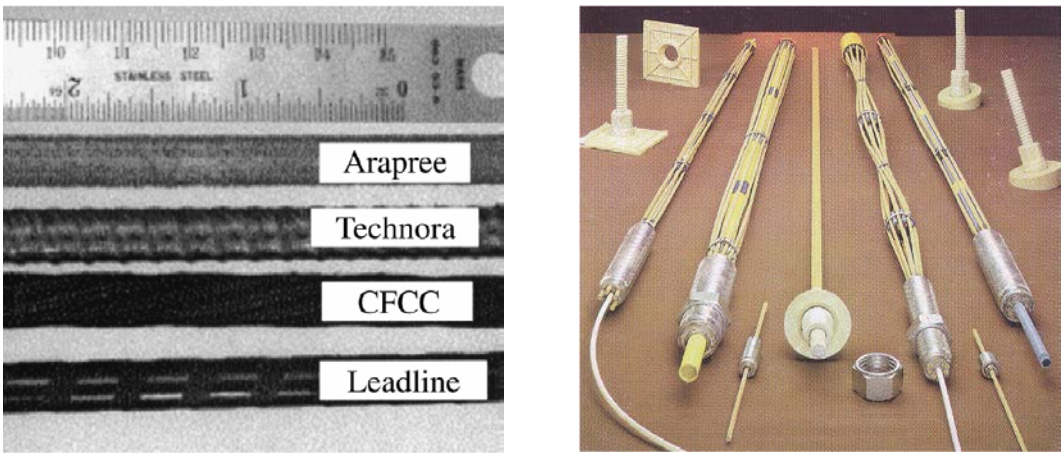

(a) (b)

Figure 3.17: FRP composites for prestressed structures; (a) four types of FRP bars [Zhang et al., 2001] and (b) FRP tendons and anchorages [Meli, 1998]

Type of prestressing FRP	Tensile strength (MPa)	Strain at failure (%)	E modulus (MPa)
Arapree (7.5 mm)	1370 - 1506	2.40	62500
Technora (8 mm)	1900 - 2140	3.70	54000
CFCC (12.5 mm)	1870 - 2120	1.57	137300
Leadline (7.9 mm)	2250 - 2600	1.30	150000

Table 3.4: Main types of prestressing FRP bars and their mechanical properties

Zhang et al. [2001] describe that tendons made of AFRP (Arapree and Technora) and CFRP (CFCC and Leadline) bars are the most commonly used for prestressed concrete (Fig. 3.17). GFRP is considered less appropriate due to its low Young´s modulus and is most commonly used as cables in mining engineering. The mechanical properties of AFRP and CFRP bars are described in table 3.4 taking into account the data reported in the works of Nanni et al. [1996], Zhang et al. [2001] and Dolan et al. [2001]. FRP compared to prestressing steel is more resistant to corrosion, equal or superior tensile strength, insensitivity to electromagnetic fields, 15 to 20% lighter and the possibility to incorporate optical fiber sensors for monitoring purposes. The disadvantages of FRP are

their vulnerability to fire and brittle failure with no yielding, showing a stress-strain behavior linear at all stress levels up to the point of failure. The recommended prestressing force is of about 40% of the ultimate load capacity for AFRP and 60% for CFRP due to the stress-rupture limitations.

3.3.3.3 NiTi shape memory alloys

Buehler and Wiley developed in the 60s at the U. S. Naval Ordnance Laboratory (NOL) a series of tests on specimens of Nickel-Titanium (NiTi) alloys. An unusual behavior different of traditional materials was observed. The specimens showed after a thermal cycle strains of more than 8%, returning to their original position with no final permanent deformation. This effect was named *shape memory* and the material *shape memory alloys* (SMA). The material was subjected to further research and it was found that SMA also presented the property of *superelasticity* (or pseudoelasticity) when subjected to high temperatures (see Figs. 3.18b and 5.1). NiTi SMA was later also named Nitinol SMA in honor to the laboratory where it was discovered. The fascinating behavior of this innovative material gained in a fast way the interest of the scientific community, being highly attractive for applications such as biomedical devices, energy dissipation and vibration control devices for the seismic protection of structures, aerospace structures and so on. Recently, SMA has been subjected to continuous research to use this smart material for the seismic retrofitting of ancient structures. Figure 3.18a shows the first worldwide application of a NiTi SMA device (developed by FIP®) for the seismic protection of the façade of the Basilica of San Francesco in Assisi.

(a)

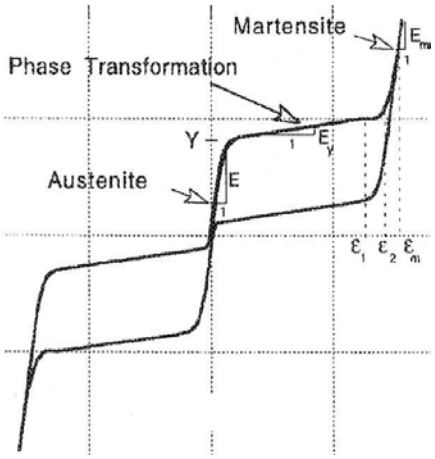

(b)

Figure 3.18: NiTi SMA; (a) Installing of a device in the Basilica of San Francesco in Assisi [Castellano, 2001] and (b) characteristic stress-strain relationship [Wilde et al., 2000]

SMA has the ability to undergo reversible micromechanical phase transition processes by changing their crystallographic structure. This capacity results in two major

features at the macroscopic level which are the superelasticity and the shape memory effect [Fugazza, 2003]. The SMA behavior is characterized by two main transformation phases, the austenite (A) and the martensite (S). These phases could be either thermal or stress induced. When a SMA specimen is subjected to uniaxial tensile stress above the austenite start stress σ_s^{A-S}, the phase transformation from austenite to martensite starts (forward transformation). At austenite finish stress σ_f^{A-S}, the phase transformation is complete (martensite). When the specimen is subjected to high stress $\sigma > \sigma_f^{A-S}$, the material exhibits the elastic behavior of the martensite phase. If unloading, the reverse transformation starts at a stress σ_s^{S-A} and is completed at a stress σ_f^{S-A}. The large deformations between both phases (forward and reverse) lead to the formation of a hysteretic loop in the loading/unloading stress-strain diagram (see Figs. 3.18b and 5.1).

Type of SMA wire	E (MPa)	ε_L (%)	σ_s^{AS} (MPa)	σ_f^{AS} (MPa)	σ_s^{SA} (MPa)	σ_f^{SA} (MPa)
GAC® (0.64 x 0.46 mm)	47000	3	350	350	125	125
NDC® (1.49 mm)	60000	8	520	600	240	200
FIP® (2.01 mm)	80000	7	590	670	250	200

Table 3.5: Main mechanical properties of the commercial NiTi SMA wires

Auricchio [1995], Auricchio and Sacco [1997], Desroches and Smith [2003] and Fugazza [2003] describe that the most common SMA devices used for engineering purposes are made of NiTi wires, due to its relatively low cost and superior behavior compared to other SMA compositions. The main manufacturers of NiTi SMA are *GAC International*, *NDC (Nitinol Devices and Components)* and *FIP Industriale* (table 3.5). SMA possesses a unique combination of novel properties such as shape memory affect (large recoverable strains) and superelasticity, high energy dissipation and hysteretic damping capacity, re-centering capabilities, fatigue and corrosion resistance. All these properties have converted SMA in a highly attractive material for engineering applications, especially for the seismic protection of structures. Desroches and Smith [2003] affirm that SMA presents a brittle connection when welded to another material. Dependency to the ambient temperature due to its thermoelastic nature (an increase in temperature is equivalent to a decrease in stress). Moreover, its cyclic behavior presents low damping capacity in the austenite form (4-8%) compared to its martensite form (15-20%).

3.3.4 Applications of prestressing in historical masonry towers

Past intervention techniques used in ancient masonry towers have been used more as local strengthening of certain vulnerable structural parts than for a real improvement of the global behavior of the structure against earthquakes. This is consequence of the limitations in the existing materials in those periods added to the lack of technology and knowledge about the real behavior of these structural elements (Figs. 3.19 and 3.20).

(a) (b)

Figure 3.19: Presence of prestressed metal bars in Italian old masonry towers; (a) bell tower at the Roman Palatino and (b) the civic tower of the "palazzo vecchio" in Florence

Figure 3.20: Metal bars in the upper internal part of the "Torre Grossa" in San Gimignano

A couple of metal bars of rectangular transversal section were usually applied in horizontal way and in two directions in the internal part of towers, at belfry, in order to generate a better connection between walls in the X and Y direction and to provide with this more stability, and to avoid the out-of-plane collapse of the upper walls in case of the occurrence of an earthquake (Figs. 3.19a and 3.20). By the other hand, the tower of Figure 3.19b presents an application of the metal bars at the perimeter of the upper part of the tower as belts aimed at fasting, to avoid with this the overturning. Figure 3.20 depicts the old prestressing system described in section 3.3.2, including connections between segments, tightener and the anchorage inserted through the wall.

The leaning tower of Pisa

One famous case of the application of post-tensioned steel tendons corresponds to the historical masonry tower of Pisa, Italy. The tower has a total height of 58.36 m with an external diameter of 15.54 m and an internal one of approximated 7.37 m. For this important monument the seismic protection is not considered as the main problem as it was mentioned in section 2.4.6.4. This worldwide famous tower has been presenting since its construction geotechnical issues (soil settlements) that started to generate its inclination, inducing with this critical concentration of stresses at certain parts of the structure. Sanpaolesi [1993] and Pavese [1997] describe in their works that its safety was evaluated as a first stage, followed by the analysis of the most suitable retrofitting technique. A band of 18 post-tensioned steel tendons with a diameter of 15 mm each was horizontally installed at the identified critical section to confine the tower at this zone and to increase its overall strength. Fischli [1994] affirms that additionally a counterweight of 600 ton was installed on the north side of the foundation, aimed to stop its inclination and to induce to the tower to reverse. Even when these intervention works were considered as satisfactory in that time for the preservation of the monument, nowadays exists big concerning and controversy between the research community about the safety of the tower and the use of different retrofitting measures, because the vulnerability of the tower to suffer a sudden collapse is still imminent.

The General Post Office clock tower of Sydney

Another important case of the application of prestressing steel tendons corresponds to the historical clock tower of the General Post Office in Sydney, Australia (Fig. 3.21).

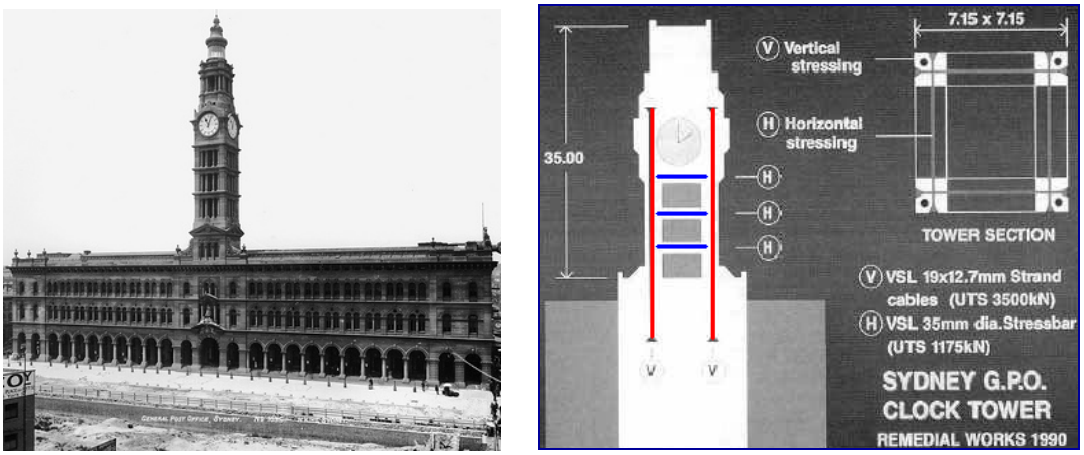

(a) (b)

Figure 3.21: The General Post Office clock tower in Sydney, Australia; (a) general view and (b) details of the retrofitting measure [Ganz, 1990]

Ganz [1990, 2002] describes that the retrofitting intervention in this clock tower was finished in 1990 with the aiming of increasing its global seismic performance by means

of vertical and horizontal prestressing as depicted in Figure 3.21b. Four vertical post-tensioned steel tendons (19 strands of 12.7 mm diameter each and ultimate tensile strength of 3500 kN) were installed in drilled holes of 100 mm diameter trough the corners of the tower. The four tendons were anchored and post-tensioned with prestressing forces of 1771 kN. Twelve horizontal prestressing bars of 35 mm diameter each and ultimate tensile strength of 1175 kN were installed at floor levels. The vertical and horizontal tendons were installed unbounded in order to allow the monitoring and future adjustment of the prestressing forces to compensate volumetric changes.

The bell tower of the church of San Giorgio

This historical masonry tower is located in Trignano, municipality of San Martino in Rio, Reggio Emilia, Italy (Fig. 3.22a). The tower has a total height of 18.5 m with a square base of 3 x 3 m, an average wall thickness of 0.36 m and is surrounded on three edges by the adjacent building up to the height of 11 m. It was strongly damaged by an earthquake occurred on October 15th, 1996 (magnitude 4.8, intensity VII).

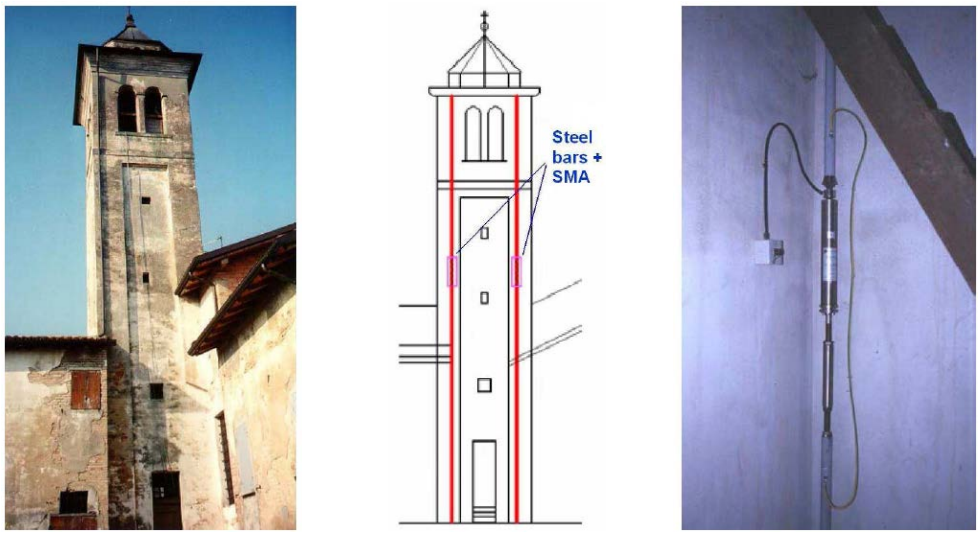

(a) (b) (c)

Figure 3.22: The bell tower of the church of San Giorgio in Trignano; (a) general view; (b) location of the retrofitting and (c) installation of the devices [Indirli et al., 2001]

In 1999 the structure was rehabilitated by means of a replacement of the damaged bricks and sealed up of cracks with especial mortars, as well as the application of new plaster on the internal and external walls. For the retrofitting intervention all the floors were restructured using lighter materials such as timber and the bells were substituted. Moreover, a combination of devices such as steel tendons and SMA were vertically installed and without drilling at the four internal corners of the tower aimed to increase its bending and shear resistance. Each of the four devices was integrated by six segments of steel tendons (to facilitate their assemblage) combined with one SMA

developed by FIP® located at the third floor (Figs. 3.22b-c). Every SMA was fabricated with 60 NiTi superelastic wires (1 mm diameter and 300 mm length). The combined devices were anchored at the top and foundation of the tower and post-tensioned with a prestressing force of 20 kN (80 kN total force) in order to apply a uniform distribution of compressive stresses to the masonry and to keep the applied force constant. This retrofitting intervention has been considered as the first world wide application of this innovative smart material on a historical masonry tower. The retrofitting was verified by the occurrence of a similar earthquake on June 18th, 2000 (M4.5, intensity VI-VII), the tower showed no damage of any type. For more information about the retrofitting of this tower the reader is referred to the works of Indirli et al. [2001], Castellano [2001], Desroches and Smith [2003] and Fugazza [2003].

3.4 Summary

The monitoring and diagnosis campaigns allow obtaining valuable information about a certain historical construction under study. This information consists of structural and geometry identification, state of damages, mechanical and dynamic characteristics. These surveys aim to enhance the knowledge throughout the actual situation of the structure. This physical information allows to the engineer to construct the numerical model of the structure and furthermore its calibration or updating, in order to obtain numerical models more reliable and representative of the real behavior of the structure. These calibrated models represent the basis and reliability of the results throughout the *seismic risk assessment* of the structure in terms of seismic response and failure mechanisms. Afterwards, is necessary to proceed with the selection and analysis of the most suitable retrofitting measure aimed to reduce *the seismic risk*. In both main stages of the seismic risk management the engineer needs a suitable material model able to represent the nonlinear behavior of masonry in static and dynamic conditions depending on the objective of the study, as well as adequate structural analysis tools. Moreover, to design the strengthening solutions to improve the seismic behavior of the structure at key vulnerable parts identified in the seismic risk assessment.

The literature review of chapter 2 presented the key aspects determining the seismic vulnerability of historical masonry towers in terms of behavior and failure modes. A deep understanding of all these aspects is very helpful towards the achievement of their risk reduction, by means of decreasing their seismic vulnerability with prestressing devices, which is the main objective of this thesis. These devices intend to improve the seismic behavior of the towers and to reduce the expected damage with the application of a uniform overall distribution of compressive stresses to enhance the tensile strength of masonry and structural stability. Nowadays, there is a huge variety of available materials for the development of prestressing devices for the seismic retrofitting of structures, including traditional prestressing steel and smart materials such as FRP and NiTi SMA. These smart materials have relevant properties different than those of conventional ones that make them highly attractive for engineering applications, especially for the seismic protection of cultural heritage.

Chapter 4

Seismic Risk Assessment of Historical Masonry Towers

4.1 Introduction

Historical masonry towers have been built all over the world and constitute a relevant part of the architectural and cultural heritage of humanity. Their protection against earthquakes is a topic of great concern among the scientific community. This concern mainly arises from the strong damage or complete loss suffered by this group of structures due to these catastrophic events and the need and interest to preserve them. Although the great progress in technology, seismology and earthquake engineering, the preservation of these brittle and massive structures still represents a major challenge.

Inside the framework of the seismic risk management there are two main stages recommended to be follow as a measure to achieve the protection of the cultural heritage. These stages correspond to the seismic risk assessment and its reduction. Nowadays there is an enormous variety of methodologies to assess the seismic risk (or seismic vulnerability) of buildings ranging from simple (e.g. empirical or qualitative) to more complex quantitative approaches (e.g. analytical-experimental). The selection of the most suitable method depends on factors such as number of buildings, importance, available data, and aim of the study. The empirical methods satisfactorily allow the evaluation of a single building or a complete city in a fast and qualitative way before or after the occurrence of a seismic event (earthquake scenarios). For assessing the vulnerability of an historical building the procedure is different and more in detail than in the qualitative and rough evaluations by empirical methods. It is more complex, requires more computer resources and especial equipment, and represents more time consuming. The literature recommends applying a hybrid approach by combining empirical, analytical and experimental methods in order to obtain more reliable and quantitative results about the amount of damage caused by the seismic action over the

structure. Afterwards, these results of the seismic evaluation are helpful to design, if necessary, the retrofitting solutions.

4.2 Methodology

As aforementioned in the introductory chapter, the *general objective* of this thesis consists of the investigation of the effectiveness of different prestressing devices as a retrofitting measure for the seismic risk reduction of historical masonry towers. The *proposed methodology* to achieve the general objective is integrated by two main stages including the *assessment of risk* and the remedial measures to attain its *reduction*. In the context of this thesis the seismic risk of a certain historical structure located in a seismic zone is determined by the conjunct of the seismic hazard of the site and its structural vulnerability. In chapters 2 and 3 an intensive literature review is presented objected at describing the main aspects that determine the earthquake hazard of a site, the structural vulnerability of historical masonry towers and the recommended in literature to manage the seismic risk. This chapter is focused on the seismic risk assessment stage in terms of seismic response and failure modes. It is developed through validated analytical models of four virtual historical masonry towers commonly found in Europe with variations in geometry, roof system and boundary conditions (see Fig. 4.1).

As a first approximation, the generated 3D finite element (FE) models of the towers are evaluated by linear elastic procedures in order to obtain in a relatively simple way information about the load carrying capacity and dynamic characteristics (natural frequencies and vibration modes). In order to obtain models more reliable and representative of real structures, the numerical results are validated with theoretical back ground and experimental results on similar real towers reported in literature. Before starting with the static and dynamic nonlinear analyses of the towers, the capability of the applied masonry model to simulate the nonlinear behavior of masonry is validated with selected experimental examples reported in literature. Since the towers are theoretical, the seismic hazard is determined at a first instance in qualitative terms by the damage grades of the European Macroseismic Scale and the limit states of the performance-based design philosophy for different earthquake intensities. Moreover, the seismic action is evaluated in quantitative terms by means of the seismic coefficient obtained in the analyses. As a final approximation, intensive numerical simulations developed through a series of nonlinear static and dynamic analyses are carried out for the earthquake evaluation of the historical masonry towers. The results in terms of seismic response and failure modes are validated with reported key-behavioral characteristics and observed damages after considerable earthquakes.

4.3 Seismic risk assessment

Figure 4.1 illustrates the general view and dimensions of the four historical masonry towers under study. They are proposed taking into account typical materials, geometry, roof system and boundary conditions of different towers commonly found in Europe.

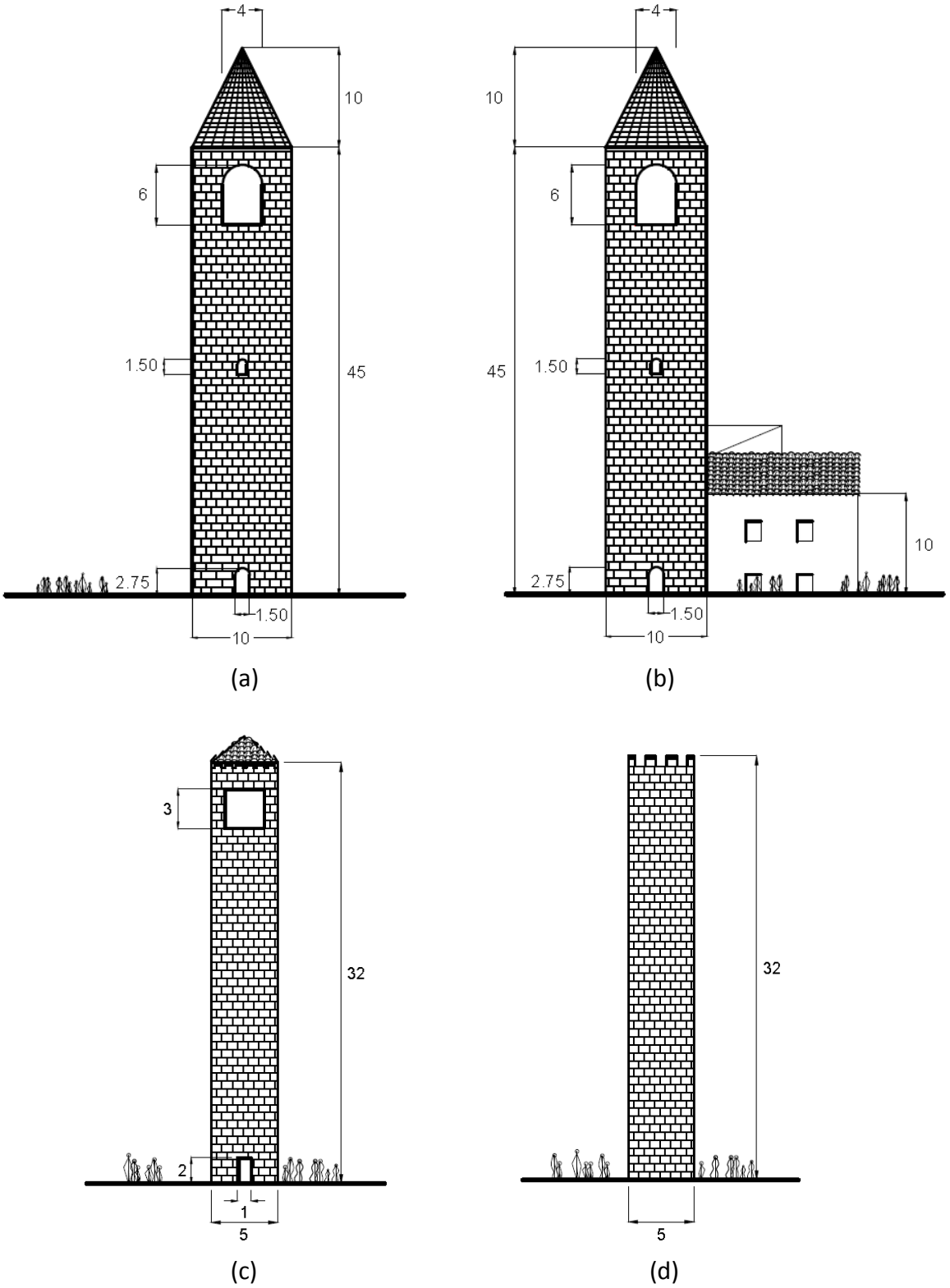

Figure 4.1: General view and dimensions (in m) of the four virtual historical masonry towers; (a) bell tower; (b) non-isolated bell tower; (c) bell tower and (d) medieval tower

The first two towers of Figure 4.1 correspond to bell towers with large openings in the four sides at the belfry level and tall and heavy masonry roof. The tower of Figure 4.1a is isolated and the one of Figure 4.1b has neighbor buildings (non-isolated). The last two are isolated and have light timber roof. One of them is representative of bell towers with only one opening at belfry (Fig. 4.1c) and the other one of medieval towers (Fig. 4.1d) with almost no openings (see table 4.1).

4.3.1 FE models definition of the historical masonry towers

Table 4.1 illustrates the 3D FE models of the four historical masonry towers developed by means of the program ANSYS®. The first two models have the same geometry and roof system but different boundary conditions. For the first model, the tower is considered isolated, and for the second one, the interaction between neighbor buildings is taken into account in the East façade at the height of 10 m and in the North at 15 m (Figs. 4.1a-b and table 4.1a-b).

Dimensions (m)	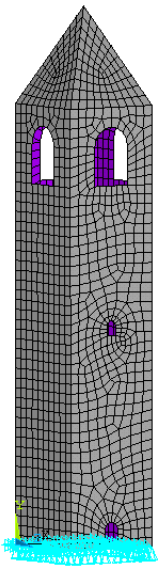 **(a)**	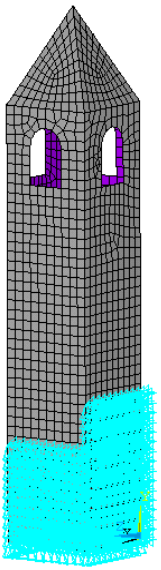 **(b)**	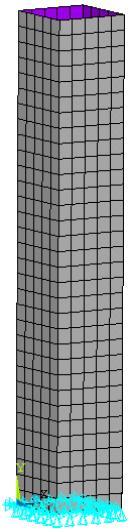 **(c)**	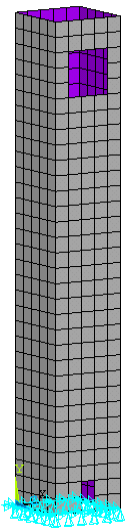 **(d)**
	Isolated	**Non-isolated**	**Isolated**	**Isolated**
Plan	10 x 10	10 x 10	5 x 5	5 x 5
Walls height (thickness)	45 (1.5)	45 (1.5)	32 (1.5)	32 (1.5)
Cover height (thickness)	10 (0.15)	10 (0.15)	-----	-----
Elements (nodes)	2050 (2125)	2050 (2125)	640 (660)	629 (656)
DOF	12627	12627	3900	3876

Table 4.1: Summary of dimensions and FE models of the four historical masonry towers

The third and fourth models have a light timber roof common of this kind of structures that could be neglected in the analyses (see Figs. 4.1c-d and table 4.1c-d). Both models are isolated and have the same dimensions, being different the presence of openings in one of the towers. As a reference point at the models, the accesses at the base level are located in the South façade of the towers.

The selected FE for walls and roofs is shell43, which has four nodes and four thicknesses with six degrees of freedom at each node. This element could represent the in-plane and out-of-plane behavior and has plasticity and creep capabilities. In the generation of the four numerical models the following main assumptions were taken into account: Since the type of foundation and soil properties are not considered, all the base nodes are assumed as fixed. The main mechanical properties of the ancient masonry were taken into account average values reported in literature (see table 2.5). The selected masonry is considered as carved stone with lime mortar, average density of 2000 kg/m^3 and a Young´s modulus of 2000 MPa. The Poisson´s ratio is held constant and equal to 0.15. Regarding the strengths, 3.5 MPa is assumed for compression and 0.25 MPa for tension. At the non-isolated model (table 4.1b), the interaction with neighbor buildings in the North and East façades is simulated by a uniform distribution of linear elastic springs of constant stiffness (275 combin14 elements). The stiffness (118.68 kN/mm) is defined by considering the experimental dynamic investigations on neighbor buildings contribution on similar towers by Pallares [2006]. In the case studies of this thesis, the spring´s stiffness is obtained by the models calibration with real experimental data (see sections 2.3.2.3, 3.2.1, and chapter 6).

4.3.2 Validation of the proposed FE models by linear analysis

As a first approach and aimed at obtaining significant progress on the seismic risk assessment of the virtual towers without the convergence problems related to nonlinear analyses, static and dynamic linear evaluations such as vertical loading and modal are developed. This first approach based on linear principles permits to determine the presence and magnitude of tensile and compressive stresses in the masonry structure generated by vertical loading, as well as the dynamic properties (frequencies and vibration modes) in the modal analysis. In the generation of structural models of real historical constructions there are many assumptions and uncertainties regarding the determination of geometry, material properties, support and boundary conditions. In this case, the linear analyses could be used to calibrate (or up-date) the initial model with the experimental data by adjusting geometry, material properties and interaction with adjacent buildings. This permits to obtain models more representative of the structure under study, and with this, a reliable seismic vulnerability assessment.

4.3.2.1 Simulation and analysis of load bearing capacity

This approach is often used to assess the vertical load carrying capacity of a building under self weight and service conditions. In the case of historical masonry towers the vertical load plays an important role in the seismic behavior, because these structures

were constructed by empirical rules only to withstand their self weight. These massive structures are extremely heavy and slender, presenting important inertia forces amplifications during an earthquake that could generate strong damage. Moreover, this long-term heavy loads and progressive damage of masonry could lead to a sudden collapse as in the cases of Venice (1902), Pavia (1989) and Goch (1992) (see section 2.4.6.3). Therefore is important for the seismic analysis to firstly evaluate the distribution of vertical stresses at different parts of the structure and to verify that they are not higher than the intrinsic strength. In the case of historical towers usually the zone most over stressed is the bottom of the structure. This compression could generate the local failure of masonry (see Fig. 2.10) and may be the trigger of the sudden collapse (global failure). This linear static analysis could be helpful as well for the identification of concentration of stresses at structures that present differential settlements in poor soil conditions (e.g. tower of Pisa, Italy and the Metropolitan Cathedral of Mexico City).

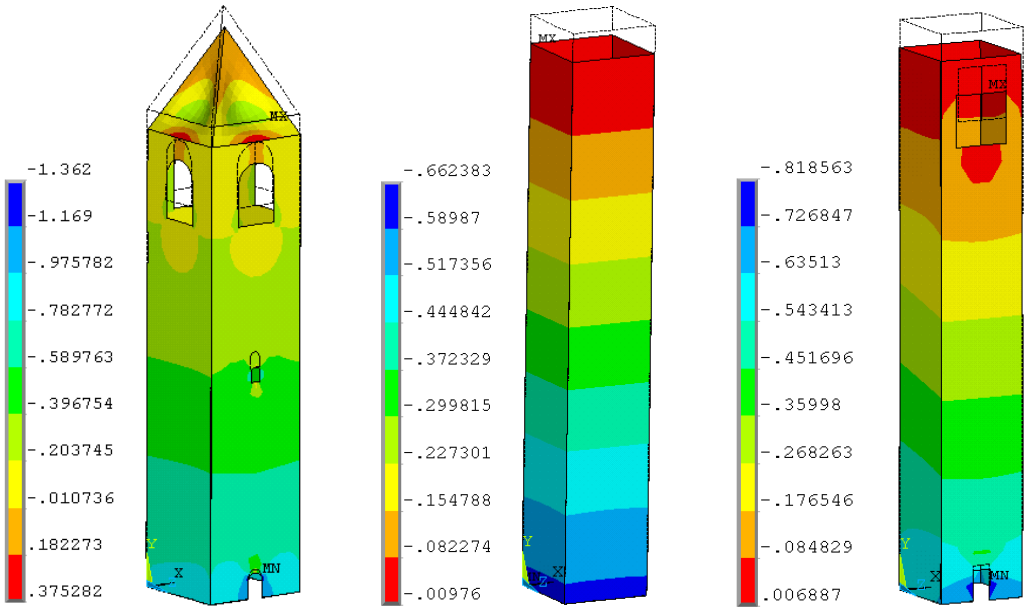

(a) (b) (c)

Figure 4.2: Vertical distribution of stresses at the FE models [units in MPa]

The models with triangular roof present the same vertical distribution of stresses because they have the same mass (interaction with neighbor buildings has no influence). Therefore only one tower is depicted (Fig. 4.2a). In the case of the other two towers (Figs. 4.2b and c), there is a small variation of mass by the presence of openings. The higher the mass, the higher the compressive stresses at the bottom part. However, the maximum values are present at the doors due to the reduction of the resistant area (see Figs. 4.2a and c). The two towers with triangular roof present tensile stresses at the base of the cover. This is in agreement with real behavior observed in similar structures. The important flexion of the roof due to the heavy weight and height generates

horizontal cracking similar to the case of domes that tends to open at the lower part due to tensile stresses by elevated self weight and temperature effects. This triangular roof definitely could have been collapsed since its construction. Therefore is quite common to observe in Europe tall triangular roofs of this type made of timber, and when built with masonry, have reduced inclination and height. The analysis revealed that the complete tower is basically in linear conditions, since the level of compressive stresses are lower than the assumed masonry strength, and tensile stresses are not present in a large zone. These results allowed the validation of the FE models of the towers regarding vertical loading, concluding that the towers were stable to satisfactorily resist at least their own self weight as expected in most of the historical constructions.

When real masonry towers are assessed, these results of vertical distribution of stresses may be used to compare those obtained from the experimental in-situ campaigns developed in different parts of the structure, usually by means of flat jack tests. Subsequently, with this experimental data is possible to calibrate the initial FE model in the static field. It could be analyzed again, and if it was successfully calibrated, the results of the vertical stresses are in agreement with those of the flat jack tests.

4.3.2.2 Simulation and analysis of vibration characteristics

In order to obtain a first estimation of the dynamic response of the four virtual towers, the linear investigations are extended to dynamic analyses.

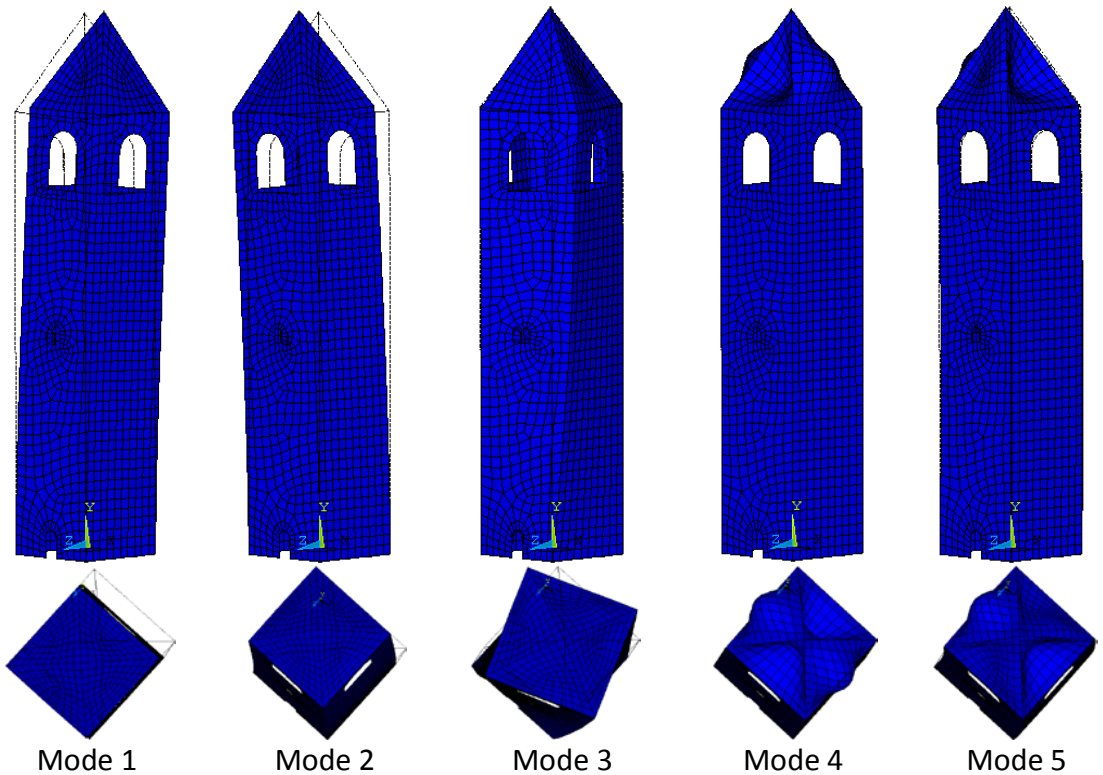

Figure 4.3: Vibration modes of the isolated bell tower with masonry roof (type a)

Mode no.	Vibration mode	Frequency (Hz)		Period (s)	
		Isolated tower	Non-isolated tower	Isolated tower	Non-isolated tower
1st	Bending N-S	1.046	1.293	0.956	0.773
2nd	Bending E-W	1.051	1.133	0.951	0.883
3rd	Torsion	3.313	3.702	0.302	0.270
4th	Vertical	3.464	3.464	0.289	0.289
5th	Vertical	3.935	4.138	0.254	0.242

Table 4.2: Modal parameters of the two bell towers with masonry roof (type a and b)

As in the case of the vertical loading analyses, the modal evaluations of FE models are relatively fast due to the progress of recent decades on computational tools. As a first stage, the dynamic parameters of the isolated and non-isolated towers with masonry roof are numerically obtained. The resulting *vibration modes* of both towers are similar, therefore only the modes of the isolated tower (type a) are depicted in Figure 4.3. By the other hand, the *natural frequencies* of the non-isolated model (type b) are higher (lower periods) as it was expected due to the increment of stiffness (about 24% in the N-S direction and 8% in the E-W) generated by the assumed contact with neighbor buildings (table 4.2).

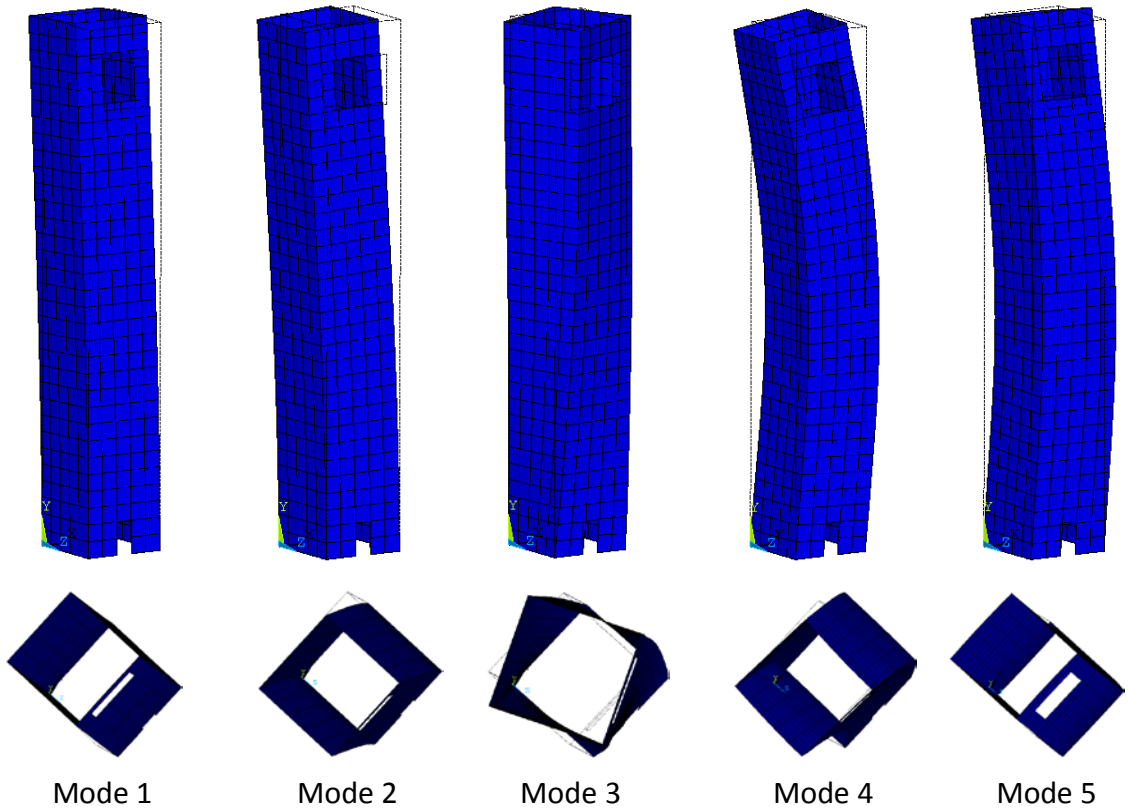

Figure 4.4: Vibration modes of the isolated tower with timber roof (type d)

Analyzing the results of Figure 4.3 and table 4.2, it could be observed that the two fundamental vibration modes of both towers correspond to a general flexion. This low frequencies (high periods of about 1 s) and vibration modes are representative of the real behavior of slender and tall structures as in the case of historical masonry towers, which are highly vulnerable to earthquake motions (see section 2.4.6). The higher modes represent torsion and a particular problem of vertical vibration due to the tall and heavy roof. Afterwards, the natural frequencies and vibration modes of the isolated towers with timber roof (type c and d) are numerically obtained as presented in Figure 4.4 and table 4.3. In this case the vibration modes and frequencies are similar as in the case of the towers with heavy roof (type a and b), the two fundamental vibration modes of these towers correspond as well to a general flexion in the two orthogonal directions.

Mode no.	Vibration mode	Frequency (Hz)		Period (s)	
		Medieval tower	Bell tower	Medieval tower	Bell tower
1st	Bending N-S	1.064	1.076	0.940	0.929
2nd	Bending E-W	1.064	1.083	0.940	0.923
3rd	Torsion	4.732	4.723	0.211	0.212
4th	Bending E-W	5.255	5.162	0.190	0.194
5th	Bending N-S	5.255	5.272	0.190	0.190

Table 4.3: Modal parameters of the two towers with timber roof (type c and d)

To validate the numerical natural frequencies of the virtual towers obtained in the modal analysis, an extensive literature review was developed. Bachmann et al. [1997] and Casolo [1998] describe in their works that the natural frequencies of slender masonry towers are measured between 0.9 and 2 Hz (periods between 1.11 and 0.5 s). The Spanish Standard NCSE [2002] considers a masonry structure as slender when its first natural period is comprised between 0.75 s < T < 1.25 s (0.8 Hz < f < 1.33 Hz). The same Standard proposes an analytical formula to approximately assess the first frequency of masonry bell towers (see Eq. 4.1). Where L corresponds to the plan dimension in the vibration direction and H is the height of the tower. The suitability and efficiency of this equation as a first and quick estimation (or validation of numerical and experimental results) of the first natural frequency of real masonry bell towers have been proved by many researchers in Europe, e.g. Ivorra and Pallares [2006], Ivorra et al. [2008] and Bayraktar et al. [2009].

$$\omega_1 = \frac{\sqrt{L}}{0.06\,H\sqrt{\frac{H}{2\,L+H}}} \quad \text{(Hz)} \qquad [4.1]$$

As a result of applying Eq. 4.1 to the four FE models of the virtual towers in the vibration direction E-W, the isolated tower with masonry roof (type a) is supposed to

have a first natural frequency of 1.119 Hz. The result is in good agreement with the one obtained in the numerical simulation for the same direction (1.051 Hz). For the case of the non-isolated tower with masonry roof (type b) is expected a greater first natural frequency as a consequence of the contact with neighbor buildings. The increment in stiffness is obtained in the numerical simulations (see table 4.2). For the case of the two towers with timber roof, Eq. 4.1 does not consider the influence of openings in the total mass. Therefore both first natural frequencies in the E-W direction are the same and correspond to 1.334 Hz (numerical simulations 1.064 Hz and 1.083 Hz).

$$f_1 = \frac{a}{2\pi}\sqrt{\frac{EI}{\mu H^4}} \quad \text{(Hz)} \qquad [4.2]$$

$$\omega = \sqrt{\frac{K}{m}} \quad \text{(Hz)} \qquad [4.3]$$

Another approach found in literature for obtaining the first frequency of slender structures is the developed by BVE [2000]. Eq. 4.2 considers the slender structure as a cantilever beam of any material, uniform cross section and uniformly distributed loads. Here E corresponds to the material Young´s modulus (N/m^2), μ the uniformly distributed load (Kg/m), H the length of the beam (m), I the moment of inertia (m^4), and a is a constant value (for cantiliver beams with fixed footing a = 3.52). Eq. 4.2 is used to obtain the first frequency of the isolated tower with triangular roof (type a). The mass contribution of the triangular roof and walls (discounting openings) is represented as a distributed load. The estimated first frequency corresponds to 0.987 Hz and higher for the stiffer non-isolated with heavy roof (type b). This equation allows obtaining similar results like those of the numerical simulations (1.051 Hz). For the medieval (type c) and bell towers (type d) with timber roof, the expected first frequencies are in the order of 0.850 Hz and 0.859 Hz respectively (numerically 1.064 Hz and 1.083 Hz).

Reference	Modal	NCSE [2002]	Error	BVE [2000]	Error
	E-W	E-W	(%)	E-W	(%)
Isolated heavy roof	1.051	1.119	6.47	0.987	6.09
Non-isolated heavy roof	1.133	1.119	1.24	0.987	12.89
Isolated light roof	1.064	1.334	25.38	0.850	20.11
Isolated light roof (openings)	1.083	1.334	23.18	0.859	20.68

Table 4.4: Comparison of frequencies (Hz) between modal analysis and the equations

Table 4.4 presents a resume of the first natural frequencies estimated by Eqs. 4.1 and 4.2, as well as the comparison to those obtained in the numerical simulations. The slight difference in the first natural frequencies of the towers with timber roof is due to

the mass. Eq. 4.2 is based on Eq. 4.3, which represents the frequency of a system of one DOF. In this equation m corresponds to the mass and K to the stiffness respectively. So, it could be noticed that the higher the mass, the lower the frequency of the structure.

Reference	Tower height	Frequency (Hz)		Period (sec)	
		1st	2nd	1st	2nd
Ramos et al. [2010]	20.40	2.15	2.58	0.47	0.39
Bayraktar et al. [2009]	22.00	2.56	2.66	0.39	0.38
Ivorra et al. [2008]	33.90	2.15	2.24	0.47	0.45
Slavik [2002]	35.00	1.10	1.30	0.91	0.77
Ivorra and Pallares [2006]	41.00	1.29	1.49	0.78	0.67
Abruzzese et al. [2009]	41.00	1.26	1.29	0.79	0.78
Lund et al. [1995]	43.50	1.38	1.82	0.72	0.55
Abruzzese et al. [2009]	45.50	1.05	1.37	0.95	0.73
Russo et al. [2010]	58.00	0.61	0.73	1.64	1.37
Gentile and Saisi [2007]	74.10	0.59	0.71	1.69	1.41

Table 4.5: Natural frequencies of real historical masonry towers

As a final validation, the natural frequencies obtained with the modal analysis and equations could be compared to experimental results obtained by different authors throughout dynamic characterization in real historical masonry towers with different heights. Here it could be observed that the frequency reduces with the height increasing, the structure is more slender, and due to this more flexible (see table 4.5).

4.3.3 Validation of the applied masonry constitutive model

In this section, the capability of the applied masonry constitutive model to simulate the different failure behavior of masonry structures is validated by means of the theoretical background presented in chapter 2 and selected experimental examples reported in literature (see section 3.2.2.2). Preliminary, the compressive and shear failure behavior of two walls with geometry and material representative of historical masonry is evaluated. The experimental results on masonry shear walls tested at the TU Eindhoven by Raijmakers and Vermeltfoort [1992] and Vermeltfoort and Raijmakers [1993] serve as a final verification of the material model.

4.3.3.1 Uniaxial compression tests on ancient masonry walls

The objective of this first numerical test is to analyze the performance of the model to predict the softening phenomenon of masonry under uniaxial compression and to compare the results to similar experimental tests. This phenomenon is associated with quasi-brittle materials as concrete and masonry and is characterized by a gradual decrease of strength under a continuous increase of deformation (Fig. 4.5).

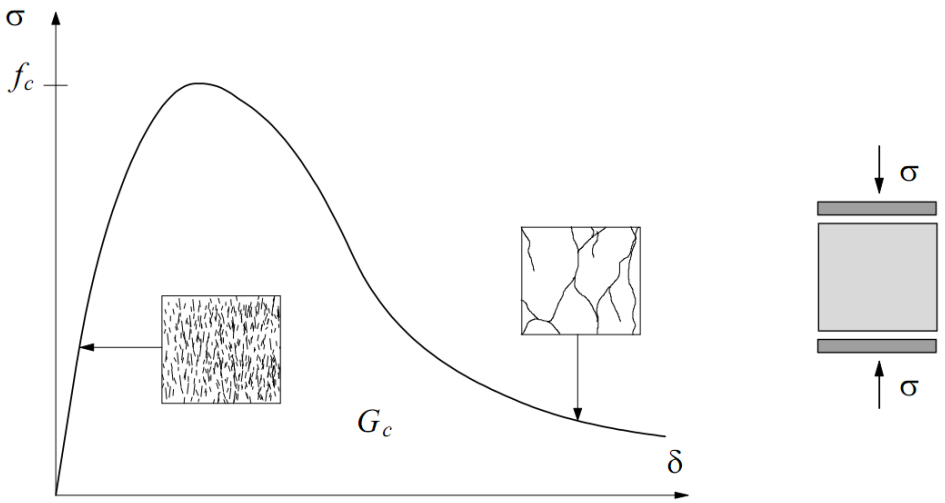

Figure 4.5: Typical behavior of quasi-brittle materials under uniaxial compression and definition of fracture energy (f_c denotes the compressive strength) [Lourenço, 1996]

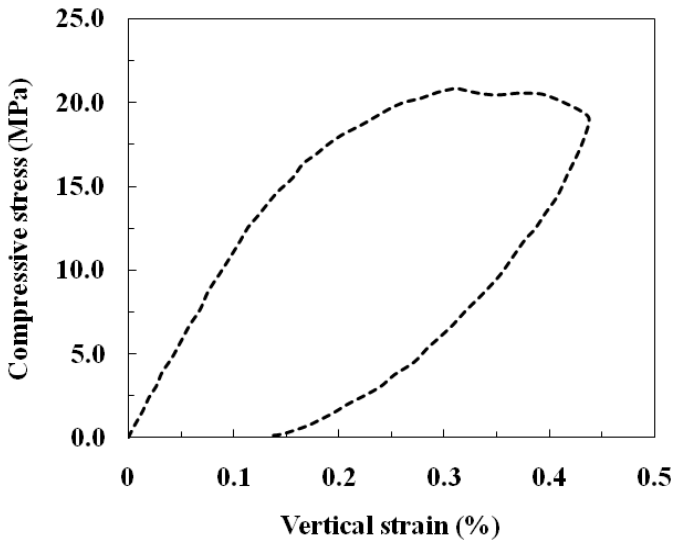

Figure 4.6: Envelope of experimental results on masonry walls subjected to uniaxial compression tests [Van der Pluijm and Vermeltfoort, 1991]

The reference results are the experimentally obtained by Van der Pluijm and Vermeltfoort [1991]. The researchers tested different masonry panels subjected to uniaxial compression tests by means of deformation control. The envelope of experimental results showed a maximum compressive strength in the order of 20.8 MPa and a vertical strain of 0.32% (typical value) as depicted in Figure 4.6.

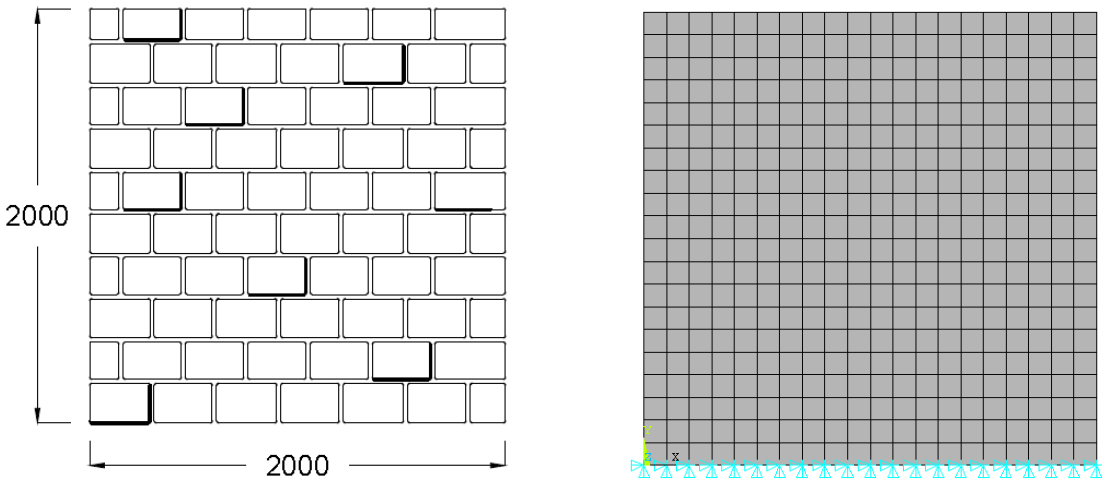

(a)

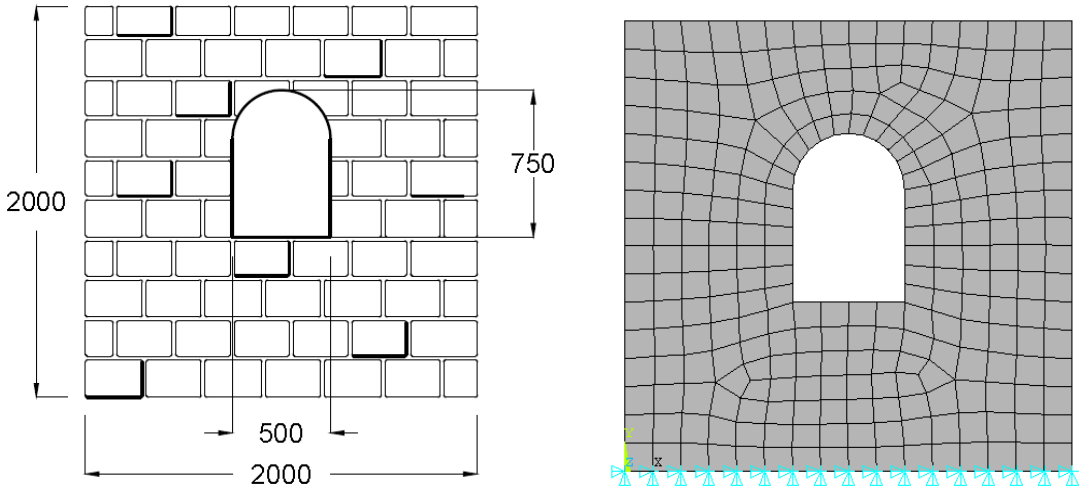

(b)

Figure 4.7: Dimensions (mm) and FE models of walls representative of old masonry structures; (a) simple wall and (b) wall with central opening

To validate the applied material model of Gambarotta and Lagomarsino [1997] under uniaxial compression load, one wall with geometry and material representative of historical masonry is evaluated. The wall has a thickness of 300 mm and dimensions of 2000 x 2000 mm (see Fig. 4.7a).

The considered masonry type is organized (see Fig. 2.7a), made of carved stone with lime mortar. The FE model is constructed with shell43 elements as shown in Figure 4.7a. The elastic parameters are the same like those used in the linear analyses of the virtual

towers previously described in section 4.3.1. The inelastic parameters are taken from Urban [2007] mentioned in section 3.2.2.2. In order to numerically simulate a traditional uniaxial compression test, the FE model is firstly loaded with gravitational force, and then, the uniaxial compression is applied under monotonically increased vertical displacement control. The results show a maximum vertical force at yielding of 2019 kN and a maximum displacement of 6.51 mm (see Figs. 4.8a and 4.9a).

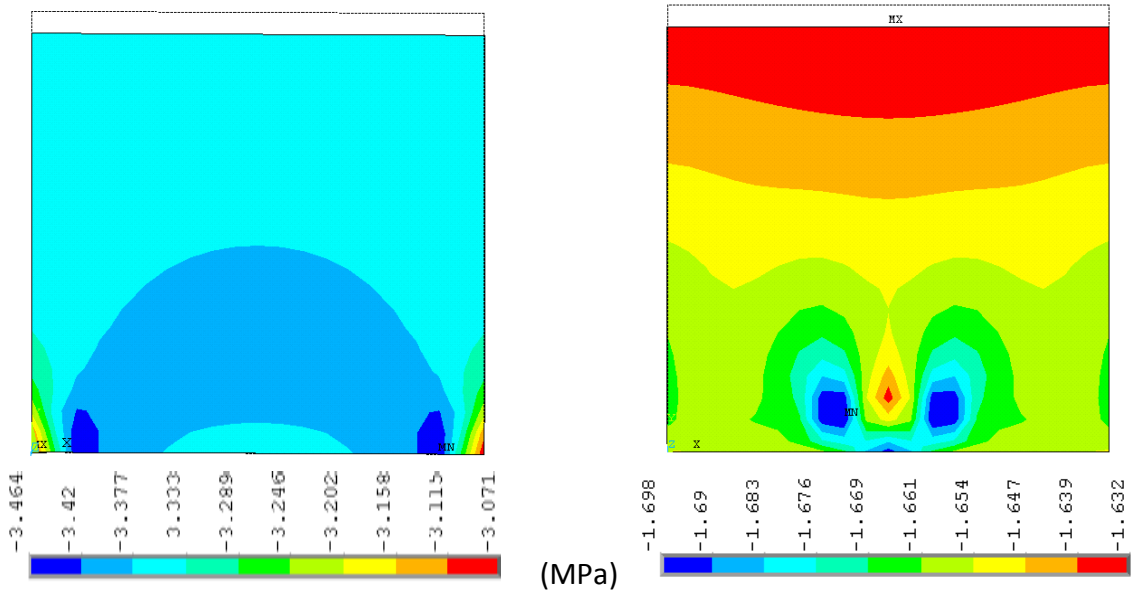

Figure 4.8: Simple wall. Vertical stress contours at a vertical displacement of: (a) 6.51 mm (yielding) and (b) 6.72 mm (after yielding)

Figures 4.8 and 4.9 illustrate the results of the numerical simulation at yielding and after yielding by means of the vertical stress distribution and the damage, represented by the vertical plastic strain contours. Due to visual purposes, the nodal solution is presented, instead of the element solution with the meshes.

By increasing the deformation, is evident a high concentration of stresses at the wall bottom, leading to the formation of a collapse mechanism represented by brittle failure with explosive behavior due to crushing of the compressed zone, firstly by the wall toes at yielding (Figs. 4.8a and 4.9a) and subsequently the rest of the base as illustrated in Figures 4.8b and 4.9b. Figure 4.10 depicts the stress-strain curve of the numerical compression test on the simple wall. It is worth noting that the model is capable to capture the softening behavior of masonry up to the yielding of the material as shown in Figure 4.5 and the post-peak behavior of the experimental tests of Figure 4.6, characterized by a descending branch.

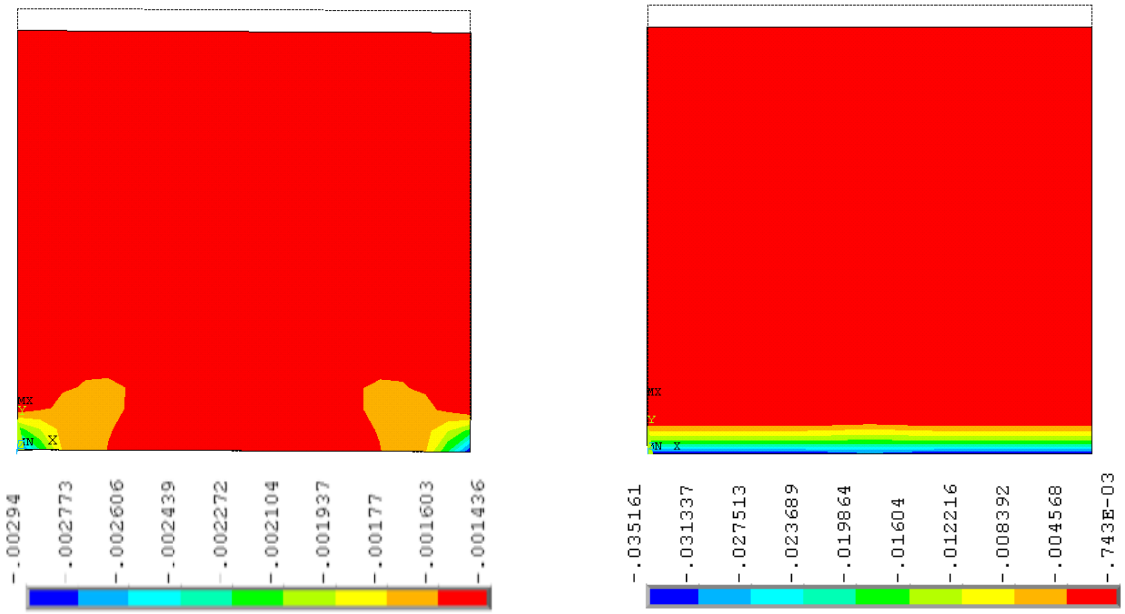

(a) (b)

Figure 4.9: Simple wall. Vertical plastic strain contours at a vertical displacement of: (a) 6.51 mm (yielding) and (b) 6.72 mm (after yielding)

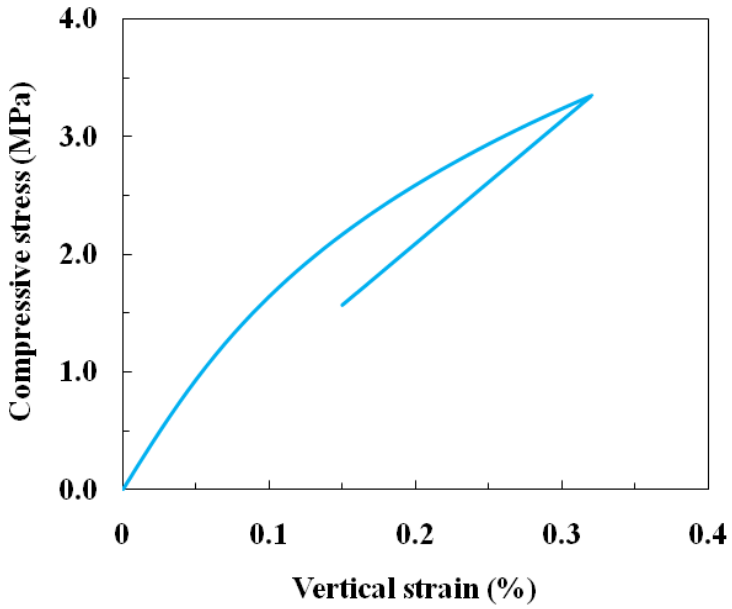

Figure 4.10: Simple wall. Vertical stress-strain curve

4.3.3.2 In-plane load tests on ancient masonry walls

In order to validate the capability of the applied constitutive model to simulate the nonlinear behavior of masonry, the walls of Figure 4.7 are subjected to numerical tests

under in-plane lateral loading. The masonry is made of carved stone with lime mortar. The FE models are built with shell43 elements and the used material data is described in section 4.3.1 and 3.2.2.2. In order to numerically simulate a traditional in-plane load test, the FE models are firstly loaded with gravitational force and no other precompression to allow a free top rotation. In a second stage, the horizontal force is applied under monotonically increased top displacement control. The main failure modes of masonry walls under static lateral loading are described in section 2.4.4. Failure occurs as: (1) bed joint sliding, (2) stepped cracking by low vertical loading (trough head and bed joints), (3) diagonal cracking by high vertical loading (trough joints and units), (4) horizontal cracking and rocking by bending, and (5) masonry crushing.

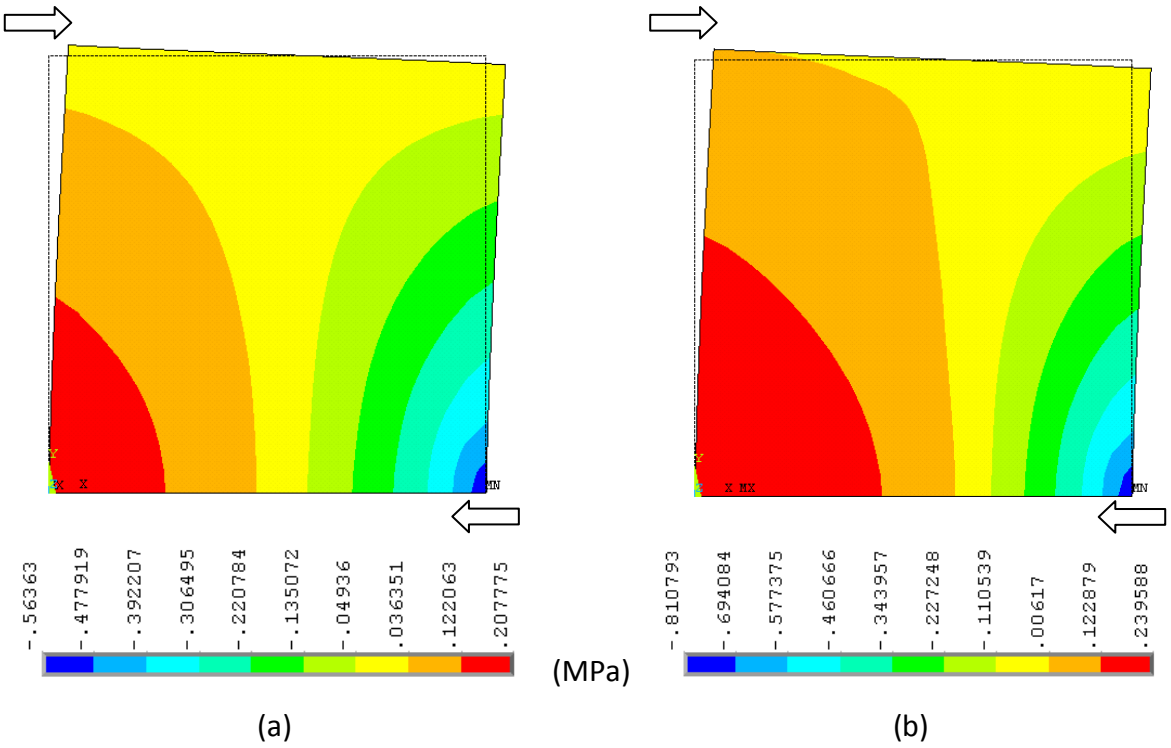

Figure 4.11: Simple wall. Vertical stress contours at a displacement of: (a) 0.5 mm and (b) 0.8 mm (failure mechanism)

The results of the in-plane load test of the simple wall are depicted in Figures 4.11 and 4.12. At an early load stage, the wall presents the initial generation of a horizontal crack at the base due to bending as depicted in Figures 4.11a and 4.12a. At increasing displacement, the horizontal crack is extended, leading to a base uplifting and a sudden brittle collapse of the wall due to the low vertical loading. This could be described from the tensile stress distribution of Figure 4.11b and the damage (plastic strains) of Figure 4.12b. Moreover, this brittle behavior could be clearly observed in the load-displacement diagram of Figure 4.15. The simple wall reaches a maximum lateral force of 47 kN for a top displacement of about 0.8 mm.

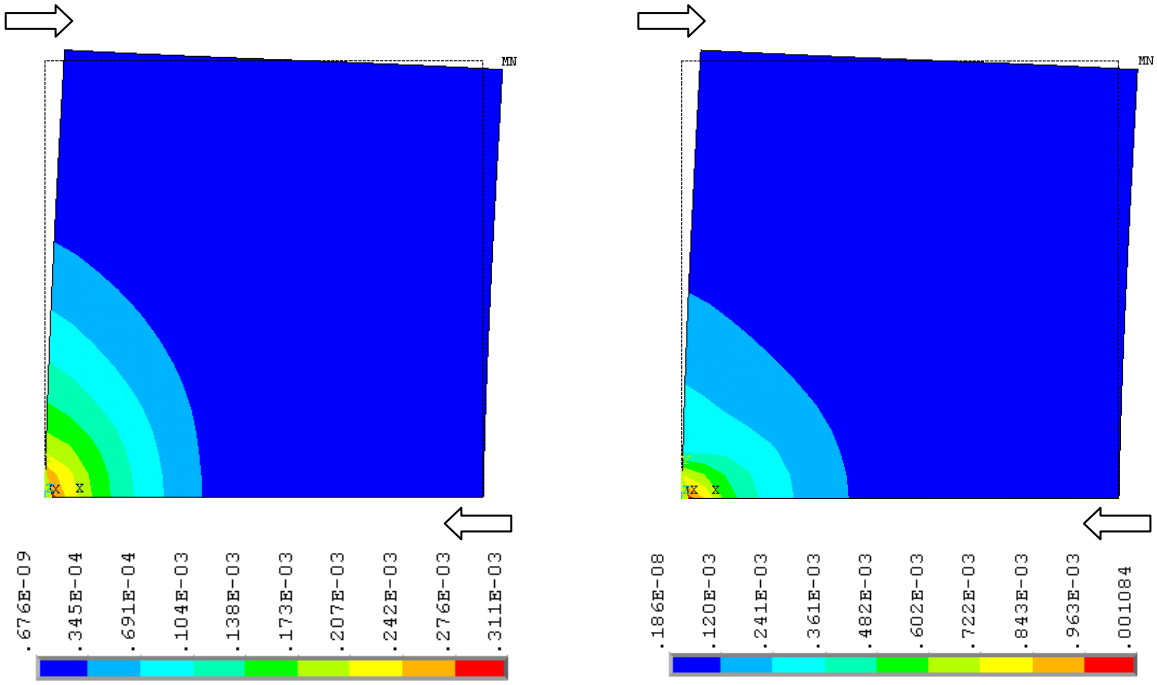

(a) (b)

Figure 4.12: Simple wall. Principal plastic strain contours at a displacement of: (a) 0.5 mm and (b) 0.8 mm (failure mechanism)

By the other hand, the wall with opening presents a different behavior. At a displacement of 1.5 mm, the early presence of horizontal cracks due to bending is evident at the lower middle part of the wall as well as the start of a stepped crack at the upper and bottom parts of the window (see Figs 4.13a and 4.14a). Subsequently, a complete failure mechanism is formed at a displacement of 2.6 mm represented by the extension of the horizontal and stepped cracks through the mortar joints due to the low vertical loading (see Figs 4.13b and 4.14b).

The load-displacement diagram of Figure 4.15 depicts the linear and nonlinear behavior of both numerical models of the walls, being stiffer the behavior of the one with solid section. The wall with opening presents about 21% more lateral force capacity and 225% more top displacement, withstanding an ultimate force of 57 kN at 2.6 mm. This contrast in strength and ductility in the wall with opening is due to the different crack pattern that leads to more energy dissipation as explained in section 2.4.4. The same tendency in masonry shear walls of solid section and with opening was experimentally observed by Raijmakers and Vermeltfoort [1992] and Vermeltfoort and Raijmakers [1993], and by means of numerical investigations by Lourenço [1996].

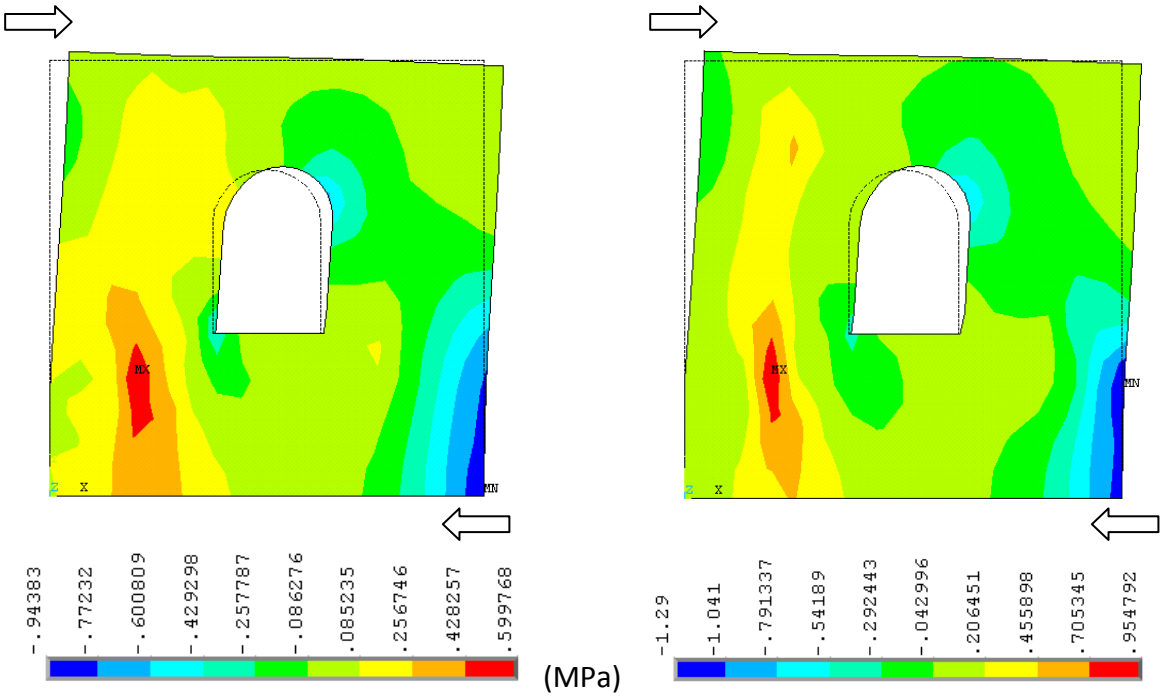

Figure 4.13: Wall with opening. Vertical stress contours at a displacement of: (a) 1.5 mm and (b) 2.6 mm (failure mechanism)

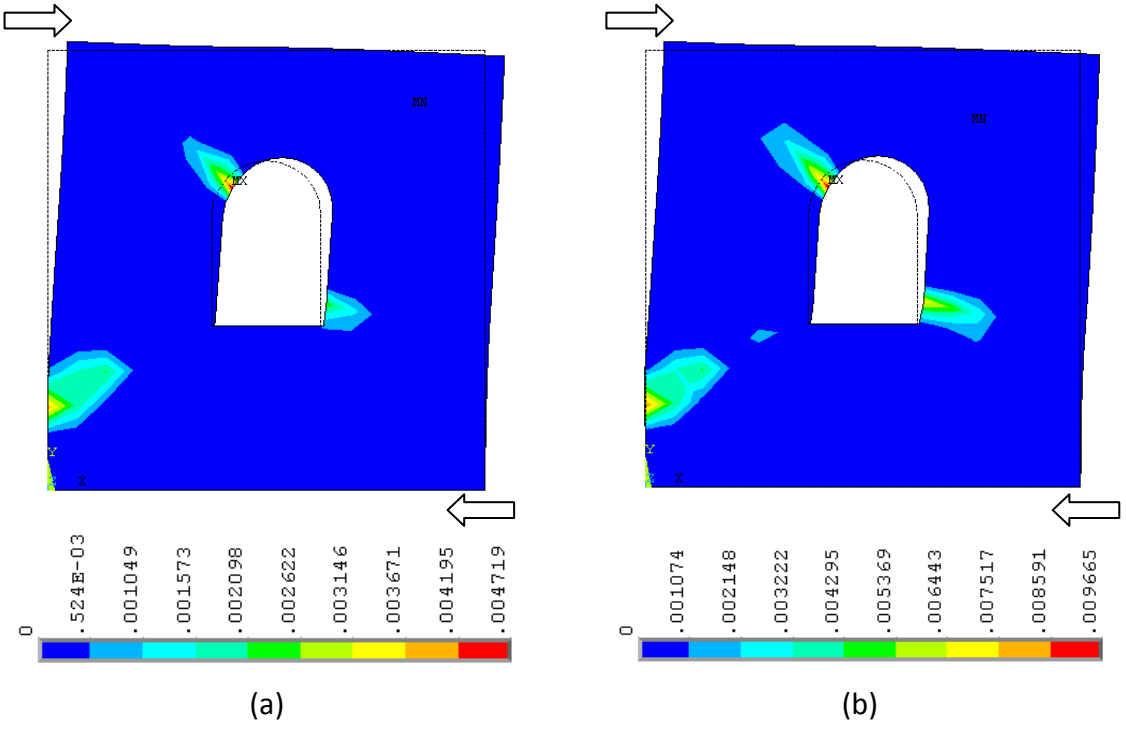

Figure 4.14: Wall with opening. Principal plastic strain contours at a displacement of: (a) 1.5 mm and (b) 2.6 mm (failure mechanism)

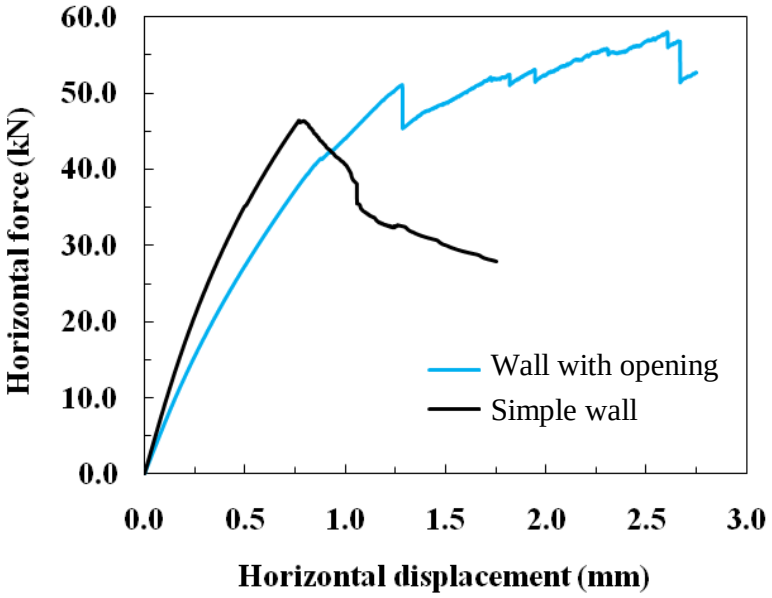

Figure 4.15: Simple wall and wall with opening. Load-displacement diagram

4.3.3.3 Masonry shear walls tests of the TU Eindhoven

Experimental tests on masonry shear walls with and without opening were carried out at the TU Eindhoven by Raijmakers and Vermeltfoort [1992] and as well as by Vermeltfoort and Raijmakers [1993]. The walls have dimensions of 990 x 1000 mm, built up with 18 courses, from which 16 courses are active and two courses are clamped in steel beams. The walls are made of wire-cut solid clay bricks with dimensions 210 x 52 x 100 mm and 10 mm thick cement: lime: sand (1:2:9) mortar [Lourenço, 1996]. The selected wall to numerically simulate this experimental test is the named J2G, which corresponds to the one with a central opening depicted in Figure 4.16a.

The FE model of the wall (see Fig. 4.16b) is firstly loaded with a precompression of 0.30 MPa (30 kN) and subsequently a horizontal load is monotonically increased under top displacement control. The top and bottom clamped courses with the steel beams aim to keep the wall in horizontal position with no top rotation (see Figs. 4.16-19). The selected FE elements for the numerical simulation of this experimental test are shell43. The material parameters described by Lourenço [1996] and the inelastic parameters of section 3.2.2.2 are taken into account in the analysis. The FE model is firstly loaded with the gravitational force and in a subsequent step the precompression is applied. Afterwards, the horizontal force is applied under monotonically increased top displacement control. The numerical results of Figures 4.18a and 4.19a illustrate an early formation of stepped cracks at two corners of the opening and horizontal cracks arise at the base and top opposite side of the loading direction. The concentration of compressive stresses at the top and bottom toes of the wall becomes evident. Subsequently, at a displacement of about 7.5 mm and a lateral force of 47 kN (Fig. 4.20), the wall reaches its ultimate limit capacity, leading to the formation of a predominant

collapse mechanism (Fig. 4.17) represented by the extension of the horizontal and stepped cracks and the failure by crushing of the compressed top and bottom toes (see Figs. 4.18b and 4.19b). Due to the relative low vertical loading, the horizontal cracks are formed through bed mortar joints and the stepped cracks through both, bed and head mortar joints as depicted in the experimental crack pattern of Figure 4.17.

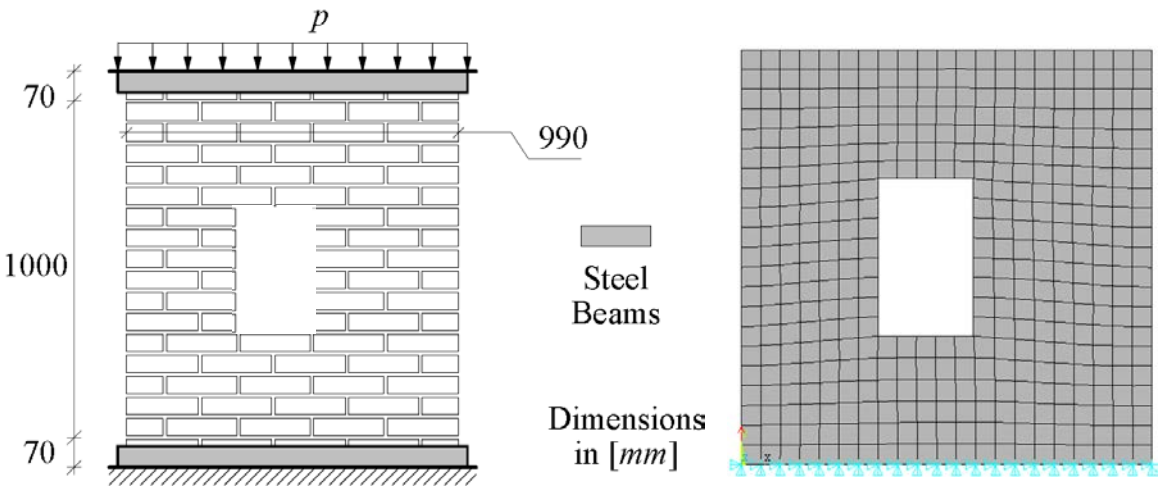

Figure 4.16: Wall J2G of TU Eindhoven. (a) dimensions [Lourenço, 1996] and (b) FE model

The load-displacement diagram of Figure 4.20 depicts the comparison between the experimental and numerical results of the in-plane load test on the wall J2G with opening. It is worth noting that the wall reaches its ultimate limit capacity at a displacement of about 7.5 mm and a lateral force of 47 kN. The material model is able to satisfactorily capture the linear and nonlinear behavior of the experimental test.

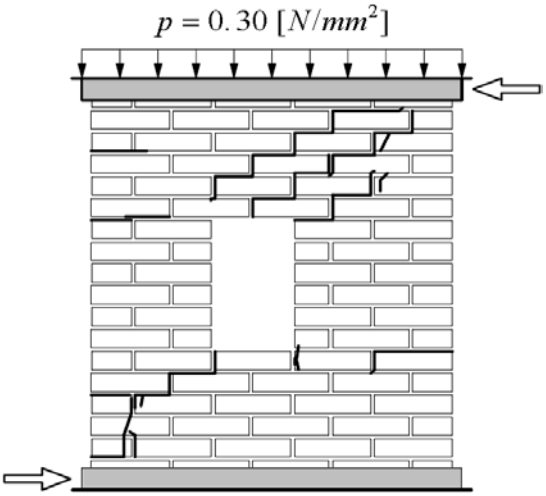

Figure 4.17: Wall J2G. Experimental crack pattern at final stage [Lourenço, 1996]

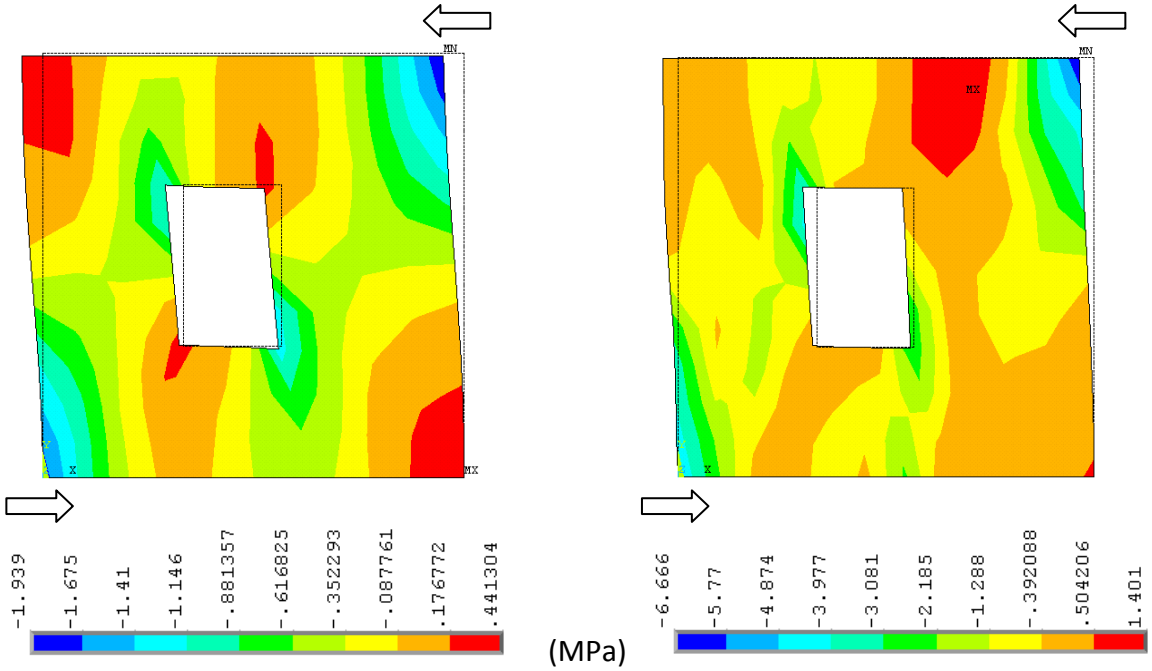

Figure 4.18: Wall J2G. Vertical stress contours at a displacement of: (a) 1 mm and (b) 7.5 mm (failure mechanism)

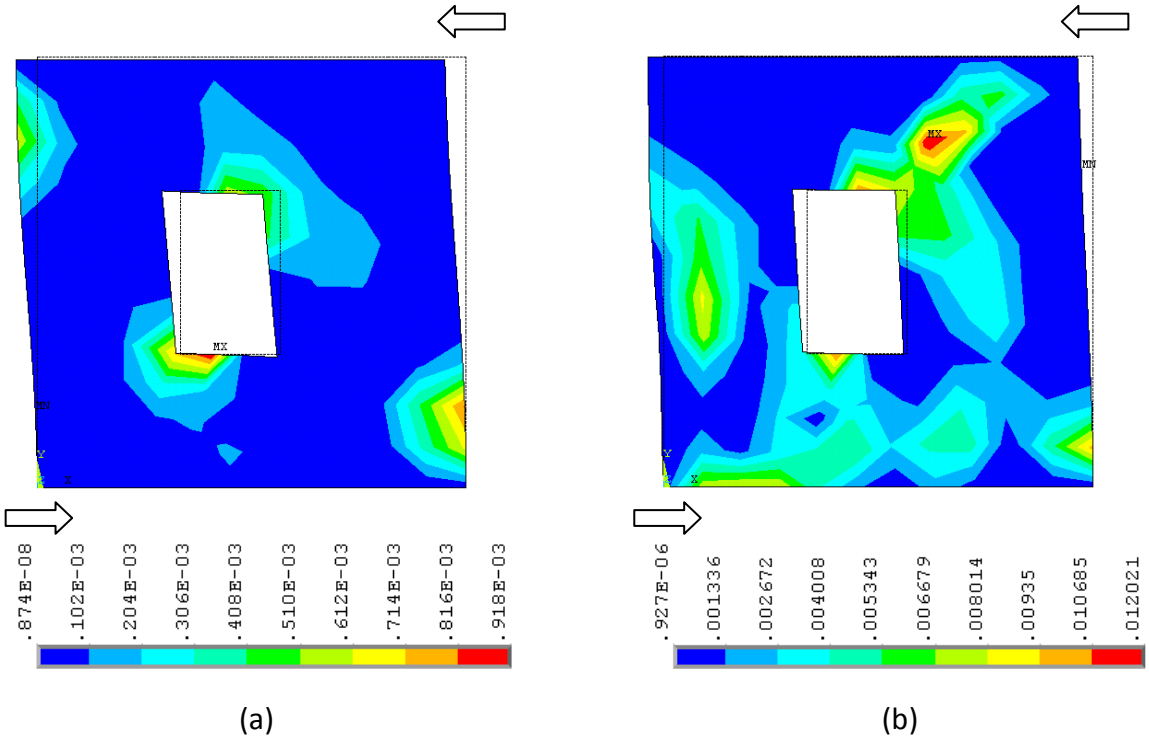

Figure 4.19: Wall J2G. Principal plastic strain contours at a displacement of: (a) 1 mm and (b) 7.5 mm (failure mechanism)

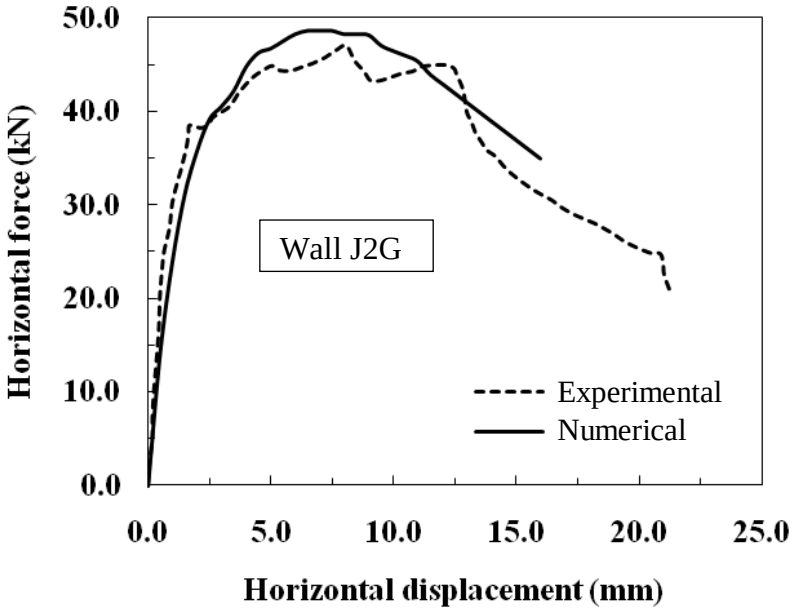

Figure 4.20: Wall J2G. Numerical and experimental load-displacement diagram

In this section a comparison between numerical and experimental results in terms of failure mechanisms and load-displacement diagram is developed. With the applied material model and numerical method, a satisfactory agreement between experimental and numerical results is obtained, allowing with this, a final validation.

4.3.4 Determination of the earthquake hazard

The seismic hazard of a certain site is the probability of occurrence of a potential damaging earthquake, characterized for being an inevitable event out of human control. In general terms, the seismic hazard level depends on the proximity of the site to a seismic source with events of enough magnitude to generate significant seismic intensities at the zone under study. The *risk management* of historical masonry structures subjected to earthquake ground motion is integrated by the *seismic risk assessment* and the remedial measures to attain its *reduction*. The seismic risk assessment of a certain building located in a zone with moderate to high seismicity involves two fundamental stages: the *earthquake hazard* of the research zone and the *structural vulnerability* of the building. Therefore, the determination of the earthquake hazard plays an essential role in the seismic risk assessment stage. This hazard is recommended in literature to be estimated by considering a combination of seismological, geophysical, geological and geotechnical studies with the history of earthquakes and observed damage at the site under study.

The severity of the ground shaking at the site depends on major factors such as seismic source and proximity, wave types, regional geology, topography and inherent characteristics of the earthquake (hypocenter, rupture mechanism, magnitude, intensity, duration, content of frequencies, and so on). Nowadays, in the majority of

regions subjected to earthquakes, there are available studies to determine the seismic actions recommended for the design of modern buildings. These studies may serve as a basis for the seismic assessment of historical constructions, but a specific evaluation of the seismic hazard is always needed, mainly based on the history of occurred events and the behavior of the construction under study and other similar [Meli, 1998].

4.3.4.1 The damage grades of the European Macroseismic Scale

The European Macroseismic Scale [Grünthal, 1998] or also known among the research community as EMS-98, corresponds to a quite significant approach to relate damage over a series of structural types to seismic intensities, where damage and intensity have different levels assigned in qualitative terms. In this research work the seismic risk assessment (or seismic vulnerability) of the virtual towers is developed as a first stage by means of the pushover method, obtaining as a result the capacity curves and failure mechanisms. In order to obtain a link between the capacity curves and the seismic vulnerability, the method developed by Lang [2002] and Lang and Bachmann [2003] is used. The authors assessed the seismic vulnerability of existing buildings in a focused area in Basel, Zurich by correlating the capacity curves of the structure and the classification of damage proposed by the EMS-98. This scale distinguishes between five damage grades ranging from negligible damage to total destruction (or collapse). Afterwards, these damage grades could be defined as points at the capacity curve of the building as shown in figure 4.21.

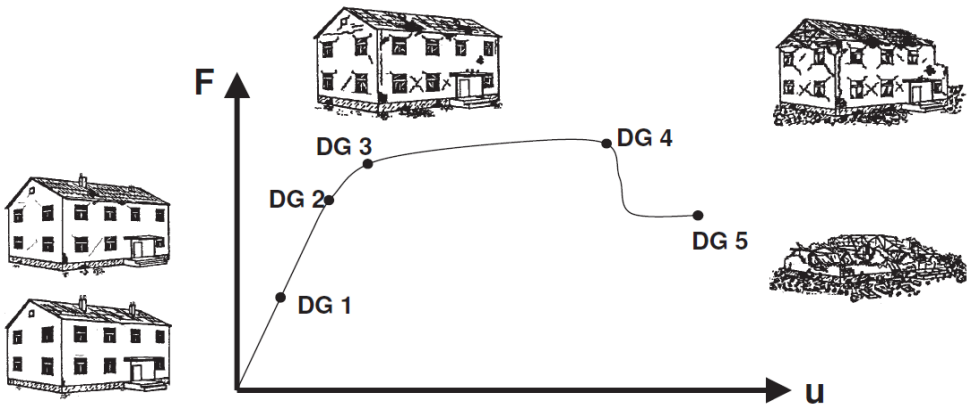

Figure 4.21: Connection of the EMS-98 with a capacity curve [Lang, 2002]

For every of these damage grades, the EMS-98 relates them to a seismic intensity mainly based on observed damages during post-earthquake investigations in reinforced concrete structures and different masonry buildings with variations in materials and level of seismic design. The damage classification for unreinforced masonry buildings is resumed as follows disregarding the damage in non-structural components: DG 1: No structural damage (Intensity V), DG 2: Slight structural damage (VI), DG 3: Moderate

structural damage (VII), DG 4: Heavy structural damage (VIII) and DG 5: Collapse (Intensities IX to XII). Afterwards, this is summarized in table 4.6.

DG	Description	Intensity	Description	Identification at the capacity curve
1	No damage	V	Strong	Elastic state (stiffness is major than zero)
2	Slight damage	VI	Slightly damaging	Yield state. The behavior becomes nonlinear (stiffness starts to reduce)
3	Moderate damage	VII	Damaging	Major strength degradation. The nonlinear behavior increases (stiffness tends to zero)
4	Heavy damage	VIII	Heavily damaging	Point at which the structure reaches an ultimate limit state (stiffness is equal to zero)
5	Collapse	IX-XII	Destructive-devastating	Collapse state (stiffness is minor than zero)

Table 4.6: Damage grades, seismic intensities and identification at the capacity curves

4.3.4.2 The limit states of the performance-based design

In recent years, a new design philosophy for building codes has been discussed within the engineering community. New building codes for earthquakes must adopt a performance-based design philosophy aimed at constructing structures which have predictable seismic performance under multiple levels of earthquake intensity [krawinkler, 1999] and [Leelataviwat et al., 1999]. Whether the response of a structure to loading is acceptable or not depends on the requirements that must be satisfied, including safety against collapse and/or limitations on damage. Each of these requirements may be termed as a limit state and its violation represents the attainment of an undesirable condition for the structure [Simioni, 2009]. The current version of the European Code (EC-8) [Eurocode 8, 2004] for the design of structures for earthquake resistance specifies three limit states as performance requirements and are summarized as follows disregarding the damage in non-structural components:

- Damage Limit State (DLS): the structure is slightly damaged, with structural elements prevented from significant yielding and retaining their strength and stiffness properties. Permanent drifts are negligible. The structure does not need reparation.

- Significant Damage Limit State (SDLS): the structure is significantly damaged, with some residual lateral strength and stiffness. Vertical elements are capable of sustaining vertical loads. Moderate permanent drifts are present. The structure can sustain aftershocks of moderate intensity. The structure is likely to be uneconomic to repair.

- Ultimate Limit State (ULS): the structure is heavily damaged, with low residual lateral strength and stiffness, although vertical elements are still capable of sustaining vertical loads. Large permanent drifts are present. The structure is near collapse and could probably not survive another earthquake, even of moderate intensity.

Limit state	Earthquake design level	Earthquake Intensity	PGA (g)	Probability of Exceedance	Return period
DLS	Occasional	VI	0.10 – 0.22	20% in 50 years	72 years
SDLS	Rare	VII	0.22 – 0.38	10% in 50 years	475 years
ULS	Very rare	≥ VIII	> 0.38	2% in 50 years	970 years

Table 4.7: Performance-based design limit states and earthquake action parameters

In order to relate the earthquake hazard with the performance requirements specified by the EC-8, Gioncu and Mazzolani [2002] propose the design parameters related to the three limit states in terms of earthquake design level, PGA, probability of exceedance and return period, based on a 50 years phase of observation (table 4.7). The earthquake intensities associated to these limit sates are taken from table 4.6 proposed by the EMS-98 based on the modified Mercalli intensity (MMI). In the same table, the description for these earthquake intensities could be related to the earthquake design level of table 4.7. In both classifications, EMS-98 and the limit states of the performance-based design, damages in non-structural components are disregarded because this thesis is only focused in historical masonry towers where the presence of these components is limited compared to other historical buildings (e.g. churches).

4.3.4.3 The seismic coefficient

The seismic coefficient of a structure is determined by the ratio between the ultimate horizontal load carrying capacity calculated by the different seismic analysis methods (e.g. pushover) and the vertical loading. The seismic coefficient is typically expressed as a fraction or percentage of the gravity (g). Meli [1998] suggests as a reference, that typical values of seismic coefficient for historical masonry buildings located in zones of intermediate to high seismic hazard range between 0.1 and 0.3. By the other hand, the codes, e.g. MDS-CFE [1993], specify higher seismic coefficients for the earthquake design of new buildings ranging between 0.50 and 0.86 depending on the level of seismicity and soil type of the zone under study. The damage grades of the EMS-98, the limit states of the performance-based design and the seismic coefficient are used in the earthquake analyses of the virtual towers.

4.3.5 Nonlinear static earthquake analysis

Series of nonlinear static analyses based on the traditional pushover procedure are carried out for the earthquake evaluation of the virtual masonry towers by assuming that the earthquake acceleration is constant throughout time (static), modeled as concentrated lateral inertia forces proportional to the mass of the elements. The pushover analysis is a simple and efficient technique to study the response of a building by incrementally applying lateral loads or displacements. It allows developing a base shear versus top displacement diagram, also known as capacity curve. Moreover, the elastic limit (yielding) and stiffness degradation until the structure reaches an ultimate

limit state and collapse could be identified. This procedure provides good estimations for structures which mainly vibrate in the fundamental mode.

4.3.5.1 Capacity curves and failure mechanisms

The general view and dimensions of the four virtual historical masonry towers under study are illustrated in Figure 4.1 and the 3D FE models are described in section 4.3.1. For the nonlinear simulations, the considered inelastic material parameters are the previously described in section 3.2.2.2. These seismic analyses by the pushover method are intended at obtaining the capacity curves and failure mechanisms of the towers in order to investigate their in-plane and out-of-plane behavior. The typical failure mechanisms of historical masonry towers are described in section 2.4.6. The seismic behavior of this type of structures is mainly governed by the low tensile strength of masonry. The failure mechanisms are summarized as follows: (1) horizontal cracking at the tower´s body due to bending behavior, (2) stepped or diagonal cracking at the tower´s body by shear stresses, (3) vertical cracking at the tower´s body due to horizontal tensile stresses induced by the detachment from other vertical elements (e.g. the façade or nave of a church) (4) partial or total collapse of belfries due to shear stresses and bending behavior, and (5) masonry crushing at the compressed toes.

The first four failure mechanisms are in agreement with the identified by Peña and Meza [2010] in the post-earthquake observations in 172 colonial churches with bell towers after two major earthquakes occurred in 1999 in Puebla and Oaxaca, Mexico. The authors identified that the damage of the small dome of the belfry is minimum compared to the above mentioned failure mechanisms and no masonry crushing at the tower's base was presented. By the other hand, Curti et al. [2008] observed in 31 Italian bell towers damaged by the 1976 Friuli earthquakes that the belfry is the most vulnerable part of the tower due to the presence of large openings, leading to the pillars to be slender and by the top masses. This amplifies the seismic motion causing critical effects in the higher parts of the tower. Alcocer et al. [1999] describe that the key damages in bell towers of churches have shown that the main behavior of these elements is in the plane of the façade. The out-of-plane behavior is generally less important and is only regarded with the detachment of the façade from the nave.

For the numerical simulations, the FE models are firstly loaded with the gravitational force, and in a subsequent stage, the horizontal force is applied under monotonically increased top displacement control. In comparison to the failure mechanisms obtained in the validation of the applied masonry constitutive model of section 4.3.3, here the distribution of stresses is not depicted anymore, because it was used to link the yielding of masonry with the principal plastic strain contours representing the damage. Moreover, for practical purposes results more clear to depict only the plastic activity, because when the material yields occurs a redistribution of stresses, but the plastic hinges (cracking) remain active. In the analyses of the four FE models of the towers the displacement-based load pattern is applied through a considerable number of steps and

sub-steps especially in the nonlinear range in order to attain convergence. The time of computational calculation for every analysis is in the order of 8 hours.

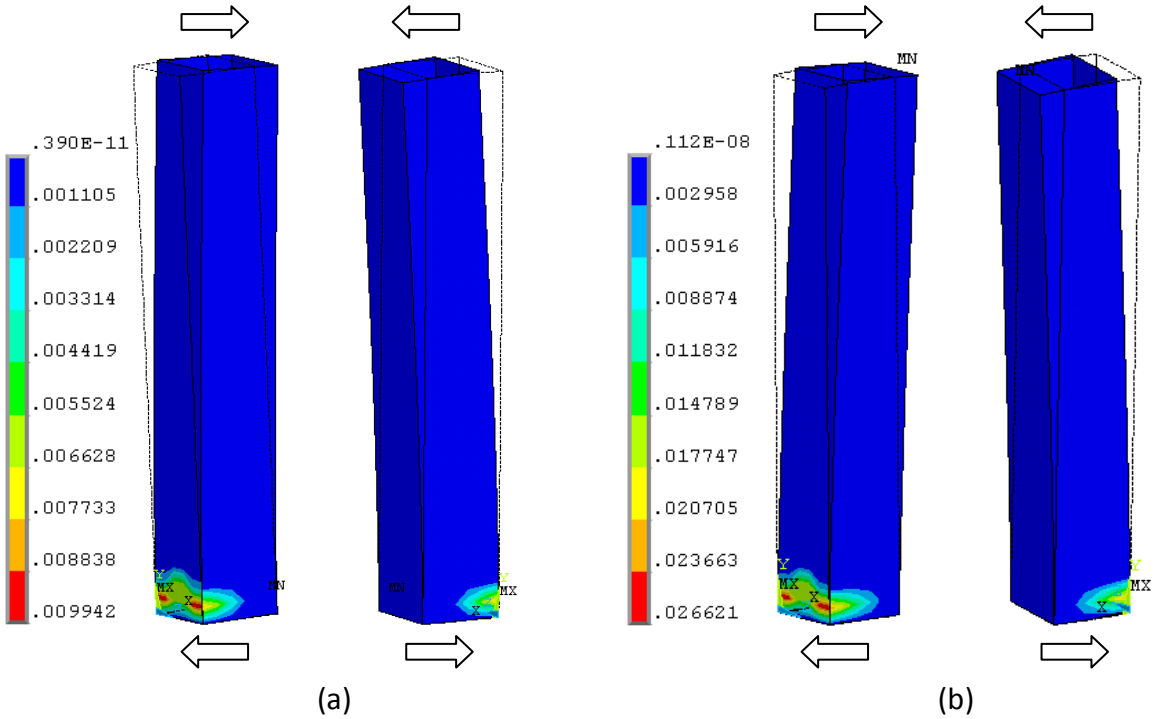

Figure 4.22: Isolated tower with light roof (type c). Principal plastic strain contours (front and back) at a displacement of: (a) 155 mm (DG 3, SDLS) and (b) 265 mm (DG 4, ULS)

The results of the analysis of the isolated tower with timber roof are depicted in Figure 4.22. It is worth noting that the tower presents a global bending behavior represented by the initial formation of horizontal cracks (see Fig. 4.22a) due to vertical tensile stresses at the base level at a displacement of 155 mm, which corresponds to a damage grade (DG) 3 and a limit state of significant damage (SDLS) defined in section 4.3.4. The tower reaches an ultimate limit state (ULS) and a damage grade 4 at a displacement of 265 mm. The final collapse mechanism (see Fig. 4.22b) is formed due to the extension of the horizontal cracks. The failure by masonry crushing is not presented, due to the maximum value of stress in the compressed in-plane and out-of-plane toes is in the order of 3.086 MPa, which is lower than the intrinsic strength (3.5 MPa). By the other hand, the isolated tower with timber roof and openings presents a different behavior as illustrated in Figure 4.23. The tower shows at a displacement of 185 mm the initial formation of horizontal cracks due to vertical tensile stresses as in the case of the similar tower but at different height out-of-plane and in the plane of the posterior part (see Fig. 4.23a). The presence of diagonal cracks is evident by shear stresses in the plane of the main door. The tower reaches an ultimate limit state at a displacement of 325 mm, represented by a final failure mechanism due to the extension of the horizontal and diagonal cracks (see Fig. 4.23b). This tower is close of failing by masonry crushing at

the in-plane and out-of-plane compressed toes, with a maximum compressive stress in the order of 3.305 MPa.

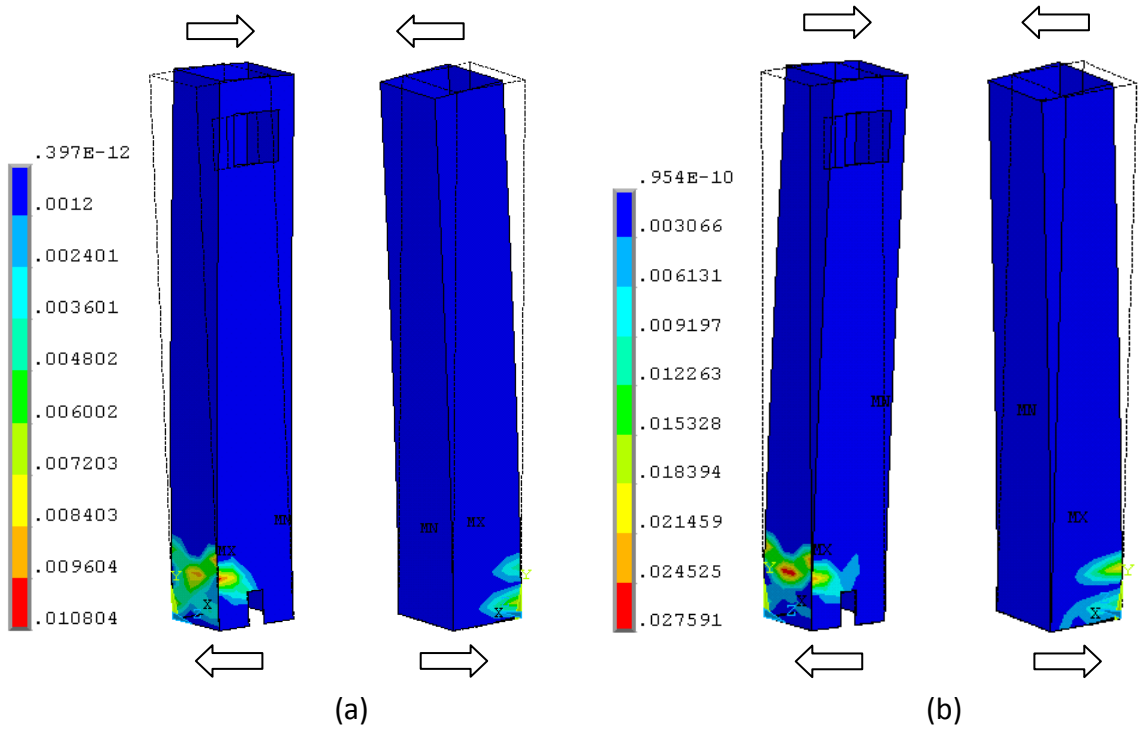

Figure 4.23: Isolated tower with light roof and openings (type d). Principal plastic strain contours (front and back) at: (a) 185 mm (DG 3, SDLS) and (b) 325 mm (DG 4, ULS)

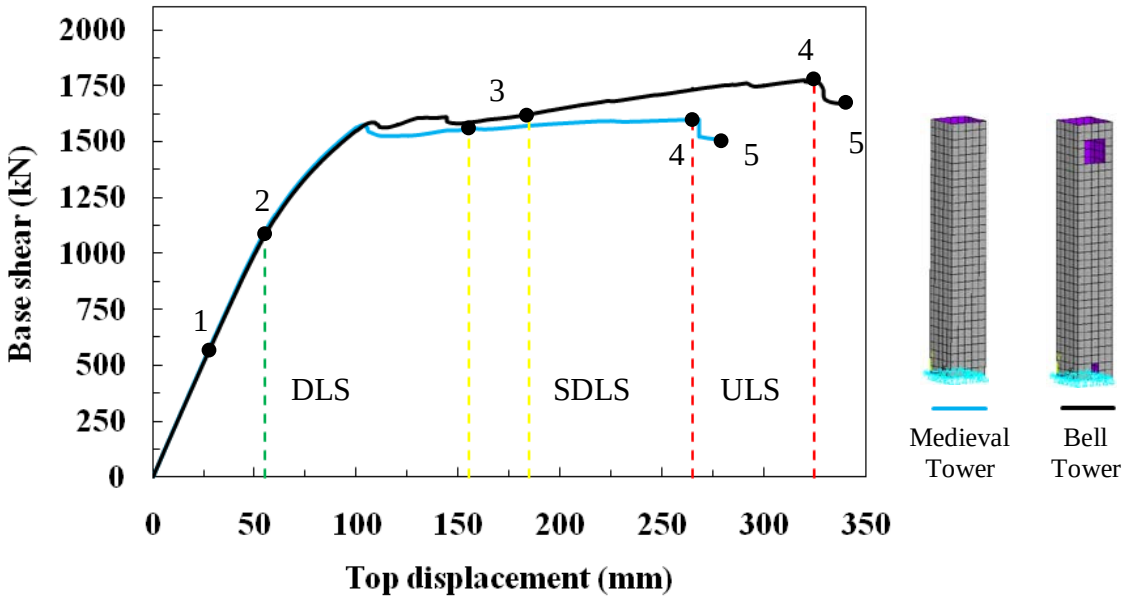

Figure 4.24: Medieval and bell tower (type c and d). Capacity curves of towers in original state with the five damage grades of theEMS-98 and three limit states of the EC-8

Figure 4.24 shows the capacity curves (force-displacement) of the two isolated towers (type c and d) with timber roof and the representative damage grades of the EMS-98 and the limit states of EC-8. It could be observed that both towers present similar linear behavior, reaching the yielding (DG 2, DLS) at the same load of 1100 kN and a displacement of 55 mm. The towers present different nonlinear behavior at a DG 3 and SDLS, being more evident the difference in the ultimate limit state (DG 4, ULS). The tower with openings shows about 9% more lateral force and 23% more displacement (F= 1750 kN and U= 325 mm) than the tower with no openings. This tendency is similar to the observed in the case of the two walls of section 4.3.3.2.

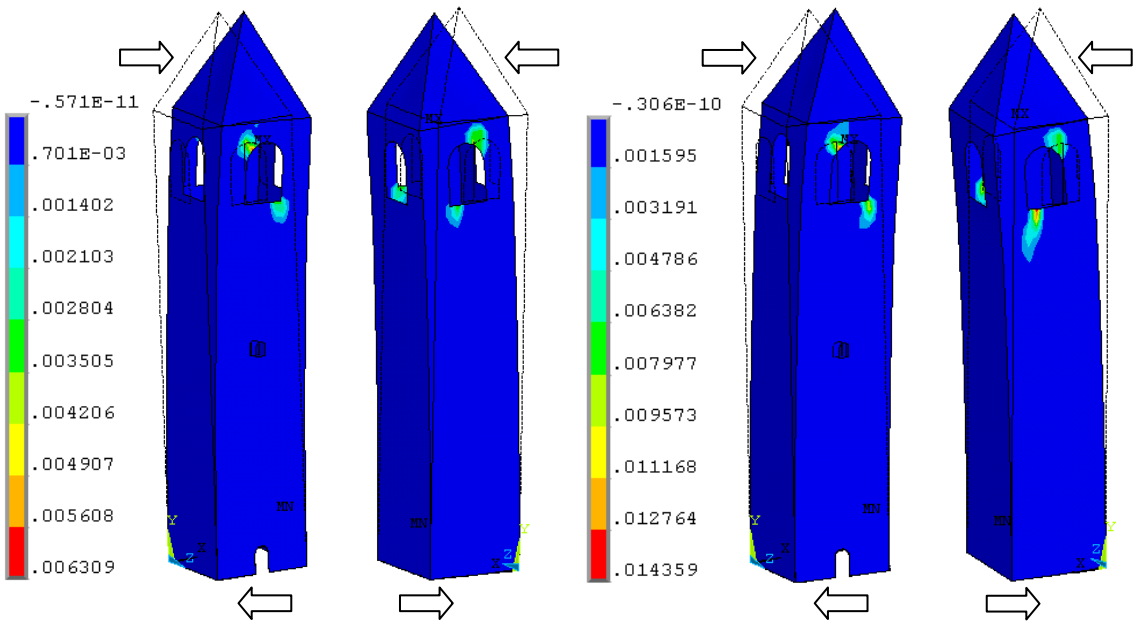

Figure 4.25: Isolated tower masonry roof (type a). Principal plastic strain contours (front and back) at a displacement of: (a) 80 mm (DG 3, SDLS) and (b) 115 mm (DG 4, ULS)

In the isolated tower case a (Fig. 4.25) and the non-isolated tower case b with masonry roof (Fig. 4.26), the results of the analyses illustrate a failure mechanism governed by diagonal cracking due to in-plane shear stresses at the large openings (front and back) at belfries. This is due to the reduction of the resistant area at this weakened part. The final failure mode in both towers is suddenly formed by the extension of the diagonal cracks at the in-plane windows (Figs. 4.25b and 4.26b). These large cracks could lead to the collapse of the belfries, placing in a situation of danger the adjacent buildings and people inside or in the surroundings (Figs. 2.21 and 2.22d-f).

This seismic behavior and failure mode are characteristic of these structures and are in complete agreement with the described in section 2.4.6. As in the analyses of the two towers with timber roof, the masonry crushing of the in-plane and out-of-plane compressed toes is not observed. This is due to the fact that these towers with masonry

roof are stiffer than the others (Figs. 4.24 and 4.27), presenting both maximum compressive stresses of approximately 1.4 MPa, being lower than the intrinsic strength of 3.5 MPa.

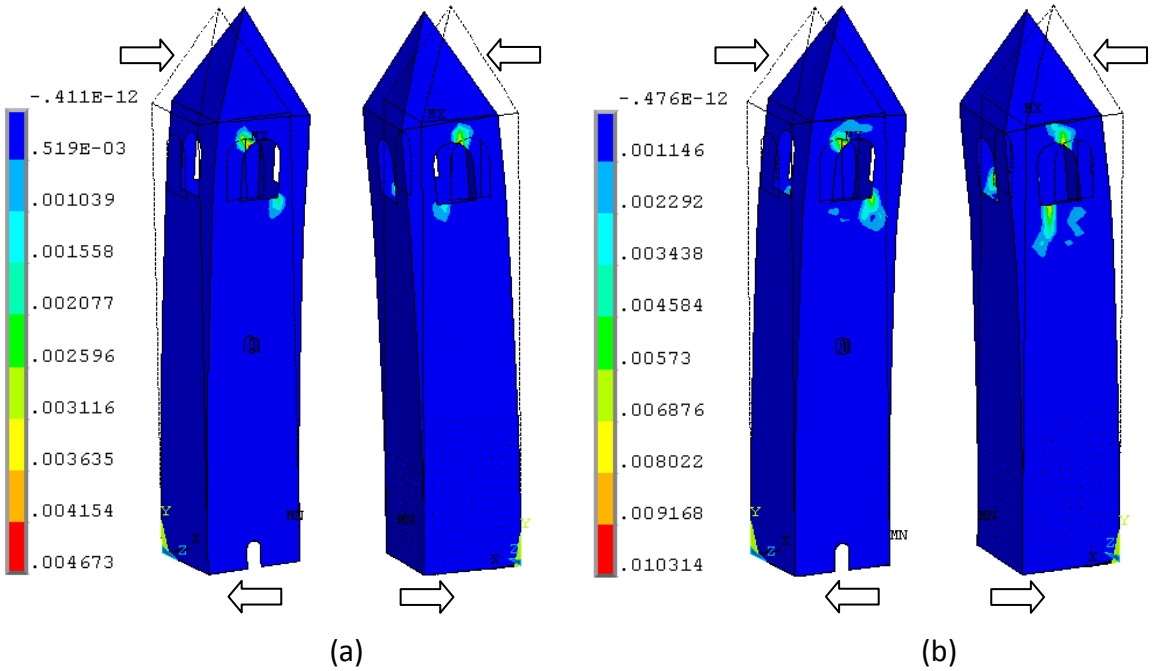

Figure 4.26: Non-isolated tower masonry roof (type b). Principal plastic strain contours (front and back) at: (a) 70 mm (DG 3, SDLS) and (b) 105 mm (DG 4, ULS)

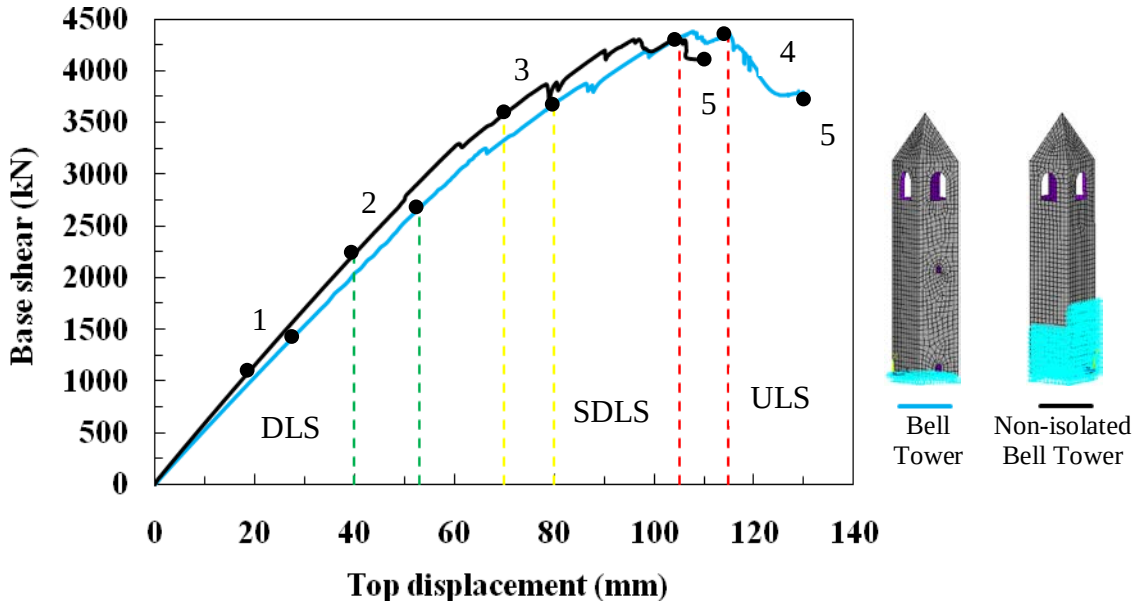

Figure 4.27: Isolated and non-isolated bell tower (type a and b). Capacity curves of towers in original state with the damage grades of the EMS-98 and limit states EC-8

Figure 4.27 illustrates the capacity curves of the two towers with triangular roof (type a and b) and the representative damage grades of the EMS-98 and the limit states of EC-8. It is worth noting that the linear behavior of both towers is different. The non-isolated tower is stiffer than the isolated one due to the interaction with adjacent buildings as it was observed in the modal analysis, reaching the yielding (DG 2) at a displacement of 40 mm and a lateral force of 2220 kN. By the other hand, the isolated tower approximately presents 22% more lateral force and about 33% more displacement capacity (F= 2700 kN and U= 53 mm) at the same yielding stage. In the nonlinear range, both towers present similar lateral load capacity but different displacement. This behavior continues until both towers reach ultimate conditions, showing the isolated one about 10% more displacement (F= 4350 kN and U= 115 mm).

Comparing the capacity curves of the four FE models of the virtual historical masonry towers illustrated in Figures 4.24 and 4.27, it is worth noting that the towers with masonry roof are more resistant to lateral loading, but in contrast, present less ductile behavior. Table 4.8 summarizes the results of the seismic evaluation of the four virtual historical masonry towers by the pushover method in terms of the damage grades of the EMS-98 and the limit states of the EC-8. The respective seismic coefficients calculated at ultimate lateral conditions are presented in table 4.9.

FE model reference	**Limit states EC-8 and Damage grades EMS-98**					
	DLS and DG 2		**SDLS and DG 3**		**ULS and DG 4**	
	***F* (kN)**	***U* (mm)**	***F* (kN)**	***U* (mm)**	***F* (kN)**	***U* (mm)**
Isolated with timber roof	1100	55	1553	155	1600	265
Isolated with timber roof and openings	1100	55	1623	185	1750	325
Isolated with masonry roof	2700	53	3670	80	4350	115
Non-isolated with masonry roof	2220	40	3600	70	4300	105

Table 4.8: Seismic analysis summary of the towers

In the seismic analysis summary of table 4.8 could be observed that in the DLS and DG 2 the four towers present similar displacement, being stiffer the tower with the assumed adjacent buildings. The difference is evident in the lateral carrying capacity, withstanding the stiffer tower about 100% more lateral load and the isolated with masonry roof around 145%. Regarding the seismic action and according to tables 4.6 and 4.7, the towers would reach this damage grade (slight damage) and initial damage limit state for an occasional-slightly damaging earthquake of intensity VI and ground motion between 0.10g and 0.22g (reparable damage). In the SDLS and DG 3 the towers with masonry roof present more lateral strength capacity but in contrast less ductility for a seismic intensity VII (rare-damaging earthquake) and PGA between 0.22g and 0.38g

(reparable damage). The towers with timber roof (type c and d) show different seismic behavior between them at ultimate conditions (ULS and DG 4), presenting the tower with openings about 9% more force and 23% more displacement. By the other hand, the towers with masonry roof (type a and b) have similar strength and ductility eachother but in comparison to the towers with timber roof are more resistant but less ductile as previously mentioned. The loss of the towers would present for a very rare earthquake of seismic intensity equal or higher than VIII (PGA > 0.38g).

FE model reference	Lateral force (kN)	Vertical loading (kN)	Seismic coefficient
Isolated timber roof	1600	18900	0.085
Isolated timber roof and openings	1750	18511	0.095
Isolated masonry roof	4350	50876	0.086
Non-isolated masonry roof	4300	50876	0.085

Table 4.9: Seismic coefficients summary of the towers

In the summary of seismic coefficients of table 4.9, it could be observed that the two towers with timber roof (type c and d) have similar vertical loading, with a small variation in the tower with openings (less mass). By the other hand, the tower with openings (type d) shows more lateral force capacity of about 150 kN due to the different seismic behavior induced by the openings. The towers with masonry roof (type a and b) present the same vertical loading because they have the same mass (interaction with neighbor buildings has impact on the stiffness but not on the mass). Regarding lateral force, both towers show similar capacity, presenting 50 kN more the isolated one (type a). Compared to the towers with masonry roof, the towers with timber show about 2.5 times less force and vertical loading. Because of this relationship, the four towers have similar seismic coefficient. The obtained low values of seismic coefficient represent in quantitative terms the high vulnerability of this type of structures to seismic actions. These seismic coefficients are in complete agreement with the typical values of ancient masonry buildings in the range between 0.1 and 0.3 suggested by Meli [1998]. Which in contrast for modern buildings, the seismic coefficients are in the range between 0.5 and 0.86. In conclusion, the four virtual historical masonry towers would reach an ultimate limit state or collapse under an earthquake ground motion of 0.1g. The seismic coefficient allows obtaining more reliable results (quantitative) than the qualitative damage indicators.

4.3.6 Nonlinear dynamic earthquake analysis

As aforementioned in section 3.2.3.1, the static-based approaches as the pushover do not give information about the hysteretic behavior of the structure, which is helpful to assess stiffness and strength degradation, and the dissipation of energy. This is due to

the static approaches do not take into account motion and damping, and nor the physical characteristics of earthquakes such as PGA, duration of the intensive phase and vibration frequencies. Moreover, changes in the modal properties due to the nonlinear behavior of masonry are not taken into account.

Nonlinear dynamic earthquake analysis is a powerful tool for the study of the structural seismic response. A set of ground motion records or artificially generated time-history representations can give an accurate evaluation of the anticipated seismic performance of structures [Mwafy and Elnashai, 2001]. This is the most adequate and comprehensive analysis procedure to evaluate the nonlinear seismic response of structures, but the currently available computer hardware and design software effectively limit both size and complexity of structures, which may be analyzed using this procedure. At present, there is no general purpose nonlinear analysis software which permits practical evaluation of large structures [Lee, 2008]. In order to validate the capability of the applied material model of Gambarotta and Lagomarsino [1997] to represent the nonlinear behavior of masonry in dynamic conditions, the tower with timber roof and no openings of Figure 4.1d and table 4.1c is used in the investigations.

4.3.6.1 Seismic response and failure mechanisms

The high mass of historical masonry towers and flexibility due to their slenderness generate that these structures present during an earthquake important inertia forces and top displacements. This amplification of the earthquake ground motion is presented when the predominant vibration period of the ground motion is similar to that of the fundamental vibration period of the tower, leading to a high dynamic amplification of the structural response by the resonance phenomena. In order to investigate the response of the tower with timber roof and no openings (type c) of Figure 4.1d and table 4.1c under base excitation, time varied displacements are taken into account. The loading history (seismic input) is represented by two scaled sinusoidal functions $f(t) = \sin(2\pi t/T)$, with maximum displacement of 100 mm and 200 mm respectively (Fig. 4.28). Due to symmetry and practical purposes the two base excitations are applied in the horizontal direction along the X axis (X and –X). The predominant vibration period considered in both base excitations is T= 1 s, which is similar to the fundamental vibration period of the tower, T= 0.94 s (see table 4.3), in order to generate a dynamic amplification (resonance), which is as above mentioned, the worst case for historical masonry towers under earthquake conditions. For the analysis are used the inelastic parameters of section 3.2.2.2 and moreover to account for damping effects in the dynamic simulations, the FE program uses the Rayleigh damping coefficients of mass and stiffness. The mass damping coefficient (α= 0.62) and stiffness damping coefficient (β= 0.0003) proposed by Urban [2007] to represent a larger range of damping ratios for a great frequency range are used in this study. These damping coefficients represent for masonry structures the decreasing of mass damping with the increasing of frequency and the opposite for stiffness damping with the increasing of frequency. The Rayleigh

damping allows obtaining a more realistic behavior of the structure under dynamic loading than assuming a constant damping ratio usually 5% of the critical for all modes.

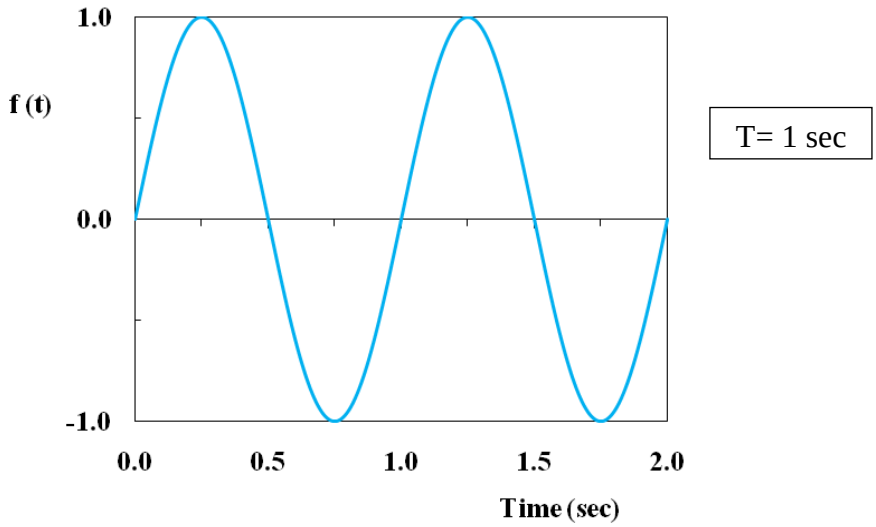

Figure 4.28: Sinusoidal wave for earthquake base excitation

Figure 4.29 shows the results of the dynamic analysis for the two base excitations in terms of top displacement time-history and plastic deformations at the moment that the structure presents the maximum response. The maximum obtained displacement for a base excitation with maximum displacement of 100 mm at the top of the tower is in the order of 110 mm (amplification of 1.1) and 207 mm (amplification of 1.035) for the base excitation with maximum displacement of 200 mm. This observed amplification at the top displacement time-history of Figures 4.29a and 4.29b allow verifying that both base excitations were correctly applied. It is worth noting that the displacement-based time-history in the analysis is applied through a considerable number of steps and sub-steps in order to attain convergence. Important computational resources are needed to run a nonlinear time-history analysis. The required calculation time was in the order of 48 hours for the base excitation with maximum displacement of 100 mm and about 100 hours for the one of 200 mm. In both loading cases the tower presents an early state of yielding (tensile stresses appear) with plastic deformations much lower than 0.1% (Figs. 4.29a and 4.29b), when in contrast, by the pushover method, this tower showed yielding at 55 mm and a major stiffness degradation with a clear nonlinear behavior at 155 mm (Figs. 4.22a and 4.24). It is true that there are differences between the seismic response and failure mechanisms in the static and dynamic approaches as above mentioned, but this clear underestimation of damage is not reasonable.

Moreover, higher amplifications were expected in the induced resonance analyses by using artificially generated time-histories with predominant vibration periods similar to the fundamental vibration period of the tower. In earthquake conditions, the base of the structure tends to follow the ground motion, meanwhile for inertia, the structural mass is opposed to be displaced and to follow the movement of its base. This leads to

the generation of inertia forces proportional to the mass of the structure. Meli [1998] affirms that due to the flexibility of masonry bell towers and the high inertia forces generate that the structure vibrates in a different way of that of the terrain, and when the phenomenon of resonance is present, the top amplification could be of about 2.3 times higher than the ground motion registered at the base. Chavez and Meli [2010] observed by parametric analysis that the seismic response and failure mechanisms of historical masonry structures are very sensitive to the tensile strength assumed in the numerical model and to the amount of internal damping.

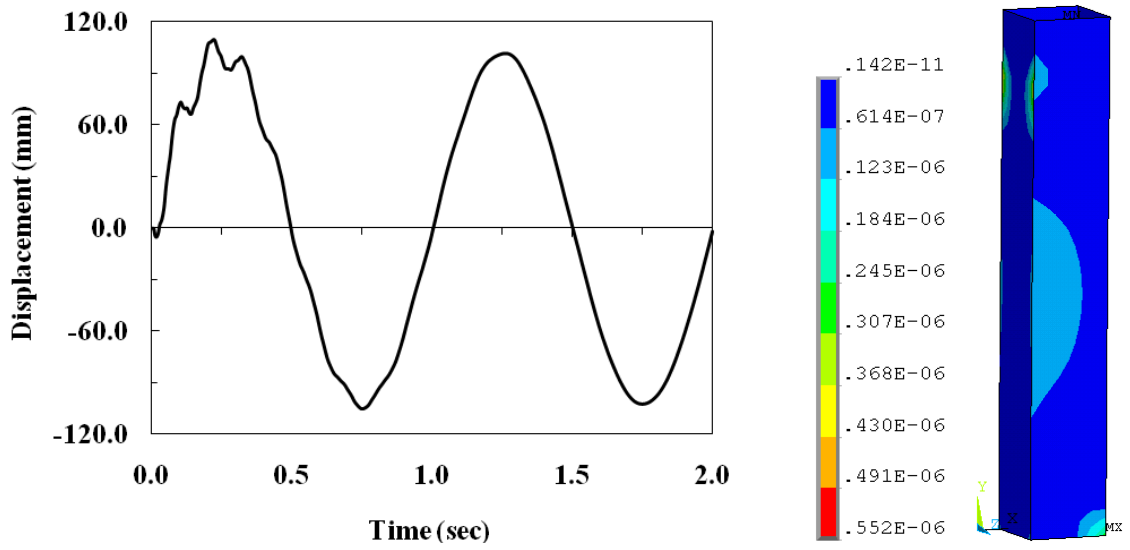

(a)

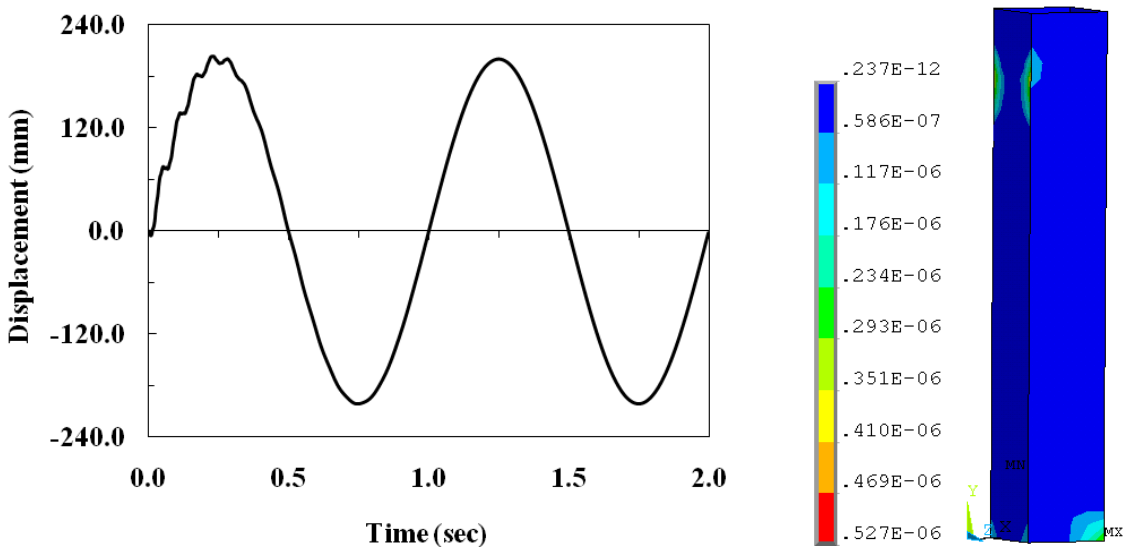

(b)

Figure 4.29: Seismic response and damage for a base excitation with maximum displacement of: (a) 100 mm and (b) 200 mm

4.4 Summary and conclusions

A proposed methodology for the seismic risk assessment of historical masonry towers was described. It was developed through four validated 3D FE models representative of towers usually found in Europe. As a first approximation on the seismic risk assessment, the FE models were subjected to linear elastic investigations on their load carrying capacity and dynamic characteristics. These initial analyses permitted to validate the models with theoretical background and experimental data on similar towers reported in literature. This validation plays an important role to obtain models representative of real towers, and with this, more reliable results in the seismic risk evaluation. This validation could be useful when there is no experimental data available to calibrate the model, and when it is available, as a practical pre-calibration. The proposed strategy to simulate the interaction with neighbor buildings is envisaged to simplify the model construction and the nonlinear analyses, because normally the modeling of non-isolated towers is done by including the façade or nave of the church.

The capability of the applied model to simulate the nonlinear behavior of masonry and collapse modes identified at shear walls was validated with reported experimental examples, obtaining a satisfactory agreement. Intensive numerical simulations developed through a series of nonlinear static and dynamic analyses were carried out. The seismic analysis by the pushover approach successfully permitted to obtain the overall seismic response of the towers represented by the capacity curves and the in-plane and out-of-plane failure modes. The huge impact of the low tensile strength of masonry and large openings at belfries on the seismic behavior was observed, failing in a brittle mode by shear stresses. The medieval tower presented the characteristic bending behavior with horizontal cracks in-plane and out-of-plane. The similar tower with openings presented a mixed failure mode of bending and shear stresses at the bottom, being more resistant and ductile. The same trend was observed in the validation of the material model and was corroborated with reported experimental observations. The few investigations reported in literature on the seismic behavior of historical masonry towers are mainly focused on the in-plane behavior and disregard horizontal cracking and crushing out-of-plane. The more flexible towers were close to present crushing in both planes. The behavior and damage types were validated with the seismic vulnerability aspects described in chapter 2 and the reported post-earthquake observations on more than 200 towers. The seismic hazard was included in qualitative terms at the capacity curves for different damage grades and limit states, and quantitatively by the seismic coefficient represented by the ratio between lateral force and vertical loading. A drawback of the seismic coefficient is that ductility is not considered, which is quite important to evaluate energy dissipation. The three approaches permitted to satisfactorily assess the seismic risk of the four towers. All of them presented an imminent high risk to seismic actions as expected. The results of the nonlinear dynamic earthquake analysis of one tower in terms of seismic response and failure mechanisms were identified as not reasonable. However, further research is required on this complex and challengeable approach regarding the material parameters and internal damping.

Chapter 5

Seismic Risk Reduction of Historical Masonry Towers

5.1 Introduction

As aforementioned in previous chapters, the risk management of a certain building located in a seismic zone is integrated by two huge and complex stages corresponding to the assessment of risk and its reduction. In chapter 4, a proposed procedure for the seismic risk assessment of historical masonry towers was described. The proposal was developed through four validated 3D FE models representative of European towers. The FE models and the results of the seismic evaluation in terms of behavior and failure mechanisms (in-plane and out-of-plane) were validated with theoretical background and the seismic vulnerability aspects on towers described in chapter 2. Moreover, for the validation was considered reported experimental data on similar towers and observed damages after considerable earthquakes on more than 200 towers. The seismic risk assessment of historical masonry towers and the possible achievement of the seismic risk reduction are the main characteristics of the proposed methodology. The present chapter aims at describing the second stage of the proposal, corresponding to the remedial measures to attain the seismic risk reduction of historical towers.

5.2 Methodology

In the context of this thesis, the seismic risk of a certain historical structure located in a seismic zone is determined by the conjunct of the seismic hazard of the site and its structural vulnerability. Since the seismic hazard is unavoidable and it is not in our hands to reduce it or modify it, therefore this research work is aimed at reducing the structural vulnerability of historical towers by the implementation of prestressing devices in order to attain the seismic risk reduction. The devices are vertically and externally located at key locations inside the towers in order to give to the retrofitting the characteristic of reversibility, respecting in all senses the architectonic and historical value of the

structure. The post-tensioned devices intend to improve the seismic performance of the towers and to reduce the expected damage with the application of a uniform overall distribution of compressive stresses to the masonry to increase confinement, ductility, lateral strength and energy dissipation, achieving with these improvements the seismic risk reduction. Firstly, the capability of the applied material model to simulate the super-elastic response of SMA is validated with reported experimental results. Moreover, an extensive parametric study on a selected tower is carried out based on more than 100 nonlinear static simulations aimed at investigating the impact on the seismic performance of different parameters such as tendon material (steel, FRP and combinations with SMA), prestressing level, changes in tendon forces and SMA superelasticity. Afterwards, from the parametric study a prestressing device and three prestressing levels are recommended as a retrofitting measure of the four proposed European towers. Moreover, the results of the seismic risk assessment of the towers in original conditions and retrofitted are compared in order to determinate the level of the obtained seismic risk reduction.

5.3 Validation of the applied SMA constitutive model

In the present section, the capability of the applied Shape Memory Alloy (SMA) constitutive model to simulate the superelastic (or pseudo elasticity) behavior of Nickel-Titanium (NiTi) wires of different fabricants is validated by means of theoretical back ground and reported experimental examples. The applied SMA material model was developed by Auricchio [1995] and is included in the finite element software ANSYS®. The model is able to describe the superelastic behavior of NiTi SMA, which is a flexible material that can undergo very large deformations in loading and unloading cycles without permanent deformations. Three different phases could be observed in the uniaxial stress-strain diagram representing the superelastic behavior of SMA (Fig. 3.18b). These phases consist with the austenite (linear elastic), martensite (also linear elastic) and the transition (nonlinear phase) between these two phases. The complete loading and unloading cycle leads to the formation of a hysteretic loop (plateau) that could be observed in the stress-strain diagram. This superelastic behavior, generally not present in traditional materials, could be used for energy dissipation and vibration control purposes in the seismic retrofitting of structures (section 3.3.3.3).

5.3.1 Uniaxial tensile tests on NiTi SMA wires

The most common SMA devices used for engineering purposes are made of NiTi wires, due to their relative low cost and superior behavior compared to other SMA compositions. The main manufacturers of NiTi SMA are *GAC International, NDC (Nitinol Devices and Components) and FIP Industriale* (see table 3.5). In order to validate the superelasticity behavior of the applied SMA material model developed by Auricchio [1995], the three commercial NiTi SMA wires of different fabricants are subjected to numerical tests under uniaxial tension. The results of the numerical simulations are compared to the reported experimental results by Fugazza [2003]. Due

to similitude in the results and for representative reasons, from the three evaluated NiTi SMA wires, here is only illustrated the results of the numerical simulation on the GAC® NiTi SMA and the comparison with experimental results. In general, when a SMA specimen is subjected to a uniaxial tensile stress above the austenite start stress $\sigma_s^{A\text{-}S}$, the phase transformation from austenite to martensite starts (forward transformation). At austenite finish stress $\sigma_f^{A\text{-}S}$, the phase transformation is complete. When the specimen is subjected to a high stress $\sigma > \sigma_f^{A\text{-}S}$, the material exhibits the elastic behavior of the martensite phase. If unloading, the reverse transformation starts at a stress $\sigma_s^{S\text{-}A}$ and is completed at a stress $\sigma_f^{S\text{-}A}$. The large deformation between both transformation phases (forward and reverse) leads to the formation of a hysteretic loop in the loading/unloading stress-strain diagram (see Fig. 5.1).

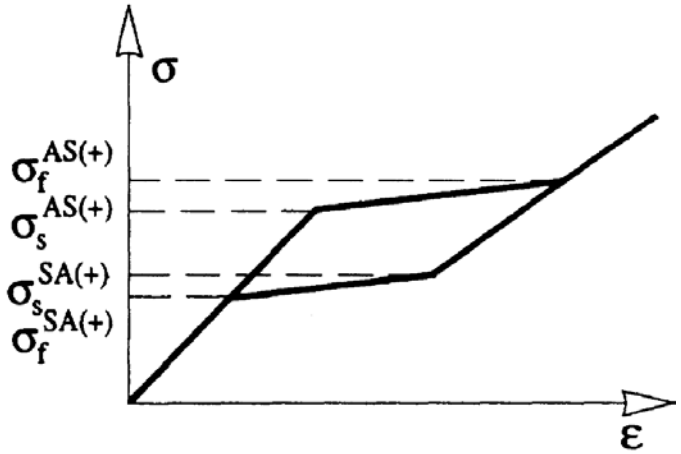

Figure 5.1: One-dimensional superelastic behavior of a SMA [Auricchio and Sacco, 1997]

The tested NiTi SMA wire has a rectangular cross section of 0.64 x 0.46 mm and a length of 5 mm. The 3D FE model is constructed with only one solid185 element fixed at the base. This element is the recommended to simulate the superelastic SMA behavior and is defined by eight nodes with three translational DOF at each node. Table 3.5 presents the main mechanical properties of the commercial GAC® NiTi SMA wire, including the E modulus of the austenite and martensite phases and the maximum recoverable strain (elastic deformation). This table also contains the material parameters representing the initial and final stress values for the transformation of austenite in martensite (forward transformation) and for the transformation of martensite in austenite (reverse transformation) respectively. The uniaxial tension is applied under monotonically increased vertical force control until reaching the complete austenite phase transformation at a stress $\sigma_f^{A\text{-}S}$ (350 MPa) and afterwards unloaded in order to induce the complete reverse transformation. The results of the numerical simulation on the GAC® NiTi SMA are compared with a reported experimental test as illustrated in Figure 5.2. The numerical and experimental results of the stress-strain diagram show a satisfactory agreement. The main difference between the other two evaluated SMA wires and the GAC® one is in the elastic modulus as well as the start and

final stresses in the austenite and martensite phases (table 3.5), with higher strengths and higher recoverable strains of 7% (FIP® SMA) and 8% (NDC® SMA) leading to a higher hysteretic loop, and with this to more energy dissipation and vibration control.

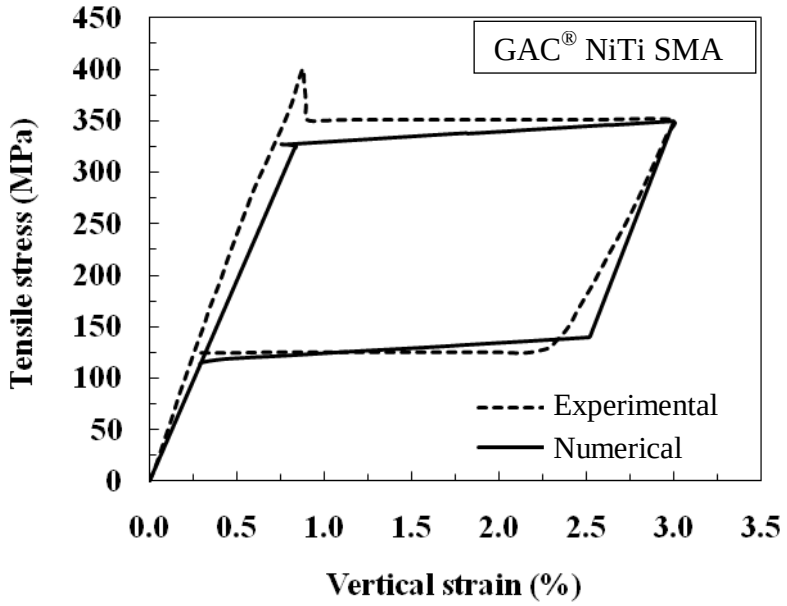

Figure 5.2: GAC® NiTi SMA. Numerical and experimental vertical stress-strain diagram

As a result of experimental tests on NiTi SMA wires, evidences have shown different material properties between traction and compression as well as different elastic properties between austenite and martensite [Auricchio and Sacco, 1997]. The main drawback of the material model is the inability to account for the different elastic properties between austenite and martensite. Figure 5.2 illustrates a good agreement in the elastic properties of the austenite phase but a clear overestimation in the martensite one. However, it is worth noting that the model is able to satisfactorily capture the superelastic behavior of SMA, the maximum recoverable strain and both transformation phases (forward and reverse) that lead to the formation of the hysteretic loop.

5.4 Parametric numerical study by nonlinear static analysis

The technique of prestressing has been successfully used to improve the seismic behavior of concrete structures. The adaptation of this technique to the seismic retrofitting of the cultural heritage has gained in recent decades especial interest for many researchers around the world. However, very few applications of this technique can be found in historical masonry towers as described in section 3.3.4. The present section aims at describing an extensive parametric study based on a series of nonlinear static simulations by means of the traditional pushover procedure. More than 100 nonlinear static simulations with a calculation time of about 10 hours each are carried out on a selected historical masonry tower. Due to practical purposes, only the most

relevant results are here reported. The parametric study aims at investigating the impact on the seismic performance of different parameters such as tendon material (steel, FRP and combinations with SMA), prestressing level, changes in tendon forces and SMA superelasticity. The results of the parametric study are compared eachother, highlighting the advantages and drawbacks of the evaluated prestressing devices and prestressing force levels in terms of seismic performance and observed failure mechanisms at the historical tower. Afterwards, from the parametric investigation a prestressing device and three prestressing levels are recommended as a retrofitting measure of the virtual towers of chapter 4.

5.4.1 Prestressing devices under study

In the context of this thesis a prestressing device is a structural member axially stressed in tension and is integrated by three main parts, the top and bottom anchorages and the tendon (see Fig. 3.15). Normally, the material of the anchorages used for prestressed concrete and masonry structures has been of high resistance steel and more recently of fiber reinforced plastics (FRP). By the other hand, the tendon could be usually fabricated of both mentioned materials as well as of NiTi SMA. This investigation is focused on different tendon materials including prestressing steel and smart materials such as FRP of different fibers (aramid and carbon) and NiTi SMA of different fabricants. The different tendon materials under investigation are summarized in table 5.1. One tendon could be made of several wires or bars depending on the prestressing force and the designed cross section.

- Steel	**- Prestressing steel**	- Cold drawn wire (5 – 7 mm)
- FRP	**- Aramid FRP (AFRP)**	- Arapree bar (7.5 mm)
		- Technora bar (8 mm)
	- Carbon FRP (CFRP)	- CFCC bar (12.5 mm)
		- Leadline bar (7.9 mm)
- SMA	**- GAC International**	- NiTi wire (0.64 x 0.46 mm)
	- NDC Devices	- NiTi wire (1.49 mm)
	- FIP Industriale	- NiTi wire (2.01 mm)

Table 5.1: Different tendon materials under investigation

The mechanical properties, general characteristics and behavior of the different tendon materials and anchorages as well as their advantages and drawbacks are described in section 3.3.3. Due to the fact that SMA wires are quite expensive, this material is recommended to be used in small quantities as a part of a device.

5.4.2 Location of prestressing devices at the towers

The prestressing devices are vertically and externally located at key locations inside the towers in order to give to the retrofitting the characteristic of reversibility (removable), respecting in all senses the architectonic and historical value of the structure. Compatibility, durability and reversibility are fundamental aspects recommended in literature to be taken into account for the seismic retrofitting of cultural heritage. Reversibility is definitely the most important aspect, because if the applied technique shows deficiencies in terms of compatibility and durability that increase the seismic vulnerability of the structure or there is a new material/technique that allows a better seismic performance, this old retrofitting could be substituted by the new one.

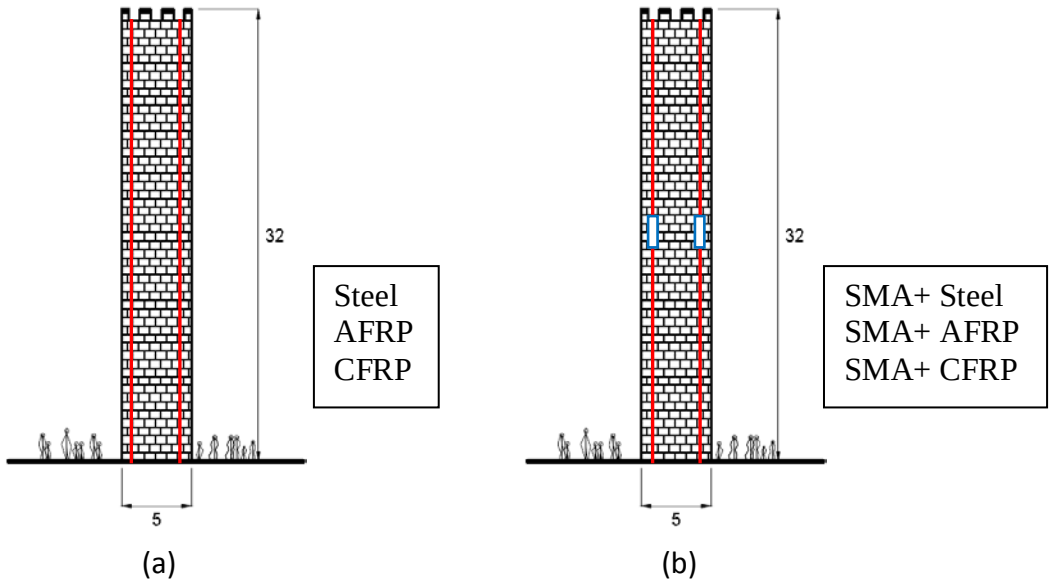

Figure 5.3: Location of prestressing; (a) uniform devices and (b) combined devices

From the four virtual historical masonry towers described and analyzed in chapter 4, the medieval tower (type c) was selected to develop the parametric study due to its simplicity and size. The external prestressing of Figure 5.3a consists of four devices vertically located and without drilling in the internal corners of the tower, anchored at the top and foundation respectively. For this case, the tendon material could be made of steel, AFRP (Arapree and Technora) and CFRP (CFCC and Leadline). Due to the high cost of SMA, the NiTi SMAs of the three fabricants described in table 5.1 are used in combination with different tendon segments of steel, AFRP and CFRP. The SMAs are located at the middle part of the tower as shown in Figure 5.3b. The used FE elements to simulate the tendons correspond to link10 (only tension) and solid185 for the SMA.

5.4.3 Determination of prestressing forces and strengthening design

This section aims to determine the prestressing forces and strengthening design of the different prestressing devices studied through the parametric study. In order to conform

to the fundamental requirements of structures under seismic action, the EC-8 specifies that at ultimate limit state shall be checked the ultimate capacity of the retrofitting device in terms of strength and deformability, in order to avoid an exceedance. The design of the retrofitting measure by means of prestressing is commonly horizontally or vertically applied with the addition of steel or FRP tendons. Horizontal external prestressing has been mainly used in the cultural heritage to provide stability out-of-plane in walls or to reduce the tensile stresses generated by supports opening of vaults, arches and domes. By the other hand, vertical external prestressing has proved to be more suitable to increase the in-plane lateral strength and ductility of masonry walls by providing tensile strength at key locations. The level of improvement strongly depends on the level of the prestressing force, so, the higher the initial prestressing force the higher the lateral strength and ductility. Especial careful may be taken into account in order to use this technique in historical masonry towers. Firstly, an optimal prestressing level may be designed, due to high prestressing levels could lead to local damage at the top anchorage zone, or a sudden collapse even in static conditions by an exceedance of compressive stresses at the bottom (see section 2.4.6.3). Moreover, in seismic conditions, the compressed in-plane and out-of-plane toes could fail by crushing as well, and with this, to a brittle failure due to the explosive behavior of this mechanism. The proposal of an optimal prestressing force and device by means of the present parametric study is an important particular objective of this thesis.

In this research work different prestressing force levels are studied. The prestressing forces are determined by taking into account as a pattern different percentages of the vertical loading. Only the most important results are here presented and could be summarized in three prestressing levels such as low (5% of vertical loading), medium (15% of vertical loading) and high (30% of vertical loading). The prestressing devices are designed for these prestressing levels and reviewed in static and seismic conditions taking into account the mechanical properties and safety factors mentioned in section 3.3.3. Moreover, in seismic conditions, the devices are checked at the point where the structure reaches its ultimate limit state in order to verify that their ultimate capacity is not exceeded as specified in the EC-8. Due to the top rotation of the tower by the natural bending behavior, the tendons experience an elongation and a shortening respectively. This elongation represents an increasing in the tendon prestressing force and increasing of the compression applied to the masonry. In the case of shortening the opposite occurs, a decreasing in the tendon prestressing force and decreasing of the compression induced to the masonry. The impact of different applied prestressing forces and devices on the seismic performance of ancient masonry towers and changes in prestressing forces are the main characteristics of the present parametric study.

5.4.3.1 Seismic analysis with low prestressing level

As above mentioned, the selected tower to develope the parametric study consists of the medieval tower (type c). The seismic analysis of this tower in original state in terms of capacity curve and failure mechanisms is described in section 4.3.5.1. This tower is

retrofitted and reanalyzed with the same material parameters and analysis approach. The results of the seismic analysis in original state and retrofitted with different prestressing forces and devices are compared eachother in order to evaluate the seismic performance improvement in terms of lateral strength, ductility and energy dissipation.

Device ø=27 mm	**E (MPa)**	**A_T (mm^2)**	**No. of wires / bars**	**σ_{Acting} (MPa)**	**$\sigma_{Permissible}$ (MPa)**	**Comment**
Steel	210000	560	11 wires (7 mm)	421.88	1169	$\sigma_{Acting}<\sigma_{Perm}$ **o.k.**
Arapree	62500	560	10 bars (7.5 mm)	421.88	548	$\sigma_{Acting}<\sigma_{Perm}$ **o.k.**
Technora	54000	560	8 bars (8 mm)	421.88	760	$\sigma_{Acting}<\sigma_{Perm}$ **o.k.**
CFCC	137300	560	3 bars (12.5 mm)	421.88	1122	$\sigma_{Acting}<\sigma_{Perm}$ **o.k.**
Leadline	150000	560	8 bars (7.9 mm)	421.88	1350	$\sigma_{Acting}<\sigma_{Perm}$ **o.k.**

Table 5.2: Designed devices for a low prestressing level of 0.05Fv

In this first case, a low prestressing level is taken into account corresponding to a 5% of the vertical loading (0.05Fv). The total vertical loading of this tower is in the order of 18900 kN, so the total applied prestressing tensile force results in 945 kN (a precompression of 0.045 MPa). Four vertical prestressing devices are considered for the retrofitting measures, one in every corner of the tower with a prestressing force each of 236.25 kN. The prestressing devices are designed/reviewed for this initial prestressing force in static and seismic conditions by taking into account the mechanical properties and safety factors of section 3.3.3. For steel is recommended not to exceed a 70% or 80% of the ultimate tensile strength, meanwhile for FRP is of about 40% of the ultimate load capacity for AFRP and 60% for CFRP due to limitations of these materials by presenting brittle failure with no yielding when reaching ultimate conditions. By the other hand, for SMA there is no safety factor in literature, just is recommended not to exceed the ultimate tensile strength of the complete austenite phase transformation ($\sigma_f^{A\text{-}S}$). Tables 5.2 and 5.3 present the designed devices for this low prestressing level. It is worth noting that the cross sections are overdesigned due to at a first instance the changes in the prestressing forces at ultimate limit state of the tower are unknown.

Device ø=56 mm L=400 mm	**E (MPa)**	**A_T (mm^2)**	**No. of NiTi wires**	**σ_{Acting} (MPa)**	**$\sigma_{Permissible}$ (MPa)**	**Comment**
GAC® SMA	47000	2500	7083 wires (0.64 x 0.46 mm)	94.5	350	$\sigma_{Acting}<\sigma_{Perm}$ **o.k.**
NDC® SMA	60000	2500	1078 wires (1.49 mm)	94.5	600	$\sigma_{Acting}<\sigma_{Perm}$ **o.k.**
FIP® SMA	80000	2500	592 wires (2.01 mm)	94.5	670	$\sigma_{Acting}<\sigma_{Perm}$ **o.k.**

Table 5.3: Designed SMA devices for a low prestressing level of 0.05Fv

Since the technique of prestressing does not substantially increase the mass nor the stiffness of the tower, the seismic performance could be obtained by increasing the overall tensile strength by the induced precompression to the masonry with the post-tensioned devices. Figure 4.2b illustrates the vertical distribution of stresses at the medieval tower in static conditions. It could be observed that the maximum average compressive stresses at the bottom are in the order of 0.59 and 0.66 MPa respectively, which are lower than the intrinsic strength of 3.5 MPa. By retrofitting the tower with the low prestressing level 0.05Fv, the concentration of compressive stresses at the bottom are checked again and are of about 0.68 MPa, which approximately corresponds to the applied precompression of 0.045 MPa, being the tower stable in static conditions. This initial check is quite important to verify that the prestressing is correctly applied and moreover to check that the applied prestressing force does not induce a sudden collapse of the tower by exceeding its compressive strength. The redistribution of compressive stresses in seismic conditions (ULS) is verified again. This could lead to stress concentrations at localized parts of the structure (in-plane and out-of-plane), mainly at the compressed toes, and with this to a brittle failure by masonry crushing.

Capacity curves and failure mechanisms

The results of the seismic analyses of the retrofitted medieval tower with uniform and combined devices with low prestressing level are illustrated in Figures 5.4 and 5.5. In the case of the combined devices with SMA of different fabricants (GAC®, NDC® and FIP®), the results of the seismic analyses (low, medium and high prestressing levels) in terms of capacity curves and failure mechanisms are quite similar, therefore only the results of the combined devices with GAC® SMA are presented. It is worth noting that the tower presents at ultimate conditions a failure mechanism governed by bending behavior. The failure modes and plastic deformation of the retrofitted tower with uniform and combined devices do not present important variations. Due to illustrative and practical purposes (Fig. 5.4), only the failure modes of the retrofitted tower with one uniform device (steel) and one combined (SMA+steel) are presented.

The retrofitted tower with uniform devices reaches an ULS at a total displacement of 270 mm and presents large in-plane and out-of-plane horizontal cracks (Fig. 5.4a). Due to symmetry of the tower, only the front view is illustrated. By the other hand, the retrofitted tower with combined devices reaches ultimate conditions at a displacement of 265 mm with similar horizontal cracks out of the plane as in the case of the uniform devices, but different height of the horizontal cracks in the plane (Fig.5.4b). This slight different behavior of the retrofitted tower with combined devices at ULS could be observed by comparing both plastic activities and lateral displacements. The failure by masonry crushing is not present, due to the maximum value of stress in the compressed in-plane and out-of-plane toes is in the order of 3.177 MPa for the case of the uniform devices and 3.149 MPa for the combined devices, which are in both cases lower than the intrinsic strength (3.5 MPa).

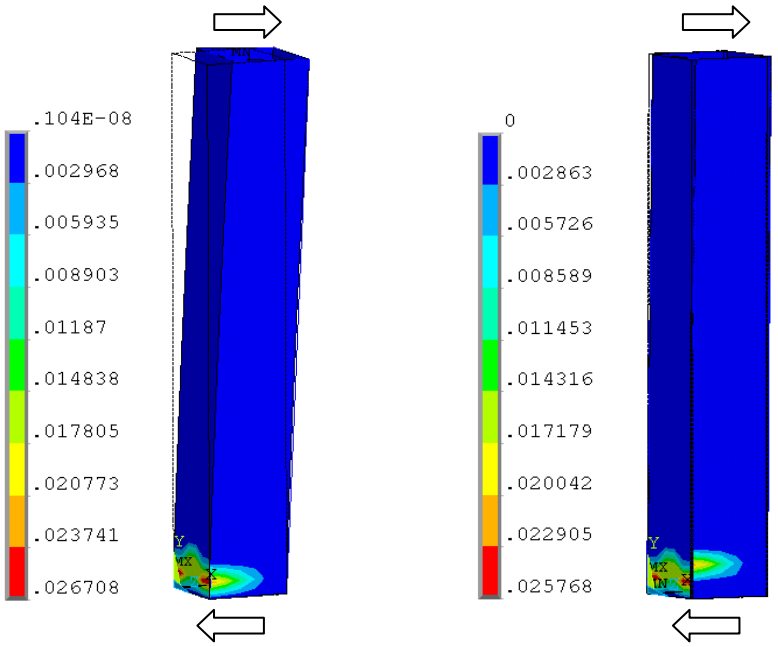

Figure 5.4: Retrofitted medieval tower (0.05Fv). Principal plastic strain contours at ULS: (a) uniform devices at U_H= 270 mm and (b) combined devices at U_H= 265 mm

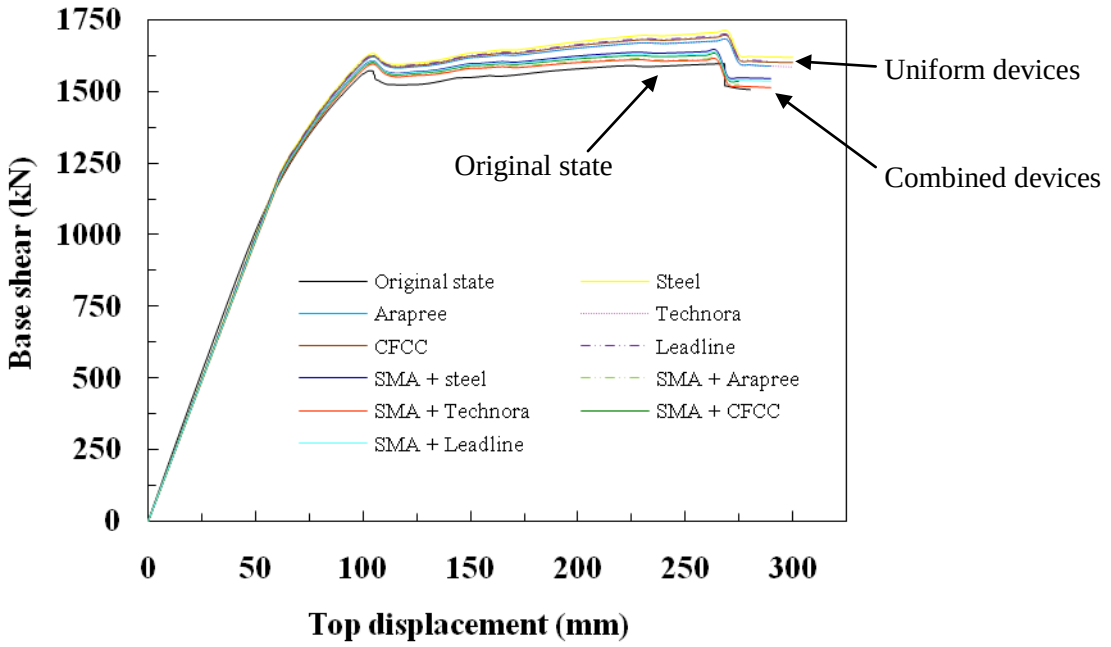

Figure 5.5: Medieval tower. Comparison of capacity curves in original state and retrofitted (0.05Fv) with the uniform and combined devices

Figure 5.5 illustrates the comparison of capacity curves (force-displacement) of the medieval tower in original state and retrofitted with the uniform and combined devices. It could be observed that both retrofitting cases do not increase the stiffness of the

tower in the linear elastic range. The differences in terms of lateral force and displacement are more obvious in the nonlinear behavior, increasing both retrofitting measures the seismic performance. The retrofitted tower with the uniform devices reaches an ULS for the five cases at a displacement of 270 mm but different base shear, being steel the one that allows more capacity, in the order of 1708 kN. By the other hand, the combined devices present a displacement of 265 mm and lower lateral load capacity as presented in table 5.4.

Device	**Steel**	**Ara.**	**Tech.**	**CFCC**	**Lead.**	**SMA + Steel**	**SMA + Ara.**	**SMA + Tech.**	**SMA + CFCC**	**SMA + Lead.**
F (kN)	1708	1679	1677	1694	1696	1642	1614	1613	1629	1631
U (mm)	270	270	270	270	270	265	265	265	265	265

Ara: Arapree; Tech: Technora; Lead: Leadline

Table 5.4: Seismic analysis summary of the retrofitted medieval tower (0.05Fv) at ULS

Changes in prestressing forces

In order to verify that the ultimate capacity of the prestressing devices is not exceeded as specified in the EC-8, the devices are checked at the point where the structure reaches the ULS. As aforementioned, in seismic conditions the tower experiences important top rotation due to its natural bending behavior, leading to elongation and shortening of the tendons. The elongation increases the tendon prestressing force and the compression applied to the masonry. In the case of shortening the opposite occurs.

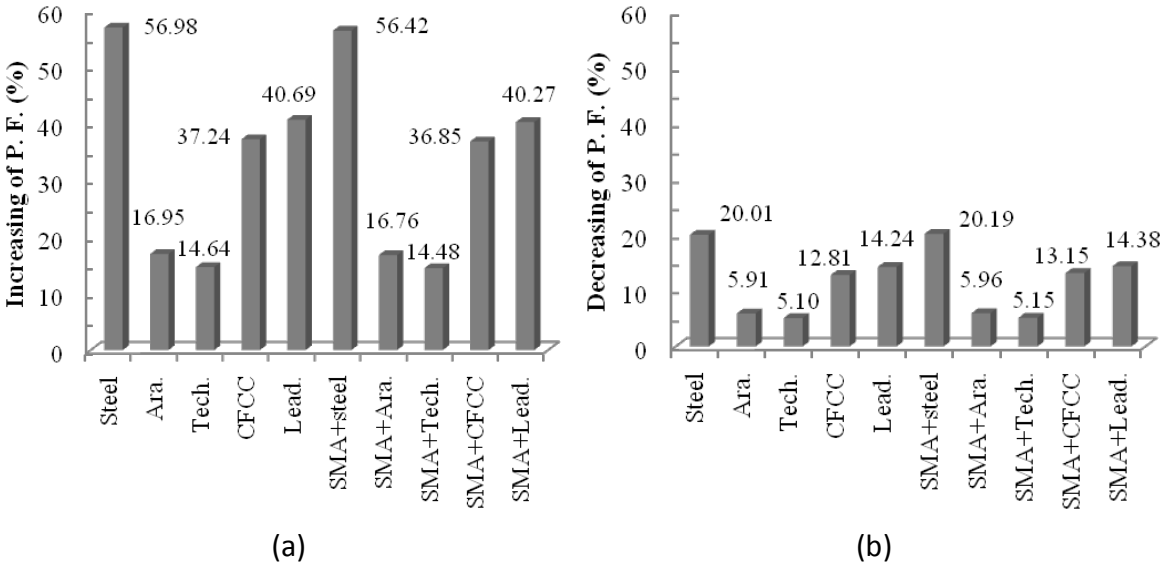

(a) (b)

Figure 5.6: Medieval tower. Changes of prestressing forces (0.05Fv) at ULS: (a) increasing in left tendons and (b) decreasing in right tendons

Figure 5.6 illustrates the changes of prestressing forces at ULS for a low prestressing level due to top rotation. It could be observed that the left tendons are the ones that present higher changes in the prestressing forces due to the increase in height because of the flexural cracks opening (Fig. 5.4). Each of the left tendons presents different force increasing depending of the E modulus of the tendon material (see tables 5.2-5.3). Steel is the stiffer prestressing device and technora the less stiff. So, the higher the E modulus, the higher the changes in prestressing forces. Comparing the increasing in prestressing forces of Figure 5.6a, it is worth noting a small decreasing in the combined devices in the order of 1%. This is due to the different displacement at ULS (265 mm), compared to the uniform devices (270 mm). So, the higher the ductility, the higher the changes in prestressing forces and plasticity. Moreover, the localized stiffness contributed by the overdesigned SMA device may explain the different crack pattern (Fig. 5.4) and seismic performance (force and displacement capacity) observed in Figure 5.5 and table 5.4. The combined devices present a lower force capacity of about 4% and 2% of lower displacement. For this increasing in prestressing forces at ULS, the safety of the devices is reviewed again and in any case occurs an exceedance of the design strengths ($\sigma_{Acting}<\sigma_{Perm}$) due to the overdesigned cross sections. Figure 5.6b illustrates the decreasing of the prestressing forces in the right tendons due to the shortening. These changes are lower compared to the ones presented in the elongated tendons because the change in height (decrease) is lower at the compressed tower's part.

5.4.3.2 Seismic analysis with medium prestressing level

In this second case, a medium prestressing level is considered and corresponds to a 15% of the vertical loading (0.15Fv). The total vertical loading of this tower is of 18900 kN, so the total applied prestressing tensile force is 2835 kN (a precompression of 0.135 MPa). Four prestressing devices vertically and externally located in every corner of the tower are considered for the retrofitting with a post-tensioned force each of 708.75 kN. Tables 5.5 and 5.6 illustrate the designed devices for this medium prestressing level. The concentration of compressive stresses at the base of the tower is checked again and is of about 0.74 MPa, which approximately corresponds to the applied precompression of 0.135 MPa. The tower is stable in static conditions due to the stresses at the bottom are lower than the compressive masonry strength.

Device ø=46 mm	**E (MPa)**	**A_T (mm^2)**	**No. of wires / bars**	**σ_{Acting} (MPa)**	**$\sigma_{Permissible}$ (MPa)**	**Comment**
Steel	210000	1680	33 wires (7 mm)	421.88	1169	$\sigma_{Acting}<\sigma_{Perm}$ **o.k.**
Arapree	62500	1680	29 bars (7.5 mm)	421.88	548	$\sigma_{Acting}<\sigma_{Perm}$ **o.k.**
Technora	54000	1680	25 bars (8 mm)	421.88	760	$\sigma_{Acting}<\sigma_{Perm}$ **o.k.**
CFCC	137300	1680	10 bars (12.5 mm)	421.88	1122	$\sigma_{Acting}<\sigma_{Perm}$ **o.k.**
Leadline	150000	1680	26 bars (7.9 mm)	421.88	1350	$\sigma_{Acting}<\sigma_{Perm}$ **o.k.**

Table 5.5: Designed devices for a medium prestressing level of 0.15Fv

Device ø=67 mm L=400 mm	E (MPa)	A_T (mm^2)	No. of NiTi wires	σ_{Acting} (MPa)	$\sigma_{Permissible}$ (MPa)	Comment
GAC® SMA	47000	3500	9917 wires (0.64 x 0.46 mm)	202.5	350	$\sigma_{Acting}<\sigma_{Perm}$ **o.k.**
NDC® SMA	60000	3500	1509 wires (1.49 mm)	202.5	600	$\sigma_{Acting}<\sigma_{Perm}$ **o.k.**
FIP® SMA	80000	3500	828 wires (2.01 mm)	202.5	670	$\sigma_{Acting}<\sigma_{Perm}$ **o.k.**

Table 5.6: Designed SMA devices for a medium prestressing level of 0.15Fv

Capacity curves and failure mechanisms

As in the case of the low prestressing level, the tower presents in both retrofitting cases (uniform and combined devices) a failure mechanism governed by bending behavior with the presence of similar out-of-plane horizontal cracks and at different height in the plane (see Fig. 5.7). The maximum plastic strain values in the retrofitted tower with the uniform devices (Fig. 5.7a) are approximately 10% higher than in the case of the retrofitting with combined devices (Fig. 5.7b). This is due to the tower reaches an ULS at 15 mm more displacement, which leads to a more ductile behavior and with this to a higher concentration of stresses at the compressed toes in the order of 3.342 MPa. By the other hand, the retrofitted tower with combined devices presents compressive stresses in the order of 3.260 MPa, with no crushing in both retrofitting cases.

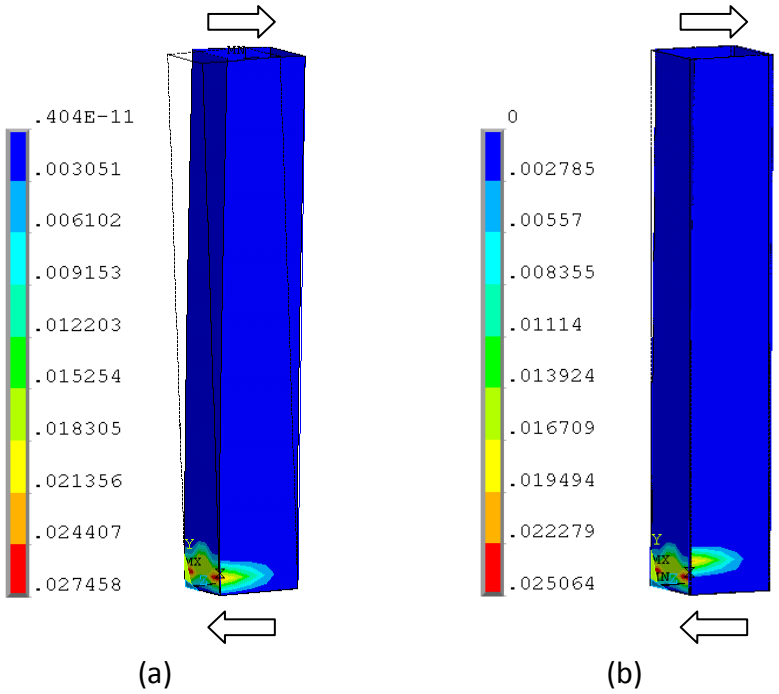

Figure 5.7: Retrofitted medieval tower (0.15Fv). Principal plastic strain contours at ULS: (a) uniform devices at U_H= 285 mm and (b) combined devices at U_H= 270 mm

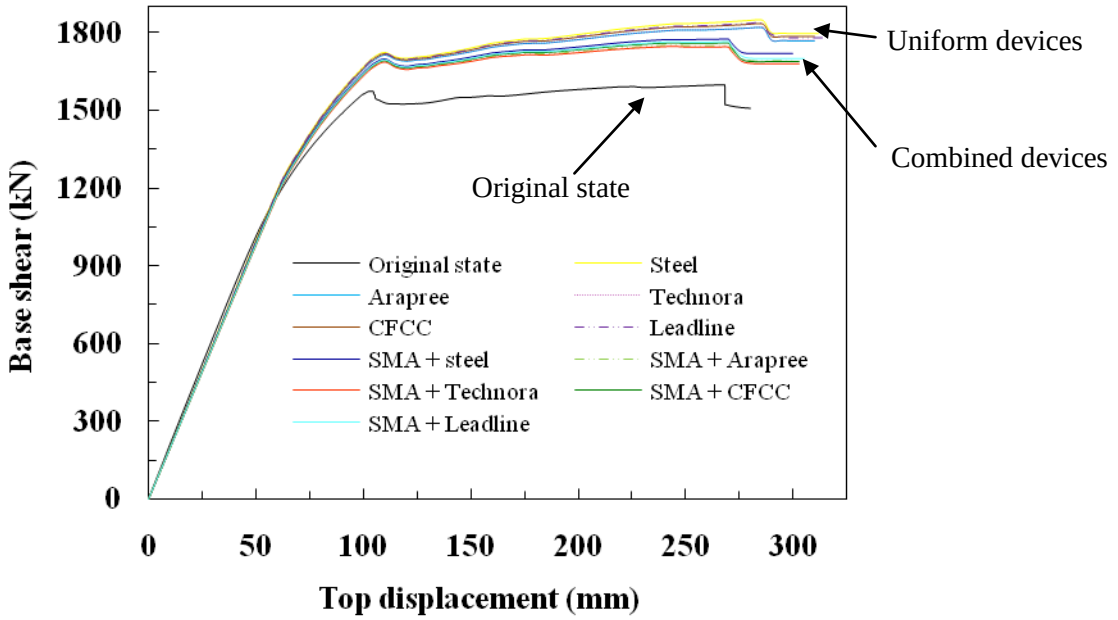

Figure 5.8: Medieval tower. Comparison of capacity curves in original state and retrofitted (0.15Fv) with the uniform and combined devices

Device	Steel	Ara.	Tech.	CFCC	Lead.	SMA + Steel	SMA + Ara.	SMA + Tech.	SMA + CFCC	SMA + Lead.
F (kN)	1850	1821	1820	1836	1839	1776	1749	1747	1763	1765
U (mm)	285	285	285	285	285	270	270	270	270	270

Ara: Arapree; Tech: Technora; Lead: Leadline

Table 5.7: Seismic analysis summary of the retrofitted medieval tower (0.15Fv) at ULS

It could be observed in the comparison of capacity curves for this intermediate prestressing level, that both retrofitting cases (uniform and combined) considerably improve the seismic performance of the tower by increasing the lateral load capacity and displacement (see Fig. 5.8). The retrofitted tower with the uniform devices reaches an ULS for the five cases at a displacement of 285 mm but different lateral force, being steel the one that presents better performance (1850 kN). By the other hand, the combined devices present lower displacement (270 mm) and force capacity due to the concentration of stresses induced by the localized SMA stiffness (table 5.7).

Changes in prestressing forces

For this intermediate prestressing level the changes of prestressing forces are analyzed at ULS in order to verify that the ultimate capacity of the devices is not exceeded and the transmitted compressive stresses to the masonry. The changes of prestressing forces in left and right tendons for the two retrofitting cases and all the devices are illustrated in

Figure 5.9. It is worth noting that in the case of the low prestressing level the changes of prestressing forces depend on the E modulus of the device, location with respect to the seismic loading (left or right) and the resulting bending top rotation. It could be observed as well for this prestressing level how the changes of prestressing forces have reduced about 65% in comparison to the low level. This is due to the reduction of the top rotation by the increasing of the precompression. The safety analysis of the devices indicates that in any case the design strengths are exceeded ($\sigma_{Acting}<\sigma_{Perm}$), because of the overdesigned cross sections.

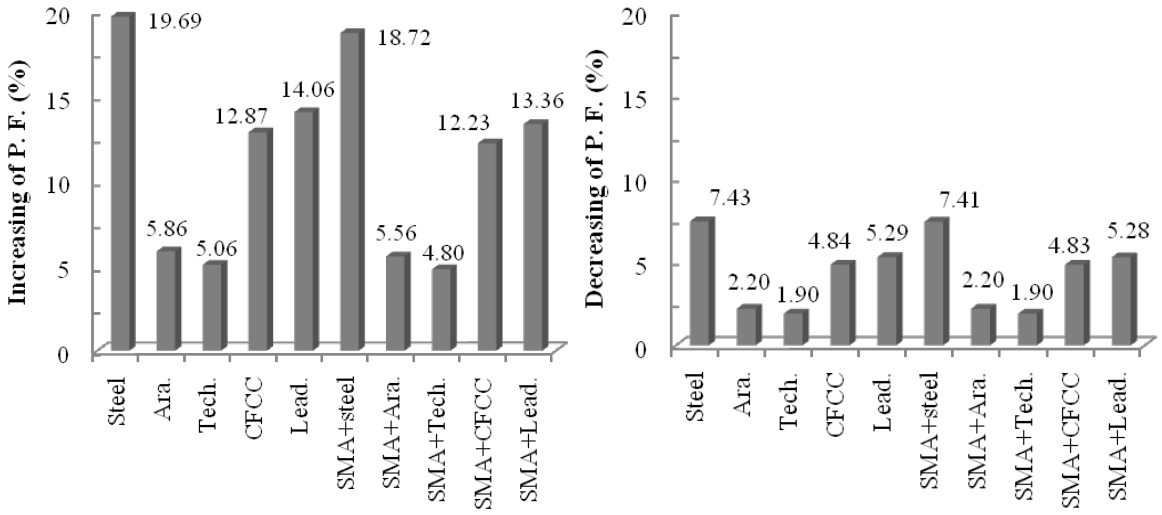

(a) (b)

Figure 5.9: Medieval tower. Changes of prestressing forces (0.15Fv) at ULS: (a) increasing in left tendons and (b) decreasing in right tendons

5.4.3.3 Seismic analysis with high prestressing level

In this final case, a high prestressing level is taken into account corresponding to a 30% of the vertical loading (0.30Fv). A post-tensioned force of about 1417.5 kN is applied to each device, resulting in a total force of 5670 kN and a precompression of 0.269 MPa.

Device ø=65 mm	E (MPa)	A_T (mm^2)	No. of wires / bars	σ_{Acting} (MPa)	$\sigma_{Permissible}$ (MPa)	Comment
Steel	210000	3360	65 wires (7 mm)	421.88	1169	$\sigma_{Acting}<\sigma_{Perm}$ **o.k.**
Arapree	62500	3360	57 bars (7.5 mm)	421.88	548	$\sigma_{Acting}<\sigma_{Perm}$ **o.k.**
Technora	54000	3360	50 bars (8 mm)	421.88	760	$\sigma_{Acting}<\sigma_{Perm}$ **o.k.**
CFCC	137300	3360	21 bars (12.5 mm)	421.88	1122	$\sigma_{Acting}<\sigma_{Perm}$ **o.k.**
Leadline	150000	3360	51 bars (7.9 mm)	421.88	1350	$\sigma_{Acting}<\sigma_{Perm}$ **o.k.**

Table 5.8: Designed devices for a high prestressing level of 0.30Fv

Device ø=91 mm L=400 mm	E (MPa)	A_T (mm^2)	No. of NiTi wires	σ_{Acting} (MPa)	$\sigma_{Permissible}$ (MPa)	Comment
GAC® SMA	47000	6500	18417 wires (0.64 x 0.46 mm)	218	350	$\sigma_{Acting}<\sigma_{Perm}$ **o.k.**
NDC® SMA	60000	6500	2802 wires (1.49 mm)	218	600	$\sigma_{Acting}<\sigma_{Perm}$ **o.k.**
FIP® SMA	80000	6500	1538 wires (2.01 mm)	218	670	$\sigma_{Acting}<\sigma_{Perm}$ **o.k.**

Table 5.9: Designed SMA devices for a high prestressing level of 0.30Fv

The designed devices for this high prestressing level are summarized in tables 5.8 and 5.9. The concentration of compressive stresses at the bottom of the tower in static conditions is in the order of 0.80 MPa, which is lower than the masonry strength. It is worth noting that the cross sections are proposed with a certain level of overdesign in order to withstand this high prestressing level in static conditions including a safety factor due to the possible changes in prestressing forces at ULS.

Capacity curves and failure mechanisms

As in the two previous prestressing levels, the tower presents in both retrofitting cases a flexural failure mode with the presence of similar out-of-plane horizontal cracks and at different heights in the plane (see Fig. 5.10).

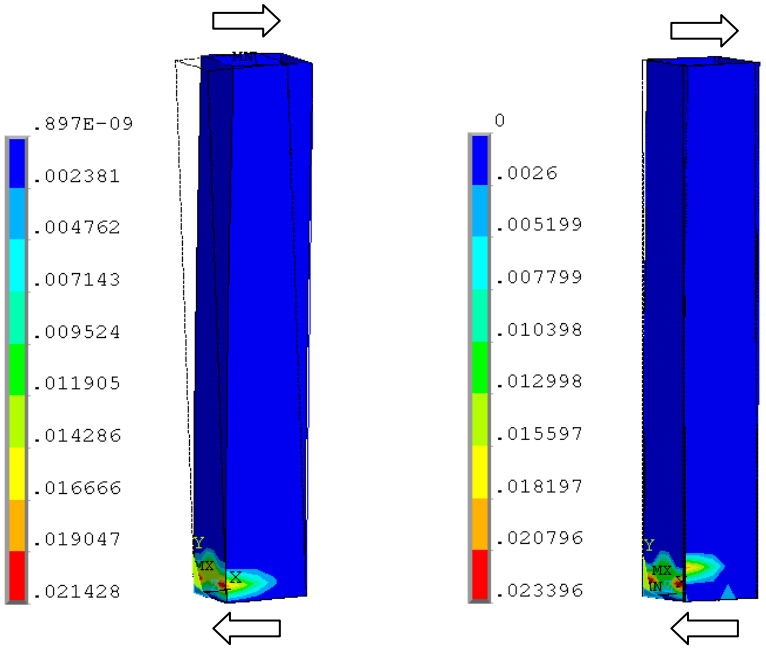

Figure 5.10: Retrofitted medieval tower (0.30Fv). Principal plastic strain contours at ULS: (a) uniform devices at U_H= 260 mm and (b) combined devices at U_H= 275 mm

In this case, the opposite of the low and medium prestressing levels occurs regarding the plastic activity and displacement capacity at ultimate conditions of the tower. The maximum plastic strain values in the retrofitted tower with uniform devices (Fig. 5.10a) are approximately 8.5% lower than in the case of the retrofitting with combined devices (Fig. 5.10b) and presents 15 mm less displacement. This increase in displacement presented by the retrofitted tower with the combined devices leads to a stress concentration at the compressed toes in the order of 3.388 MPa, becoming evident the early formation of a slight vertical cracking in the plane because the compressive strength of masonry (3.5 MPa) is almost reached. By other instance, the retrofitted tower with uniform devices presents compressive stresses of 3.344 MPa with no vertical cracking. A possible reason to explain this contrast in displacement could be related to the precompression level and high concentration of stresses at the SMA near to the austenite start stress (beginning of the superelasticity). This led to a global less stiff behavior of the devices than in former prestressing levels.

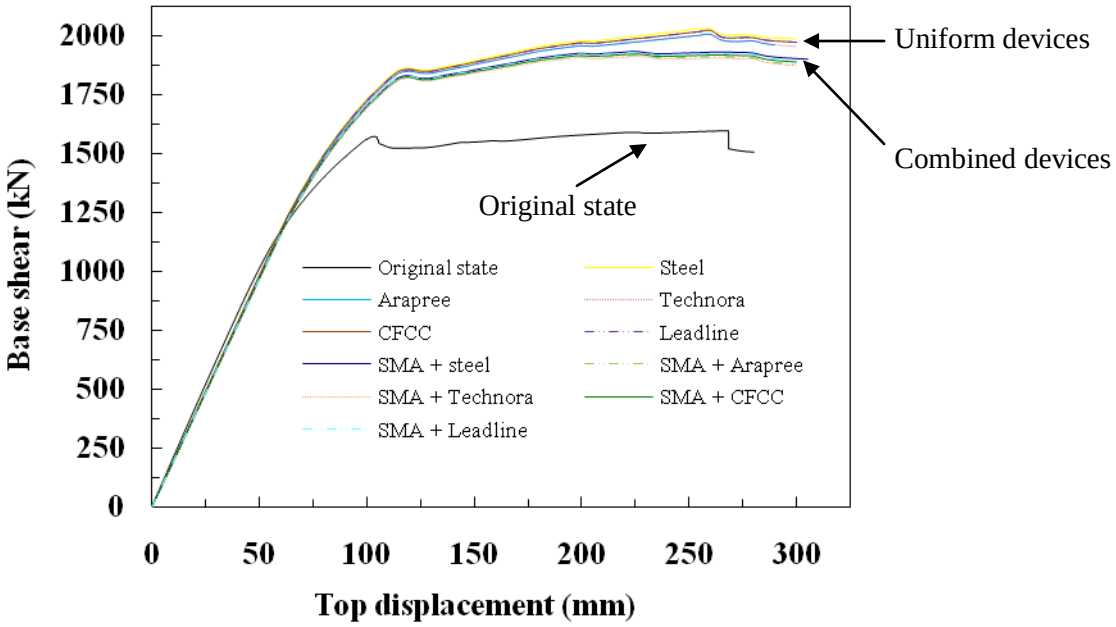

Figure 5.11: Medieval tower. Comparison of capacity curves in original state and retrofitted (0.30Fv) with the uniform and combined devices

Device	Steel	Ara.	Tech.	CFCC	Lead.	SMA + Steel	SMA + Ara.	SMA + Tech.	SMA + CFCC	SMA + Lead.
F (kN)	2026	2009	2008	2021	2023	1931	1907	1906	1919	1921
U (mm)	260	260	260	260	260	275	275	275	275	275

Ara: Arapree; Tech: Technora; Lead: Leadline

Table 5.10: Seismic analysis summary of the retrofitted medieval tower (0.30Fv) at ULS

In the comparison of capacity curves of Figure 5.11 retrofitted with the uniform and combined devices, it could be observed that the linear behavior of the tower is substantially increased, presenting the start of the nonlinear behavior at a lateral load of about 1450 kN and a displacement of 75 mm. The uniform devices permit to improve in a better way as in the two first prestressing levels the lateral force capacity of the tower, but in contrast present 15 mm of less displacement as above mentioned. It is worth noting that in both retrofitting cases the tower presents a different post-peak behavior after reaching the ULS, characterized for a more stable failure in comparison to the low and medium prestressing levels. The results of the seismic analyses for this high level are summarized in table 5.10.

Changes in prestressing forces

As above mentioned, in this high prestressing level, the retrofitted tower with the combined devices reaches at ULS for the five cases about 15 mm more lateral displacement than in the retrofitting with the uniform devices. This increase in displacement is reflected in the changes of prestressing forces of Figure 5.12 due to top rotation. However, this high prestressing level induces that the top rotation reduces due to the precompression. By comparing the changes of prestressing forces in the left tendons of this level, in comparison to the low level, there is a reduction of these changes in the order of 85%, and 57% less than in the intermediate level. In any case the design strength of the tendons is exceeded ($\sigma_{Acting}<\sigma_{Perm}$) due to the overdesigned cross sections and the small increasing in prestressing forces. In the seismic risk reduction of the historical towers of section 5.5, these cross sections are optimized taking into account the increasing in prestressing forces at ultimate conditions in dependency of the proposed prestressing level and post-tensioned device.

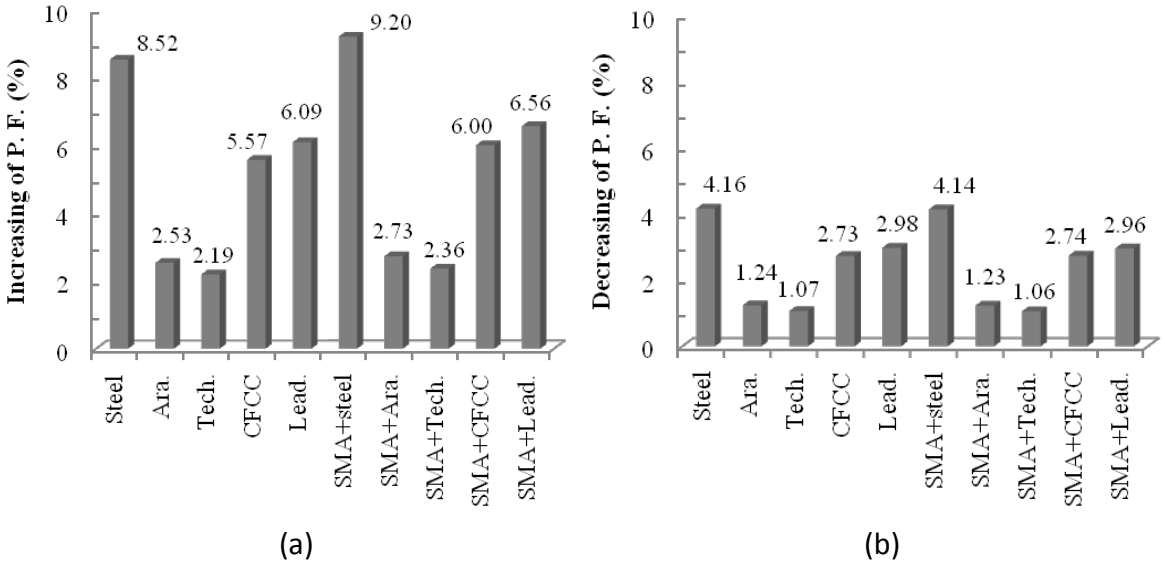

Figure 5.12: Medieval tower. Changes of prestressing forces (0.30Fv) at ULS: (a) increasing in left tendons and (b) decreasing in right tendons

5.4.3.4 Seismic analysis with SMA induced superelasticity

In the seismic analyses of the retrofitted tower with low, medium and high prestressing levels no especial behavior was observed in the combined devices with SMA in terms of changes of prestressing forces and seismic performance contribution. In the low and medium prestressing levels was observed a lower contribution in lateral force and displacement capacity in comparison to the uniform devices with no SMA. This was related to the contributed localized stiffness by the SMA device. This contribution was also reflected by means of slight differences in the changes of prestressing forces in the elongated and shortened tendons respectively. In the high prestressing level the combined devices allowed obtaining more displacement and higher changes in tendon forces than the uniform devices, but in contrast presented lower lateral force contribution as in former prestressing levels. However, in both retrofitting cases (uniform and combined) the seismic performance of the tower was successfully enhanced. Unfortunately, in the parametric study was not observed the superelasticity behavior of SMA which is characterized for keeping the prestressing forces constant. This is due to the post-tensioned forces in static conditions and at ULS did not reach the austenite start stress ($\sigma_s^{A\text{-}S}$) of the three SMA of different fabricants used in the parametric study. This led to a similar linear stress-strain behavior of traditional materials. It mainly occurred due to the overdesigned cross sections of the SMA devices.

This section aims at inducing the SMA superelasticity in order to quantitatively verify its contribution in the seismic performance of the tower and in the changes of prestressing forces. The methodology to do so is based by following the process carried out in orthodontics. The shape memory effect in NiTi wires is produced by temperature and not by stress; meanwhile the superelasticity effect is achieved by inducing a martensite forward transformation by stress (deformation) or a reverse martensite transformation by temperature. So, the arch wires are initially adjusted at room temperature, and the oral temperature (about 35°C) activates the martensite reverse transformation by providing a light and constant force for a long period of time. For the seismic analysis with SMA induced superelasticity the NDC® NiTi wire is selected due to its larger strain capability (8%) in comparison to the FIP® and GAC® wires and low E modulus (table 3.5). The stress-induced martensite transformation is aimed at designing the cross section of the SMA device for the initial prestressing force in static conditions at the austenite start stress ($\sigma_s^{A\text{-}S}$= 520 MPa), and with the increasing of the post-tensioning force at ULS of the tower to reach the forward transformation branch up to the austenite final stress ($\sigma_f^{A\text{-}S}$= 600 MPa) at a strain of 8%. If the tensile stresses continue instead of following the unloading path, the large deformation could lead to the failure of the SMA as observed in the experimental tests of Zurbitu et al. [2009]. The authors observed as well that the unloading in the incomplete stress-induced martensite transformation branch leads to the formation of a plateau with lower energy dissipation than that observed in the complete martensite transformation. By comparing the austenite start and final stresses of the selected NDC® NiTi wire for the seismic analysis with induced superelasticity, it could be observed that the allowed increase in stress is in

the order of 15.4% (80 MPa). Due to this restriction, only the devices that showed in the three prestressing levels (low, medium and high) changes of prestressing forces lower than this percentage are selected for the investigations with stress-induced martensite transformation (see Figs. 5.6, 5.9 and 5.12). Table 5.11 illustrates the selected stiffer and weaker tendon materials (steel and technora) combined with SMAs, as well as the respective cross sections and initial post-tensioning forces.

Prestressing level	Device	A_T (mm^2)	No. of wires / bars	σ_{Acting} (MPa)	$\sigma_{Permissible}$ (MPa)	Comment
Low 0.05Fv= 945 kN 236.25 kN each	Technora ø=27 mm	560	8 bars (8 mm)	421.88	760	$\sigma_{Acting}<\sigma_{Perm}$ **o.k.**
	SMA ø=24 mm	454	195 wires (1.49 mm)	520	600	$\sigma_{Acting}<\sigma_{Perm}$ **o.k.**
Medium 0.15Fv= 2835 kN 708.75 kN each	Technora ø=46 mm	1680	25 bars (8 mm)	421.88	760	$\sigma_{Acting}<\sigma_{Perm}$ **o.k.**
	SMA ø=42 mm	1363	586 wires (1.49 mm)	520	600	$\sigma_{Acting}<\sigma_{Perm}$ **o.k.**
High 0.30Fv= 5670 kN 1417.5 kN each	Technora ø=65 mm	3360	50 bars (8 mm)	421.88	760	$\sigma_{Acting}<\sigma_{Perm}$ **o.k.**
	Steel ø=65 mm	3360	65 wires (7 mm)	421.88	1169	$\sigma_{Acting}<\sigma_{Perm}$ **o.k.**
	SMA ø=59 mm	2726	1172 wires (1.49 mm)	520	600	$\sigma_{Acting}<\sigma_{Perm}$ **o.k.**

Table 5.11: Designed combined devices for the stress-induced martensite transformation

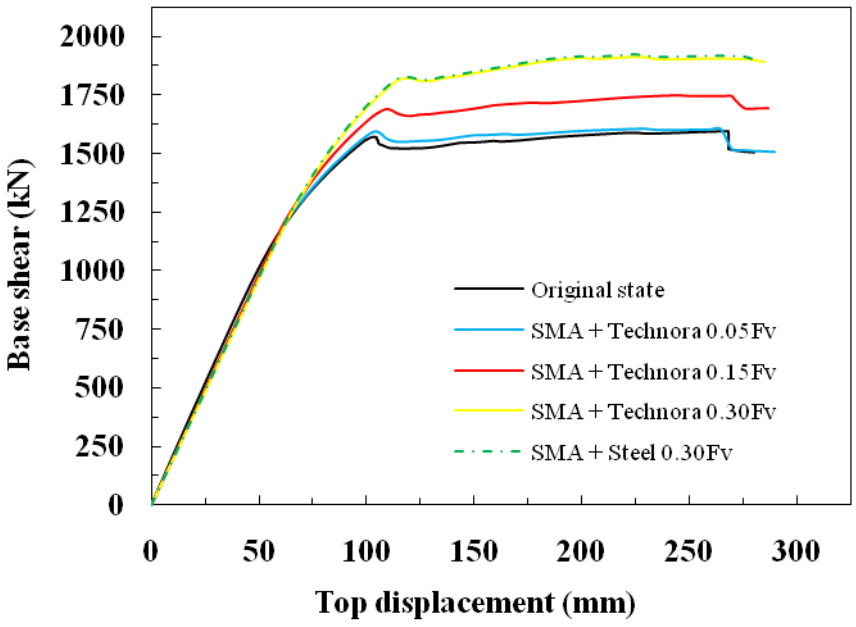

Figure 5.13: Medieval tower. Comparison of capacity curves in original state and retrofitted with SMA induced superelasticity

The results of the seismic analysis of the retrofitted medieval tower with SMA induced superelasticity in terms of capacity curves are illustrated in Figure 5.13. By comparing the capacity curves of the three prestressing levels of Figures 5.5, 5.8 and 5.11, it could be observed that the stress-induced martensite transformation of the SMA has no impact in further improvement of the lateral load and displacement capacity as the observed without transformation. The tower presents ultimate conditions at the same displacements with minimum variations in the lateral forces (less than 1%). This trend is also reflected in the failure mechanisms. The tower fails as well for bending and presents the same crack patterns with minimum variations (about 1%) in the plastic activity compared to the similar analysis with the same prestressing device and force, but without the induced transformation (see Figs. 5.4, 5.7 and 5.10). The maximum values of stress at the compressed toes (in-plane and out-of-plane) are almost the same as well, and in all cases lower than the intrinsic strength (3.5 MPa).

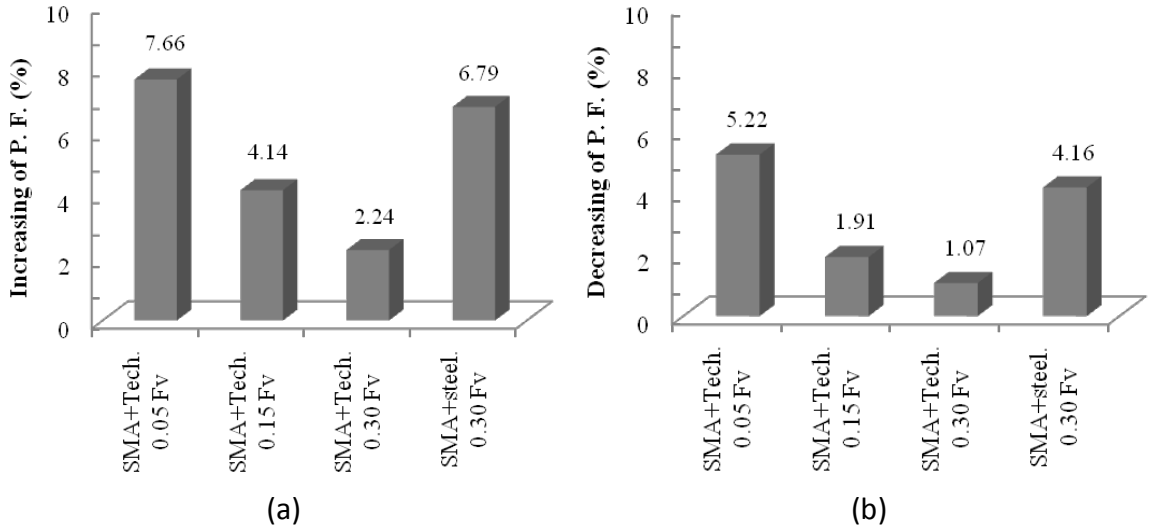

Figure 5.14: Medieval tower. Changes of prestressing forces at ULS with SMA induced superelasticity: (a) increasing in left tendons and (b) decreasing in right tendons

The decreasing of forces in the right tendons with the induced transformation (Fig. 5.14b) are similar than those observed without it (Figs. 5.6b, 5.9b and 5.12b). The impact is observed in the elongated left tendons (Fig. 5.14a), with a substantial reduction of the increasing of forces. For the case of the combined SMA with technora and a low prestressing level, the reduction is of about 47.10%. By the other hand, in the medium level a reduction of about 13.75% is achieved and 5.08% in the high level. A contrast in the combined SMA with steel and high prestressing level is observed, with a reduction in the order of 26.20%. This variation is due to the high E modulus of steel (210000 MPa) in comparison to that of the technora FRP (54000 MPa). It is worth noting in Figure 5.14a that the increasing of prestressing forces is lower than the allowed increase in stress/force of 15.4%. In any case the failure of the devices is presented.

5.4.4 Findings and proposed prestressing levels and devices

The evaluation and comparison of the nonlinear static analyses results presented through the parametric study led to the following comments:

Low prestressing level

- In any case of the three prestressing levels (PL) was observed failure by crushing at the tower's base, due to the compressive stresses were lower than the strength. The seismic analyses results (force and plasticity) for the three PL and combined devices (CD) with three different SMAs showed minimum variations (1%) and the same failure mode.

- The tower with UD showed flexural failure as in original state and ULS in the five cases at 270 mm but different load. Steel showed more force capacity (1708 kN). The retrofitted with CD reached for all the cases 265 mm with similar horizontal cracks out of the plane as with the UD but lower force capacity and other height of in-plane cracks.

- The tower with CD showed 3.52% less plastic deformation due to the 5 mm of less displacement compared to UD. Both cases enhanced the tower's seismic performance (CD: force and UD: force and displacement). At ULS the failure by masonry crushing was not observed. The maximum stress in the compressed in-plane and out-of-plane toes was 3.177 MPa (UD) and 3.149 MPa (CD), in both cases lower than the intrinsic strength.

- Left tendons showed higher changes in prestressing forces (PF) due to the increase in height by the flexural cracks opening. The different increasing of PF depended on the E modulus of the tendon material. Steel was the stiffer prestressing device (PD) and technora the weaker. So, the higher the E modulus, the higher the changes in PF.

- Comparing the increasing in PF, a small reduction in the CD in the order of 1% was observed. This is due to the localized stiffness induced by the overdesigned SMA device. This explained the different crack pattern and seismic performance between the UD and CD. The CD showed lower lateral load capacities (4%) and displacement (2%).

- At ULS the tower experienced important top rotation by natural bending behavior. The cracks opening led to elongation of the left tendons and this considerably increased the PF and the compression to the masonry. In the shortened right tendons the opposite was observed, but lower due to the change in height was minor at the compressed top. There was no device failure due to the overdesigned cross sections.

Medium prestressing level

- As in the low PL, the tower failed by bending and same crack pattern. The retrofitted tower with UD reached an ULS for the five cases at 285 mm but different lateral force, being as well steel the one that presented better performance (1850 kN). The CD presented 270 mm and lower lateral force by the SMA stiffness contribution.

- The plasticity in the retrofitted tower with UD was 10% higher than with CD due to the 15 mm of more displacement at ULS. This led to a more ductile behavior and

concentration of stresses at the compressed toes (3.342 MPa). The tower with CD showed high compressive stresses as well (3.260 MPa), with no crushing in both cases.

- Both retrofitting cases (UD and CD) did not considerably increase the stiffness of the tower in the linear elastic range. The enhancement in terms of lateral force and displacement was obvious in the nonlinear range, increasing both measures the seismic performance and in a better way than the low PL.

- In this PL the changes of PF (increasing and decreasing) reduced about 65% in comparison to the low level due to the reduction in height of the flexural cracks opening induced by the three times higher precompression. In any case the devices failed.

- In the increasing of PF with UD and CD was observed a decreasing of 5% in the CD due to the SMA localized stiffness contribution. This was reflected by different seismic performance. In comparison to UD, CD showed the same rate of lower force capacity (4%) as the observed in the low PL, but three times the rate of lower displacement (6%).

High prestressing level

- As in the two previous PLs, the tower failed by bending and same crack pattern. The opposite of the low and medium PLs occurred regarding the plastic activity and displacement capacity at ULS. The maximum plastic strains values with the UD were 8.5% lower than in the case with CD and presented 15 mm less displacement.

- The high PL and increase in displacement with CD, led to a concentration of stresses at the compressed toes of 3.388 MPa with the formation of slight vertical cracking in the plane because of the masonry compressive strength (3.5 MPa) was almost reached. The tower with UD presented compressive stresses of 3.344 MPa with no vertical cracking.

- The linear strength of the tower was substantially increased, presenting the start of the nonlinear behavior at 1450 kN and 75 mm. The UD improved in a better way as in the two first PL the lateral force, but in contrast presented 15 mm of less displacement.

- In this high PL, the CD presented lower force enhancement compared to the UD but more displacement. Due to the high deformation, the SMA was near to the austenite start stress, leading to behave less stiff than former PLs. In both retrofitting cases the tower showed different post-peak behavior, failing more stable compared to former PLs.

- The increasing in displacement with CD was reflected in the changes of PF due to the augment in top rotation. However, the high PL induced less top rotation than the former PLs due to the high precompression. The changes in left tendons of this PL in comparison to the low level decreased 85% and 57% less than in the medium level.

SMA induced superelasticity

- The SMA superelasticity behavior which characterizes for keeping the PF constant was not observed through the parametric study. This was due to the post-tensioned

forces in static conditions and at ULS did not reach the SMA austenite start stress because of the overdesigned cross sections, behaving similar to traditional materials.

- The martensite transformation was successfully induced with the designed cross sections and initial PF at the austenite start stress. It permitted to observe the SMA superelasticity with the increasing of PF at ULS by reaching the forward transformation branch and without exceeding the austenite final stress that could lead to its failure.

- The difference between the austenite start stress and the austenite final stress represents the allowed increase in the changes of PF. In the case of the selected NDC® SMA for the stress-induced martensite transformation (SIMT) was 15.4%.

- In the seismic analyses, the SIMT of the SMA had no impact in further enhancement of the lateral load and displacement capacity as the observed without transformation. The same failure mode and crack pattern were observed with minimum variations of 1% in lateral forces and plastic deformations.

- The decreasing of forces in right tendons with the transformation were similar than without it. The impact was in the elongated left tendons with a substantial reduction of the increasing of PF: SMA + technora and low PL reduced 47.10%, medium PL 13.75% and high PL 5.08%. SMA + steel and high PL showed 26.20% of reduction. In all cases the increasing of PF were lower than the SMA allowed increase (15.4%).

Proposed prestressing levels and devices

Through the numerical parametric study was observed that the flexural resistance of historical masonry towers in terms of lateral load and ductility capacity could be successfully enhanced by the application of vertical prestressing. The external post-tensioned tendons located in the four corners of the tower transmit normal forces to the masonry that increases friction and resistance by reducing the tensile stresses with the applied pre-compression. The level of enhancement mainly depends on the applied normal forces and the tendon material as observed in the three different PLs under study. In the low PL, the UD showed better performance (force and displacement) than SMA with and without SIMT. Steel was the tendon material that allowed higher lateral force capacity but in contrast higher changes in PF due to its high E modulus. By the other hand, technora presented a slight reduction in force capacity compared to steel, but much lower changes in prestressing forces by its low E modulus. So, this FRP material and PL could be recommended for towers located in low seismic hazard zones. In the medium level, the UD enhanced force and displacement in a better way than SMA with and without SIMT. The technora device and this PL could be proposed for towers in zones with low to medium seismicity. For zones with medium to high seismic hazard a high PL is recommended. For this level technora and SMA + technora showed better enhancement and stable post-peak behavior. Technora allowed higher force capacity but lower displacement than SMA + technora. Especial attention is suggested in high PLs, due to the elevated normal forces and redistribution of stresses at ULS (about 10% higher than in original conditions) could lead to a brittle failure by masonry crushing.

5.5 Seismic risk reduction of the virtual historical towers

The parametric study permitted to develop a methodology for the seismic risk reduction of historical masonry towers by means of vertical external prestressing. The proposed prestressing levels and devices mainly depend on the seismic hazard of the zone under study. It is worth noting that the approach was developed through towers presenting failure modes governed by flexion. Therefore no great impact was observed in displacement enhancement due to towers failing in bending are ductile by nature. In this case the virtual medieval tower was used in the seismic analyses. Two other different failure mechanisms were identified in the seismic risk assessment evaluations presented in chapter 4. By the one hand, the bell tower with timber roof and reduced openings showed at the lower part a combined failure mode of bending and shear. This combination led to more force and displacement capacity compared to the tower failing by bending. This contrast was due to the different crack pattern that allowed more energy dissipation. The same tendency on shear walls was experimentally observed by Raijmakers and Vermeltfoort [1992] and Vermeltfoort and Raijmakers [1993] and numerically in section 4.3.3.2. The bell towers with heavy roof presented a brittle failure by shear stresses at belfry which is the most common failure mode. In this section, the possibility to enhance by retrofitting the seismic performance of towers subjected to these three failure modes is studied, mainly with medium (0.15Fv) and high prestressing levels (0.30Fv) to assess which is the maximum reachable performance.

5.5.1 Seismic risk comparison: Original state and retrofitted

As above mentioned, in the following sections the three failure mechanisms observed through the seismic risk assessment of the four virtual towers of chapter 4 are studied. The towers are retrofitted with the proposed prestressing levels and devices and reanalyzed, in order to develop a seismic risk comparison between original conditions and retrofitted. In this comparison, the level of seismic risk reduction is assessed in terms of strength, ductility and confinement enhancement, based on the limit states of the EC-8 and the damage grades EMS-98.

5.5.1.1 Flexural failure mechanism

This failure mechanism was studied through the developed parametric study. In this case is quite important to enhance the seismic performance of the tower by increasing its bending resistance without reducing its natural ductility. The retrofitted tower presents at ULS the same failure mode as in original conditions but with a clear increasing of its lateral force of 25.5% (see tables 5.12 and 5.13) and reflected as well in a reduction of the plastic activity (20%). By the other hand the retrofitted tower presents the peak load at 1.9% less displacement but a more ductile failure (post-peak behavior) induced by the confinement with the post-tensioned tendons at the tower´s corners. This means that the building is highly damaged but is still stand and capable of withstanding force and displacement, and the most important, that the monument could be reparable, instead

of the sudden brittle failure observed in original conditions (see Figs. 5.15 and 5.16). The failure by masonry crushing and the devices do not occur.

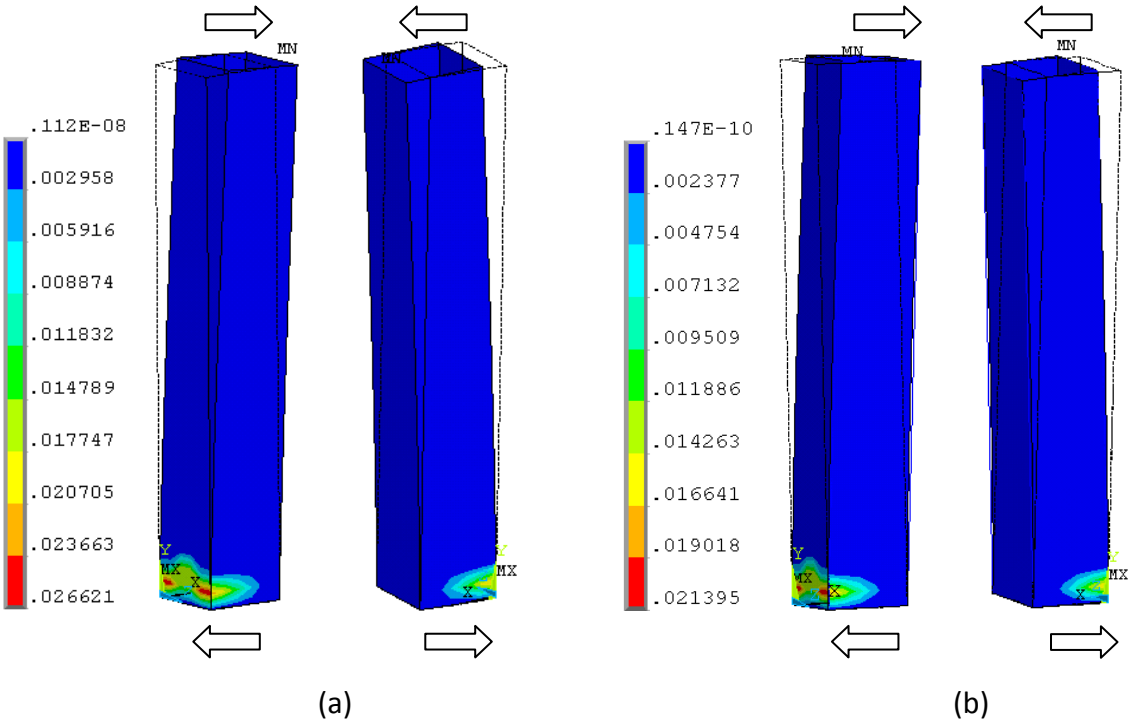

Figure 5.15: Medieval tower. Comparison of principal plastic strain contours (front and back) at ULS: (a) original state at 265 mm and (b) retrofitted 0.30Fv technora at 260 mm

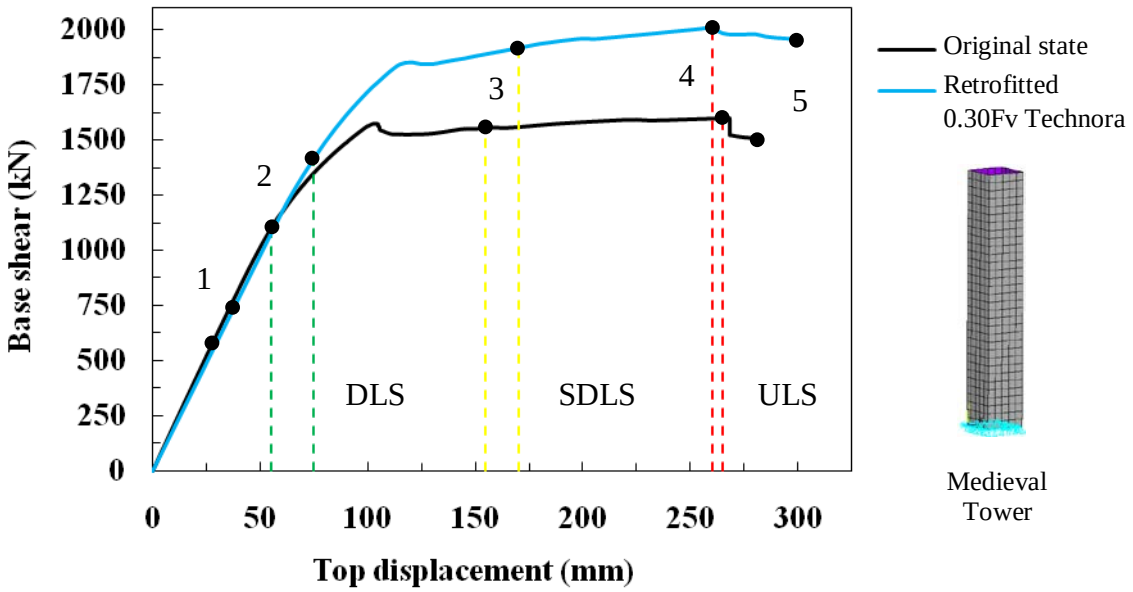

Figure 5.16: Medieval tower. Comparison of capacity curves in original state and retrofitted (0.30Fv) with the damage grades (EMS-98) and limit states (EC-8)

5.5.1.2 Flexural-shear failure mechanism

In this combined failure mode is important as in the case of the medieval tower to increase the bending resistance without considerably reducing the natural ductility. In original conditions, the combination of bending behavior and shear stresses at the lower tower´s body due to the door changes the behavior by inducing more force and displacement capacity (energy dissipation) compared to the medieval tower (Fig. 4.24). It is worth noting that the retrofitting increases the bending resistance, withstanding higher lateral force at ULS of about 21% (Figs. 5.17-18 and tables 5.12-13) and reduces the crack size and plasticity approximately 16.5%. The reduction of the crack extension is observed in the out-of-plane part of the tower and in the plane of the posterior part.

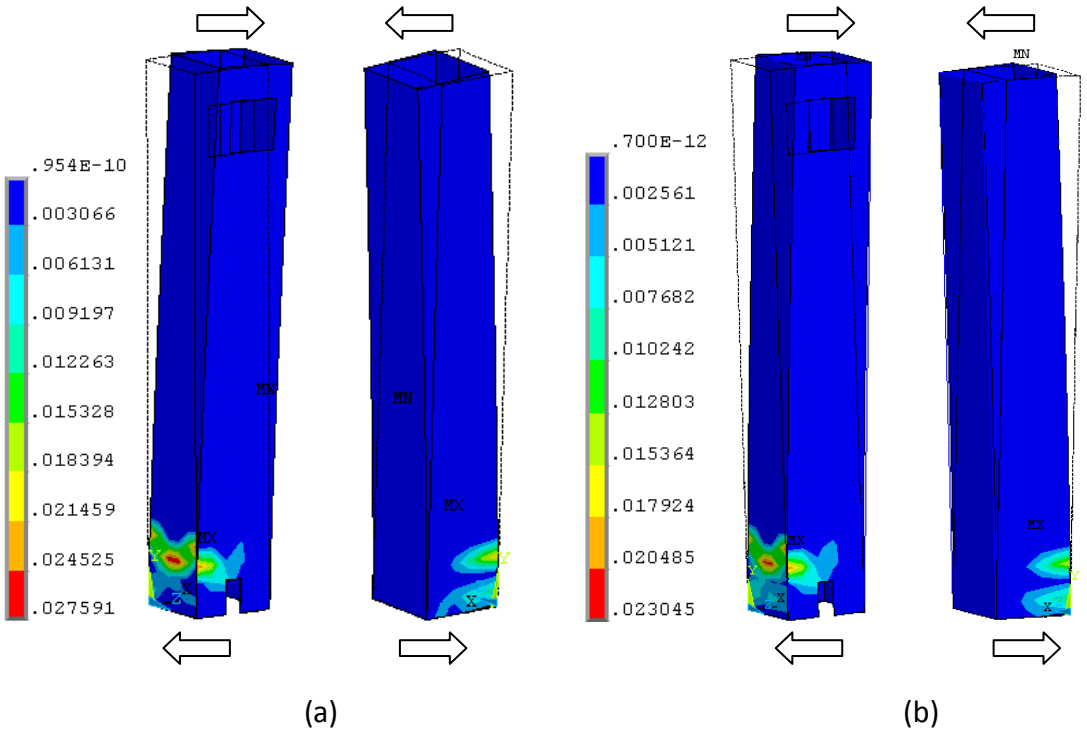

Figure 5.17: Bell tower. Comparison of principal plastic strain contours (front and back) at ULS: (a) original state at 325 mm and (b) retrofitted 0.30Fv technora at 325 mm

The failure by shear in the plane of the main door is not changed, which is favorable to the tower. Compared to the non strengthened tower, the retrofitting does not induce an enhancement of displacement capacity but presents a more ductile post-peak behavior as observed in the retrofitted medieval tower with the possibility of not to lose the structure due to the confinement. This mechanism is also favorable in order to avoid a brittle failure by masonry crushing. In original conditions the tower reached at ULS at the compressed toes stresses of about 3.305 MPa and retrofitted 3.342 MPa, in both cases lower than the strength (3.5 MPa). The failure of the devices do not occur due to the low changes of prestressing forces in the tendons (left: +2.84%, right: -1.17%) thanks to the selected technora device with low E modulus. For towers presenting flexural

failure or this combined mode is proposed the technora device for the three levels of prestressing according to the seismic hazard of the zone. The proposal is recommended for towers with a compressive strength of at least 15% higher than the maximum observed stress at the compressed toes at ULS in original conditions.

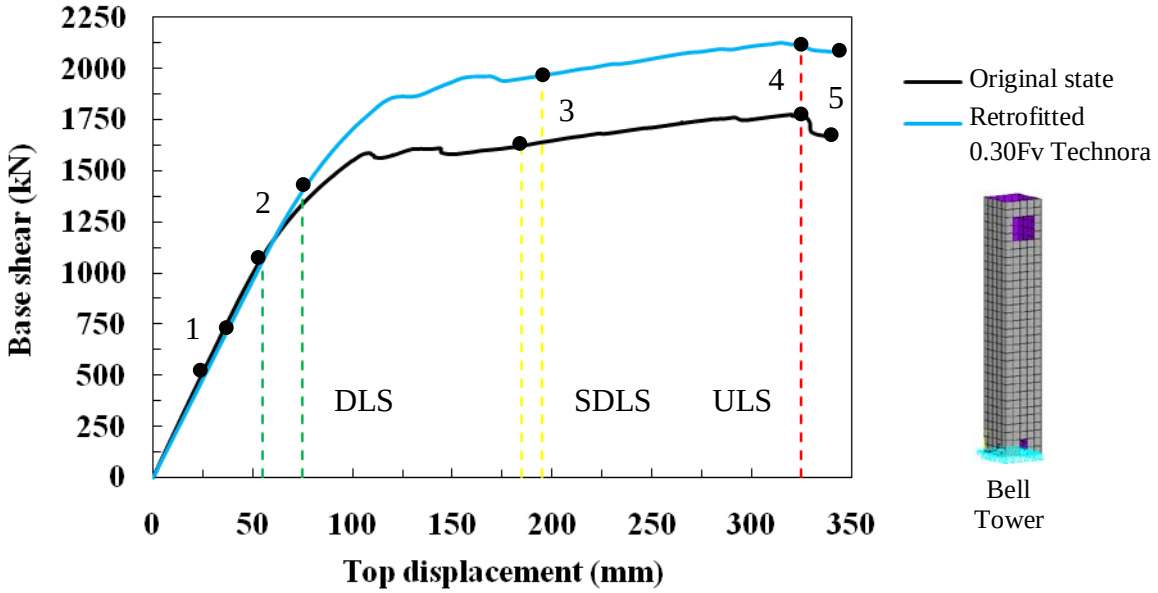

Figure 5.18: Bell tower. Comparison of capacity curves in original state and retrofitted (0.30Fv) with the damage grades (EMS-98) and limit states (EC-8)

5.5.1.3 Shear failure mechanism

This failure mode is commonly represented by shear stresses at belfry due to the large openings, and flexural cracks by the relative low vertical loading at this upper part. This leads to a brittle failure ending with the collapse of the belfry as explained in section 2.4.6.5, and numerically represented by the crack pattern in the two bell towers of chapter 4. This is the most common failure mode presented by bell towers under seismic action. As it could be observed, in the bell tower failing by a combined flexural-shear mode (section 5.5.1.2), the shear stresses were present at the lower part at the door and not at belfry because of the presence of only one window, showing good performance. The shear stresses at the door were induced by the elevated loading at this lower part and the opening itself. For towers failing by shear and bending at belfry is quite important to enhance force and displacement capacity by inducing a flexural ductile failure, but mainly confinement. For practical purposes and due to the need of developing several seismic analyses, the large bell towers of chapter 4 were substituted in the retrofitting investigations by the bell tower with more openings at belfry of Figures 5.19 and 5.21. The tower was retrofitted with medium and high prestressing levels, enhancing both cases the seismic performance in terms of force, displacement and confinement (Figs. 5.20 and 5.22). In this case the retrofitting allows lower force enhancement than in the flexural and combined failure modes, but more displacement.

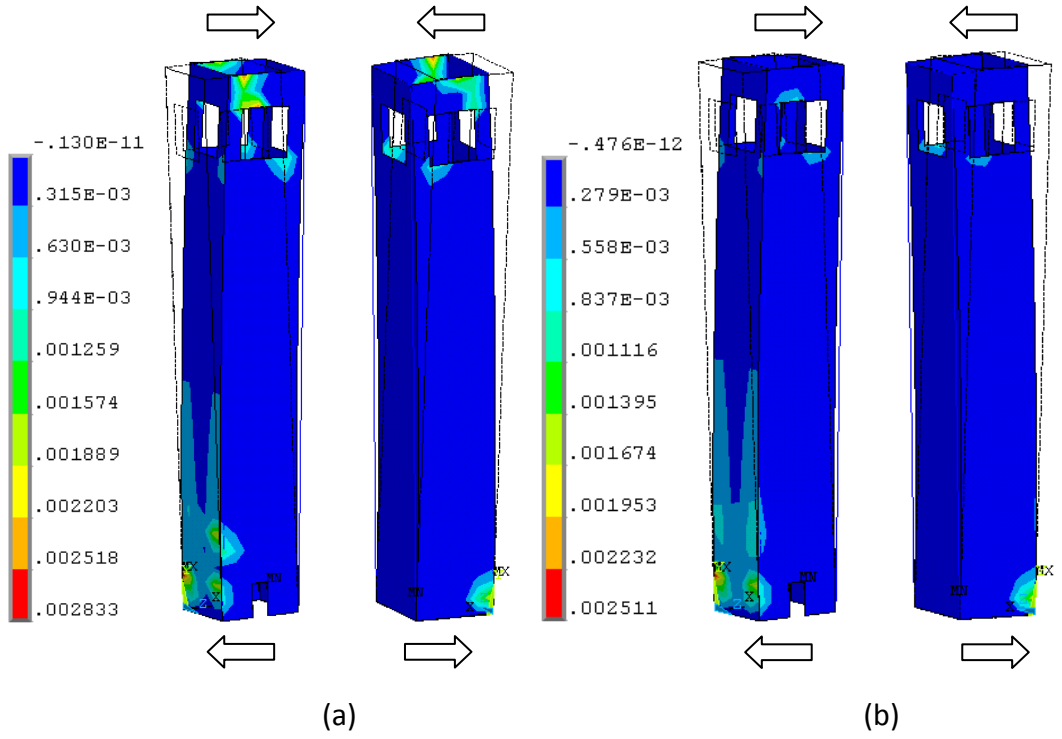

Figure 5.19: Bell tower. Comparison of principal plastic strain contours (front and back) at a displacement of 130 mm: (a) original state (ULS) and (b) retrofitted 0.15Fv technora

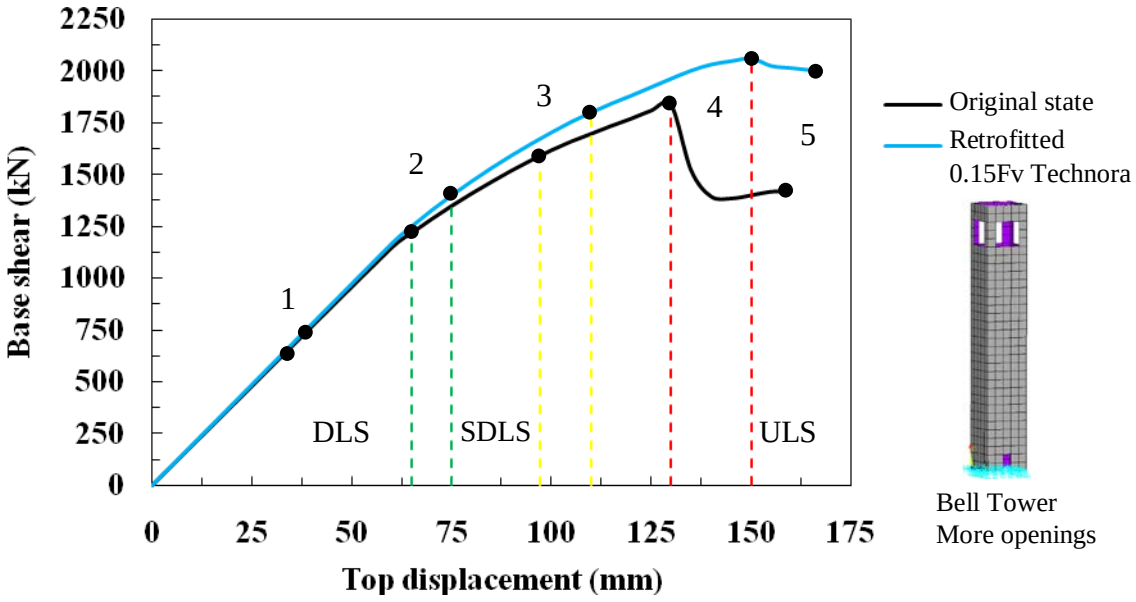

Figure 5.20: Bell tower. Comparison of capacity curves in original state and retrofitted (0.15Fv) with the damage grades (EMS-98) and limit states (EC-8)

In original state the tower fails by bending at the lower body and a loss of belfry by a combination of shear in the plane and out-of-plane bending. It is worth noting in the

comparison of Figures 5.19 and 5.21 the way that both retrofitting measures substantially reduce the damage by decreasing the plastic activity and the extension of cracks especially at belfry. At ULS, both retrofitting levels present similar failure mode as in original state but a more ductile post-peak behavior which could be interpreted as an increase of confinement that avoids the collapse of the belfry (Figs. 5.20 and 5.22). The maximum reached stress at the compressed toes at ULS of this tower in original state is in the order of 2.25 MPa, much lower than in the ductile flexural failures. Retrofitted with the medium prestressing level, the tower reaches stresses of about 2.535 MPa and changes of prestressing forces in the left tendons of +2.38% (increasing) and -1.86% (decreasing) in the right ones. In the high level the tower presents compressive stresses in the order of 2.634 MPa and lower changes of prestressing forces than in the medium level due to the higher normal forces (left: +1.06%, right: -0.95%). For towers presenting this failure mode and a compressive strength of at least 15% higher than the maximum observed stress at the compressed toes at ULS is proposed the technora device for the three levels of prestressing according to the seismic hazard. Tables 5.12 and 5.13 present the seismic analysis summary of the virtual towers in original state and retrofitted, as well as the seismic risk reduction comparison in terms of the increasing of force, displacement and seismic coefficient for the three limit states of the EC-8 and the damage grades EMS-98. It is worth noting that the retrofitting has more impact in the flexural and combined modes than in the failure of belfry (see tables 4.8 and 4.9).

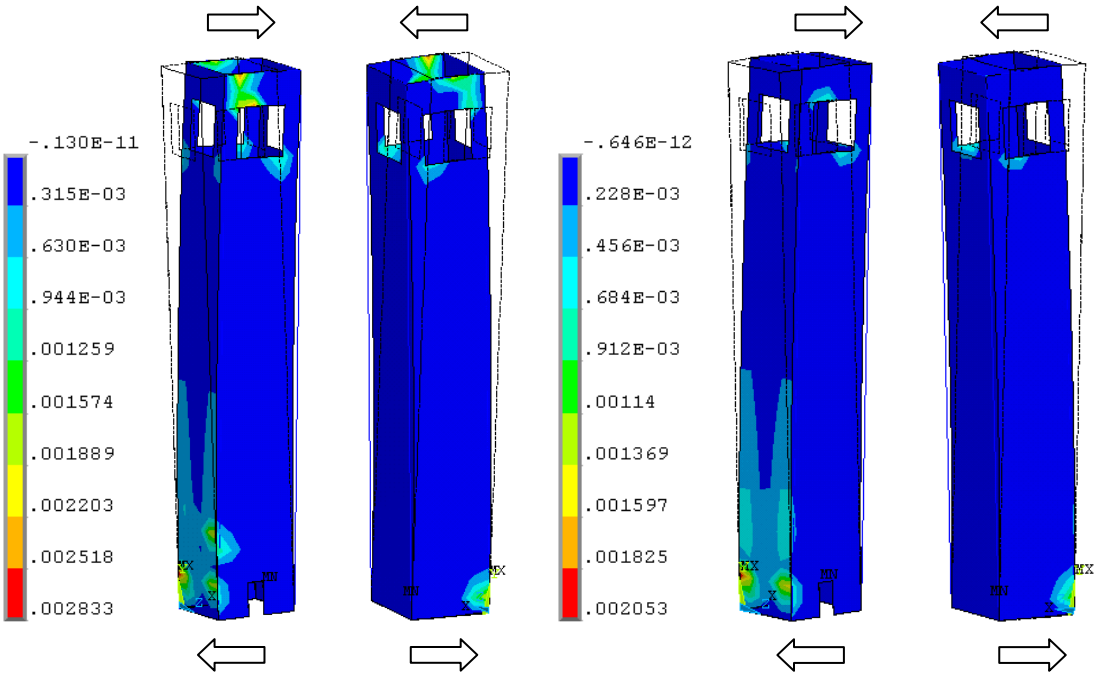

Figure 5.21: Bell tower. Comparison of principal plastic strain contours (front and back) at a displacement of 130 mm: (a) original state (ULS) and (b) retrofitted 0.30Fv technora

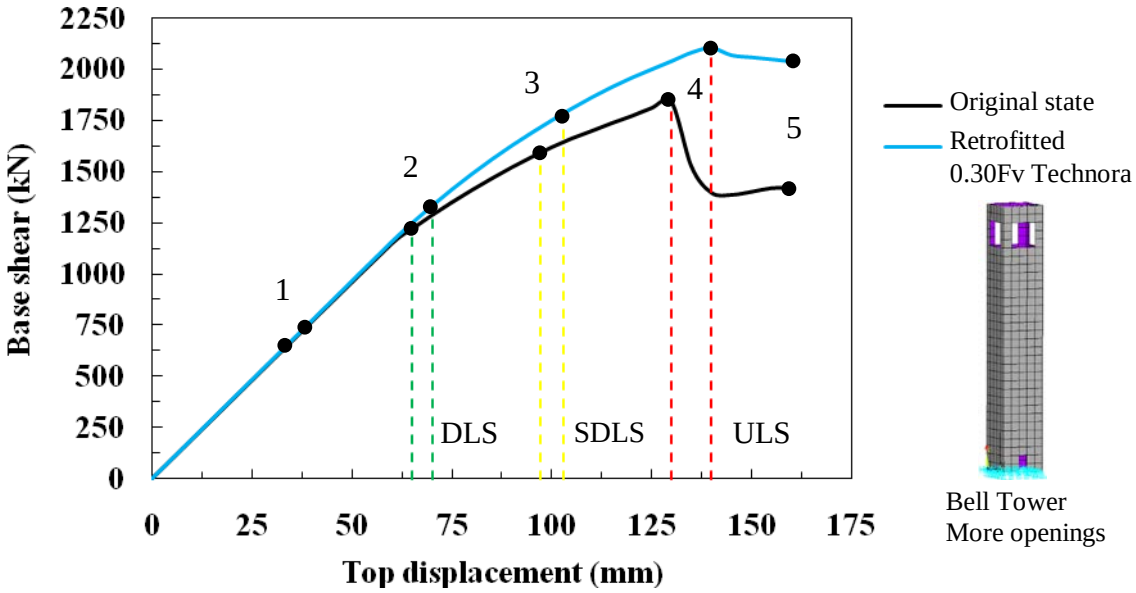

Figure 5.22: Bell tower. Comparison of capacity curves in original state and retrofitted (0.30Fv) with the damage grades (EMS-98) and limit states (EC-8)

Ref.	Limit states EC-8 and Damage grades EMS-98												S.C. $_R$
	DLS DG 2				SDLS DG 3				ULS DG 4				
	F_{OS}	U_{OS}	F_R	U_R	F_{OS}	U_{OS}	F_R	U_R	F_{OS}	U_{OS}	F_R	U_R	
1 $_{30\%}$	1100	55	1430	75	1553	155	1916	170	1600	265	2008	260	0.106
2 $_{30\%}$	1100	55	1430	75	1623	185	1966	195	1750	325	2119	325	0.115
3 $_{15\%}$	1245	65	1397	75	1600	97	1771	110	1839	130	2056	150	0.117
3 $_{30\%}$	1245	65	1340	70	1600	97	1755	103	1839	130	2106	140	0.119

1: medieval tower; 2: bell tower; 3: bell tower more openings; $_{OS}$: original state; $_R$: retrofitted; %: PL; S.C: seismic coefficient; F: force (kN); U: displacement (mm)

Table 5.12: Seismic analysis summary of the towers in original state and retrofitted

FE model reference	Limit states EC-8 and Damage grades EMS-98						Seismic Coeff. %
	DLS DG 2		SDLS DG 3		ULS DG 4		
	F %	*U %*	*F %*	*U %*	*F %*	*U %*	
1 $_{30\%}$	30.0	36.4	23.4	9.7	25.5	0.0	24.7
2 $_{30\%}$	30.0	36.4	21.1	5.4	21.1	0.0	21.1
3 $_{15\%}$	12.2	15.4	10.7	13.4	11.8	15.4	12.5
3 $_{30\%}$	7.6	7.7	9.7	6.2	14.5	7.7	14.4

Table 5.13: Seismic risk reduction comparison by the increment of F, U and S.C.

5.6 Summary and conclusions

A methodology for the seismic risk reduction of historical masonry towers with external prestressing devices was proposed, which corresponds to the general objective of this thesis. The devices were vertically and externally located at the four internal corners to be removable if needed. Vertical prestressing was selected due to it has proved to be more suitable to increase the in-plane lateral strength and ductility of masonry walls by providing tensile strength at key locations. Horizontal prestressing has been mainly used in the cultural heritage to provide stability out-of-plane in walls or to reduce the tension generated by supports opening of vaults, arches and domes. The capability of the applied model to simulate the superelastic behavior of SMA was validated with reported experiments, showing a satisfactory agreement despite of the inability to account for the different elastic properties between phases. An extensive parametric study on a selected tower was carried out based on more than 100 nonlinear static simulations aimed at investigating the impact on the seismic performance of different parameters as tendon material, prestressing level, tendon force changes and SMA superelasticity. The last did not show upgrading of seismic performance due to the small SMA contribution by the device size and vertical location. If the material is in austenite phase behaves as a conventional one. The stress-induced transformation in vertical prestressing has only impact in keeping the applied forces with lower variations than other material in low and medium prestressing levels. The AFRP technora showed good performance in force and displacement enhancement with low changes in tendon forces because of its low E modulus, being favorable to interact with such a poor material like old masonry.

The parametric study allowed proposing three prestressing levels based on the desirable seismic performance enhancement and the earthquake hazard. The suitability was tested through three different failure modes identified in the virtual towers of chapter 4 by estimating the level of seismic risk reduction between original state and retrofitted. The risk reduction was evaluated by combining the capacity curves with the seismic hazard (qualitatively: EC-8 and EMS-98; quantitatively: seismic coefficient). Especial attention is suggested when using high prestressing levels due to this could generate brittle failure by masonry crushing at the compressed toes. The three proposed levels are suggested for towers with compressive strength at least 15% higher than the maximum stress showed in original state at ULS. Prestressing enhanced force capacity and confinement of towers failing by pure bending and combined with shear in not larger areas without increasing the natural ductility, which is favorable due to masonry crushing could occur by higher prestressing levels than 0.30Fv or an increasing in ductility. In towers with belfry failure, prestressing permitted to increase displacement but lower force than towers failing by bending due to the brittleness of this mode. The post-peak behavior showed an increase in confinement which is favorable to avoid belfry failure that could damage people or adjacent buildings. The improvement level in the three failure modes was also reflected in the seismic risk reduction. Considering the recent performance based design philosophy where ductility enhancement is quite important for energy dissipation, the medium prestressing level (0.15Fv) is the optimal.

Chapter 6

Case Studies

6.1 Introduction

In this chapter the proposed methodology for the seismic risk assessment and reduction of ancient masonry towers by external prestressing devices is validated by proving its effectiveness on two real historical masonry towers located in zones with different level of seismicity in Mexico and Italy. The case studies correspond to the north bell tower of the Cathedral of Colima, Mexico and the medieval tower "Torre Grossa" of San Gimignano, Italy. The 3D FE models are calibrated with experimental data and validated as in the case of the virtual towers. The seismic analyses are developed trough the pushover and the capacity spectrum method including the seismic demand determined in the seismic hazard characterization of the research zones. The towers are assessed in original conditions and retrofitted with the most effective device and optimal prestressing level that satisfactorily allowed the seismic risk reduction of the virtual towers. Finally, the advantages and limitations of this proposed approach in the seismic risk management of historical masonry towers are described.

6.2 The north bell tower of the Cathedral of Colima, Mexico

This first case study is located (Latitude 19° 14´ N and Longitude 103° 43´ W) in the historical center of Colima, Mexico which is characterized by its very high seismic hazard with interplate earthquakes as described in the following section. The cathedral was approximately built in 1889 and has two bell towers connected to the main façade and nave. The building is considered as one of the most important monuments of all the state of Colima by the great historical and cultural value that this building represents for the residents. The north bell tower (left in Figs. 6.6 and 6.7a) is selected as one of the case studies of this research because it has been strongly damaged due to historical earthquakes (section 6.2.2), showing once almost a total belfry collapse (Fig. 6.6b). Moreover, is quite interesting to compare the seismic analysis results obtained with a different approach and material model by other researchers in this tower in particular.

6.2.1 Earthquake hazard characterization

The state of Colima is located in the Mexican Littoral in the Pacific Ocean with an extension of 5455 km^2. Colima has ten municipalities and adjoins with the states of Jalisco in the NW direction and with Michoacan in the SW. (Fig. 6.1). At national level, the seismic hazard of Mexico is divided in four main zones ranging from A to D, where A represents low hazard and D very high. In the seismological context Colima is distinguished by its important exposure, being considered one of the Mexican states under most significant seismic hazard (Figs. 6.1b and 6.2a). Figure 6.2a presents a seismic hazard map of Mexico based on several studies in seismology and seismic risk by CENAPRED [2010] for different return periods with expected PGA higher than 0.20g. MDS-CFE [1993] assigns a 0.4g value to the state of Colima (rock site) for a return period of 100 years (Fig. 6.1b). Bandy et al. [1995] and Ramirez-Gaytan [2008] describe that the seismic hazard of Colima is determined by three main sources: the active Volcano of Colima that generates constant microseismicity (M<3.5); the Jalisco block located between the Rivera and North American plates and the convergence zone between the Cocos, Rivera and North American plates in front of the coastal area (Fig. 6.2b).

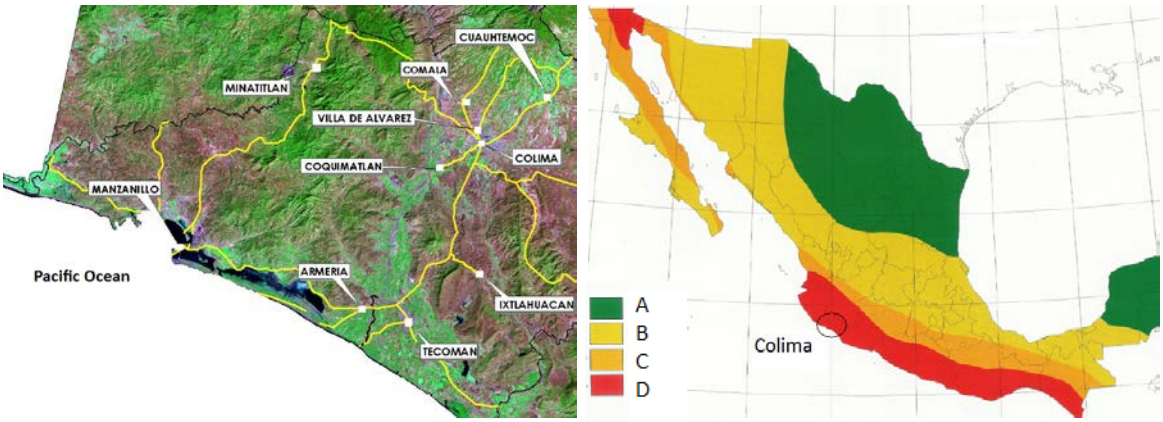

(a) (b)

Figure 6.1: Seismic hazard of Colima; (a) Colima region [DCW, 2004] and (b) seismic hazard of Mexico, low (A), moderate (B), high (C) very high (D) [MDS-CFE, 1993]

Mexico is located in the *Circum-Pacific Ring,* characterized by its high seismicity *interplate*. The seismic activity is generated by the convergence of the Cocos and North American plates (6 cm/year in average) and the Rivera and North American plates (4.5 cm/year) [Bandy et al., 1995]. In the boundaries between plates have occurred major to great earthquakes (according to table 2.1) causing strong damage to the cities of Manzanillo, Tecoman, Colima, Guadalajara and Mexico (see tables 2.2 and 6.1). The black arrows depicted in the tectonic map of Figure 6.2b represent the convergence direction of the Rivera and Cocos plates with reference to the North American plate. The great difficulty to estimate the seismic hazard in the zone between the states of Colima and Jalisco is due to the lack of reliable values of the velocity of convergence between

the Rivera and North American plates [Ramirez-Gaytan, 2008]. Bandy et al. [1995] estimate a displacement of convergence between 2 and 5 cm per year. The triple point of contact of the Rivera, Cocos and North American plates is characterized as well for being a zone of diffuse seismicity that difficults the successful estimation of the seismic hazard [Pardo and Suarez, 1995]. Moreover, the other triple point of contact of the Pacific, Cocos and Rivera plates is also complex to define and in addition due to the lack of a kinematic model able to represent the absolute and relative movement of the four plates in relation to the Jalisco block and the study area of Colima [UCOL et al., 1997].

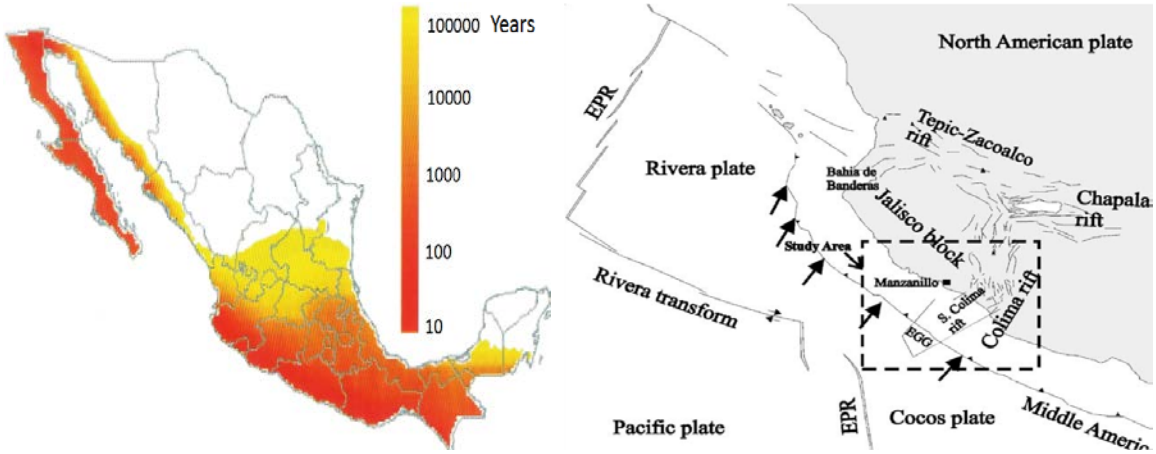

(a) (b)

Figure 6.2: Seismic hazard map of Mexico; (a) for different return periods (PGA>0.20g) [CENAPRED, 2010] and (b) Tectonic map of the occident of Mexico [Bandy et al., 1995]

No	Date	Latitude N	Longitude W	Magnitude M_w	Intensity MMI Colima City	Comment
1	03.06.1932	19.80°	104.00°	8.0	VIII	R and NA
2	18.06.1932	18.95°	104.42°	7.8	IX	Replica of 1
3	15.04.1941	18.85°	102.94°	7.6	X	C and NA
4	30.01.1973	18.39°	103.21°	7.6	VIII	C and NA
5	09.10.1995	18.79°	104.47°	8.0	VII	R and NA
6	21.01.2003	18.63°	104.13°	7.5	VIII	C and NA

Plates that generated the earthquake: R= Rivera; NA= North American; C= Cocos

Table 6.1: Information of the principal earthquakes occurred in Colima, Mexico [UCOL et al., 1997], [Zobin, 2004], and [Rodriguez-Lozoya et al., 2007]

Historically, Colima has been subjected to very important earthquakes of more than M7.5 and intensities (felt in different cities of the region) ranging from VII to X based on the Modified Mercalli Intensity (MMI). The most recent strong earthquakes that have affected the region occurred on October 9th, 1995, with a M8 and on January 21st, 2003, M7.5 (table 6.1 and Fig. 6.3). The cities that presented the maximum intensities were

Manzanillo and Colima. SMIS and EERI [2006] and SSN [2010] describe that intensities larger than VII have occurred about seven times in 100 years. The 1995 earthquake also generated a tsunami in the coasts of the states of Colima and Jalisco with waves between 2 and 10 m height that partially flooded 200 km of coast [Borerro et al., 1997].

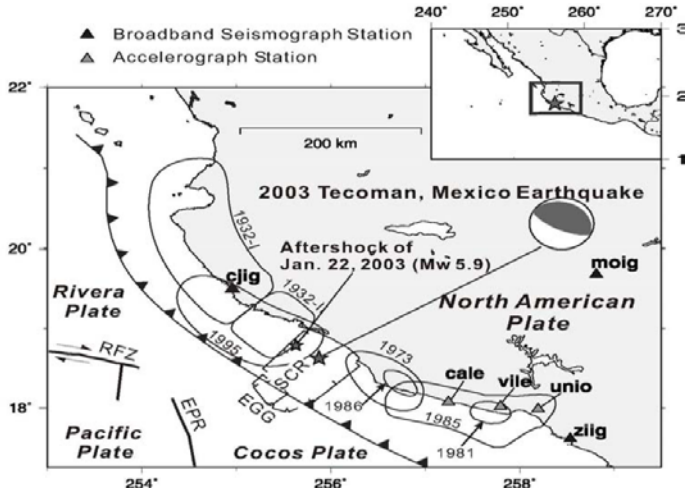

Figure 6.3: Geographical map with the location and area of rupture of the principal earthquakes occurred in Jalisco, Colima and Michoacan [Yagi et al., 2004]

The map of Figure 6.3 depicts the location and area of rupture of the main seismic events described in table 6.1 occurred in the states of Jalisco, Colima and Michoacan. It could be observed the world famous 1985 M8.1 earthquake occurred in the coast of Michoacan that generated strong damage to Mexico City (350 km away from the epicenter) causing more than 20000 deaths (table 2.2). Several studies have been developed in the state of Colima aimed to identify and to characterize the seismic source by different methodologies: e. g. Courboulex et al. [1997] and Escobedo et al. [1997] by means of teleseismic data; CENAPRED, National Autonomous University of Mexico (UNAM) and the University of Colima (UCOL) by studying the recorded replicas of the 1995 earthquake; DeMets et al. [1995] and Melbourne et al. [1997] by GPS and more recently, in 2008 UNAM and UCOL installed two temporary networks in the coastal zone. The 1995 earthquake (M8) was generated by the *subduction* of the *Rivera plate* beneath the *North American plate* with an epicenter located about 24 km in front of the harbor of Manzanillo and a depth of 20 km. The estimated size of the rupture area was of about 170 x 70 km with *directivity* to the NW. Despite Mexico City is located 550 km away from Manzanillo (far-source site), the earthquake was felt with large duration but moderate intensity in the city center (also named zone of the lake), characterized by poor soil conditions with dominant periods of about 2.5 s [UCOL et al., 1997]. The Manzanillo Power Plant which is located 30 km from the epicenter measured the only strong motion record of the earthquake that was obtained within 100 km from the rupture plane. In addition, various records at distances greater than 120 km were obtained from strong motion arrays in Guadalajara and Mexico City. The Power Plant registered PGA of 0.395g

in the EW, 0.395g in the NS, and 0.309g in the vertical. The accelerograms presented in both horizontal directions approximately 20 cycles exceeding 0.2g and about ten cycles higher than 0.3g. Strong shaking lasted about 30 s and a total duration of about 100 s (Fig. 6.4a) [UCOL et al., 1997] and [GEER, 2010].

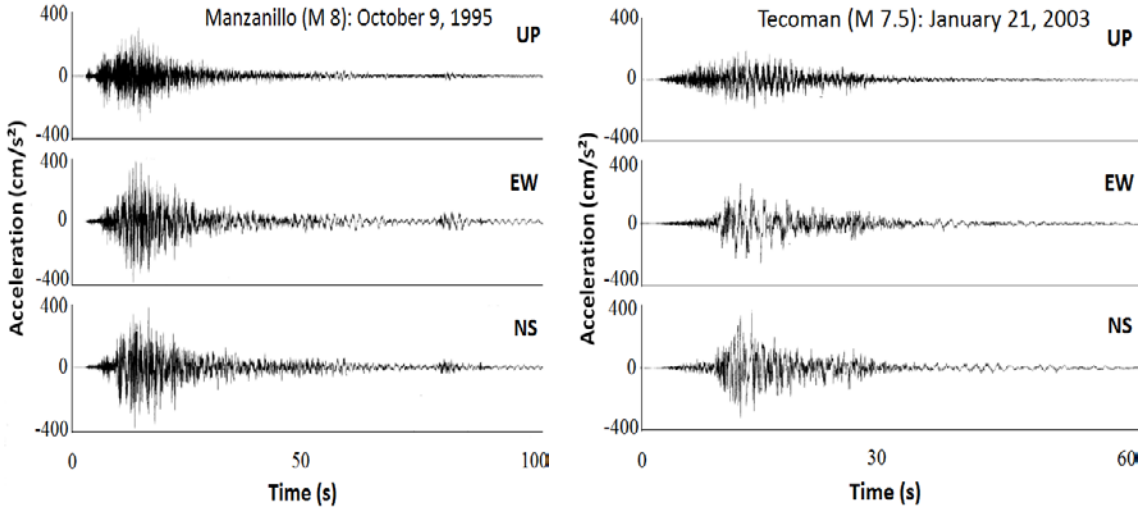

Figure 6.4: Records of the Manzanillo and Tecoman earthquakes [SMIS and EERI, 2006]

The 1995 earthquake was felt with intensities between VIII and IX in the harbor (near-source site) and VII in Colima City (intermediate-source site), located 100 km away in the NE (Fig. 6.1). Manzanillo presented strong damage in the harbor facilities and mainly in masonry and adobe housing. The damage in Colima City was minimum compared to Manzanillo. The most recent earthquake that has caused strong damage to the city occurred on January 21st, 2003 (M7.5). SMIS and EERI [2006] describe that it was caused by the subduction of the Cocos plate beneath the North American plate with an epicenter in front of the Tecoman coasts (60 km SW from Colima City and 60 km SW from Manzanillo) and a depth of 9 km. The studies indicated rupture *directivity* to the NE (Fig. 6.1a), which explains the high intensity (VIII) and observed damages in masonry and adobe structures in Colima City (Figs. 2.13 and 2.21). As in the 1995 earthquake, the only accelerograms were recorded by the Power Plant. The PGA were of about 0.266g in the EW, 0.378g in the NS and 0.190g in the vertical. The records (Fig. 6.4b) showed three cycles in the EW and ten in the NS exceeding 0.2g. Strong shaking lasted about 20 s and a total duration of about 60 s. Luhr and Carmichael [1981] describe that Colima is located in a Plateau slight inclinated to the SW in the graben (or rift) of Colima, surrounded by the grabens of Tepic-Zacoalco and Chapala (Fig. 6.2b), forming a triple point. Based on geotechnical and geophysical studies, Silva and Esquivel [1976] and Tejeda and Silva [2003] proposed a geotechnical classification of five zones for Colima City: Alluvial–lacustrine zone (NW) with granular deposits of fine materials; volcanic sediments from the NE to the SW including the City Center (good geotechnical conditions); alluvial zone by consolidated rivers and swamps; fluvial zone in the surroundings of rivers (granular deposits); and fillings and mines (NW) in the city limits.

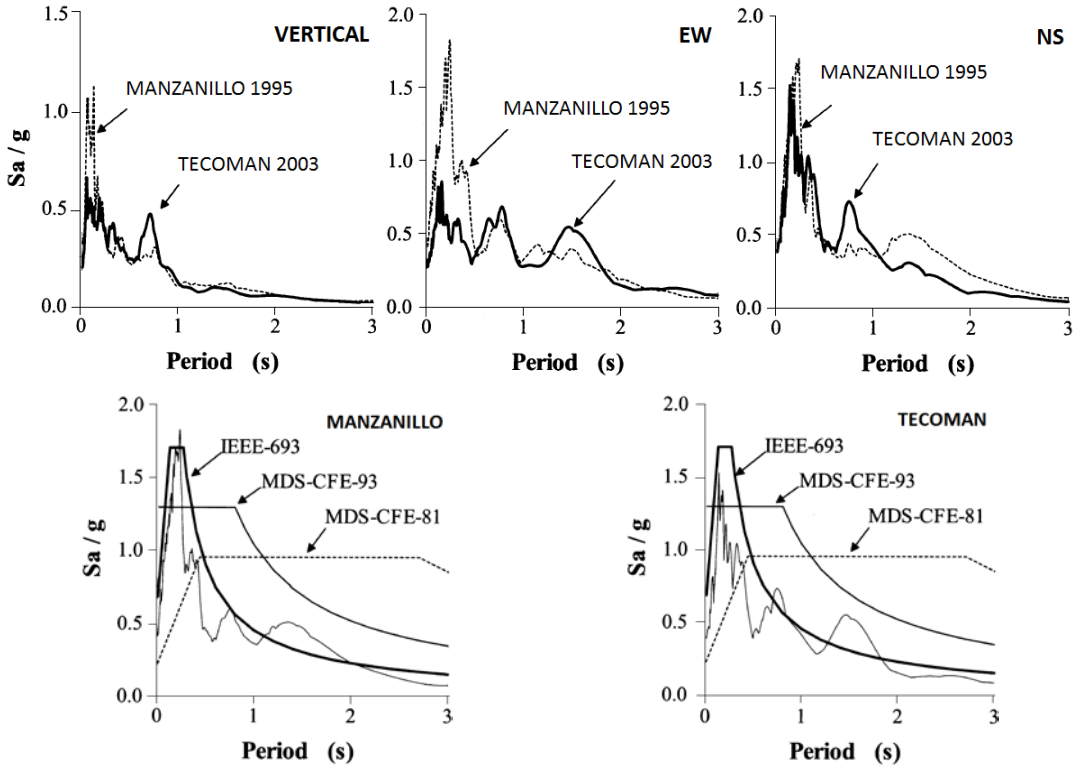

Figure 6.5: Response spectra of the Manzanillo and Tecoman earthquakes and comparison between the response and design spectra [SMIS and EERI, 2006]

To assess the *local site effects* (*seismic amplification and directivity*) in Colima City, UCOL et al. [1997] and SMIS and EERI [2006] developed several studies based on replicas of the 1995 and 2003 earthquakes and by ambient noise. It was done due to any station of Colima City recorded the ground motion by technical problems, only the Power Plant. The authors observed an important seismic amplification from two to six due to poor soil conditions. This explains the presence of areas of high damage concentration observed after the 2003 earthquake. Figure 6.5 depicts the absolute spectral accelerations (5% damping) of the 1995 and 2003 earthquakes recorded by the Power Plant. The maximum accelerations of the NS component are similar for both events. The EW component of the 2003 earthquake represents about 50% of the acceleration of the 1995 for periods between 0.1 and 0.5, which indicates a notorious effect of *directivity* in the Tecoman earthquake. The response spectra are compared to the design spectra (return period of 475 years, rock site) specified in three codes used in Mexico, MDS-CFE [1981 and 1993] and IEEE-693 [1997]. For the Tecoman earthquake (M7.5) it was expected more damage. However, if the attenuation relationships proposed by Youngs et al. [1997] are used in addition of the tool of PEER [2011], the results suggest PGA between 0.11 and 0.21g (rock site) for an interplate seismic source with epicentral distance of 60 km and focal depth of 9 km. For soft soil conditions PGA between 0.16 and 0.33g. This last PGA level is in accordance with the level of observed damage. This method is quite helpful when there are no records available at a certain site.

6.2.2 Historical analysis and actual conservation state

As aforementioned, the Cathedral of Colima was approximately built in 1889 after the Colonial period. Two years later it was finished the construction of the adjacent chapel. The materials used for its construction were fired clay bricks and carved stones with lime mortar for all the vertical elements such as walls and towers and empty fired clay basins in a matrix of mortar for the vaults. Colima City has been subjected to strong earthquakes due to its proximity to an important seismic source as described in the seismic hazard characterization. About ten years after its construction the building was damaged by an earthquake, presenting moderate damage in the towers and cupola but strong non-structural damage. In 1941 occurred a M7.6 earthquake generated by the subduction of the Cocos plate beneath the North American plate. The strong ground motion was felt in the city with an intensity of X (Table 6.1). It highly damaged the building, generating important cracking in walls, cupola, vaults and the partial collapse of the north bell tower. The belfry collapsed almost totally, falling down in a highly transited street (see Fig. 6.6b), causing for luck just small injuries to some pedestrians. For the tower´s reconstruction, materials with similar characteristics were used.

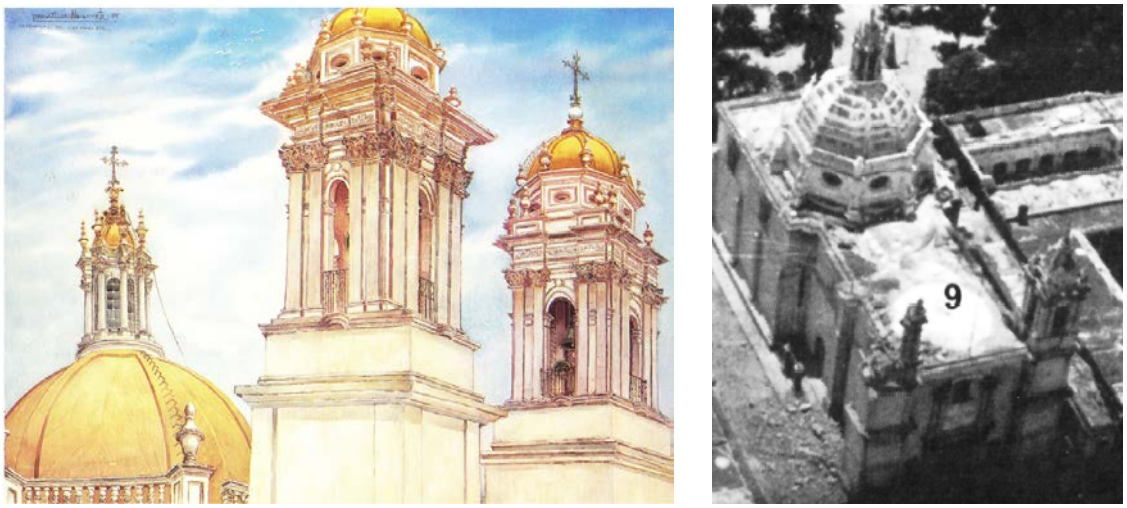

(a) (b)

Figure 6.6: The Cathedral of Colima, Mexico; (a) view of the two towers and the cupola [Guzman et al., 1986] and (b) observed damage after the 1941 earthquake [Zobin, 2004]

Afterwards, in 2003 the city was struck again by another important earthquake with the same rupture mechanism of the occurred in 1941. The M7.5 earthquake was felt this time with lower intensity (VIII) but caused strong damage to the building (Fig. 6.8a). The restoration and strengthening works were developed by INAH [2003]. The wall thickness was increased by adding thin concrete walls. The vaults were strengthened with a mesh covered by mortar and some beams were included at the level of belfries. Nowadays, the structure is in a good conservation state as illustrated in Figure 6.7a thanks to the intervention which has shown good performance after recent moderate seismic events.

6.2.3 Structural characterization by experimental campaigns

The main structural components of the Cathedral were described in section 6.2.2. There is no information available regarding the structural characteristics in terms of mechanical and dynamic data. During the intervention works developed by INAH [2003], the experimental campaigns were limited to characterize the type of materials of the different structural components by sampling. The strengths of materials were not assessed, nor the level of stresses at vertical elements and dynamic characteristics. During the present research several technical visits were developed in order to assess by visual inspections the actual conservation state of the building, a photographic survey, and most importantly, to characterize in a simple way the dynamic characteristics of the bell tower under study (left in Fig. 6.7a). A portable vibration analyzer (triaxial accelerometer) CSI RBM Consultant® was used, consisting in one sensor and its data acquisition control (Fig. 6.7b). The used excitation was induced by means of ambient vibration (traffic and wind) and registered at the level of belfry.

(a) (b)

Figure 6.7: Dynamic characterization by experimental campaigns; (a) General view of the Cathedral and the adjacent municipal building and (b) portable vibration analyzer

Afterwards, from the acquisition control, the registered data is transferred to a computer and managed with the device software. By means of the vibration spectra, the natural frequency is graphically determined. The results of the two orthogonal directions are 1.4067 Hz in the E-W direction and 1.6222 Hz in the N-S. In order to obtain models more representative of the real structure and more reliable results in the seismic risk management, they are calibrated with the experimental data (see section 6.2.5).

6.2.4 Review of previous works

The present section is aimed at reviewing previous research works on this case study in order to compare the results with the obtained in the present research work. The seismic performance of the north bell tower was previously assessed by Preciado [2007]

and Orduña et al. [2008] by 3D limit analysis. This approach is a suitable tool to assess the in-plane and out-of-plane nonlinear behavior of small to medium structures as explained in section 3.2.3.2. The great advantage of this proposal is that parameters of strength are only needed. The rigid blocks are modeled depending on the direction of the seismic loading (+X, -X, +Y or –Y), observed damage after real earthquakes in similar structures and failure mechanisms reported in literature. The interaction between the 3D rigid blocks and foundation is modeled trough frictionant interfaces with no tensile strength. Both towers and the main façade were modeled for the analysis. The –X direction was selected due to the observed strong damages in the 1941 and 2003 earthquakes. To define the macroblocks (Fig. 6.8b), the observed crack pattern after the 2003 seismic event (Fig. 6.8a) and other suggestions of Orduña [2003] were considered.

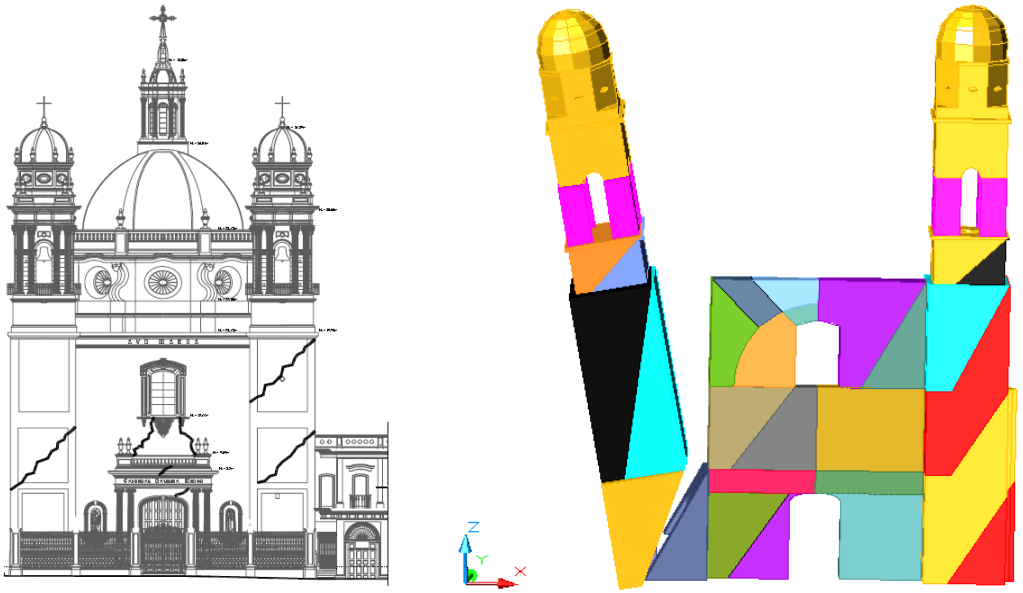

(a) (b)

Figure 6.8: Seismic analysis of the Cathedral; (a) observed crack pattern due to the 2003 earthquake and (b) failure mechanism (–X) [Preciado, 2007] and [Orduña et al., 2008]

Due to the lack of information about the material parameters as above mentioned, the authors used typical values reported in literature. By means of the reports of INAH [2003] it was observed that the façade is formed by brick masonry with lime mortar and both towers with brick and carved stone masonry at different heights. In the analysis was considered a density of 1.6 ton/m^3 (brick masonry) and 2 ton/m^3 (carved stone), 0.6 of friction coefficient, a compressive strength of 2.5 MPa and a tensile strength of 0.25 MPa. The failure mode (Fig. 6.8b) showed a separation of the north tower from the façade and a combination of in-plane shear and out-of-plane bending cracks at the tower´s lower body with a seismic coefficient at ULS (peak) of 0.12. The retrofitting proposals were not analyzed. The impossibility to assess ductility and to calibrate the model with experimental data are the main drawbacks of this proposal.

6.2.5 Seismic risk assessment and reduction

The seismic analyses of the north bell tower of the Cathedral of Colima are developed considering two directions (-X and +X) and the respective calibrated models with the experimental data. Due to symmetry, no considerable changes are expected in the other two directions (-Y and +Y). In the +X model the interaction with the façade (South, L= 4 m) and the nave (East, L= 2 m) up to the height of 20 m is considered by a horizontal distribution of linear elastic springs (combin14) with constant stiffness (10 kN/mm). The +X model is proposed without springs in order to simulate a disconnection with the façade and nave. The tower has a square plan of 6 x 6 m with a wall thickness of 1.5 m and 31 m height. With the cover (0.10 m thick) the tower has a total height of 37 m and a reinforced concrete slab at belfry (total mass of 1707.4 Ton). The 3D FE models are integrated by 859 shell43 elements and 906 nodes with 5367 DOF. The material properties for both models are only integrated by brick masonry (see section 6.2.4) as observed in the newly developed visual inspections in addition of table 2.5 and the inelastic parameters of section 3.2.2.2. Using Eq. 4.1 (L= 6 m, H= 31 m), a first natural frequency of 1.5508 Hz or higher is expected due to the interaction with the Cathedral. Both numerical models are calibrated trough modal analyses in the dynamic field with the experimental data of section 6.2.3, obtaining a good agreement: (+X) E-W 1.4193 Hz and N-S 1.6174 Hz; (-X) E-W 1.4897 Hz and N-S 1.5142 Hz.

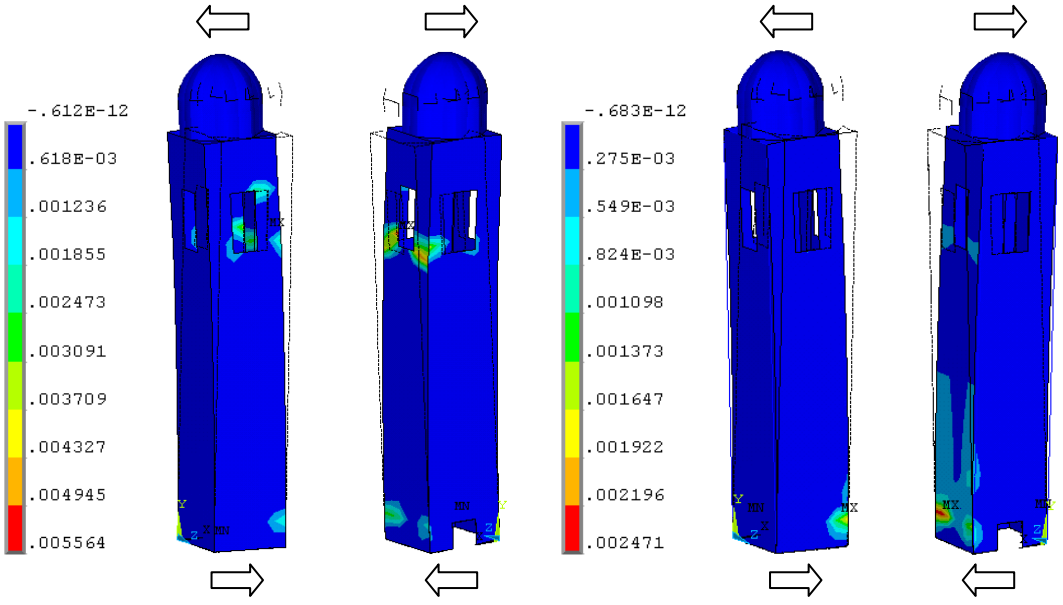

Figure 6.9: Comparison of principal plastic strains (front and back) at a displacement of 100 mm for a seismic action in –X (S-N): (a) original state (ULS) and (b) retrofitted 0.30Fv

The failure mode of the tower without springs for a seismic action in the –X direction is presented in Figure 6.9a. Flexural cracks at the lower body and failure of belfry by a combination of flexural cracks out of the plane and shear in the plane are observed. The

model with springs (+X direction) is stiffer as expected, presenting the failure of belfry by flexural and shear cracks (Fig. 6.10a). This brittle behavior is due to the large openings and the short column effect which reduces the flexural height of slender structures. The different seismic performances of both models could be observed in Figure 6.11.

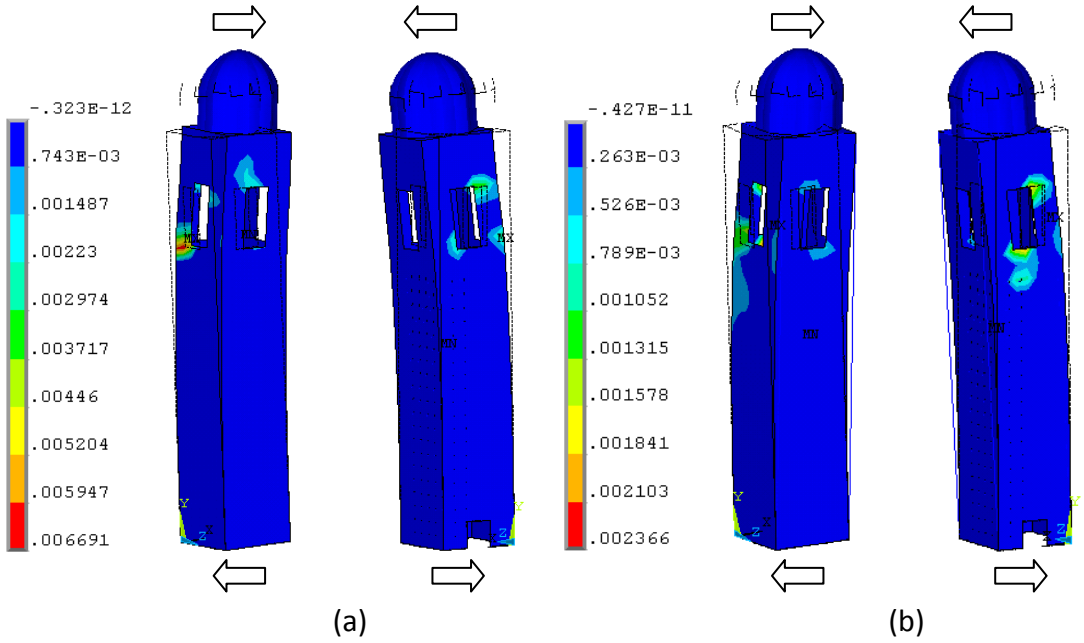

Figure 6.10: Comparison of principal plastic strains (front and back) at a displacement of 75 mm for a seismic action in +X (N-S): (a) original state (ULS) and (b) retrofitted 0.30Fv

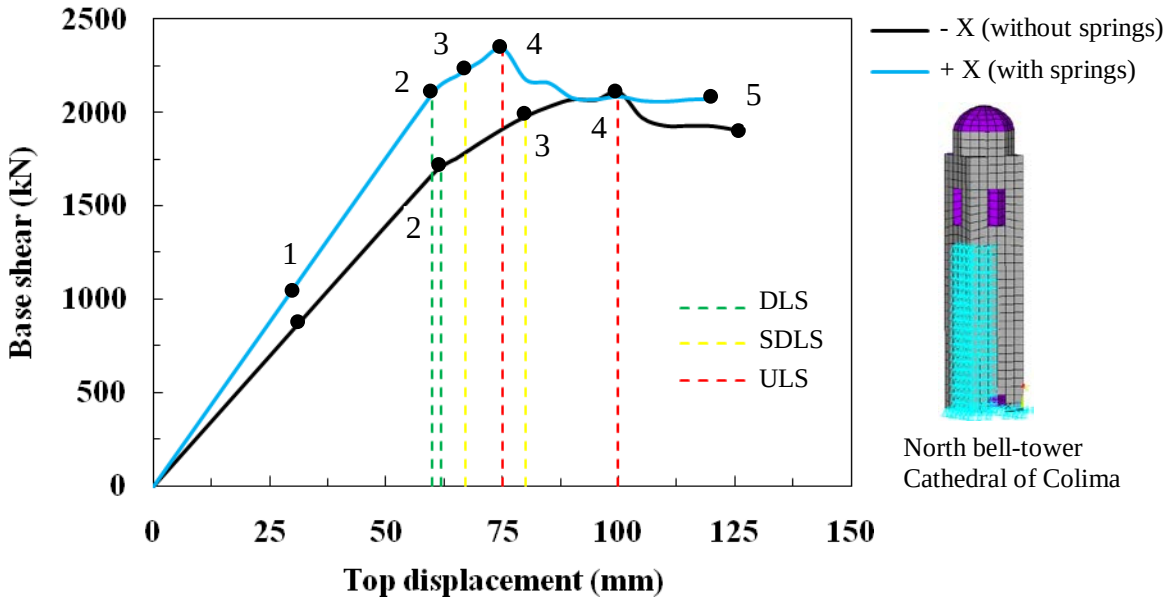

Figure 6.11: Comparison of capacity curves in original state for a seismic action in –X and +X with the damage grades (EMS-98) and limit states (EC-8)

Four technora devices and two prestressing levels are proposed because of the high seismicity of the region, 0.15Fv (At= 1000 mm^2, 15 bars of 8 mm) and 0.30Fv (At= 2000 mm^2, 30 bars of 8 mm). For practicity only the results of the high prestressing level are presented. It is worth noting that prestressing considerably reduces damage at belfry (Figs. 6.9b and 6.10b). The seismic performance is enhanced by increasing force, displacement and confinement (Fig. 6.12). The assessment and risk reduction summaries are presented in tables 6.2-3. The seismic coefficient of the –X model in original state (0.126) is in good agreement with the obtained by other researchers (0.12) and observed damages after passed earthquakes. At ULS no crushing is observed: -X original state 1.80 MPa, retrofitted 2.38 MPa; +X original state 1.15 MPa, retrofitted 1.48 MPa.

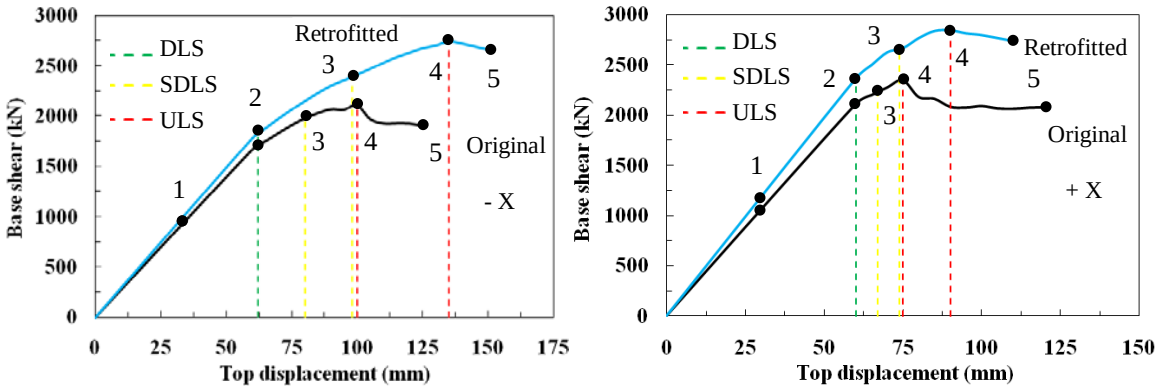

(a) (b)

Figure 6.12: Comparison of capacity curves in original state and retrofitted (0.30Fv) with the damage grades (EMS-98) and limit states (EC-8): (a) –X and (b) +X with springs

Ref.	Limit states EC-8 and Damage grades EMS-98												S.C. OS	S.C. R
	DLS DG 2				SDLS DG 3				ULS DG 4					
	F_{OS}	U_{OS}	F_R	U_R	F_{OS}	U_{OS}	F_R	U_R	F_{OS}	U_{OS}	F_R	U_R		
- X	1740	62	1820	62	1970	80	2380	98	2105	100	2741	135	0.126	0.164
+ X	2108	60	2368	60	2240	67	2650	74	2345	75	2849	90	0.140	0.170

$_{OS}$: original state; $_R$: retrofitted; S.C: seismic coeff.; F: force (kN); U: displacement (mm)

Table 6.2: Seismic assessment summary of the north bell tower in original state and retrofitted 0.30Fv for an earthquake action in –X and +X (springs)

FE model reference	Limit states EC-8 and Damage grades EMS-98						Seismic Coeff. %
	DLS DG 2		SDLS DG 3		ULS DG 4		
	F %	*U %*	*F %*	*U %*	*F %*	*U %*	
-X	4.6	0.0	20.8	22.5	30.2	35.0	30.2
+X	12.3	0.0	18.3	10.5	21.5	20.0	21.4

Table 6.3: Seismic risk reduction comparison between original state and retrofitted (0.30Fv) by the increment of F, U and S.C. for an earthquake action in –X and +X (springs)

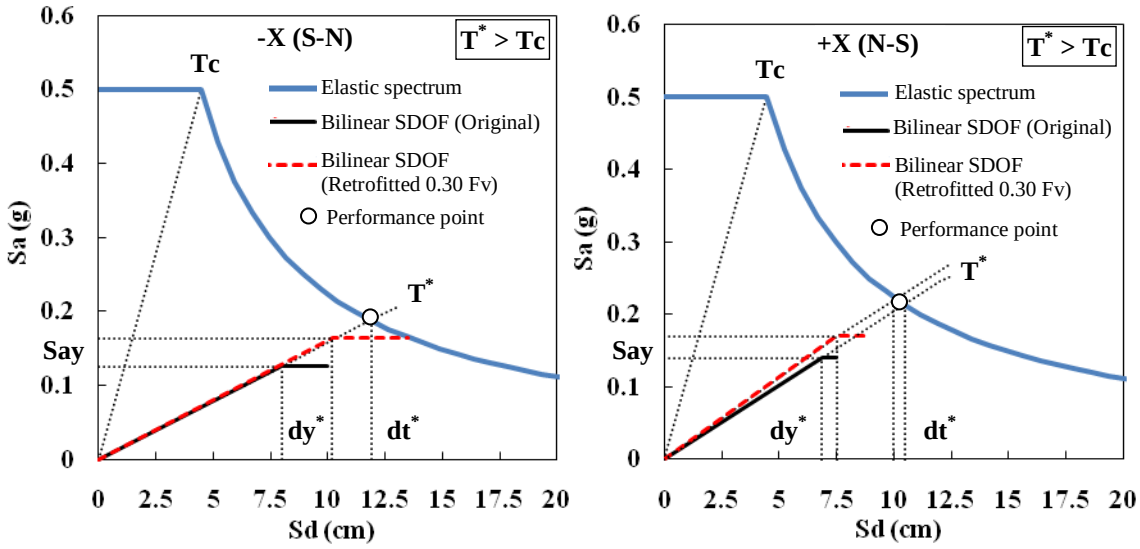

(a) (b)

Figure 6.13: Seismic evaluation of the north bell tower of the Cathedral of Colima by the capacity spectrum method: (a) –X direction and (b) +X direction (springs)

FE model reference	m* (Ton)	dy* (mm)	Fy* (Ton)	Say (g)	dm* (mm)	dt* (mm)	Comment
-X Original state	1707.4	80	215	0.126	100	119.2	Loss of belfry
-X Retrofitted 0.30 Fv	1707.4	102	279.4	0.164	135	119.2	Reparable
+X Original state	1707.4	68.5	239	0.140	75	105	Loss of belfry
+X Retrofitted 0.30 Fv	1707.4	75	290.5	0.170	90	100	Loss of belfry

m*: mass; dy*: yield displacement; Fy*: yield force; Say: yield acceleration;
dm*: maximum displacement; dt*: target displacement (performance point)

Table 6.4: Seismic evaluation summary of the bell tower (capacity spectrum method)

Moreover, the capacity spectrum method proposed by Fajfar [2000] is used. The aim is to graphically identify the performance point by the intersection between the capacity curve transformed in a equivalent SDOF system and the seismic demand represented by the elastic spectrum properly reduced (appendix A). Figure 6.13 illustrates the converted capacity curves and the elastic response spectrum based on the seismic risk characterization (appendix B). Since $T^* > Tc$ (Fig. A.2b), the target displacement is directly obtained without reducing the elastic spectrum. The tower seismic performance in original state (seismic action in –X and +X) is not satisfactory, presenting belfry failure (table 6.4). The retrofitted tower (0.30Fv) is able to withstand a seismic action in –X, but not enough in +X due to the façade constraint. Even by applying a medium level (0.15Fv) that allows more ductility enhancement, the maximum obtained displacement (100 mm) is lower than the target one (105 mm). To bring the additional ductility, a combination of the technora devices with an internal wrapping of belfry (GFRP sheets) is suggested.

6.3 The medieval tower (*Torre Grossa*) of San Gimignano, Italy

San Gimignano (Latitude 43° 28´ N and Longitude 11° 03´ E) is a medieval town located in the north of Italy in the Tuscany region close of Siena and has an extension of approximately 138 km^2. This town is very famous for its masonry towers and in recent decades has been designated a world heritage site. The selected tower as a case study is the "Torre Grossa" (big tower) due to its importance in comparison to the other towers, ancientness and available data (e.g. historical, structural and experimental).

6.3.1 Earthquake hazard characterization

The Tuscany (*Toscana*) region is surrounded and crossed by major mountain chains. Located in the north-central part of Italy, between the Tyrrhenian Sea and the central Apennines with an extension of about 22990 km^2 (see Fig. 6.14a). Tuscany adjoins in the northern part with the regions of Liguria (NW) and Emilia-Romagna (NE), with Marche in the East and in the southern part with Lazio (SW) and Umbria (SE). According to the OPCM Italian code, at national level, the seismic hazard of Italy is divided in four main zones ranging from 1 to 4, where 4 represents slight hazard, 3 moderate, 2 strong and 1 major (Fig. 6.14b). Considering this zonification, it could be observed that the seismicity of Tuscany is classified in two zones, moderate and strong seismic hazard, being part of this last the San Gimignano region (red circle in Fig. 6.14a). Another important seismic hazard map of Italy was developed by INGV [2011] as depicted in Figure 6.15. The map presents the seismic hazard by zones in terms of PGA (rock site). It is worth noting that for San Gimignano is expected a PGA value in the order of 0.125–0.150g.

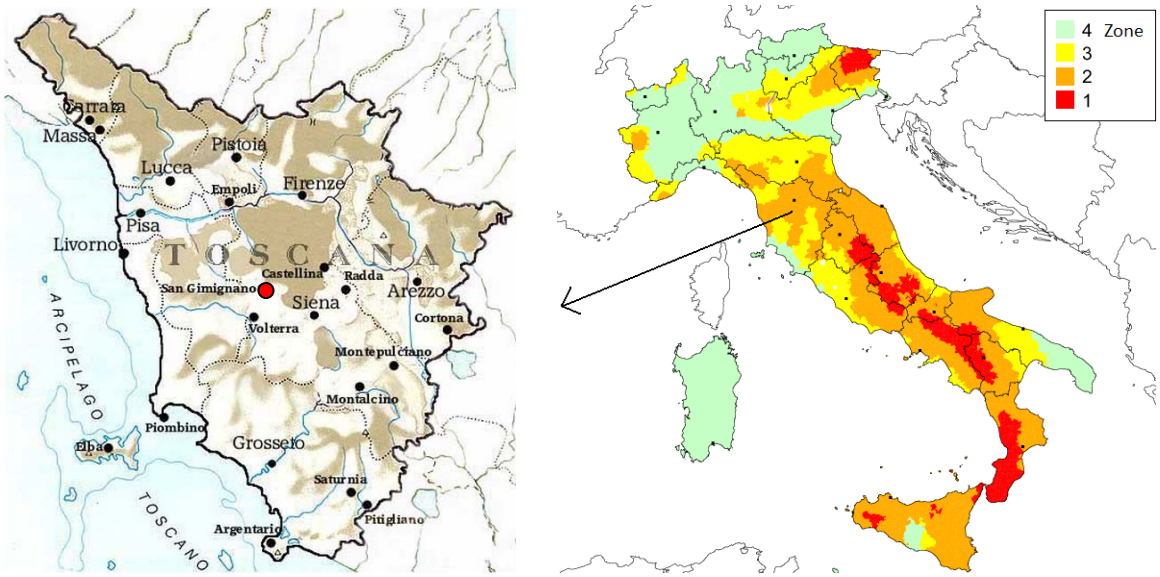

(a) (b)

Figure 6.14: Tuscany seismic hazard; (a) Tuscany region [TDR, 2011] and (b) seismic hazard regionalization of Italy, OPCM 3274 (2003) [INGV, 2011]

In the plate tectonics context, Europe has one of the most complex zonification. The Mediterranean zone including the South of Spain and the NW of Italy is characterized by subduction interplate earthquakes (the Africa plate beneath the Mediterranean microplate). By the other hand, the South of Sicily and Crete is characterized by the presence of intraslab earthquakes (the Africa plate beneath the Tyrrhenian microplate). The Italian peninsula is characterized by intraplate seismic activity represented by collision and strike-slip fault earthquakes (Fig. 6.16a). Collision earthquakes (e.g. L'Aquila and Sichuan seismic events) occur when two tectonic plates meet (compression) along a convergent fault (also known as destructive boundaries), if both plate tectonics have similar rock density the crust of the earth tends to buckle, leading to the formation of mountains (e.g. Alps, Himalayan and the Apennines), otherwise, if both rock densities of the plates are different, one plate subducts beneath the other. By the other hand, the strike-slip earthquakes occur when two tectonic plates slide and grind against each other along a transform fault (e.g. Loma Prieta, San Francisco and Kobe earthquakes).

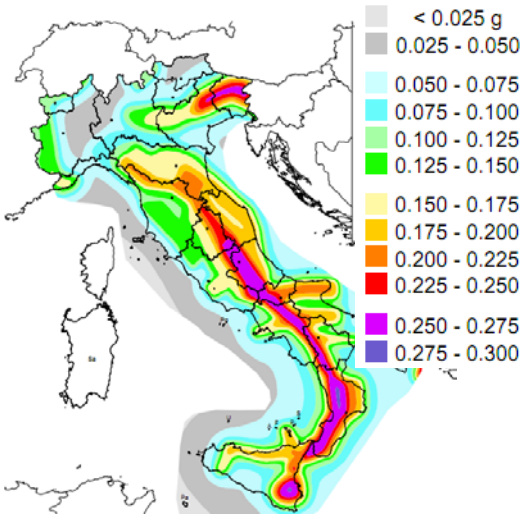

Figure 6.15: Seismic hazard map of Italy, OPCM 3519 (2006): PGA values with probability of exceedance of 10% in 50 years and a return period of 475 years [INGV, 2011]

Solarino and Cassinis [2007] describe that the geology of the Italian territory is characterized by three different zones as a result of several geodynamical processes. The first zone is determined by the collision of the Adriatic microplate and the Eurasian plate in the North of Italy, forming as a result the Alps. In the Central part, the collision between the Eurasian and African plates and the opening of the Tyrrhenian basin to the West (represented by the Tyrrhenian Sea) created the Apennines. The South is characterized by the subduction of the African plate (Ionian microplate) beneath the Eurasian plate (Tyrrhenian microplate) along the Calabrian Arc (Fig. 6.16). The geodynamical processes generate nowadays to the Alps an increment of height of about one centimeter per year, causing this stress, ground motions along the faults, especially in the Apennines. Italy lies in one of the most seismically active regions of Europe. The boundary between the African and European plates is particularly complex in the north

central Mediterranean, and mountain-building processes are active through much of the country. Most of these earthquakes occur beneath the Apennines, which form the topographic "backbone" of the country [BGS, 2011]. Lots of studies have been developed in Italy considering a combination of several research fields with the aim to characterize the plate tectonics and to reach more knowledge about the seismic hazard. One example of these approaches is the geodynamic model of Figure 6.16b developed by Devoti et al. [2008]. This model describes a transition from continental compression in the front of the chain (Adriatic side) to extension behind the chain (Tyrrhenian sector). Cuffaro et al. [2009] affirm that the northern Adriatic plate is surrounded and squeezed by the interaction of three independent subduction zones, the Apennines, the Alps and the Dinarides. GPS data has shown the horizontal pattern of motion (shortening) along the front of the three belts surrounding the northern Adriatic plate (northern Apennines: 2-3 mm/yr, southern Alps: 1-2 mm/yr and Dinarides: < 1mm/yr). Historically, Italy has been mainly subjected to earthquakes ranging from moderate to strong (see table 2.1) that have generated heavy damage to the historical patrimony and have caused the death of thousands of persons as shown in tables 2.2 and 6.5. In this last table and Figure 6.17 could be observed the seismic activity of central Italy in recent decades, as well as the complexity and diversity of the earthquake types generated by different seismic sources distributed along the Italian territory.

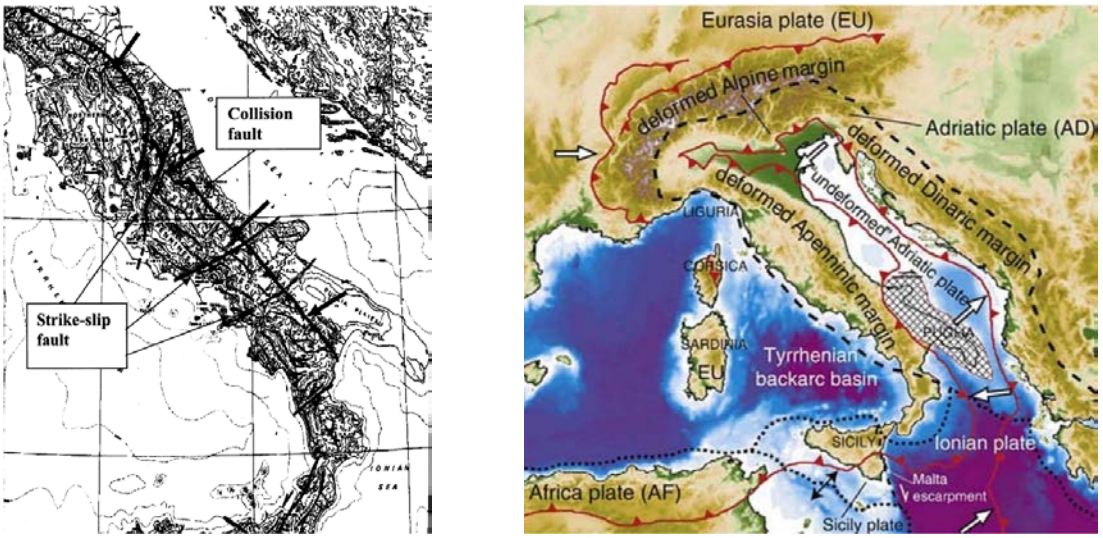

(a) (b)

Figure 6.16: Plate tectonics; (a) faults along the Apennines [Monaco and Monaco, 2005] and Geodynamic model for the Mediterranean region [Devoti et al., 2008]

The most recent destructive earthquake that has affected Italy occurred on April 6th, 2009 with M6.3 and hypocentral depth of 9 km according to INGV [2011]. The normal-faulting collision earthquake occurred in Central Italy in the Abruzzo region with an epicenter close to the city of L'Aquila. The magnitude was not so high, but due to the proximity of the seismic source, bad soil conditions and highly vulnerable historical

masonry buildings, the damage in L'Aquila was invaluable, causing the death of about 300 persons and destroying most of the cultural patrimony as shown in Figure 1.2. Gioncu and Mazzolani [2011] describe that the event presented important seismic amplification due to bad soil conditions (mainly sediments), which explains the observed high damage concentration. The location of the L'Aquila earthquake was of about 85 km NE from Rome, 115 km SE from Perugia and 371 km SE from Florence. According to USGS [2011a], the earthquake intensity in L'Aquila was of VII and was also felt in Rome (intensity IV) and Florence (intensity III) without damage (table 6.5 and Fig. 6.17).

Location	Date	Latitude N	Longitude E	Magnitude M_w	Depth km	Deaths	Fault
Irpina	23.11.1980	40.51°	15.16°	6.8	30	3000	Intraslab
Umbria	26.09.1997	43.08°	12.81°	5.8	10	11	Strike-slip
Molise	31.10.2002	41.73°	14.89°	5.9	10	28	Strike-slip
L'Aquila	06.04.2009	42.33°	13.33°	6.3	9	281	Collision

Table 6.5: Main seismic events of Italy in recent decades [USGS, 2011a] and [BGS, 2011]

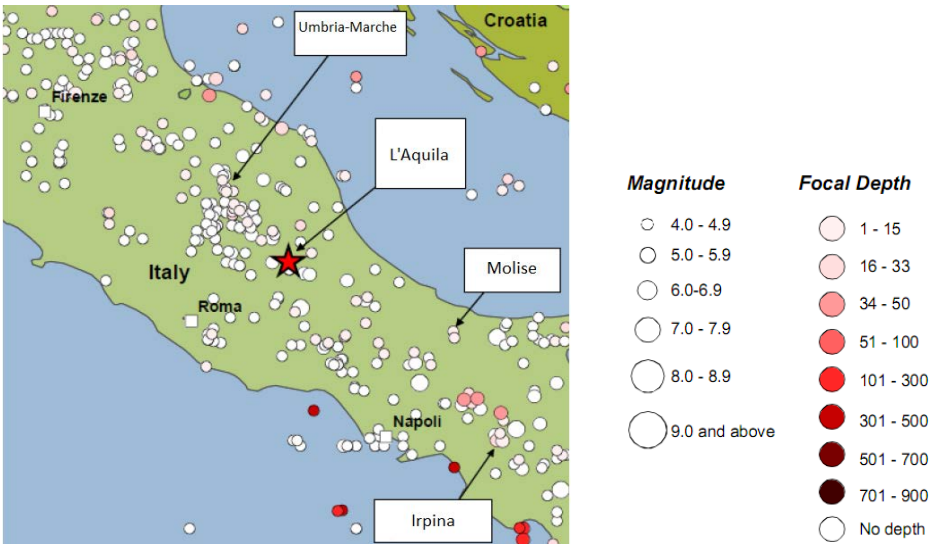

Figure 6.17: Historical seismicity of central Italy (magnitudes 5 and greater) [BGS, 2011]

Although it has been shown that PGA is a poor indicator of the damage potential of earthquake ground motions [Bertero, 1992], the amplitudes of strong shaking affecting L'Aquila and other nearby settlements in the region (within a 10 km epicentral distance) exceeded 0.3g and possibly reached up to 1g in the case of the Pettino area. As indicated by the response spectra, the frequency content of the recorded motions was high, particularly in the range 1–10 Hz (0.1–1 s), which corresponds to the range of fundamental frequencies (period) of most of the inventory of buildings in the affected region. The duration of strong shaking was short, between 5–10 seconds. In the case of shaking at the central valley station AQU, 60% of the strong-shaking energy was released

within 3 seconds. This is an important characteristic of this earthquake, as it implies that relatively large-amplitude (medium-to-high-frequency) shaking affecting the structures was sustained over only a few cycles (Fig. 6.18) [Çelebi et al., 2010]. If the attenuation relationships of Youngs et al. [1997] for subduction zone earthquakes (interplate and intraslab) are used to compare the recorded PGA (intraplate source: epicentral distance between 10 km and focal depth of 9 km), 0.30 and 0.69g for rock site are obtained and PGA between 0.43 and 0.97g for soft soil conditions. This range of PGA is in accordance with the recorded by the two stations close to L'Aquila (0.3 and 1g).

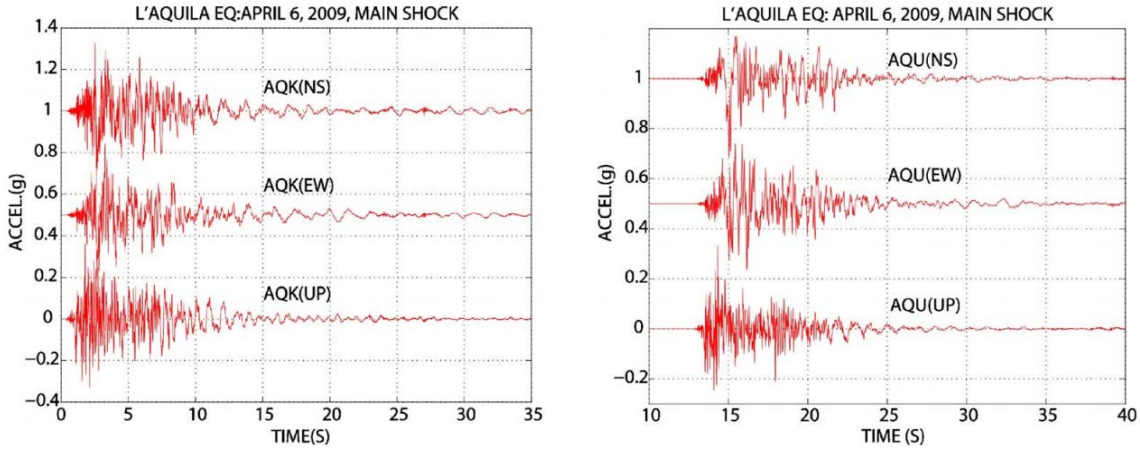

(a)

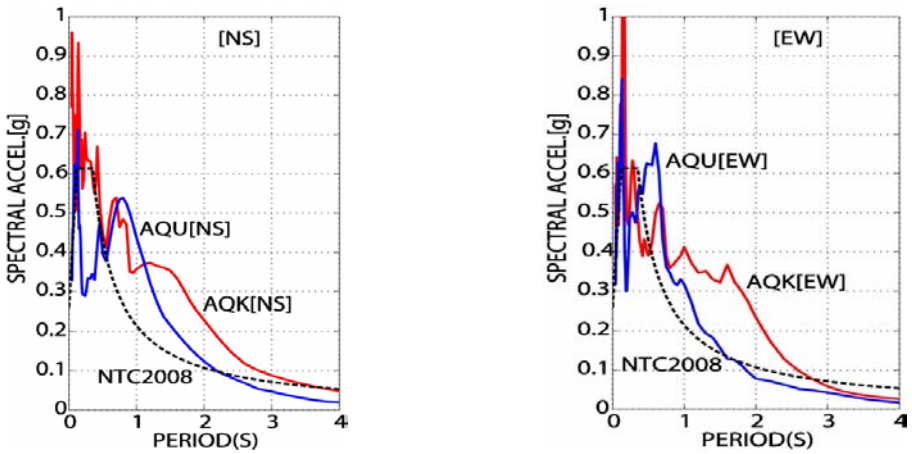

(b)

Figure 6.18: L'Aquila main shock; (a) accelerations at AQU and AQK stations and (b) comparison between response spectra and design spectra NTC 2008 [Celebi et al., 2010]

Historically, the seismic activity of Tuscany has been reduced. The only significant earthquake found in literature is briefly mentioned by USGS [2011b]. It occurred on June 29th, 1919, with a magnitude of 6.3, in the municipality (*comune*) of Mugello, located about 25 km north of the province of Florence. The earthquake caused in this place the death of more than 100 persons. Tordini [2005] describes that San Gimignano

is geologically characterized by the presence of two different types of sedimentary deposits created during the geological era of Pliocene. These consist on Limestone rock deposits (historical center and most of the town) and granular deposits of fine materials as sands and clays (surroundings). The presence of limestone rock is due to the fact that the medieval town of San Gimignano was built on the top of a hill with apparent stable soil conditions. Nowadays, there is not information available about the local site effects of the municipality of San Gimignano. As a part of a big project between local authorities and several Universities of Tuscany, including the University of Florence, a local site effects characterization has been planned to be developed in 2011.

6.3.2 Historical analysis and actual conservation state

Bartoli et al. [2000] and [2006] describe that the "Torre Grossa" was approximately built in the XIII century and is the tallest and most important among the preserved towers in the town of San Gimignano. Its cross section is square with dimensions of 9.5 x 9.5 m and a total height of about 60 m with walls of variable thickness (2.6-1.6 m). The walls are made of three layers masonry (*sacco*). The external layer is constituted by stone and mortar, the internal by brick and mortar and the filling by remains of bricks in a matrix of poor mortar. At the height of 20 m the tower is incorporated to the neighbor Town Hall (*Palazzo Comunale*) previously constructed. The floors were built with vaults of brick masonry. An internal steel stair permits to reach the top of the tower (RC slab).

(a) (b)

Figure 6.19: The medieval tower (Torre Grossa) of San Gimignano, Italy; (a) general view and (b) presence of vegetation on the South façade

As aforementioned, historically, the seismic activity of Tuscany has been reduced, being classified as moderate the seismic hazard of San Gimignano. The tower was importantly damaged due to a lightning in 1632, causing the partial collapse of a wide

part of the SW edge. About 17 years later, the collapsed part was re-constructed. Nowadays, the tower presents important vertical cracks (Fig. 6.20a) related to long-term heavy loads and the lightning, and moreover localized damage due to grenade shots during the Second World War. In the present research, several technical visits were developed to assess by visual inspections and photographic survey the actual conservation state of the building (Fig. 6.19a). Despite of the ancientness of the tower, it presents a good conservation state and is open to the public. Only at the South façade, the presence of invasive vegetation was observed. This could lead to the generation of new cracks or the extension of existing ones (Fig. 6.19b). Moreover, the presence of old metal chains was identified at the internal upper part of the tower (Fig. 3.20).

6.3.3 Structural characterization by experimental campaigns

Since the last decade the "Torre Grossa" has been subjected to extensive in-situ and laboratory testing in the framework of a big research contract (San Gimignano Project) [Bartoli and Mennucci, 2000]. The in-situ campaigns aimed at determining the global structural behavior (natural frequencies and eigenmodes) and the local masonry characteristics (local stress state and E modulus). The dynamic characteristics (lower table in Fig. 6.20b) were assessed by a vibrodyne placed at the tower´s top and recording the structural response by means of some seismic accelerometers and velocity transducers. The local stress state and E modulus were mainly assessed by double flat jack tests, meanwhile the laboratory ones consisted of crushing tests on stone samples in order to determine the ultimate strength (45-65 MPa) and mechanical characteristics.

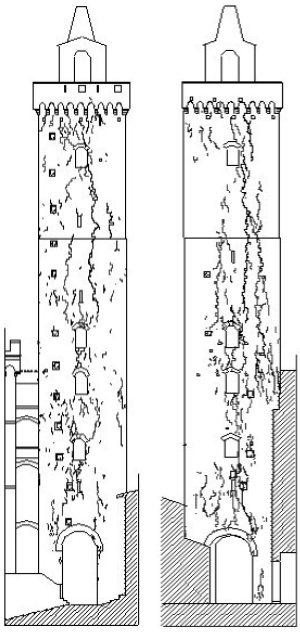

(a)

Material properties				
Material	**E modulus (Kg/cm^2)**	**Density (T/m^3)**	**Compressive Strength (kg/cm^2)**	**Tensile Strength (kg/cm^2)**
External stone masonry	110000	2.4	55	5.5
Internal filling	16000	2	16	1.6
Internal brick masonry	30000	1.8	30	3

Experimental frequencies		
Mode	**Direction**	**Frequency (Hz)**
I	East – West	1.3060
II	North – South	1.3310
III	Torsional	3.4100
IV	Vertical	-----
V	West - East	6.5500

(b)

Figure 6.20: Experimental tests and crack pattern survey; (a) cracks on North and South façades and (b) mechanical and dynamic properties [Bartoli et al., 2000 and 2006]

With the collected data a numerical model in ANSYS® was identified in the static and dynamic field. The dynamic one permitted to estimate the restrain degree offered by the neighbor City Hall. The static identification allowed obtaining an estimation of the internal filling E modulus by some creep analyses using an elastic time-dependent concrete model [Tordini, 2005]. This was an important task since no experimental data was available about the filling. The material properties are summarized in the upper table of Fig. 6.20b. As part of the surveys, the crack pattern at two sides of the tower was identified (Fig. 6.20a) and the numerical model confirmed that the lightning that hit the tower was probably responsible for the crack´s appearance [Bartoli et al., 2000].

6.3.4 Review of previous works

Bartoli et al. [2006] evaluated the seismic capacity of the Torre Grossa by using the above mentioned calibrated FE model. The tower was subjected in the X direction to base excitation (time-varied displacements) by a 20 s time-history generated according to EC-8 for a ground class B and a 475 years return period with a PGA equal to a_g=0.25g. The seismic reliability was evaluated by considering two limit states (tower overturning and mechanical collapse of a masonry panel). By considering a dynamic linear model the I limit state was carried out to determine the time-history of the eccentricity e(z,t)= M(z,t)/N(z). The tower is safe if, for each instant $|e_{max}| \leq |e_{lim}|$ where e_{max} is the maximum value assumed e(z,t) during the loading time and e_{lim} is the value of the eccentricity of the normal force producing the overturning (half length of the tower section). A coefficient of reduction $\alpha = e_{max}/e_{lim}$ was determined, that together with $a_{g1}=a_g/\alpha$ define the maximum acceleration that the tower accepts without overturning (0.0546g). The II limit state was defined trough a reduced model of an elementary panel (Fig. 6.21a) to determine that the seismic loading does not produce a local crushing at the external layer of the infill wall of the tower and the final admissible seismic input. The nonlinear behavior of masonry was based on the yield Drucker-Prager criterion and Solid65 eight nodes elements with cracking and crushing capabilities. The admissible acceleration 0.0268g was obtained by considering the acceleration that makes all combination [T(z;t), M(z;t] of shear and moment inside the collapse domain.

Stavroulaki et al. [2009] developed seismic analyses of the tower with the FE model developed in the framework of the San Gimignano Project. By the use of sinusoidal waves the seismic input was included. The tower was analyzed in original state (Model A) and retrofitted with horizontal prestressed metal cables in several locations (Models B, C and D). The analyses were developed with the FE software MARC® and the Mohr-Coulomb Parabolic criterion. The used material parameters are the described in the upper table in Fig. 6.20b. The results of the analyses are illustrated in Fig. 6.21b by means of the plastic activity which represents the crack development. Compared to the original state, the retrofitted model C showed a satisfactory reduction of damage. This reduction was not so high since the compressive stresses and development of localized tensile stresses at other locations (at the corners) were increased. Injections to enhance the strength of the filling material were recommended by the authors.

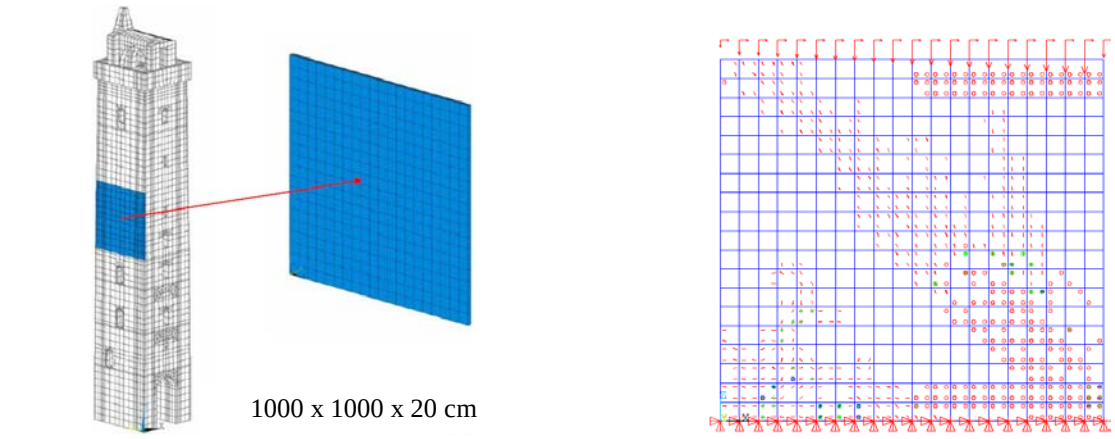

(a)

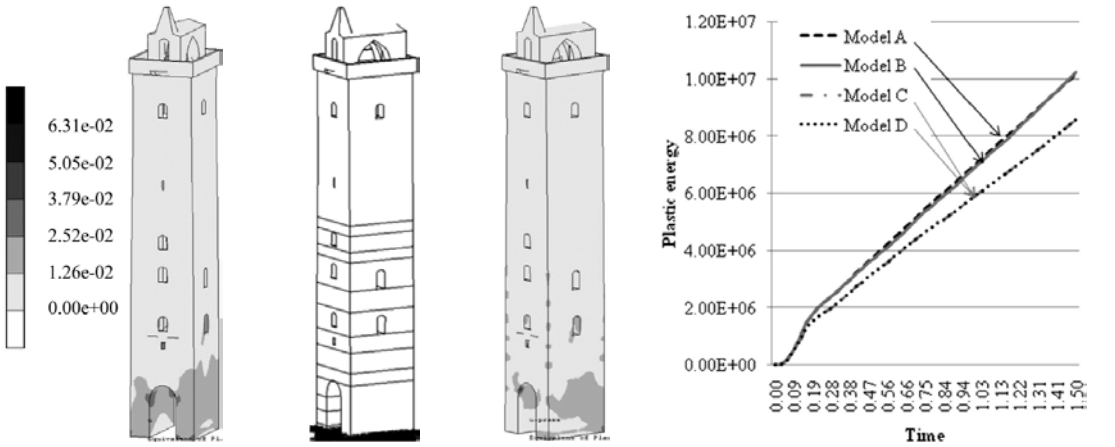

Original state Model A | Cable position Model C | Retrofitted Model C | Plastic energy vs time

(b)

Figure 6.21: Seismic analyses of the Torre Grossa; (a) panel definition and crack pattern [Bartoli et al., 2006] and (b) comparison of plastic activity [Stavroulaki et al., 2009]

6.3.5 Seismic risk assessment and reduction

In the seismic analyses of the "Torre Grossa" only one direction of the seismic action is considered and two prestressing levels (medium and high). The selected direction is the –X (S-N), which corresponds to the most vulnerable due to the constraint offered by the neighbor municipal building (*Palazzo Comunale*) up to the height of about 20 m (L= 6 m). The developed FE model in the San Gimignano Project is not used in the present research. The main reason is that the model has been built with eight nodes solid elements (soild45) representing the three layers of masonry, which is not suitable for the material model of Gambarotta and Lagomarsino [1997] due to the fact that it correctly works trough simplified models with four nodes shell elements (shell43). The FE model is rebuilt considering the interaction with the municipal building by springs (combin14) of constant stiffness (10 kN/mm). The model has a square plan of 9.5 x 9.5 m

with wall thickness of 2 m and 50 m height. At the top has a concrete slab and a substructure (belfry), reaching the total height of 57 m (total mass of 6043.8 Ton, San Gimignano Project model 6042 Ton). The 3D FE model has 2340 shell43 elements and 2402 nodes (14316 DOF). An equivalent layer with average properties of the three masonry materials is considered: E modulus of 1700 MPa, mass density of 1.8 Ton/m^3 with a constant Poisson's ratio of 0.15, compressive strength of 3.5 MPa (about 10% of tensile strength) and the inelastic parameters of section 3.2.2.2. With the use of Eq. 4.1 (L= 9.5 m, H= 50 m), a first natural frequency of 1.2072 Hz or higher is expected due to the interaction with the adjacent building. The numerical model is calibrated by modal analyses with the dynamic experimental data of section 6.3.3, obtaining a good agreement: E-W 1.2927 (flexural) Hz, N-S 1.3323 Hz (flexural) and 3.1131 Hz (torsional).

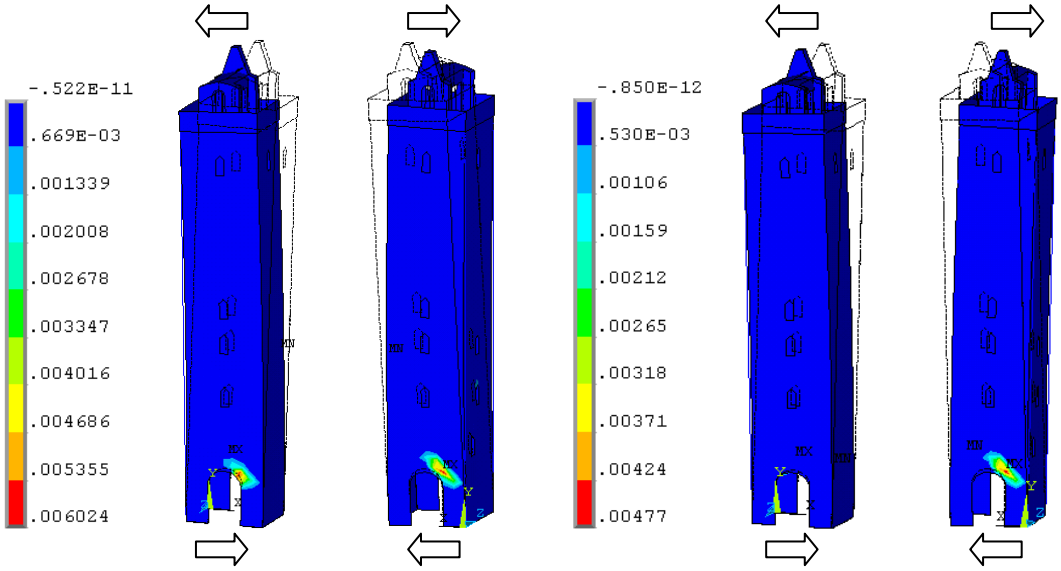

Figure 6.22: Comparison of principal plastic strains (front and back) at a displacement of 105 mm for a seismic action in –X (S-N): (a) original state (ULS) and (b) retrofitted 0.15Fv

The tower presents at the plane of the W façade horizontal flexural cracks and diagonal shear cracks at the E façade (Figs. 6.22a and 6.23a) with brittle behavior as expected due to the large openings and the neighbor building (Fig. 6.24). For retrofitting, two prestressing levels with four technora devices are proposed: medium 0.15Fv (At= 3360 mm^2, 50 bars of 8 mm) and high 0.30Fv (At= 6720 mm^2, 100 bars of 8 mm). It is worth noting that the retrofitting considerably reduces the damage by completely decreasing the plasticity at the W façade and substantially at the E façade depending on the prestressing level (Figs. 6.22b and 6.23b). The seismic performance is satisfactorily enhanced as observed in tables 6.6 and 6.7. It could be observed that the seismic coefficient of the model in original state (0.042) is in good agreement with the obtained by other researchers (0.055), reflecting its high vulnerability. At ULS no failure by crushing is observed: original 1.60 MPa, 0.15Fv 1.95 MPa and 0.30Fv 2.32 MPa.

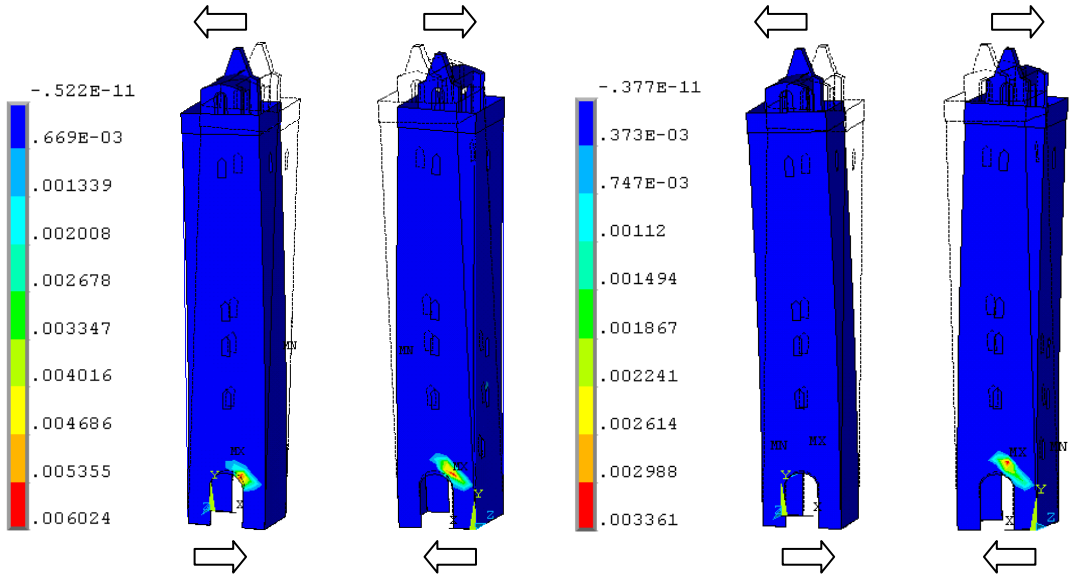

(a) (b)

Figure 6.23: Comparison of principal plastic strains (front and back) at a displacement of 105 mm for a seismic action in –X (S-N): (a) original state (ULS) and (b) retrofitted 0.30Fv

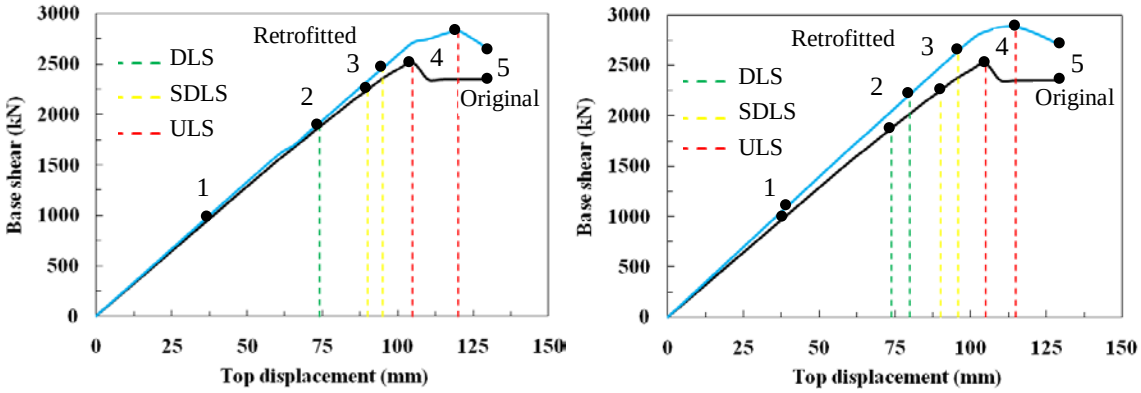

(a) (b)

Figure 6.24: Comparison of capacity curves in original state and retrofitted with the damage grades (EMS-98) and limit states (EC-8): (a) 0.15Fv and (b) 0.30Fv

FE model reference	Limit states EC-8 and Damage grades EMS-98						S. C.
	DLS DG 2		SDLS DG 3		ULS DG 4		
	F	***U***	***F***	***U***	***F***	***U***	
Original state	1940	74	2249	90	2516	105	0.042
Retrofitted 15%	1940	74	2464	95	2830	120	0.048
Retrofitted 30%	2208	80	2625	96	2880	115	0.049

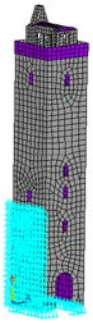

%: PL; S.C: seismic coefficient; F: force (kN); U: displacement (mm)

Table 6.6: Seismic analysis summary of the Torre Grossa in original state and retrofitted 0.15Fv and 0.30Fv for an earthquake action in –X

FE model reference	Limit states EC-8 and Damage grades EMS-98						Seismic Coeff. %
	DLS DG 2		SDLS DG 3		ULS DG 4		
	F %	*U %*	*F %*	*U %*	*F %*	*U %*	
Retrofitted 15%	0.0	0.0	9.6	5.6	12.5	14.3	14.3
Retrofitted 30%	13.8	8.1	16.7	6.7	14.5	9.5	16.7

Table 6.7: Seismic risk reduction comparison at the Torre Grossa by the increment of F, U and S.C. for an earthquake action in –X

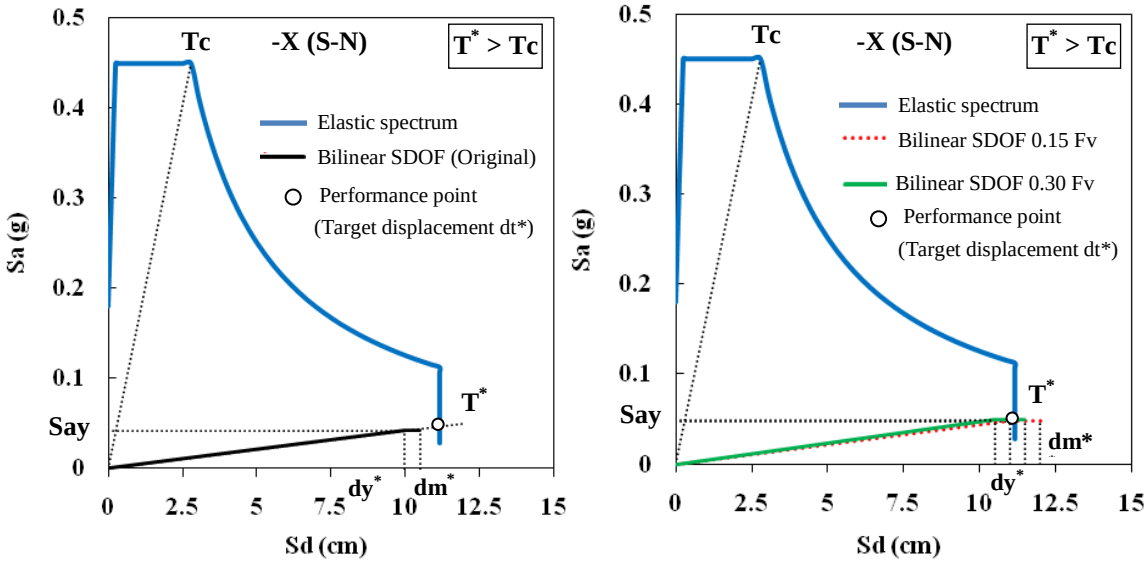

Figure 6.25: Seismic evaluation of the Torre Grossa by the capacity spectrum method: (left) original state and (right) retrofitted with 0.15Fv and 0.30Fv

FE model reference	m* (Ton)	dy* (mm)	Fy* (Ton)	Say (g)	dm* (mm)	dt* (mm)	Comment
Original state	6043.8	100	256.5	0.042	105	111.7	Loss of tower
Retrofitted 15%	6043.8	110	288.5	0.048	120	111.7	Reparable
Retrofitted 30%	6043.8	105	293.6	0.049	115	111.7	Reparable

m*: mass; dy*: yield displacement; Fy*: yield force; Say: yield acceleration; dm*: maximum displacement; dt*: target displacement (performance point)

Table 6.8: Seismic assessment summary of the Torre Grossa (capacity spectrum method)

Figure 6.25 and table 6.8 illustrate the results of the seismic analysis by the capacity spectrum method with the capacity curves converted in bilinear equivalent SDOF and the elastic response spectrum based on the seismic risk characterization (appendix C). It is worth noting that the seismic performance of the tower in original state is not satisfactory, leading to its collapse. By the other hand, both retrofitting levels (0.15Fv and 0.30Fv) allow to the tower to be able to withstand the seismic action ($dm^* > dt^*$).

6.4 Summary and conclusions

The present chapter described applications of the proposed methodology for the seismic risk management (assessment and reduction) of historical masonry towers by external prestressing devices. The proposal was applied in two real historical towers located in seismic zones, in order to validate the approach and to prove its effectiveness. The case studies consisted of the north bell tower of the Cathedral of Colima, Mexico, and the medieval tower "Torre Grossa" of San Gimignano, Italy. The 3D FE models of the towers were calibrated with data experimentally obtained and validated as in the case of the four virtual towers with key behavioral characteristics and observed failure mechanisms after real important earthquakes. Firstly, the seismic hazard of the sites under study was characterized considering a combination of studies (e.g. seismological, geophysical, and geological) with the history of earthquakes. The level of seismic hazard was estimated by identifying the main seismic sources and expected earthquake characteristics. The relationships of Youngs et al. [1997] included in PEER [2011] is a suitable tool to measure (or to compare) the local site effects of a real earthquake in terms of PGA by taking into account the seismic source, epicentral distance, focal depth and soil conditions. The results were compared with the level of observed damage and recorded PGA after real earthquakes in Colima, Mexico and L'Aquila, Italy, obtaining quite good agreement. Afterwards, the FE models of both case studies were successfully calibrated in the dynamic field with experimental data, proving the equation of NCSE [2002] to be suitable as a practical pre-calibration, obtaining good agreement between the analytical first natural frequency and the experimental one.

The seismic risk assessment and its reduction were developed through two methodologies with different level of refinement. The first one consisted to the seismic evaluation by the pushover method of the towers in original state and retrofitted with the proposed device and prestressing levels depending on the seismic hazard of the site and desirable performance enhancement determined in chapter 5. The seismic hazard was included in qualitative terms at the capacity curves for different damage grades and limit states, and quantitatively by the seismic coefficient. The failure modes and force-displacement diagrams showed the high vulnerability of the towers. The crack patterns were similar to the observed after real earthquakes. Moreover, the seismic coefficients were in complete agreement with the obtained by other researchers, proving the reliability of the obtained results. The retrofitting considerably reduced the damage (plasticity) depending on the prestressing level. The seismic performance enhancement was also reflected in the seismic risk reduction comparisons. At ULS no failure by crushing was observed nor devices failure, due to the proposed material kept the prestressing forces almost constant with changes of about ±1.5%. Complementary, the capacity spectrum method was used. The seismic performance of both case studies in original state was not satisfactory. The retrofitted towers (with extra measures for the Colima tower) were able to withstand the local seismicity, proving with this risk reduction the effectiveness of the present proposal. Once again, the medium level (0.15Fv) proved to be the optimal prestressing level due to the ductility enhancement.

Chapter 7

Synopsis

7.1 Summary

Existing historical masonry towers are distributed all over the world and constitute a relevant part of the architectural and cultural heritage of humanity. Their protection against earthquakes is a topic of great concern among the scientific community. This concern mainly arises from the strong damage or complete loss suffered by these structures due to earthquakes and the need and interest to preserve them. Although the great progress in technology, seismology and earthquake engineering, the preservation of these brittle and massive structures still represents a major challenge. Seismic risk management of the built environment is integrated by two great stages, the assessment and the remedial measures to attain its reduction. The seismic risk of a structure located in a seismic zone is determined by the conjunct of the seismic hazard and the vulnerability of the structure. In the relevant literature the seismic risk is also known as seismic vulnerability and there is a great variety of methods for its evaluation. The selection of the most suitable approach depends on different factors such as number of buildings, importance, available data and aim of the study. For more reliable results, the literature recommends applying a hybrid approach, which is a combination of the empirical, analytical and experimental.

In the present research work, a practical methodology for the seismic risk management of historical masonry towers by external prestressing devices (PDs) was proposed in the framework of the International Graduate College 802. The investigation was divided in two major stages, the seismic risk assessment and the remedial measures to attain its reduction. Firstly, the most relevant aspects that determine the seismic vulnerability of historical masonry towers were described and compared to those observed in post-earthquake investigations. The seismic risk assessment stage was developed through four validated 3D FE models representative of European towers. The models were subjected to linear elastic investigations to validate them with theoretical background and reported experimental data on similar towers. This validation could be

useful when there is no experimental data available to calibrate the model, and when it is available, as a practical pre-calibration. The capability of the applied model to simulate the nonlinear behavior of masonry was validated with reported experimental examples, obtaining a good agreement. Intensive numerical simulations based on nonlinear analyses were carried out. The pushover approach successfully permitted to obtain the tower's seismic response in-plane and out-of-plane. The huge impact of the low tensile strength of masonry and large openings at belfries on the seismic performance was observed, failing in a brittle mode by shear stresses. Towers failing by bending and combined bending and shear showed similar resistance but more ductility. The behavior and damage types were validated with the seismic vulnerability aspects and reported post-earthquake observations on more than 200 towers. The seismic hazard was qualitatively included at the capacity curves for different damage grades and limit states, and quantitatively by the seismic coefficient. These permitted to satisfactorily assess the seismic risk of the four towers. They presented an imminent high risk to seismic actions as expected. The results of the nonlinear dynamic earthquake analysis of one tower in terms of seismic response and failure modes were identified as not reasonable.

The seismic risk reduction stage included the addition of vertical external prestressing at the four internal corners of the towers to be removable and to increase the strength and ductility of masonry by providing tensile strength at key locations. Firstly, an extensive parametric study on a selected tower was carried out based on more than 100 nonlinear static simulations aimed at investigating the impact in the seismic performance of different parameters such as tendon material, prestressing level (PL), changes in tendon forces and SMA superelasticity (previously validated with reported experimental data). The parametric study allowed proposing a device and three PLs based on the desirable seismic performance enhancement and the earthquake hazard. The suitability was proved through the three different failure modes identified in the virtual towers by assessing the level of seismic risk reduction between original conditions and retrofitted. Finally, the proposal was applied in two real historical towers located in seismic zones of Mexico and Italy to validate it and to prove its effectiveness. The FE models were built and calibrated in the dynamic field with data experimentally obtained and validated as in the case of the four virtual towers. The seismic risk and reduction evaluations were developed by the pushover method and the damage/limit state indicators, and by the capacity spectrum method involving the seismic demand determined in the hazard characterizations. The results by the first approach showed the high vulnerability of the towers. The crack patterns were similar to the observed after real earthquakes and the seismic coefficients were in good agreement with the obtained by other researchers. The retrofitting considerably reduced the damage depending on the PL and reflected in the seismic risk reduction. At ULS no failure by crushing was observed nor devices failure due to the proposed material and PLs. By the capacity spectrum method was observed that the seismic performance of both case studies in original state was not satisfactory. By implementing the retrofitting (with extra measures for the Colima tower) they were able to withstand the local seismicity, proving with this risk reduction the effectiveness of the present proposal.

7.2 Conclusions and outlook for further research

The research carried out in these years permitted to identify the most important aspects that determine the vulnerability of historical masonry towers under earthquake ground motion. A deep understanding of these main aspects was the basis towards the achievement of their risk reduction, by decreasing their seismic vulnerability with external PDs, which corresponds to the main objective of this thesis. The two major stages at which the investigation was developed allowed highlighting the suitability of the proposal. In particular, in the seismic risk assessment stage, the proposed validation strategy combined with the nonlinear static pushover method permitted to evaluate the seismic performance of the four virtual European towers in terms of failure modes and force-displacement diagrams. Especial attention was focused on the in-plane and out-of-plane failure modes, due to the few investigations reported in literature on the seismic behavior of historical masonry towers are mainly focused on the in-plane behavior and disregard horizontal cracking and crushing out-of-plane. The material model of Gambarotta and Lagomarsino [1997] was able to satisfactorily simulate the main failure modes of masonry towers by comparing the results with the reported post-earthquake observations on more than 200 towers. The damage indicators EMS-98, limit states EC-8 and seismic coefficient permitted to satisfactorily assess the seismic risk of the four towers. They presented an imminent high risk to seismic actions as it was expected. The results of the nonlinear dynamic earthquake analysis of one tower in terms of seismic response and failure modes were identified as not reasonable. Further research is recommended on this complex and challengeable approach regarding the material parameters and internal damping.

In the seismic risk reduction stage the PDs were vertically and externally proposed in order to respect in all senses the cultural value of the towers and to be removable. Vertical prestressing was selected due to it has proved to be more suitable to increase the in-plane lateral strength and ductility of masonry walls by providing tensile strength at key locations. Horizontal prestressing has been mainly used in the cultural heritage to provide stability out-of-plane in walls or to reduce the tension generated by supports opening of vaults, arches and domes. A practical way to determine the prestressing forces (PFs) based on the tower´s weight was proposed. An extensive parametric study allowed proposing a device and three PLs (low, medium and high) based on the desirable seismic performance enhancement and the earthquake hazard. SMA did not show high upgrading of the seismic performance due to the size of the device and the vertical location. If a SMA is in austenite phase behaves as a conventional material. The superelasticity in vertical prestressing has only impact in keeping the applied forces with lower variations than other material in low and medium PLs. The AFRP technora showed different levels of seismic performance enhancement depending on the PL and failure mode, keeping almost constant the PFs by its low E modulus, being favorable to interact with such a poor material as old masonry. Especial attention is suggested when using high PLs due to this could generate brittle failure by masonry crushing at the compressed toes in static and seismic conditions. The three proposed PLs are suggested

for towers with compressive strength at least 15% higher than the maximum stress presented in original state at ULS. Prestressing allowed enhancing the lateral force capacity and confinement of towers failing by pure bending and combined with shear in a small area without increasing the natural ductility, which is satisfactory due to the crushing of masonry could occur by PLs higher than 0.30Fv or an increasing in ductility. In towers with belfry failure, prestressing increased displacement but lower force than in towers failing by bending due to the brittleness of this mode. The post-peak behavior showed an increase in confinement which is favorable to avoid belfry's failure that could harm people or adjacent buildings.

Considering the recent performance based design philosophy where ductility enhancement is quite important for energy dissipation, the medium PL (0.15Fv) is the optimal. The proposed technora device and PL are valuable for systematic and practical applications. This research has contributed to find out that the implementation of a simple device is able to successfully reduce the seismic risk of towers. The suitability and good agreement with the results obtained by other researchers at the case studies in original conditions, and the attainment of seismic risk reduction permitted to validate the effectiveness of the present proposal. The high seismic hazard of Colima and the brittleness of the belfry due to the large openings and reduced performance by the adjacent façade, led to suggest in combination with PDs an internal wrapping of belfry with GFRP sheets, to be reversible and to bring the additional strength and ductility. Further research is suggested regarding the use of GFRP sheets in terms of seismic performance and numerical simulation.

In all the cases the towers were assumed as fixed disregarding the actual state of the foundation and soil. In seismic conditions an exceedance of the load bearing capacity could lead to tower overturning or soil failure. Even when the soil-structure interaction has been a topic of intensive research in this decade, so less could be found in literature about ancient masonry towers, being an interesting topic for further research. The seismic analyses were developed on the "Torre Grossa" by considering an equivalent layer with average properties of the three masonry types due to the material model´s limitation and to simplify the simulations, obtaining acceptable agreement in the results. However, most of the ancient buildings, especially in Italy have been built with this constructive technique, therefore further intensive research is recommended on the mechanical experimental campaigns and simulation to account for a suitable representation of the three materials interaction and damage in earthquake conditions.

Finally, the investigation of an additional mechanism that works together with the external PDs able to go from passive to active prestressing before earthquakes is suggested, to avoid an increasing of long-term loads and to improve the PDs durability.

Appendix A

Determination of the target displacement [EC-8, 2004]

A.1 General

The target displacement is determined from the elastic response spectrum $S_e(t)$. The capacity curve derives from the pushover analysis for values of the control displacement ranging between zero and the value corresponding to 150% of the target displacement. The following relation between normalized lateral forces F_i and normalized displacements Φ_i is assumed:

$$\overline{F_i} = m_i \Phi_i \quad [A.1]$$

where m_i is the mass in the i-th storey. Displacements are normalized in such a way that $\Phi_n = 1$, where n is the control node usually denoting the roof level. Then, $F_n = m_n$.

A.2 Transformation from the MDOF system to an equivalent SDOF system

The mass of the equivalent SDOF system m^* is determined as:

$$m^* = \sum m_i \Phi_i = \sum \overline{F_i} \quad [A.2]$$

and the transformation factor is given by:

$$\Gamma = \frac{m^*}{\sum m_i \Phi_i^2} = \frac{\sum \overline{F_i}}{\sum \left(\frac{\overline{F_i}^2}{m_i} \right)} \quad [A.3]$$

The force F^* and displacement d^* of the equivalent SDOF system are computed as:

$$F^* = \frac{F_b}{\Gamma} \quad [A.4]$$

$$d^* = \frac{d_n}{\Gamma} \quad [A.5]$$

where F_b and d_n are, respectively, the base shear force and the control node displacement of the MDOF system.

A.3 Determination of the idealized elasto-perfectly plastic F vs d relationship

The yield force F_y^*, representing also the ultimate strength of the idealized system, is equal to the base shear force at the formation of the plastic mechanism. The initial stiffness of the idealized system is determined in such a way that the areas under the actual and the idealized force-deformation curves are equal (see Fig. A.1). Based on this assumption, the yield displacement of the idealized SDOF system d_y^* is given by:

$$d_y^* = 2\left(d_m^* - \frac{E_m^*}{F_y^*} \right) \quad [A.6]$$

where E_m* is the actual deformation energy up to the formation of the plastic mechanism.

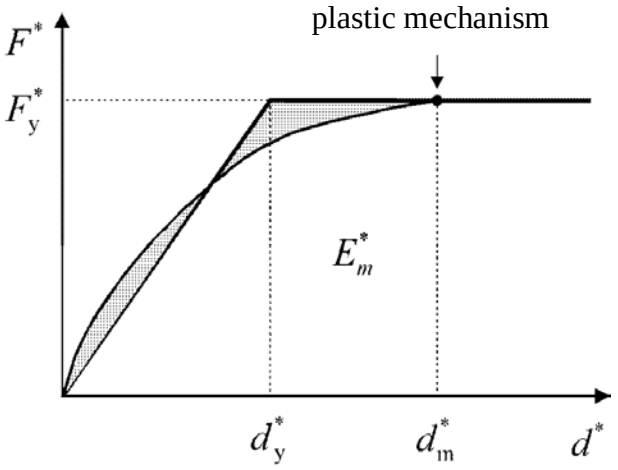

Figure A.1: Determination of the idealized elasto-perfectly plastic F VS d relationship

A.4 Determination of the period of the idealized equivalent SDOF system

The period T^* of the idealized equivalent SDOF system is determined as:

$$T^* = 2\pi\sqrt{\frac{m^* d_y^*}{F_y^*}} \quad [A.7]$$

A.5 Determination of the target displacement of the equivalent SDOF system

The target displacement of the structure with period T^* and unlimited elastic behavior is given by:

$$d_{et}^{*} = S_e(T^{*})\left[\frac{T^{*}}{2\pi}\right]^2 \qquad [A.8]$$

where $S_e(T^*)$ is the elastic acceleration response spectrum at the period T^*. For the determination of the target displacement d_t^* for structures in the short-period range and for structures in the medium and long-period range different expressions should be used, as indicated below. The corner period between the short and medium-period range is Tc (see Fig. A.2).

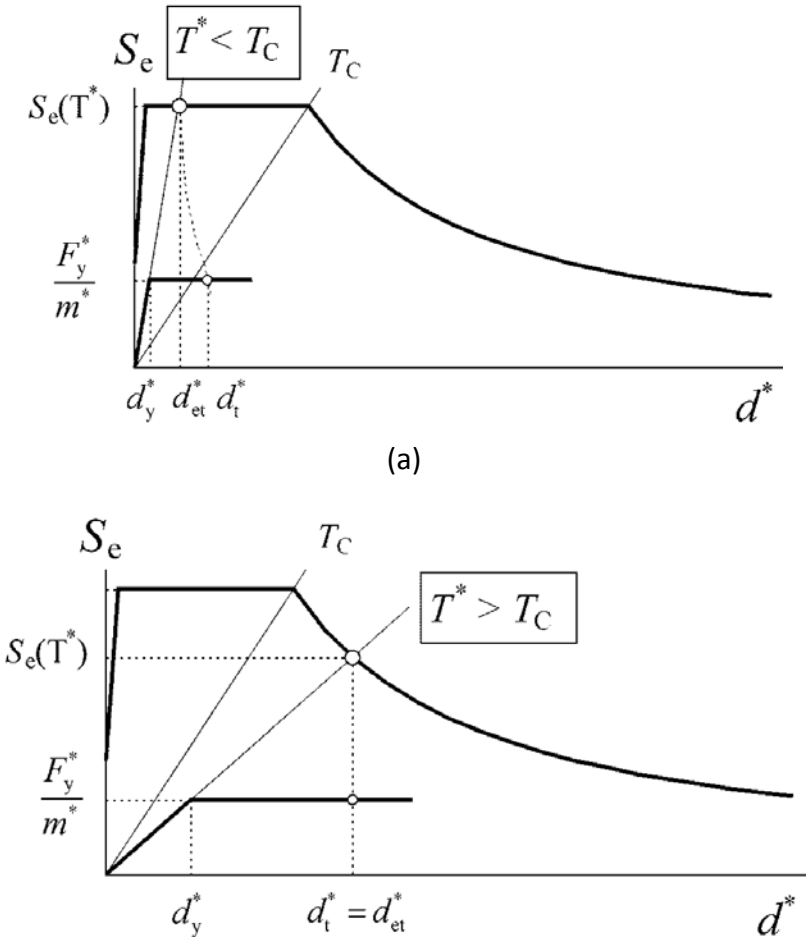

Figure A.2: Determination of the target displacement for the equivalent SDOF system; (a) short period range and (b) medium and long period range

Figure A.2a: $T^* < Tc$ (short period range)

If $F_y^* / m^* \geq S_e(T^*)$, the response is elastic and

$$d_t^* = d_{et}^* \qquad [A.9]$$

If $F_y{}^* / m^* < S_e(T^*)$, the response is nonlinear and

$$d_t^* = \frac{d_{et}^*}{q_u}\left(1 + (q_u - 1)\frac{T_C}{T^*}\right) \geq d_{et}^* \qquad [A.10]$$

where q_u is the ratio between the acceleration in the structure with unlimited elastic behavior $S_e(T^*)$ and in the structure with limited strength $F_y{}^* / m^*$:

$$q_u = \frac{S_e(T^*)m^*}{F_y^*} \qquad [A.11]$$

Figure A.2b: $T^* \geq Tc$ (medium and long period range)

$$d_t^* = d_{et}^* \qquad [A.12]$$

$d_t{}^*$ need not exceed 3 $d_{et}{}^*$

Figures A.2a-b are plotted in acceleration-displacement format. The period T^* is represented by the radial line from the origin of the coordinate system to the point at the elastic response spectrum defined by coordinates $d^* = S_e(T^*) \cdot (T^* / 2\pi)^2$ and $S_e(T^*)$.

A.6 Determination of the target displacement of the equivalent MDOF system

The target displacement of the MDOF system corresponding to the control node is given by the expression:

$$d_t = \Gamma d_t^* \qquad [A.13]$$

Appendix B

Elastic response spectrum and parameters for Colima City [MDS-CFE, 1993] and [NTCDF, 2004]

For the horizontal components of the seismic action, the elastic response spectrum a= $S_e(T)$ is defined by the following expressions:

$$a = a_0 + (c - a_0)\frac{T}{T_a}; \quad T < T_a \qquad [B.1]$$

$$a = c; \quad T_a \leq T \leq T_b \qquad [B.2]$$

$$a = qc; \quad T > T_b \qquad [B.3]$$

$$q = (T_b/T)^r \qquad [B.4]$$

Where

$S_e(T)$ is the elastic response spectrum;
T is the vibration period of a linear single-degree-of-freedom (SDOF) system;
a_0 is the design ground acceleration involving the soil factor of the site;
T_a is the lower limit of the period of the constant spectral acceleration branch;
T_b is the upper limit of the period of the constant spectral acceleration branch;
c is the seismic coefficient or design coefficient;
r is the parameter that controlls the descendent spectral acceleration branch;
q is the parameter that determines the descendent spectral acceleration branch;

According to the Mexican codes MDS-CFE [1993] and NTCDF [2004], as well as the seismic hazard characterization developed in section 6.2.1 of this thesis, the historical center of Colima City is characterized as soil type I (stable) and seismic hazard zone D,

with a maximum PGA value (rock site) of 0.50g (a_0) with a probability of exceedance of 10% in 50 years and a return period of 475 years. Table B.1 presents the summary of the needed parameters to develop the normalized elastic response spectrum.

Seismic hazard	Ground type	a_0 (g)	c	T_a (s)	T_b (s)	r
zone D	I	0.5	0.5	0.0	0.6	1

Table B.1: Parameters describing the elastic response spectrum for the historical center of Colima City

Figure B.1 illustrates the normalized elastic response spectrum for the historical center of Colima City. The dashed line indicates the fundamental period T_0 of the north bell tower of the Cathedral.

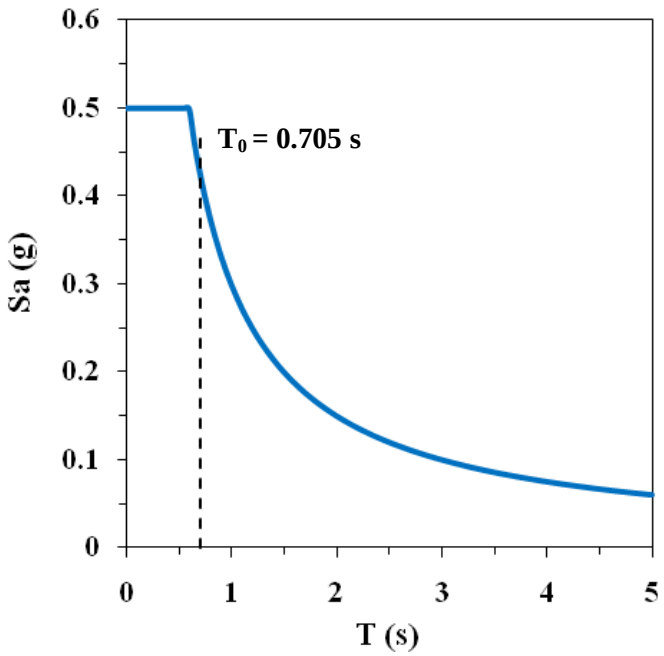

Figure B.1: Elastic response spectrum for the historical center of Colima City

The elastic displacement response spectrum $S_{De}(T)$, shall be obtained by direct transformation of the elastic acceleration response spectrum $S_e(T)$, using the following expression:

$$S_{De}(T) = S_e(T)\left[\frac{T}{2\pi}\right]^2 \qquad [B.5]$$

Appendix C

Elastic response spectrum and parameters for San Gimignano [EC-8, 2004] and [INGV, 2011]

For the horizontal components of the seismic action, the elastic response spectrum $S_e(T)$ is defined by the following expressions:

$$0 \le T \le T_B : S_e(T) = a_g \cdot S \cdot \left[1 + \frac{T}{T_B} \cdot (\eta \cdot 2{,}5 - 1)\right] \quad \text{[C.1]}$$

$$T_B \le T \le T_C : S_e(T) = a_g \cdot S \cdot \eta \cdot 2{,}5 \quad \text{[C.2]}$$

$$T_C \le T \le T_D : S_e(T) = a_g \cdot S \cdot \eta \cdot 2{,}5\left[\frac{T_C}{T}\right] \quad \text{[C.3]}$$

$$T_D \le T \le 4\text{s} : S_e(T) = a_g \cdot S \cdot \eta \cdot 2{,}5\left[\frac{T_C T_D}{T^2}\right] \quad \text{[C.4]}$$

Where

$S_e(T)$ is the elastic response spectrum;

T is the vibration period of a linear single-degree-of-freedom (SDOF) system;

a_g is the design ground acceleration on type A ground;

T_B is the lower limit of the period of the constant spectral acceleration branch;

T_C is the upper limit of the period of the constant spectral acceleration branch;

T_D is the value defining the beginning of the constant displacement response range;

S is the soil factor;

η is the damping correction factor with a reference value of $\eta=1$ for 5% viscous damping

According to the Italian code OPCM 3519 (2006), INGV [2011], the medieval town of San Gimignano is characterized as soil B and seismic hazard zone 2, with a maximum PGA (rock site) of 0.150g (a_g) with a probability of exceedance of 10% in 50 years and a return period of 475 years (see section 6.3.1). Table C.1 presents the summary of the needed parameters to develop the normalized elastic response spectrum. Considering the maximum acceleration at rock site (0.150g) and the soil factor (1.2) of Table C.1, the maximum acceleration at the site results in 0.18g and could be observed in Figure C.1.

Seismic hazard	Ground type	S	T_B (s)	T_C (s)	T_D (s)
Zone 2	B	1.2	0.15	0.5	2.0

Table C.1: Parameters describing the elastic response spectrum for San Gimignano

Figure C.1 illustrates the normalized elastic response spectrum for the medieval town of San Gimignano. The dashed line indicates the fundamental period T_0 of the Torre Grossa.

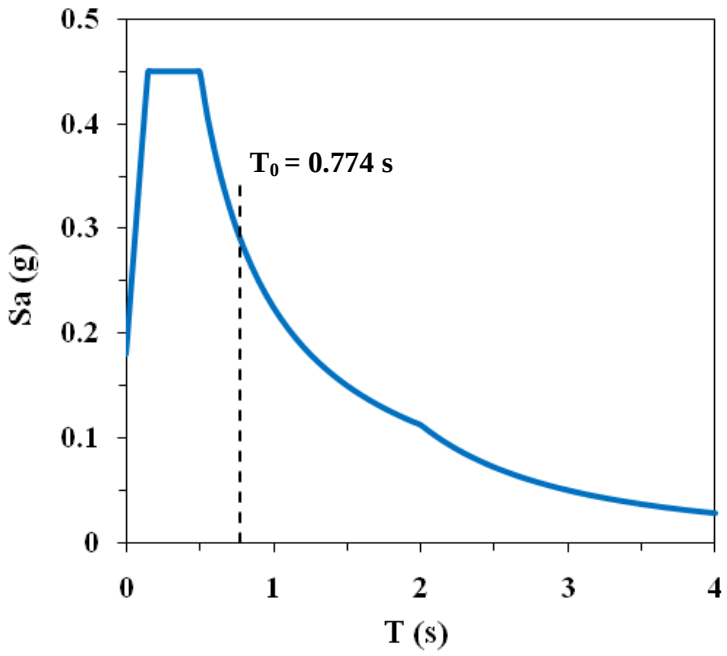

Figure C.1: Elastic response spectrum for the medieval town of San Gimignano

The elastic displacement response spectrum $S_{De}(T)$, shall be obtained by direct transformation of the elastic acceleration response spectrum $S_e(T)$, using the following expression:

$$S_{De}(T) = S_e(T)\left[\frac{T}{2\pi}\right]^2 \qquad [C.5]$$

References

Abruzzese, D. and Vari, A. [2004]. *"Seismic resistance of masonry towers."* 4th International Seminar on Structural Analysis of Historical Constructions. November 10-13, Padova, Italy.

Abruzzese, D., Miccoli, L. and Vari, A. [2009]. *"Dynamic investigations on medieval masonry towers: Seismic resistance and strengthening techniques."* Proceedings of the 1st International Conference on Protection of Historical Buildings (PROHITECH 09), June 21-24, 2009, Rome, Italy.

Aguiar, R., Barbat, A., Caicedo, C. and Canas, J. [1994]. *"Seismic vulnerability of buildings (in Spanish)"*. Monographs of Seismic Engineering, Published by the International Center of Numerical Methods (CIMNE), Barcelona, Spain.

Alcocer, S. M., Aguilar, G., Flores, L., Bitrán, D., Durán, R., López, O. A., Pacheco, M. A., Reyes, C., Uribe, C. M. and Mendoza, M. J. [1999]. *"The Tehuacan earthquake of June 15th, 1999 (in Spanish)"*. National Center for the Prevention of Disasters, Technical Report IEG/03/99, Mexico.

Araiza, J. C. [2003]. *"Dynamic assessment of structural building components"*. Doctoral thesis, Politechnical University of Catalunya, Barcelona, Spain.

ATC-40 [1996]. Applied Technology Council. *"Seismic evaluation and retrofit of concrete buildings."* Redwood City, USA.

Auricchio, F. [1995]. *"Shape memory alloys: Micromechanics, macromodeling and numerical simulations."* Doctoral thesis, University of California at Berkeley.

Auricchio, F. and Sacco, E. [1997]. *"A one-dimensional model for superelastic shape-memory alloys with different elastic properties between martensite and austenite."* International Journal of Non-Linear Mechanics, 32: 1101-1114.

Bachmann, H., Ammann, W. and Deischl, F. [1997]. *"Vibration problems in structures: Practical Guidelines."* Springer Verlag, Berlin, 50-55.

Badoux, M., Elgawady, M. A. and Lestuzzi, P. [2002]. *"Earthquake simulator tests on unreinforced masonry walls before and after upgrading with composites."* 12th European Conference on Earthquake Engineering, September 9-13, 2002, London, UK. Paper reference 862.

Bandy, W., Mortera-Gutierrez, C., Urrutia-Fucugauchi, J. and Hilde, T. W. C. [1995]. *"The subducted Rivera-Cocos plate boundary: Where is it, what is it, and what is its relationship to the Colima rift?."* Geophysical Research Letters, Vol. 22: pp. 3075-3078.

Bartoli, G. and Mennucci, A. [2000]. *"Project San Gimignano, la Torre Grossa: Inspection and diagnosis investigations (in Italian)."* Proceedings of the 1st Congress on Diagnosis for the Protection of the Cultural Heritage, December 6-7, San Gimignano, Italy.

Bartoli, G., Casamaggi, C. and Spinelli, P. [2000]. *"Numerical modelling and analysis of monumental buildings: A case study."* Department of Civil Engineering, University of Florence, Italy.

Bartoli, G., Betti, M., Spinelli, P. and Tordini, B. [2006]. *"An innovative procedure for assessing the seismic capacity of historical tall buildings: The Torre Grossa masonry tower."* Proceedings of the 5th International Conference on Structural Analysis of Historical Constructions (SAHC), November 6-8, 2006, New Delhi, India.

Bartoli, G., Betti, M., Orlando, M. and Spinelli, P. [2008]. *"In situ testing and structural assessment of an historic masonry dome."* Proceedings of the 12th International Conference on Structural Faults and Repair, June 10-12, Edinburgh, Scotland.

Bayraktar, A., Türker, T., Sevim, B., Altunisik, A. C. and Yildirim, F. [2009]. *"Modal parameter identification of Hagia Sophia bell-tower via ambient vibration test."* Journal of Nondestructive Evaluation 28: 37-47.

Bazan, E. and Meli, R. [2003]. *"Seismic design of buildings (in Spanish)."* Limusa Editorial, Mexico.

Bazrafshan, E. [2009]. *"Investigation of non-strengthened and post-tensioned masonry towers in case of earthquake loading by means of numerical simulations."* Master thesis, Technical University of Braunschweig, Germany.

Beconcini, M. L., Bennati, S. and Salvatore, W. [2001]. *"Structural characterization of a medieval bell tower: First historical, experimental and numerical investigations."* Proceedings of the 3rd International Seminar on Structural Analysis of Historical Constructions (SAHC), University of Minho, Guimaraes, Portugal.

Benedetti, D. and Petrini, V. [1984]. *"Seismic vulnerability of masonry buildings: Proposal of an assessment methodology."* The Construction industry, Vol 18: pp. 66-78, Rome, Italy.

Bennati, S., Salvatore, W., Nardini, L. and Della Maggiora, M. [2002]. *"Bell´s dynamic action on a historical masonry tower."* Proceedings of the 4th International Conference on Structural Dynamics (EURODYN), September 2-5, Munich, Germany.

Bertero, V. V. [1992]. *"Lessons learned from recent catastrophic earthquakes and associated research (in Spanish)."* 1st Intern. Conference Torroja, Monograph 410–411, Madrid, Spain.

BGS [2009]. British Geological Survey, Centre for Sustainable Mineral Development. http://www.bgs.ac.uk/mineralsuk/mines/stones/home.html. Last access 21.07.2009.

BGS [2011]. *"Seismic alert: Central Italy 6 April 2009."* British Geological Survey, Natural Environment Research Council. http://www.bgs.ac.uk/. Last access 16.03.2011.

Binda, L., Gatti, G., Mangano, G., Poggi, C. and Sacchi-Landriani, G. [1992]. *"The collapse of the civic tower of Pavia: A survey of the materials and structure."* Masonry International 11-20.

Binda, L. [2008]. *"Learning from failure: Long-term behaviour of heavy masonry structures."* Polytechnic of Milano, Italy. Published by WIT press, GB.

Bolt, B. A. [1999]. *"Earthquakes."* W. H. Freeman and Company, 4th Edition, New York.

Bonett, R. L. [2003]. *"Vulnerability and seismic risk of buildings: application to urban environments in zones of high and moderate hazard (in Spanish)."* Doctoral thesis, Politechnical University of Catalunya, Barcelona, Spain.

Borerro, J., Ortiz, M., Titov, V. and Synolakis, C. [1997]. *"Field survey of Mexican tsunami produces new data and unusual photos."* Eos, Trans. AGU, Vol. 78, No. 8, pp. 85-88.

BVE [2000]. *"Rules for the classification of steel ships."* Bureau Veritas AII (3.2), Beams of uniform section and uniformly distributed load.

Caicedo, C., Barbat, A.H. and Canas, J.A. [1994]. *"Seismic vulnerability of buildings (in Spanish)."* Published by the International Center of Numerical Methods (CIMNE), monograph IS-6. Barcelona, Spain.

Calderini, C. [2004]. *"A constitutive model for masonry: Formulation and implementation for the analysis of complex structures (in Italian)."* Doctoral thesis, University of Genoa, Italy.

Calderini, C. and Lagomarsino, S. [2006]. *"A micromechanical inelastic model for historical masonry."* Journal of Earthquake Engineering 10(4): 453-479.

Casolo, S. [1998]. *"A three-dimensional model for the vulnerability analysis of a slender medieval masonry tower."* Journal of Earthquake Engineering, Vol. 2, No. 4: 487-512.

Casolo, S. and Milani, G. [2010]. *"A simplified homogenization-discrete element model for the nonlinear static analysis of masonry walls out-of-plane loaded."* Journal of Engineering Structures, Vol. 32, No. 8: 2352-2366.

Castellano, M. G. [2001]. *"Innovative technologies for earthquake protection of architectural heritage."* Proceedings of the International Millennium Congress: More than two thousand years in the history of Architecture, UNESCO-ICOMOS, September 10-12, 2001, Paris, France.

Çelebi, M., Bazzurro, P., Chiaraluce, L., Clemente, P., Decanini, L., DeSortis, A., Ellsworth, W., Gorini, A., Kalkan, E., Marcucci, S., Milana, G., Mollaioli, F., Olivieri, M., Paolucci, R., Rinaldis, D., Rovelli, A., Sabetta, F. and Stephens, C. [2010]. *"Recorded motions of the 6th April 2009 M_w 6.3 L'Aquila, Italy, earthquake and implications for building structural damage: Overview."* Earthquake Spectra, Vol. 26, No. 3, pp. 651-684.

CENAPRED [2010]. *"Seismology and seismic risk."* National Center for the Prevention of Disasters, Mexico. http://www.cenapred.gob.mx. Last access 20.12.2010.

Chavez, M. and Meli, R. [2010]. *"Numerical simulation of the seismic response of a Mexican colonial model temple tested in a shaking table."* Proceedings of the 7th International Conference on Structural Analysis of Historic Constructions (SAHC), October 6-8, 2010, Tongji University, Shanghai, China.

Chopra, A. K. [2001]. *"Dynamics of structures: Theory and applications to Earthquake Engineering."* Published by Prentice-Hall, Upper Saddle River, New Jersey, USA.

Courboulex, F., Singh, S. K., Pacheco, J. F. and Ammon, C. J. [1997]. "*The 1995 Colima-Jalisco, Mexico, earthquake (M_w= 8.0): A study of the rupture process*." Geophysical Research Letters, Vol. 24, No. 9, pp. 1019-1022.

Croci, G. and D'Ayala, D. [1993]. "*Recent developments in the safety assessment of the Coliseum."* Conference on structural preservation of architectural heritage, Roma, Italy.

Croci, G. [1995]. *"The Coliseum: safety evaluation and preliminary criteria of intervention."* Proceedings of the 1ST International Conference on Structural Analysis of Historical Constructions (SAHC), November 8-10, 1995, Barcelona, Spain.

Croci, G. [1998]. *"The conservation and structural restoration of architectural heritage."* Advances in Architecture series. Computational mechanics publications.

Cuffaro, M., Doglioni, C. and Riguzzi, F. [2009]. *"Present geodynamics of the northern Adriatic plate."* Rendiconti online Soc. Geol. It., Vol. 3, Italy.

Curti, E., Parodi, S. and Podesta, S. [2008]. *"Simplified models for seismic vulnerability analysis of bell towers."* Proceedings of the 6th International Conference on Structural Analysis of Historical Constructions (SAHC), July 2-4, 2008, Bath, UK.

D'Ayala, D. [2000]. *"Establishing correlation between vulnerability and damage survey for churches."* Proceedings of the 12th World Conference on Earthquake Engineering (12WCEE), 30 January - 4 February, 2000, Auckland, New Zealand.

DCW [2004]. *"The highway network of the state of Colima, Mexico."* Scale 1: 1000000. Digital Chart of the World, Geographical Information System, Global Database.

DeMets, C., Carmichael, I., Melbourne, T., Sanchez, O., Stock, J., Suarez, G. and Hudnut, K. [1995]. *"Anticipating the successor to Mexico´s largest historical earthquake."* Eos, Vol. 76, No. 42, pp. 417-424.

Desroches, R. and Smith, B. [2003]. *"Shape memory alloys in seismic resistant design and retrofit: A critical review of the state of the art, potential and limitations."* School of Civil and Environmental Engineering, Georgia Institute of Technology, Atlanta, USA.

Devoti, R., Riguzzi, F., Cuffaro, M. and Doglioni, C. [2008]. *"New GPS constraints on the kinematics of the Apennines subduction."* Earth and Planetary Science Letters, 273, pp. 163-174.

Dolan, C. W., Hamilton, H. R., Bakis, C. E. and Nanni, A. [2001]. *"Design recommendations for concrete structures prestressed with FRP tendons."* FHWA Contract, Final Report, University of Wyoming, Pennsylvania State University and University of Missouri.

Dolce, M. [1994]. *"Vulnerability and Risk Analysis."* Report of the EAEE Working Group 3 in the 10th Congress of the European Conference on Earthquake Engineering, 28 August-2 September, 1994, Vienna, Austria.

DTES [2005]. *"Prestress manual: A guide for field inspection of cast-in-place post-tensioned structures."* Department of Transportation and Engineering Services, State of California, USA.

ElGawady, M. A., Lestuzzi, P. and Badoux, M. [2007]. *"Static cyclic response of masonry walls retrofitted with fiber reinforced polymers."* Journal of Composites for Construction (ASCE), Vol. 11, No. 1.

Escobedo, D., Pacheco, J. and Suarez, G. [1997]. *"Teleseismic body-wave analysis of the 9th October, 1995 (M_w= 8.0), Colima-Jalisco, Mexico, earthquake and its large foreshock and aftershock."* Accepted in Geophysical Research Letters.

Eurocode 8 [2004]. *"Design of structures for earthquake resistance - Part 1: General rules, seismic actions and rules for buildings."* European Standard.

Fajfar, P. [2000]. *"A nonlinear analysis method for performance-based seismic design."* Journal of Earthquake Spectra, 16 (3), 573-591.

FEMA-273 [1997]. *"Handbook for the seismic evaluation of existing buildings."* Federal Emergency Management Agency, Washington, USA.

Filiatrault, A. [1996]. *"Elemental Seismic Engineering and dynamic evaluation of structures."* Editions of the Polytechnical School of Montreal, Canada.

Fischli, F. [1994]. *"Leaning tower of Pisa: post-tensioning Italy's famous bell tower."* Forum on Structural Engineering, April, 1994, Pisa, Italy.

Fugazza, D. [2003]. *"Shape-memory alloy devices in earthquake engineering: Mechanical properties, constitutive modeling and numerical simulations."* Master thesis, University of Pavia, Italy.

Gambarotta, L. and Lagomarsino, S. [1997]. *"Damage models for the seismic response of brick masonry shear walls."* Part I and II. Earthquake Engineering and Structural Mechanics, Vol. 26: 441-462.

Ganz, H. R. [1990]. *"Post-tensioned masonry structures: Properties of masonry design considerations post-tensioning system for masonry structures applications."* VSL Report Series No. 2, Berne, Switzerland.

Ganz, H. R. [2001]. *"Evolution of prestressing systems."* Workshop on Durability of Post-tensioning Tendons, November 15-16, 2001, Ghent, Belgium.

Ganz, H. R. [2002]. *"Post-tensioned masonry around the world."* Proceedings of the first annual Conference of the Post-tensioning Institute, May 5-7, 2002, San Antonio, USA.

Garcia, N. [2007]. *"Functioning and structural safety of the conventual temples of the XVI century in Mexico (in Spanish)."* Doctoral thesis, National Autonomous University of Mexico (UNAM).

GEER [2010]. *"Geotechnical Extreme Events Reconnaissance: Turning disaster into knowledge."* Report of the 2003 Colima earthquake http://www.geerassociation.org. Last access 18.02.2011.

Gentile C. and Saisi A. [2007]. *"Ambient vibration testing of historic masonry towers for structural identification and damage assessment."* Construction and Building Materials 21: 1311-1321.

GES [1993]. *"Technical opinion about the collapse of the bell tower of St. Maria Magdalena in Goch, Germany ."* Gantert Engineering Studio.

Gioncu, V. and Mazzolani, F. M. [2002]. *"Ductility of seismic resistant steel structures."* Published by Spon Press, London.

Gioncu, V. and Mazzolani, F. M. [2011]. *"Earthquake Engineering for Structural Design."* Published by Spon Press, an imprint of Taylor and Francis, London and New York.

Giordano, A., De Luca, A., Mele, E. and Romano A. [2007]. *"A simple formula for predicting the horizontal capacity of masonry portal frames."* Engineering Structures 29: 2109-2123.

Giovinazzi, S. [2005]. *"The vulnerability assessment and the damage scenario in seismic risk analysis."* Doctoral thesis, Technical University of Braunschweig, Germany.

GNDT [1990]. *"Seismic risk of public buildings (in Italian)."* National Council of Investigation, National Group for the earthquake protection, Italy.

Grünthal, G. [1998]. *"European Macroseismic Scale EMS-98."* Notes of the European Center of Geodynamics and Seismology, Volume 15, Luxembourg.

GSHAP [2010]. *"Global seismic hazard map."* Global Seismic Hazard Assessment Program. http://www.seismo.ethz.ch/static/GSHAP/. Last access 19.12.2010.

Guzman, R., Aguayo, I., Martinez, J. and Alcaraz, C. [1986]. *"Colima: Semblance of a province."* Edited by the Constitutional Government of the State of Colima, Mexico.

Heyman, J. [1966]. *"The stone skeleton."* International Journal of Solids and Structures, Vol. 2, pp. 249-279.

Heyman, J. [1967]. *"On shell solutions for masonry domes."* International Journal of Solids and Structures, Vol. 3, pp. 227-241.

Heyman, J. [1969]. *"The safety of masonry arches."* International Journal of Mechanical Sciences, Vol. 11, pp. 363-385.

Huster, U. [2000]. *"Bearing behavior of natural stone masonry under central loading: Development and application of a Finite Element program (in German)."* Doctoral thesis, University of Kassel, Germany.

IEEE-693 [1997]. *"Recommended Practices for Seismic Design of Substations."* Institute of Electrical Electronic Engineers, Piscataway, NJ, USA.

INAH [2003]. *"Restoration and strengthening works on the damaged historical buildings after the 2003 Colima, Mexico earthquake."* National Institute of Anthropology and History, Mexico.

Indirli, M., Castellano, M. G., Clemente, P. and Martelli, A. [2001]. *"Demo-application of Shape Memory Alloy Devices: The rehabilitation of the S. Giorgio church bell-tower."* Proceedings of SPIE, Smart Structures and Materials.

INGV [2011]. *"Seismic hazard maps of the national territory (in Italian)."* National Institute of Geophysics and Vulcanology, Italy. http://www.ingv.it/. Last access 17.03.2011.

Ivorra, S. and Pallares F. J. [2006]. *"Dynamic investigations on a masonry bell tower."* Engineering structures 28: 660-667.

Ivorra, S., Pallares, F. J. and Adam, J. M. [2008]. *"Experimental and numerical studies on the bell tower of Santa Justa y Rufina (Orihuela-Spain)."* Proceedings of the 6th International Conference on Structural Analysis of Historical Constructions (SAHC), paper CH29, 349-355. July 2-4, 2008, Bath, UK.

Kooharian, A. [1952]. *"Limit analysis of voussoir (segmental) and concrete arches."* Journal of the American Concrete Institute, Vol. 24, No. 4, pp. 317-328.

Kozak, J. and Thompson, M. C. [1991]. *"Historical earthquakes in Europe."* Swiss Reinsurance, Zurich.

Kramer, S. L. [1996]. *"Geotechnical earthquake engineering."* Published by Prentice-Hall International Series, Upper Saddle River, New Jersey, USA.

Krawinkler, H. [1999]. *"Challenges and progress in performance-based earthquake engineering."* International Seminar on Seismic Engineering for Tomorrow (in honor of Professor Harashi Akiyama), November 26, Tokyo, Japan.

Kulhanek, O. [1990]. *"Anatomy of seismograms."* Elsevier, Amsterdam, Netherlands.

Lagomarsino, S., Podesta, S. and Resemini, S. [2002]. *"Seismic response of historical churches."* 12th European Conference on Earthquake Engineering, Paper Reference 123 (Genoa), September 9-13, 2002, London, UK.

Lang, K. [2002]. *"Seismic vulnerability of existing buildings."* Doctoral Thesis, ETH, Zurich.

Lang, K. and Bachmann, H. [2003]. *"on the seismic vulnerability of existing unreinforced masonry buildings."* Journal of Earthquake Engineering, Volume 7, Issue 3: 407-426.

Lee, S. [2008]. *"Nonlinear dynamic earthquake analysis of skyscrapers."* Proceedings of the 8th World Congress of Council on Tall Buildings and Urban Habitat, March 3-5, 2008, Dubai.

Leelataviwat, S., Goel, S. C. and Stojadinovic, B. [1999]. *"Towards performance-based seismic design of structures."* Journal of Earthquake Spectra, Volume 15, No. 3: 435-461.

Lofti, H. R. and Shing, P. B. [1994]. *"Interface model applied to fracture of masonry structures."* Journal of Structural Engineering, 120 (1), 63-81.

Lourenço, P. B. [1996]. *"Computational strategies for masonry structures."* Doctoral thesis, Delft University of Technology, Netherlands.

Lourenço, P. B. and Rots, J. [1997]. *"A multi-surface interface model for the analysis of masonry structures."* Journal on Engineering Mechanics, 123 (7), 660-668.

Lourenço, P. B., Rots, J. and Blaauwendraad, J. [1998]. *"Continuum model for masonry: Parameter estimation and validation."* Journal on Structural Engineering, 124 (6), 642-652.

Lourenço, P. B. and Pina-Henriques, J. [2006]. *"Validation of analytical and continuum numerical methods for estimating the compressive strength of masonry."* Journal on Computers and Structures 84: 1977-1989.

Luhr, J. F. and Carmichael, I. S. E. [1981]. *"The Colima volcanic complex, Mexico: Part II. Late Quaternary cinder cones."* Contributions to Mineralogy and Petrology, 76 (2), 127-147.

Lund, J. L., Selby, A. R. and Wilson, J. M. [1995]. *"The dynamics of bell towers: A survey in northeast England."* Proceedings of the 4th International Conference on Structural Repairs and Maintenance of Historical buildings. Volume 2: 45-52.

Macchi, G. [1993]. *"Monitoring medieval structures in Pavia."* Structural Engineering International, I/93.

Mazzolani, F. M. [2002]. *"Structural integrity under exceptional actions: Basic definitions and field activity."* Proceedings of the COST Seminar, April 19-20, 2002, Lisbon, Portugal.

MDS-CFE [1981]. *"Manual of Civil Constructions: Seismic Design (in Spanish)."* Federal Commission of Electricity (CFE) and Institute of Electric Research, Mexico.

MDS-CFE [1993]. *"Manual of Civil Constructions: Seismic Design (in Spanish)."* Federal Commission of Electricity (CFE) and Institute of Electrical Research, Mexico.

Melbourne, T., Carmichael, I., DeMets, C., Hudnut, K., Sanchez, O., Stock, J., Suarez, G. and Webb, F. [1997]. *"The geodetic signature of the M8.0 Oct. 9, 1995, Jalisco subduction earthquake."* Geophysical Research Letters, Vol. 24, No. 6, pp. 715-718.

Meli, R. [1998]. *"Structural engineering of the historical buildings (in Spanish)."* Civil Engineers Association (ICA) Foundation, A. C., Mexico.

Mena, U. [2002]. *"Evaluation of the seismic risk in urban zones (in Spanish)."* Doctoral thesis, Politechnical University of Catalunya, Barcelona, Spain.

Meza, J. M. [2007]. *"Method for the seismic performance assessment of historical masonry buildings (in Spanish)."* Master thesis, National Autonomous University of Mexico (UNAM).

Mistler, M. [2006]. "Deformation-based seismic measure concept for masonry constructions (in German)." Doctoral thesis, University of Aachen, Germany.

Monaco, A. and Monaco, R. [2005]. *"Urban seismic risk (in Italian)."* Editorial Syst., Naples, Italy.

Mucciarelli, M. and Magri, L. [1992]. *"For an adequate use of intensity data in site hazard estimates: Mixing theoretical and observed intensities."* Proceedings of the 10th World Conference on Earthquake Engineering (10WCEE), Madrid, Spain.

Mwafy, A. M. and Elnashai, A. S. [2001]. *"Static pushover versus dynamic collapse analysis of RC buildings."* Journal of Engineering Structures, Vol. 23, No. 5, pp. 407-424.

Nanni, A., Bakis, C. E., O´Neil, E. F. and Dixon, T. O. [1996]. *"Performance of FRP tendon-anchor systems for prestressed concrete structures."* PCI Journal: 34-44.

NCSE [2002]. *"Spanish Seismoresistant Construction Norm (in Spanish)."* General Part and Edification (Spanish standard). Ministry of Foment. Spain.

Nielsen, M. P. [1999]. *"Limit analysis and concrete plasticity."* Second edition, CRC.

NTCDF [2004]. *"Complementary Technical Norms of the Mexican Construction Code (in Spanish)."* Mexico.

Oliver, J. Huespe, A. E. Blanco S. and Linero, D. L. [2006]. *"Stability and robustness issues in numerical modeling of material failure with the strong discontinuity approach."* Computer Methods in Applied Mechanics and Engineering 195: 7093-7114.

Orduña, A. [2003]. *"Seismic assessment of ancient masonry structures by rigid blocks limit analysis."* Doctoral thesis, University of Minho, Portugal.

Orduña, A. and Lourenço, P. B. [2005a]. *"Three-dimensional limit analysis of rigid blocks assemblages. Part I: Torsion failure on frictional interfaces and limit analysis formulation."* International Journal of Solids and Structures 42(18-19): 5140-5160.

Orduña, A. and Lourenço, P. B. [2005b]. *"Three-dimensional limit analysis of rigid blocks assemblages. Part II: Load-path following solution procedure and validation."* International Journal of Solids and Structures 42(18-19): 5161-5180.

Orduña, A., Roeder, G. and Peña, F. [2007]. *"Seismic assessment of historical masonry constructions: comparative of three models of analysis (in Spanish)."* Seismic Engineering Magazine, No. 77, pp. 71-88. Mexico.

Orduña, A., Preciado, A., Galván, J. F. and Araiza, J. C. [2008]. *"Vulnerability assessment of churches at Colima by 3D limit analysis models."* Proceedings of the 6th International Conference on Structural Analysis of Historical Constructions (SAHC), July 2-4, 2008, Bath, UK.

Ötes, A. and Löring, S. [2006]. *"Bearing behavior of masonry constructions under earthquake loading (in German)."* Published in Bautechnik 83, Heft 2.

Palencia, J. C., Agüera, N., Frau, C. and Tornello, M. [2005]. *"Seismic vulnerability assessment of an educational building (in Spanish)."* 9th National Congress on Seismic Engineering, November 16-19, 2005, Chile.

Pardo, M. and Suarez, G. [1995]. *"Shape of the subducted Rivera and Cocos plates in southern Mexico: Seismic and tectonic implications."* Journal of Geoph. Research, Vol. 100, pp. 357-373.

Paulay, T. and Priestley, M. J. N. [1992]. *"Seismic design of reinforced concrete and masonry buildings."* John Wiley and sons, Inc.

Pavese, A. [1997]. *"Structural role of the colonnade in the leaning tower of Pisa."* Proceedings of the International Conference on Inspection and Monitoring of Architectural Heritage, May 15-19, 1997, Seriate, Italy.

PEER [2011]. *"PGA and spectral accelerations at a site by the attenuation relationships of Youngs et al. [1997]."* Pacific Earthquake Engineering Research. Last access 24.03.2011. http://peer.berkeley.edu/course_modules/eqrd/IntExmp/atten22.htm.

Penelis, G. G. and Kappos, A. J. [1997]. *"Earthquake-resistant concrete structures."* Published by E and FN Spon, an imprint of Chapman and Hall, London, UK.

Peña, F. and Meza, M. [2010]. *"Seismic assessment of bell towers of Mexican colonial churches."* Proceedings of the 7th International Conference on Structural Analysis of Historic Constructions (SAHC), October 6-8, 2010, Tongji University, Shanghai, China.

Preciado, A. [2007]. *"Seismic vulnerability assessment of historical constructions in the State of Colima, Mexico (in Spanish)."* Master thesis, University of Colima, Mexico.

Preciado, A., Araiza, J. C. and Orduña, A. [2007]. *"Seismic vulnerability assessment of historical constructions in the State of Colima, Mexico."* Proceedings of the International Symposium on Studies on Historical Heritage (SHH 07), September 17-21, 2007, Antalya, Turkey.

Preciado, A. and Orduña, A. [2008]. *"Seismic vulnerability assessment of historical constructions in Colima, Mexico: A correlation between damage and intensity."* University of Colima, Mexico.

Raijmakers, T. M. J. and Vermeltfoort, A. T. [1992]. *"Deformation controlled tests in masonry shear walls (in Dutch)."* Report B-92-1156, TNO-Bouw, Delft, The Netherlands.

Ramirez-Gaytan [2008]. *"Modeling of the source and simulation of accelerograms of the earthquake of Tecoman of the 21st of January, 2003, by the method of the empirical Green´s function (in Spanish)."* Doctoral thesis, National Autonomous University of Mexico (UNAM).

Ramos, L. F., Marques, L., Lourenço, P. B., De Roeck, G., Campos-Costa, A. and Roque, J. [2010]. *"Monitoring historical masonry structures with operational modal analysis: Two case studies."* Mechanical Systems and Signal Processing (2010).

Rao, D. S. P. [2007]. *"Investigations on ancient masonry structures using infrared thermography."* Proceedings of the Conference of InfraMation 2007, USA.

Rodriguez-Lozoya, H., Quintanar, L., Rebollar, C., Gomez, J, Yagi, Y., Dominguez, T., Reyes, G., Javier, C. and Alcantara, L. [2007]. *"Source characteristics of the 22nd January 2003 M_w 7.5 Tecoman, Mexico, earthquake and its rupture process"*. Journal of Geophysical Research.

Rots, J. G. [1997]. *"Structural masonry: An experimental/numerical basis for practical design rules."* Published by Balkema, ISBN 90 5410 680 8, Rotterdam, Netherlands.

Rots, J. G. and Invernizzi, S. [2004]. *"Regularized sequentially linear saw-tooth softening model."* Int. Journal for Numerical and Analytical Methods in Geomech. 28: 821-856.

Russo, G., Bergamo, O., Damiani, L. and Lugato, D. [2010]. *"Experimental analysis of the Saint Andrea masonry bell tower in Venice: A new method for the determination of tower global young´s modulus E."* Engineering Structures, Vol. 32, Issue 2: 353-360.

Safina, S. [2002]. *"Seismic vulnerability of Essential buildings (in Spanish)."* Doctoral thesis, Politechnical University of Catalunya, Barcelona, Spain.

Sandi, H. [1986]. *"Vulnerability and risk analysis for individual structures and systems."* Report of the European Association of Structural Engineering, 8th Congress of the ECEE, Lisbon, Portugal.

Sanpaolesi, L. [1993]. *"Structural behavior of the leaning tower of Pisa."* Structural Engineering International, Vol. 3, No. 1.

Schlegel, R. [2004]. *"Numerical simulations of masonry structures by homogenised and discrete modeling strategies (in German)."* Doctoral thesis, University of Weimar, Germany.

Sengupta, A. K. and Menon, D. [2009]. *"Prestressed concrete structures."* Indian Institute of Technology, Madras.

Sepe, V., Speranza, E. and Viskovic, A. [2008]. *"A method for large-scale vulnerability assessment of historic towers."* Structural control and health monitoring 15: 389-415.

Silva, C. and Esquivel, R. [1976]. *"The subsoil of Colima City (in Spanish)."* Memories of the VIII National Meeting on Soils Mechanics, Guadalajara, Mexico, Vol. II, pp. 57-61.

Simioni, P. [2009]. *"Seismic response of reinforced concrete structures affected by reinforcement corrosion."* Doctoral thesis, Technical University of Braunschweig, Germany.

Slavik, M. [2002]. *"Assessment of bell towers in Saxony."* Proceedings of the 4th Int. Conference on Structural Dynamics (EURODYN), September 2-5, Munich, Germany.

SMIE and FICA [1999]. *"Masonry edifications for housing (in Spanish)."* Mexican Society of Structural Engineering and the Civil Engineers Foundation (ICA), A. C., Mexico.

SMIS and EERI [2006]. *"Preliminary observations on the Tecoman, Colima, Mexico, earthquake of January 21st, 2003."* Mexican Society of Seismic Engineering and the Earthquake Engineering Research Institute, USA. Especial earthquake report (learning from earthquakes), March, 2006.

Solarino, S. and Cassinis, R. [2007]. *"Seismicity of the upper lithosphere and its relationship with the crust in the Italian region."* Bulletino di Geofisica Teorica e Applicata, Vol. 48 (2), pp. 99-114.

Somerville, P. [2000]. *"Seismic hazard evaluation."* Proceedings of the 12th World Conference on Earthquake Engineering (12WCEE), 30 January - 4 February, 2000, Auckland, New Zealand.

Sperbeck, S. [2009]. *"Seismic risk assessment of masonry walls and risk reduction by means of prestressing."* Doctoral thesis, Technical University of Braunschweig, Germany.

SSN [2010]. National Seismological Service of the National Autonomous University of Mexico (UNAM). http://www.ssn.unam.mx/. Last access 28.02.2010.

Stavroulaki, M. E., Bartoli, G., Betti, M. and Stavrolakis, G. E. [2009]. *"Strengthening of masonry using metal reinforcement: A parametric numerical investigation."* Proceedings of the International Conference on Protection of Historical Buildings (PROHITECH), June 21-24, Rome, Italy.

TDR [2011]. *"Map of Tuscany."* http://www.tuscandream.com. Last access 16.03.2011.

Tejeda, J. C. and Silva, C. [2003]. *"Studies on the subsoil conditions of Colima City (in Spanish)."* Faculty of Civil Engineering, University of Colima, Mexico.

Toranzo-Dianderas, L. A., Restrepo, J. I., Carr, A. J. and Mander, J. B. [2004]. *"Rocking confined masonry walls with hysteretic energy dissipators and shake-table validation."* 13th World Conference on Earthquake Engineering, August 1-6, 2004, Vancouver, Canada. Paper No. 248.

Tordini, B. [2005]. *"The Torre Grossa of San Gimignano: Structural modeling and evaluation of the safety under seismic action (in Italian)."* Bachelor thesis, University of Florence, Italy.

Turcotte, D. L. [1999]. *"The physics of earthquakes: Is it a statistical problem?."* ACES Inaugural Workshop, Australia.

UCOL [1997]. *"The macro-earthquake of Manzanillo occurred on October 9th, 1995 (in Spanish)."* University of Colima (UCOL), Government of the state of Colima and the Mexican Society of Seismic Engineering. Compiled by Arturo Tena Colunga.

Urban, M. [2007]. *"Earthquake risk assessment of historical structures."* Doctoral thesis, Technical University of Braunschweig, Germany.

USGS [2010]. *"Frequency of occurrence of earthquakes based on observations since 1900."* U. S. Geological Survey. http://earthquake.usgs.gov/earthquakes/. Last access 19.12.2010.

USGS [2011]. *"Understanding plate motions."* U. S. Geological Survey. http://pubs.usgs.gov/gip/dynamic/understanding.html#anchor19173262.
Last access 7.03.2011

USGS [2011a]. U. S. Geological Survey. http://www.usgs.gov/. Last access 22.03.2011.

USGS [2011b]. *"World historical earthquakes."* United States Geological Survey.
http://earthquake.usgs.gov/earthquakes/world/historical_mag_big.php.
Last access 22.03.2011.

Van der Pluijm, R. and Vermeltfoort, A. T. [1991]. *"Deformation controlled tension and compression tests in units, mortar and masonry (in Dutch)."* Report B-91-0561, TNO-Bouw, Delft, The Netherlands.

Vere-Jones, D., Ben-Zion, Y. and Suniga, R. [2005]. *"Statistical seismology."* Pure and Applied Geophysics, Vol. 162, 1023-1026.

Vere-Jones, D. [2006]. *"The development of statistical seismology: A personal experience."* Tectonophysics, 413, 5-12.

Vermeltfoort, A. Th. and Raijmakers, T. M. J. [1993]. *"Deformation controlled tests in masonry shear walls, Part 2 (in Dutch)."* Report TUE/BKO/93.08, Eindhoven University of Technology, The Netherlands.

Wikipedia [2009]. The free encyclopedia. http://www.wikipedia.org/. The Finite Element Method, Richard Courant, http://en.wikipedia.org/wiki/Finite_element_analysis. Alexander Hrennikoff, http://en.wikipedia.org/wiki/Alexander_Hrennikoff. Last access 21.07.2009.

Wilde, K., Gardoni, P. and Fujino, Y. [2000]. *"Base isolation system with shape memory alloy device for elevated highway bridges."* Journal of Engineering Structures 22: 222-229.

Woo, G. [1992]. *"Calibrated expert judgment in seismic hazard analysis."* Proceedings of the 10th World Conference on Earthquake Engineering (10WCEE), Madrid, Spain.

Yagi, Y., Mikumo, T., Pacheco, J. and Reyes, G. [2004]. *"Source ruptures process of the Tecoman, Colima, Mexico earthquake of January 22nd, 2003, determined by joint inversion of teleseismic body wave and near-field data."* Bulletin of the Seismological Society of America, Vol. 94, No. 5, pp. 1795-1807.

Youngs, R. R., Chiou, S. J., Silva, W. A. and Humphrey, J. R. [1997]. *"Strong ground motion attenuation relationships for subduction zone earthquakes." Seismological Research Letters*, Vol. 68, Seismological Society of America.

Zhang, B., Benmokrane, B., Chennouf, A., Mukhopadhyaya, P. And El-Safty, A. [2001]. *"Tensile behavior of FRP tendons for prestressed ground anchors."* Journal of Composites for Construction, Vol. 5, No. 2.

Zobin, V. M. [2004]. *"The earthquakes and their hazards: How to survive to them? (in Spanish)."* University of Colima, Mexico.

Zurbitu, J., Castillo, G., Urrutibeascoa, I. and Aurrekoetxea, J. [2009]. *"Low-energy tensile-impact behavior of superelastic NiTi shape memory alloy wires."* Journal of Mechanics of Materials 41: 1050-1058.